

Ground Water Flow Modeling Under Selected Levee Reaches



Mark M. Wilsnack, P.E.¹
Victor A. Kelson, Ph.D²
David J. Dahlstrom, P.G.³
Henk M. Haitjema, Ph.D⁴
Ruben Arteaga, Ph.D⁵
Lorie Brownell, P.E.⁶
John Doherty, Ph.D⁷

February, 2008

Affiliations

¹ Department of SCADA and Hydro Data Management (formerly of HESM)

² Wittman Hydro Planning Associates, Inc.

³ Barr Engineering, Inc.

⁴ Haitjema Consulting, Inc.

⁵ Department of Hydrologic and Environmental Systems Modeling, SFWMD

⁶ Taylor Engineering

⁷ Watermark Numerical Computing

Executive Summary

The South Florida Water Management District has recently completed several implementations of the finite volume, object oriented model code HSE (Hydrologic Simulation engine) at subregional scales. HSE simulates ground water flow, overland flow in wetlands, flow in canals, ground water / surface water interactions and other critical components of the hydrologic cycle. In most HSE applications at a regional or subregional scale, ground water flow within the surficial aquifer system is simulated in two dimensions. While this is appropriate for regional applications, it may be inaccurate in regions where the vertical component of ground water flow is significant. The location of a shallow, partially penetrating well with a high pumping rate would serve as an example. Another possible example may be the levees that form boundaries of the ENP and Water Conservation Areas. These engineered levees are typically located adjacent to borrow canals whose water levels may be controlled by hydraulic structures. Seepage from the Everglades and Water Conservation Areas across levees such as L-28, L-29, L-31N and L-30 is a critical component of the water budget for the ENP, the remnant Everglades and the lower east coast service areas. Its implication to water resource issues has been a subject of discussion for many years.

Currently, the HSE code utilizes a linear algorithm to move ground water and ponded surface water from the up-gradient (i.e. wetland) side of a levee / borrow canal configuration to the down-gradient side (typically the landward side). This formulation relates total seepage from the wetlands to the wetland water level, the borrow canal stage, the aquifer properties, the geometry of the ground water flow system and borrow canal, and the ambient ground water level on the landward side of the levee (Lal, 2005). In order to utilize such an algorithm as part of an HSE application, the coefficients of this formulation must be obtained *a priori* for each levee reach in question. This may be accomplished by constructing a representative two-dimensional cross section model for each levee reach and measuring ground water flows for typical gradients under saturated conditions.

In support of HSE implementations, cross sectional ground water flow models were constructed under levees C-111, L-31N, L-30, L-29, L-33, L-37, L-38, L-35A, L-36, L-6, L-7, L-8 and L-40. Each of these models was based on the analytic element method for simulating ground water flow. Since, prior to this study, the analytic element method was not used in southern Florida to simulate ground water flow underneath levees in a cross sectional sense, two test models were also implemented to help verify the suitability of the method for the intended purpose. In each case, the results from a cross sectional analytic element model were compared to those obtained from an analytic solution that was also developed as part of this effort.

The levee seepage parameters required by the HSE were derived for each of the major levee reaches listed above using the analytic element modeling code ModAem along with automated parameter estimation techniques. The uncertainty inherent to these parameters was also evaluated. These results can be incorporated into implementations of the HSE at regional or subregional scales.

Table of Contents

<u>List of Figures</u>	6
<u>List of Tables</u>	9
<u>Acknowledgements</u>	11
<u>1.0 Introduction</u>	12
<u>2.0 Application of the Analytic Element Method to Cross Section Levee Seepage Models</u>	13
2.1 <i>Specification of Boundary Conditions</i>	13
2.2 <i>Application to Test Problems</i>	14
2.3 <i>Incorporation of Cross Section Model Results into the HSE</i>	17
<u>3.0 Cross Section Models and Seepage Coefficients of Selected Levee Reaches</u>	19
3.1 <i>The C-111 Levee / Borrow Canal System located between S-176 and S-177</i>	20
3.2 <i>The C-111 Levee / Borrow Canal System located between S-177 and S-18C</i>	26
3.3 <i>The EAA L-6 Levee / Borrow Canal System</i>	30
3.4 <i>The L-7 Levee / Borrow Canal System</i>	34
3.5 <i>The L-8 Levee / Borrow Canal System</i>	38
3.6 <i>The L-29, Section 1 Levee / Borrow Canal System</i>	42
3.7 <i>The L-29, Section 2 Levee / Borrow Canal System</i>	46
3.8 <i>The L-29, Section 3 Levee / Borrow Canal System</i>	50
3.9 <i>The L-30 Levee / Borrow Canal System located South of S-335</i>	55
3.10 <i>The L-30 Levee / Borrow Canal System located North of the Bridge</i>	60
3.11 <i>The L-30 Levee / Borrow Canal System located between S-335 and the Bridge</i>	65
3.12 <i>The L-31N Levee / Borrow Canal System located between G-211 and S-331</i>	69
3.13 <i>The L-31N Levee / Borrow Canal System located north of G-211</i>	75
3.14 <i>The L-31N Levee / Borrow Canal System located south of S-331</i>	80
3.15 <i>The L-33 Levee / Borrow Canal System</i>	85
3.16 <i>The L-35A Levee / Borrow Canal System</i>	89
3.17 <i>The L-36 Levee / Borrow Canal System</i>	93
3.18 <i>The L-37 Levee / Borrow Canal System</i>	98
3.19 <i>The L-38E and L38W Levee / Borrow Canal System</i>	102
3.20 <i>The L-40 Levee / Borrow Canal System</i>	107
<u>4.0 Summary and Conclusions</u>	113
<u>5.0 References</u>	114
<u>Appendix A.</u> Development of a Closed-Form Solution to the Initial Test Problem	124
<u>Appendix B.</u> Methodology for Levee Seepage Sensitivity Analysis	127

<u>Appendix C.</u>	A Comparison of the Analytic Element Method to an Analytic Solution to Ground Water Flow under L-29, Section 1	137
<u>Appendix D.</u>	Analytic Solutions to Generalized or Proposed Levee / Borrow Canal Configurations	151
<u>Appendix E.</u>	Additional Cross Sectional Modeling of the C-111, L-31N and L-30 Corridors	166
<u>Appendix F.</u>	A Discussion of Predictive Confidence Limits by John Doherty	255

List of Figures

Figure 1. Simple Conceptual Model of an Aquifer with Poned Surface Water and a Levee	13
Figure 2. Semi-Infinite, Layered Ground Water Flow System with Dirichlet Boundaries	15
Figure 3. Locations of Canal Cross Section Models	20
Figure 4. Location of C-111 canal/levee between S-176 and S-177	21
Figure 5. Conceptualization of the levee, canal, and shallow hydrostratigraphy of C-111 between S-176 and S-177	22
Figure 6. Location of C-111 canal/levee between S-177 and S-18C	26
Figure 7. Conceptualization of the levee, canal, and shallow hydrostratigraphy of the C-111 between S-177 and S-18C	27
Figure 8. Location of EAA L-6 levee/canal conceptual model	30
Figure 9. Conceptualization of the levee, canal, and shallow hydrostratigraphy of L-6	31
Figure 10. Location of L-7 conceptual model	34
Figure 11. Conceptualization of the levee, canal, and shallow hydrostratigraphy of L-7	35
Figure 12. Location of L-8 levee/canal conceptual model	38
Figure 13. Conceptualization of the levee, canal, and shallow hydrostratigraphy of L-8	39
Figure 14. Location of L-29, Section 1 levee/canal conceptual model	42
Figure 15. Conceptualization of the levee, canal, and shallow hydrostratigraphy of the L-29, Section 1 reach	43
Figure 16. Location of L-29, Section 2 Levee/Canal Conceptual Model	46
Figure 17. Conceptualization of the levee, canal, and shallow hydrostratigraphy of the L-29, Section 2 corridor	47
Figure 18. Location of L-29, Section 3 Levee/Canal Conceptual Model	50
Figure 19. Conceptualization of the levee, canal, and shallow hydrostratigraphy of the L-29, Section 3 corridor	51

Figure 20. Location of L-30 levee/canal conceptual model located south of S-335	55
Figure 21. Conceptualization of the levee, canal, and shallow hydrostratigraphy of L-30 levee/canal located south of S-335	56
Figure 22. Location of L-30 levee/canal conceptual model located north of the bridge	60
Figure 23. Conceptualization of the levee, canal, and shallow hydrostratigraphy of the L-30 reach located north of the bridge	61
Figure 24. Location of L-30 levee/canal conceptual model located north of S-335 and south of the bridge	65
Figure 25. Conceptualization of the levee, canal, and shallow hydrostratigraphy of the L-30 Canal located north of S-335 and south of the bridge	66
Figure 26. Location of L-31N Levee/Canal Conceptual Model located between G-211 and S-331	70
Figure 27. Conceptualization of the levee, canal, and shallow hydrostratigraphy of the L-31N reach located between G-211 and S-331	71
Figure 28. Location of L-31N (north of G-211) Levee/Canal Conceptual Model	75
Figure 29. Conceptualization of the levee, canal, and shallow hydrostratigraphy of the L-31N, north of G-211 corridor	76
Figure 30. Location of L-31N levee/canal conceptual model located south of S-331	80
Figure 31. Conceptualization of the levee, canal, and shallow hydrostratigraphy of the L-31N reach located south of S-331	81
Figure 32. Location of L-33 levee/canal reach conceptual model	85
Figure 33. Conceptualization of the levee, canal, and shallow hydrostratigraphy of L-33	86
Figure 35. Conceptualization of the levee, canal, and shallow hydrostratigraphy of the L-35A.	90
Figure 36. Location of L-36 levee/canal conceptual model	93
Figure 37. Conceptualization of the levee, canal, and shallow hydrostratigraphy of L-36	94
Figure 38. Location of L-37 canal/levee	98
Figure 39. Conceptualization of the levee, canal, and shallow hydrostratigraphy of the L-37 reach	99

Figure 40. Location of the L-38E and L-38W levee/canal conceptual model	102
Figure 41. Conceptualization of the levee, canal, and shallow hydrostratigraphy of L-38E and L-38W	103
Figure 42. Locations of L-40 conceptual models	107
Figure 43. Conceptualization of the levee, canal, and shallow hydrostratigraphy of the L-40 northern reach	108
Figure 44. Conceptualization of the levee, canal, and shallow hydrostratigraphy of the L-40 southern reach	111
Figure B1. Contours of equal objective function value for a two-parameter model	131
Figure B2. Contours of a model prediction in parameter space	132
Figure B3. The critical point in parameter space	133
Figure C1. Conceptualization of the levees, canals and shallow hydrostratigraphy along section 1 of the L-29 corridor	139
Figure D1. Conceptual cross section of a generalized levee / borrow canal configuration along with the associated ground water flow system	154
Figure F1. Contour lines in parameter space of a prediction made by a linear model	257
Figure F2. Contour lines in parameter space of a prediction made by a nonlinear model	259

List of Tables

Table 1. Comparison of Analytic and GFLOW Solutions for the Hypothetical Test Problem ...	17
Table 2. Differences Between the Analytic Solution and GFLOW Results	17
Table 3. A Comparison of two GFLOW Solutions for the Hypothetical Test Problem	18
Table 4. Differences between Heads and Flows Obtained from Two GFLOW Models	18
Table 5. Hydrogeologic parameters along C-111 between S-176 and S-177	23
Table 6. Summary of historical water levels along C-111 between S-176 and S-177	23
Table 7. Seepage Rates Across C-111 between S-176 and S-177	24
Table 8. Seepage Coefficients for C-111 between S-176 and S-177	24
Table 9. Hydrogeologic parameters along C-111 between S-177 and S-18C	27
Table 10. Summary of historical water levels along C-111 between S-177 and S-18C	28
Table 11. Seepage Rates Across C-111 between S-177 and S-18C	29
Table 12. Seepage Coefficients for C-111 between S-177 and S-18C	29
Table 13. Hydrogeologic parameters along EAA L6	31
Table 14. Summary of historical water levels along EAA L6	32
Table 15. Seepage Rates Across EAA L6	33
Table 16. Seepage Coefficients for EAA L6	33
Table 17. Hydrogeologic parameters along L7	35
Table 18 Summary of historical water levels along L7	36
Table 19. Seepage Rates Across L7	37
Table 20. Seepage Coefficients for L7	37
Table 21. Hydrogeologic parameters along L8	39
Table 22 Summary of historical water levels along L8	40

Table 23. Seepage Rates Across L8	41
Table 24. Seepage Coefficients for L8	41
Table 25. Hydrogeologic parameters along L-29, Section 1	45
Table 26 Summary of historical water levels along L-29, Section 1	46
Table 27. Seepage Rates Across L-29, Section 1	47
Table 28. Seepage Coefficients for L-29, Section 1	47
Table 29. Hydrogeologic parameters along L-29, Section 2	49
Table 30 Summary of historical water levels along L-29, Section 2	50
Table 31. Seepage Rates Across L-29, Section 2	51
Table 32. Seepage Coefficients for L-29, Section 2	51
Table 33. Hydrogeologic parameters along L-29, Section 3	54
Table 34 Summary of historical water levels along L-29, Section 3	54
Table 35. Seepage Rates Across L-29, Section 3	55
Table 36. Seepage Coefficients for L-29, Section 3	56
Table 37. Hydrogeologic parameters along L-30 south of S-335	59
Table 38 Summary of historical water levels along L-30 south of S-335	59
Table 39. Seepage Rates Across L-30 south of S-335	60
Table 40. Seepage Coefficients for L-30 south of S-335	60
Table 41. Hydrogeologic parameters along L-30 north of the Bridge	64
Table 42 Summary of historical water levels along L-30 north of the Bridge	64
Table 43. Seepage Rates Across L-30 north of the Bridge	65
Table 44. Seepage Coefficients for L-30 north of the Bridge	66
Table 45. Hydrogeologic parameters along L-30 between S-335 and the Bridge	68

Table 46 Summary of historical water levels along L-30 between S-335 and the Bridge	69
Table 47. Seepage Rates Across L-30 between S-335 and the Bridge	70
Table 48. Seepage Coefficients for L-30 between S-335 and the Bridge	71
Table 49. Hydrogeologic parameters along L-31N between G-211 and S-331	74
Table 50 Summary of historical water levels along L-31N between G-211 and S-331	74
Table 51. Seepage Rates Across L-31N between G-211 and S-331	75
Table 52. Seepage Coefficients for L-31N between G-211 and S-331	76
Table 53. Hydrogeologic parameters along L-31N north of G-211	79
Table 54 Summary of historical water levels along L-31N north of G-211	79
Table 55. Seepage Rates Across L-31N north of G-211	80
Table 56. Seepage Coefficients for L-31N north of G-211	81
Table 57. Hydrogeologic parameters along L-31N south of S-331	84
Table 58 Summary of historical water levels along L-31N south of S-331	84
Table 59. Seepage Rates Across L-31N south of S-331	85
Table 60. Seepage Coefficients for L-31N south of S-331	86
Table 61. Hydrogeologic parameters along L-33	88
Table 62 Summary of historical water levels along L-33	89
Table 63. Seepage Rates Across L-33	89
Table 64. Seepage Coefficients for L-33	90
Table 65. Hydrogeologic parameters along L-35A	92
Table 66 Summary of historical water levels along L-35A	93
Table 67. Seepage Rates Across L-35A	93
Table 68. Seepage Coefficients for L-35A	94

Table 69. Hydrogeologic parameters along L-36	97
Table 70 Summary of historical water levels along L-36	97
Table 71. Seepage Rates Across L-36	98
Table 72. Seepage Coefficients for L-36	99
Table 73. Hydrogeologic parameters along L-37	99
Table 74 Summary of historical water levels along L-37	102
Table 75. Seepage Rates Across L-37	103
Table 76. Seepage Coefficients for L-37	103
Table 77. Hydrogeologic parameters along L-38E and L-38W	106
Table 78 Summary of historical water levels along L-38E and L-38W	106
Table 79. Seepage Rates Across L-38E and L-38W	107
Table 80. Seepage Coefficients for L-38E and L-38W	108
Table 81. Hydrogeologic parameters along L-40	110
Table 82 Summary of historical water levels along L-40	111
Table 83. Seepage Rates Across L-40 (northern reach)	112
Table 84. Seepage Coefficients for L-40 (northern reach)	113
Table 85. Seepage Rates Across L-40 (southern reach)	114
Table 86. Seepage Coefficients for L-40 (southern reach)	114

Acknowledgements

The authors wish to express appreciation to Lehar Brion, Ken Tarboton, Jayantha Obeysekera, Ji-Ang Song, Randy Van Zee, Sharika Senarath and David Welter for their helpful comments and guidance in establishing the objectives and priorities of this project. Special thanks should also go to Rich Sands for his role in handling the contract management duties.

1.0 Introduction

The finite volume, object oriented model code HSE (Hydrologic Simulation Engine) simulates ground water flow, overland flow in wetlands, flow in canals, ground water / surface water interactions and other critical components of the hydrologic cycle. In most HSE implementations at a regional or subregional scale, ground water flow within the surficial aquifer system is simulated in two dimensions. While this is appropriate for regional applications, it may be inaccurate in regions where the vertical component of ground water flow is significant. The location of a shallow, partially penetrating well with a high pumping rate would serve as an example. Another possible example may be the levees that form boundaries of the ENP and Water Conservation Areas. These engineered levees are typically located adjacent to borrow canals whose water levels may be controlled by hydraulic structures.

Seepage from the Everglades and Water Conservation Areas across levees such as L-28, L-29, L-31N and L-30 is a critical component of the water budget for the ENP, the remnant Everglades and the lower east coast service areas. Its implication to water resource issues has been a subject of discussion for many years. Numerical models are typically used to analyze seepage rates under these levees (e.g. SEEP2D). Strack (1989) and Haitjema (1995) emphasize that it is often beneficial to supplement complex numerical analyses with analytical models in order to improve insight into underlying processes and controlling parameters. Unfortunately, analytical solutions for levee seepage in southern Florida have been limited or customized to specific circumstances in a manner that restricts their range of application. In cases where closed-form analytic solutions are too cumbersome or are not available, approximate analytic solutions may be employed. Here we present a methodology for developing approximate analytic solutions using the analytic element method (AEM).

Currently, the HSE code utilizes a linear algorithm to move ground water and ponded surface water from the up-gradient (i.e. wetland) side of a levee / borrow canal configuration to the down-gradient side (typically the landward side). This formulation relates total seepage from the wetlands to the wetland water level, the borrow canal stage, the aquifer properties, the geometry of the ground water flow system and borrow canal, and the ambient ground water level on the landward side of the levee (Lal, 2005). In order to utilize such an algorithm as part of an HSE application, the coefficients of this formulation must be obtained *a priori* for each levee reach in question. This may be accomplished by constructing a representative two-dimensional cross section model for each levee reach and measuring ground water flows for typical gradients under saturated conditions.

The primary objectives of this study are to (i) assess the applicability of analytic element models for analyzing levee seepage in two-dimensional, vertical cross section; (ii) to develop cross sectional analytic element models for selected reaches of major levees such as L-29, L-30, L-31N and L-37; and (iii) to develop the linear coefficients needed to simulate seepage under levees in the HSE based models. In addition, approximate closed-form solutions for seepage under typical or generic levee / borrow canal configurations will be developed to facilitate implementation of the HSE at locations of proposed or future levees.

2.0 Application of the Analytic Element Method to Cross Sectional Levee Seepage Models

As with any ground water flow model, the development of the cross-sectional levee seepage model requires a depiction of the ground water flow system in a conceptual model. A simple conceptual model of the surficial aquifer in the vicinity of a levee is shown in figure 1. In this situation, the surficial aquifer system extends a very large distance from either side of the levee / borrow canal configuration with ponded surface water occurring to the left of the levee. Although the example problem in Figure 1 suggests that aquifer properties are continuous everywhere, the proposed methodology is appropriate for layered systems, subject to the limitation that the layering must be continuous everywhere.

2.1 Specification of Boundary Conditions

In this conceptual model, it is assumed that the (layered) aquifer system is laterally infinite in

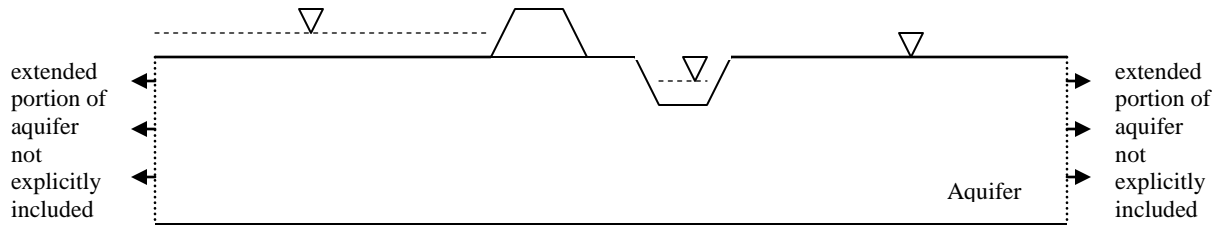


Figure 1. Simple Conceptual Model of an Aquifer with Ponded Surface Water and a Levee

extent. It may be shown that vertical flow in the system may be ignored at a lateral distance of 3λ from a partially-penetrating feature, e.g. a levee and borrow canal. The value λ is the “representative leakage length”, defined as

$$\lambda = \sqrt{KHc} \dots\dots\dots (1)$$

where K is the hydraulic conductivity, H is the aquifer thickness and c is the entry resistance of the surficial materials. This entry resistance is defined as the ratio of the thickness of the resistance layer to its vertical hydraulic conductivity. For layered systems, each flow layer has its own value of λ , based on the vertical resistance between the flow layer and all layers above. A conservative practice in layered systems is to choose the largest value of λ from among the layers.

For any cross-sectional model, it is possible to achieve an accurate ground water flow solution by truncating the model at a distance greater than 3λ from the levee and placing a vertically-oriented no-flow boundary there. However, in south Florida the value λ is often on the scale of a mile or more, and truncating at the 3λ distance is impractical.

Haitjema (2005) provides a methodology for truncating the model domain at a smaller distance from the levee. The model is truncated using vertically-oriented line-sink elements that are

configured as general-head boundary conditions (GHBs). The entry resistance for the GHB line-sinks in each layer are chosen such that the GHB approximates the flow into or out of the truncated model by the omitted portion of the aquifer; similarly, the modeled heads at the ends of the truncated model approximate the heads in the extended model. The entry resistance for the GHBs at the ends of the truncated model, denoted as c_b , is given by

$$c_b = \lambda / K \quad \dots\dots\dots (2)$$

where K is the hydraulic conductivity of the aquifer and λ is the representative leakage length provided above.

The formulation for the GHB resistance in a layered, truncated cross-sectional model as follows. In a layered model, the value λ_n for layer n (numbered from top to bottom) is given by

$$\lambda_n = \sqrt{K_n H_n \sum_{i=1}^{n-1} c_i} \quad \dots\dots\dots (3)$$

where c_i denotes the vertical resistance of the i^{th} layer. This formulation for λ essentially accounts for all of the vertical resistance between layer n and the ponded surface water. One could add to this total resistance the resistance of the top half of layer n . The GHB resistance for layer n is computed similarly as for the single-aquifer problem, except that λ_n is used. It is expected that the truncated model will be less accurate if the length of the model is far below 3λ . Below, the accuracy of the approximate truncated models and their applicability for seepage problems is examined and discussed. Unless otherwise stated, the assumption that $k_v = K$ everywhere within the ground water flow system is made.

2.2 Application to Test Problems

Shown in figure 2 is a conceptual model that can be used to perform a simple test of this approach to constructing truncated cross sectional models. The aquifer is semi infinite in length and consists of two layers separated by blankets with hydraulic conductivities that are three orders of magnitude less than those of the aquifer layers. Furthermore, the aquifer is bounded on its top by ponded surface water, on the bottom by impervious material, and on its right end by specified heads. All dimensions and aquifer properties are as shown.

2.21 Comparison with an Analytic Solution

A closed form solution to this ground water flow system can be stated as

$$h_2 = h_0 - M_2 e^{-fx} - M_4 e^{-gx} \quad \dots\dots\dots (4a)$$

$$h_4 = h_0 - jM_2 e^{-fx} - mM_4 e^{-gx} \quad \dots\dots\dots (4b)$$

where h_0 is the ponded surface water head; h_2 and h_4 are the heads within layers 2 and 4, respectively, and

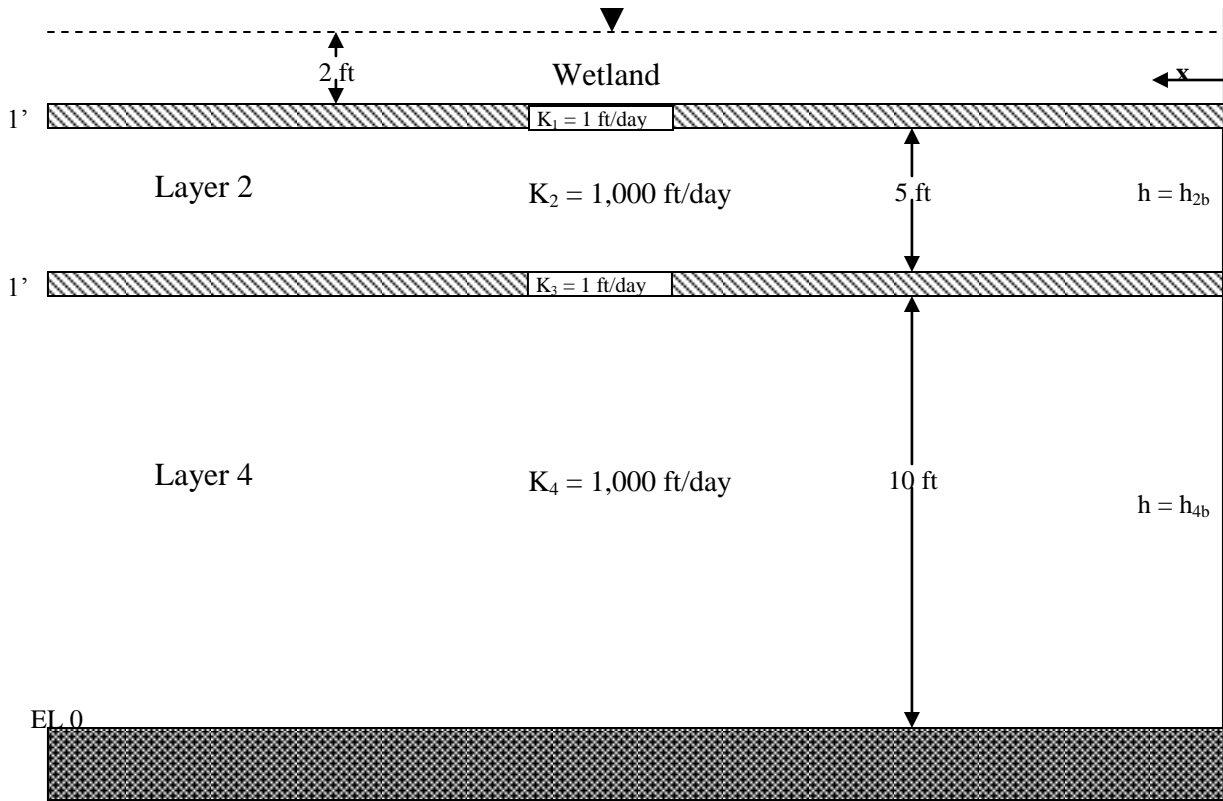


Figure 2. Semi-Infinite, Layered Ground Water Flow System with Dirichlet Boundaries

$$M_2 = \frac{(m-1)h_o - mh_{2b} + h_{4b}}{m-j} \dots\dots\dots (5)$$

$$M_4 = \frac{(1-j)h_o + jh_{2b} - h_{4b}}{m-j} \dots\dots\dots (6)$$

All other parameters within equations (4) – (7) reflect the hydraulic properties of the aquifer system and are as defined by Shea and Whitsett (1958). The derivation of this closed form solution is provided in Appendix A. Furthermore, applying Darcy’s law to equations (4) yields

$$Q_2(x) = C_2(fm_2e^{-fx} + gM_4e^{-gx}) \dots\dots\dots (7a)$$

$$Q_4(x) = C_4(fjM_2e^{-fx} + gmM_4e^{-gx}) \dots\dots\dots (7b)$$

where C_2 and C_4 denote the transmissivities of layers 2 and 4, respectively, while Q_2 and Q_4 are the ground water flow rates at a specified distance x . The amount of surface water that infiltrates

into the top aquifer over a specified distance is also of interest. The infiltration per unit length, denoted as q_w , is simply

$$q_w = C_1(h_0 - h_2) = C_1(M_2e^{-fx} + M_4e^{-gx}) \dots\dots\dots (8)$$

where C_1 is the vertical resistance to surface water flow into layer 2. The amount of surface water infiltrating over a distance equal to λ would then be

$$Q_\lambda = \int_0^\lambda q_w dx = \int_0^\lambda C_1(M_2e^{-fx} + M_4e^{-gx}) dx = C_1\left[\frac{M_2}{f}(1 - e^{-f\lambda}) + \frac{M_4}{g}(1 - e^{-g\lambda})\right] \dots\dots\dots (9)$$

With $h_0 = 21$ ft and $h_{2b} = h_{4b} = 19$ ft, equations (4) through (8) were used to compute heads and flows within layers 2 and 4 at the various locations given in table 1. Also contained in table 1 are the corresponding heads and flows computed with an analytic element model of the same ground water flow system. This model, based on the code GFLOW (Haitjema, 1995) is 600 feet in length. Applying equation (3) to the lower aquifer layer yields a λ value of about 140 feet; hence, the model length is slightly over 4λ . Additionally, a comparison between the results obtained using the two modeling approaches is provided in table 2. Agreement between head values is excellent while agreement in flow rates are good except at the left boundary. While this is most likely an artifact of the approximate nature of equation (3), the errors evident in table 2 are immaterial due to the relatively small magnitude of the flows at this boundary. Similarly, the total leakage from surface water over a length of λ from the right boundary of the model was found to be about 151 ft² / day. This agrees fairly well with the value of 148 ft²/day obtained using equation (9).

2.22 Comparisons of Different Model Lengths

The evaluation discussed above utilizes an analytic element model that is long enough to ensure that the upstream boundary contributes only a minor percentage of the total ground water flow. Due to the approximate nature of the formulation used to determine the hydraulic resistance of this boundary, this effect is desirable when making comparisons of model output to those obtained from an analytic solution. As a result, the test results shown in tables 1 and 2 help ascertain the use of analytic element models of finite length in modeling two-dimensional ground water flow in the vertical plane. However, they do not offer any insight into the errors that would be incurred if an analytic element model of shorter length was used. To address this, the same quantities shown in table 1 were also computed using an analytic element model with a truncated aquifer length of 150 feet. As in the longer model, the resistances of the vertical line sinks forming the left boundary were computed with equations (1) through (3). A comparison of the heads and flows computed with both analytic element models is given in tables 3 and 4. In this case, $Q_\lambda = 142$ cfd which differs by about 6% from the value of Q_λ computed for the longer model.

The agreement between the heads computed by each model is very good while agreement between the flow rates is good at locations that are not too distant from the downstream boundary. In contrast, the errors between flow rates become much larger within layer 4 at

Table 1. Comparison of Analytic and GFLOW Solutions for the Hypothetical Test Problem

x (ft)	Analytic Solution				GFLOW Model			
	Head (ft)		Flow (ft ² /day)		Head (ft)		Flow (ft ² /day)	
	Layer 2	Layer 4	Layer 2	Layer 4	Layer 2	Layer 4	Layer 2	Layer 4
0	19.00	19.00	122.03	101.09	19.00	19.00	125.73	99.74
50	19.85	19.48	57.35	89.60	19.84	19.48	56.07	88.69
150	20.51	20.19	18.52	52.42	20.50	20.18	18.24	52.30
300	20.83	20.70	5.78	20.02	20.82	20.69	5.76	20.25
450	20.94	20.89	2.10	7.44	20.94	20.89	2.11	7.68
600	20.98	20.96	0.77	2.76	20.98	20.96	0.782	2.06

Table 2. Differences Between the Analytic Solution and GFLOW Results

x (ft)	% Difference			
	Head		Flow	
	Layer 2	Layer 4	Layer 2	Layer 4
0	0.00	0.00	3.40	-1.34
50	-0.04	-0.02	-2.23	-1.02
150	-0.04	-0.05	-1.52	-0.23
300	-0.04	-0.03	-0.29	1.15
450	0.02	0.01	0.69	3.23
600	0.02	0.01	1.56	-25.36

locations closer to the upstream boundary. This is evidently due to the approximate nature of equation (3) for computing the resistance of the upstream vertical boundary. Hence, in order to achieve satisfactory results in practical applications involving layered ground water flow systems, it may be necessary to implement a cross sectional model long enough so that flux emitted from the upstream boundary is only a small percentage of the overall water budget.

Another comparative test similar to the one discussed above was carried out using a modified cross section of the ground water flow system underneath L-29, Section 3. This test is discussed in Appendix C.

2.3 Incorporation of Cross Section Model Results into the HSE Model

As indicated previously, the final objective of this study is to use cross section modeling results to define, for each levee reach, the linear relationship employed by the HSE for computing levee seepage rates based on wetland stages, canal stages and ambient ground water levels. By designating the upgradient or “marsh” side of the levee with the subscript “m”, the adjacent

Table 3. A Comparison of two GFLOW Solutions for the Hypothetical Test Problem

x (ft)	150-foot Model				600-foot Model			
	Head (ft)		Flow (ft ² /day)		Head (ft)		Flow (ft ² /day)	
	Layer 2	Layer 4	Layer 2	Layer 4	Layer 2	Layer 4	Layer 2	Layer 4
0	19.00	19.00	128.27	101.95	19.00	19.00	125.73	99.74
50	19.85	19.50	57.62	91.50	19.84	19.48	56.07	88.69
100	20.30	19.91	34.34	73.09	20.26	19.87	31.34	70.05
150	20.60	20.23	20.38	54.43	20.50	20.18	18.24	52.30

Table 4. Differences between Heads and Flows Obtained from Two GFLOW Models

x (ft)	% Difference			
	Head		Flow	
	Layer 2	Layer 4	Layer 2	Layer 4
0	0.00	0.00	2.0	2.2
50	0.0	0.0	2.8	3.2
100	0.2	0.2	9.6	4.3
150	0.5	0.2	11.7	4.1

borrow canal with the subscript “c” and the downgradient or “dry” side of the levee/borrow canal configuration with the subscript “d”, this linear relationship between seepage rates and stages can be expressed as

$$Q_m = K_{mc} (H_m - H_c) + K_{md} (H_m - H_d) \dots\dots\dots(10)$$

where Q_m is the total seepage under the levee and from the marsh; H_m , H_c and H_d are the heads on the marsh side of the levee, in the borrow canal and on the dry side of the borrow canal, respectively; and K_{mc} , K_{md} are coefficients that reflect the hydraulic properties of the ground water flow system. Similarly, the total ground water gained or lost by the dry side can be expressed as

$$Q_d = K_{dc} (H_d - H_c) + K_{dm} (H_d - H_m) \dots\dots\dots(11)$$

While the ground water flow into the canal is

$$Q_c = K_{cm} (H_c - H_m) + K_{cd} (H_c - H_d) \dots\dots\dots(12)$$

The quantities Q_m , Q_d and Q_c given by equations (10) - (12) can be derived from a cross section model where H_m , H_c , and H_d are the assigned boundary conditions. For each set of boundary conditions and corresponding seepage rates, equations (10) - (12) indicate that there will be six unknown coefficients. However, it should be readily apparent that $K_{md} = K_{dm}$, $K_{mc} = K_{cm}$, and $K_{cd} = K_{dc}$. In practice, it is best to solve for K_{mc} , K_{md} and K_{cd} through linear regression since

ground water flow within the analytic element model is not always strictly linear (Appendix E). A detailed description of the approach used to determine these coefficients is provided in Appendix E. Additional discussions are provided by Kelson et al (2006).

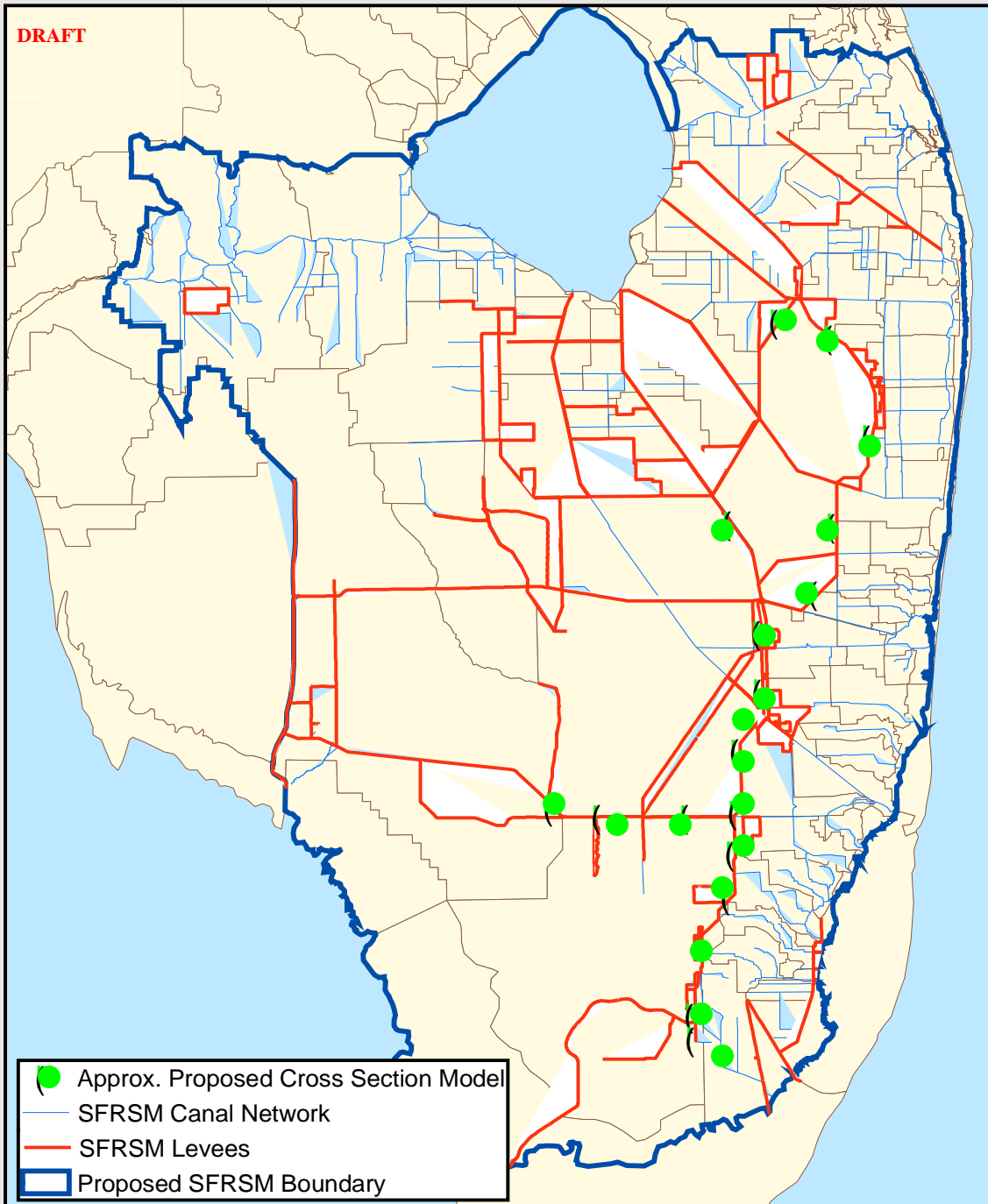
3.0 Cross Section Models and Seepage Coefficients of Selected Levee / Borrow Canal Reaches

Analytic Element based cross sectional models were developed using the ModAem code (Kelson, 2000) at representative locations within the primary levee reaches identified in figure 3. In each case, steady state discharges and heads within the ground water flow system beneath the levee / borrow canal configuration were computed under a set of representative wetland stages, canal stages and ambient ground water levels. The procedure outlined in section 2.3 was then used to determine the set of seepage coefficients. Additionally, an uncertainty analysis was conducted at each location in order to evaluate the uncertainties in the resultant coefficients due to model parameter uncertainties. This essentially provides approximate coefficient ranges that reflect the inherent uncertainty in hydraulic conductivity values. In particular, these uncertainty analyses were based on model simulations carried out in predictive analysis mode using the inverse parameter estimation code PEST (Doherty, 2004). Details on this approach are provided in Appendix B. The cross section model and resultant seepage coefficients for each levee reach are discussed in the sections that follow.

Although AEM based cross section models provide a relatively accurate and efficient means for studying ground water flow beneath existing levee reaches, it may not be feasible to conduct this type of modeling effort for every levee reach within the regional model domain. Furthermore, seepage beneath future proposed levees (e.g. those surrounding a new impoundment) may need to be simulated in a regional model. In this case, a design change in the levee / borrow canal system would necessitate modification of the supporting analytic element model. The use of analytic element modeling under these circumstances to develop the required relationships between water levels and seepage rates may prove to be impractical if a large number of designs need to be analyzed. Consequently, analytic solutions to certain generalized levee / borrow canal configurations were developed to support modeling applications that need to consider seepage under a generic or typical levee and borrow canal system constructed in common subsurface conditions. This could include seepage under future levees or existing levees that have not yet been studied in detail with the analytic element method or other modeling technique. The development of these solutions is provided in Appendix D.

In addition to the above analyses, the aforementioned modeling techniques were used to conduct a more rigorous evaluation of ground water flow under the C-111, L-31N and L-30 levee corridors. More specifically, ground water flow rates under a wider variety of boundary conditions were determined and, for certain boundary configurations, hydraulic head and streamline contours were constructed to illustrate prominent ground water flow pathways. Additionally, potential limitations in the linear relationship between seepage rates and head differentials were investigated. A separate report on these investigations is included in Appendix E.

DRAFT



Proposed Cross Section Model Locations

Figure 3. Approximate Locations of the Cross Section Models

The C-111 Levee / Borrow Canal System located between S-176 and S-177

Figure 4 shows the C-111 canal located between S-176 and S-177. The 1966 USACE As-Built drawings, DOQQ aerial images, the interpretation of data collected from USGS control well G-3319, and the hydrogeologic conceptualization along the C-111 canal (Fish and Stewart, 1991) provided the information for the development of the conceptual model (Figure 5). The Detail Design Memorandum (USACE, 1965) and the Gee & Jenson Frog Pond reports (Genereux et al., 1995) provided additional subsurface information. Frog Pond, the L-31W levee, and the Everglades National Park lie west of the study area. The control structures located along this levee reach include S-176 and S-177.

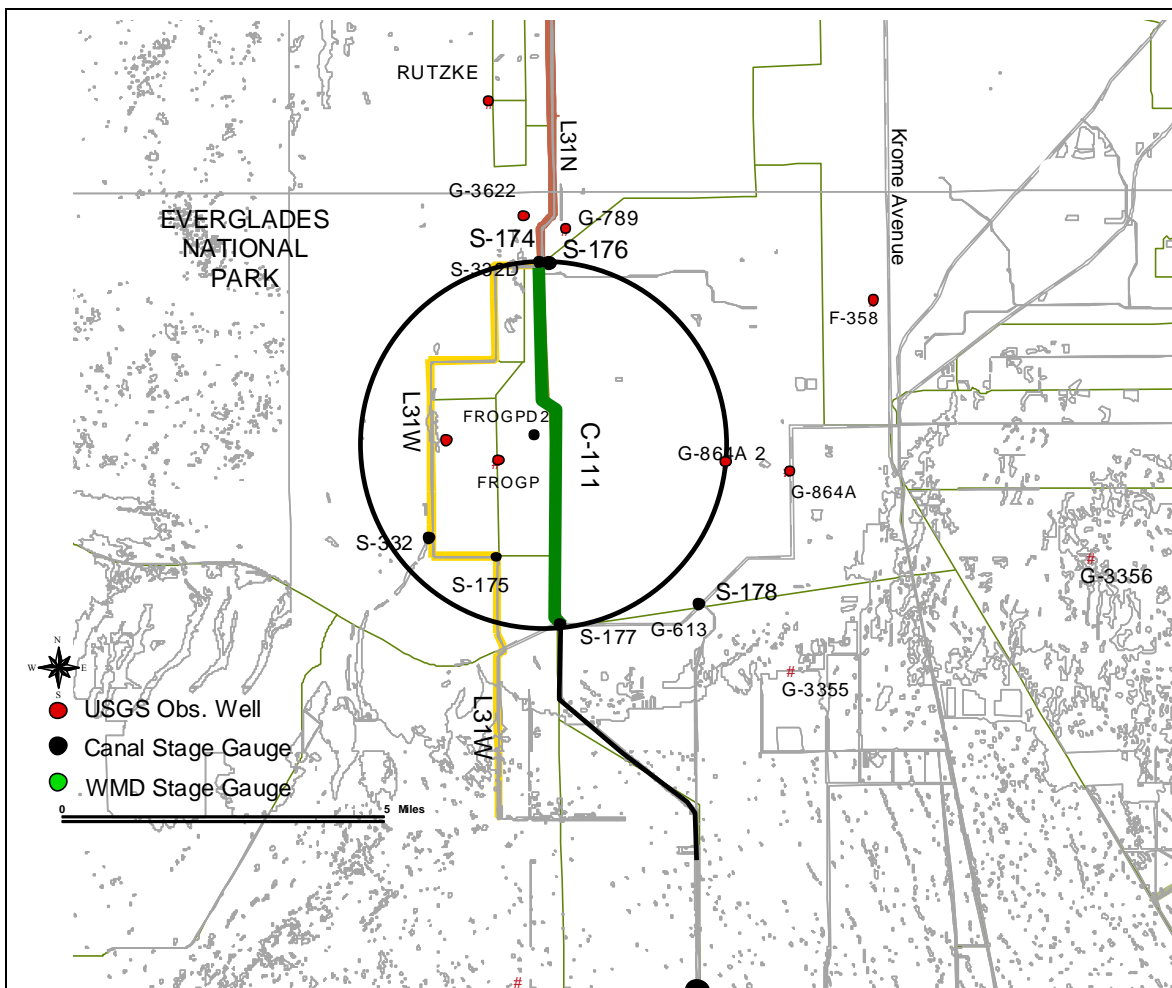


Figure 4. Location of C-111 canal/levee between S-176 and S-177

Conceptual Model

Existing ground elevations in this area lie approximately between +5.5 ft and +6 ft above mean sea level (MSL). The 10-ft wide levee crest lies at approximately +29 ft MSL. The levee side slopes extend 2:1 (H:V) from the crest and a minimum 40-ft berm (lying at approximately +11 ft

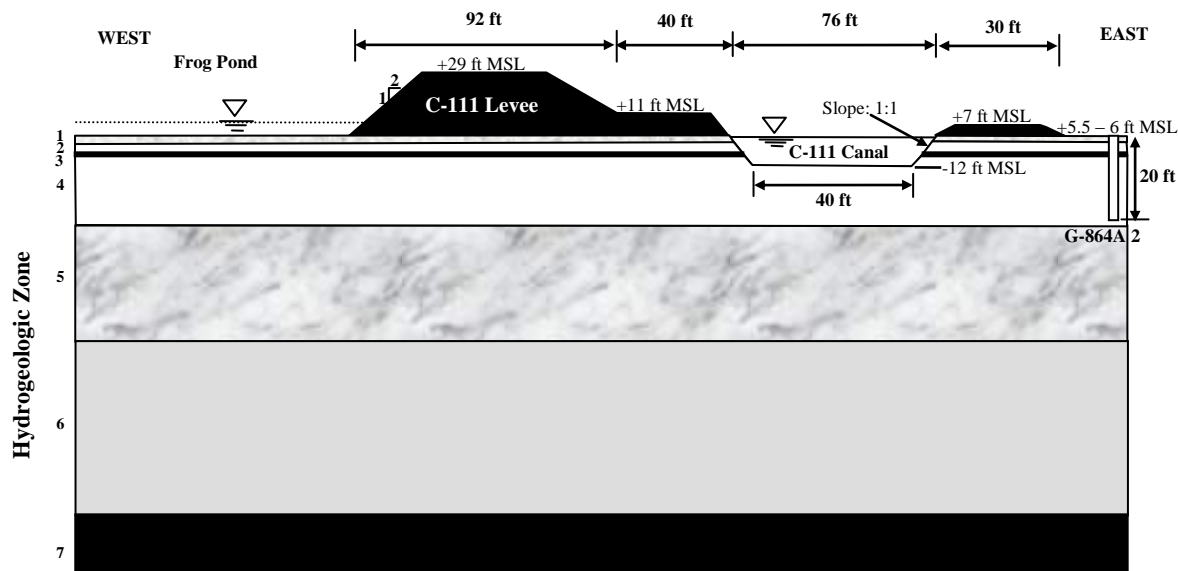


Figure 5. Conceptualization of the levee, canal, and shallow hydrostratigraphy of C-111 between S-176 and S-177 (NTS)

MSL) extends between the side slope and the C-111 canal. A 30-ft berm, located on the opposite side of the canal, lies at approximately +7 ft MSL. Side slopes of 1:1 side slopes, a bottom width of 40 ft, and a bottom elevation of approximately -12 ft MSL characterize the C-111 canal.

Table 5 summarizes the pertinent hydrogeologic parameters, corresponding to the seven zones identified in Figure 5.

Historical extreme and average water elevations on the C-111 canal are available at Structure S-176 on the northern end of the canal reach. The appropriate water level record at this location is S176_TW. On the east side of the canal there are no nearby surface or groundwater stage gauges available. The nearest groundwater observation well, USGS well G-864A_2, is located about 2.6 miles east of the C-111 canal. On the west side of C-111, a groundwater observation well, FORGPD2_G, is located in the Frog Pond area about 1,400 ft west of the C-111 levee. Table 6 summarizes the historical extreme and average water levels in the canal and at opposite sides of the levee.

Analytic Element Model

The model domain was truncated 1600 ft north and south of the C-111 levee. The “zero” point in the profile axis was set on the south edge of the borrow canal. Inhomogeneity domains were extended over the range $-2000 < x < +2000$, for accurate solutions at the ends of the model domain. The use of the truncated domain made it necessary to set GHB conditions at the ends of the model, with resistance computed according to the profile modeling documentation. All strings of inhomogeneity doublets were subdivided as necessary beneath major surface boundary conditions (e.g. at edges of ponded regions) and at the GHB elements that bounded the left and right ends of the model domain.

Table 5. Hydrogeologic parameters along C-111 between S-176 and S-177

Zone ID		Feature/Description	Range of Hydraulic Conductivity, K (ft/day)	Thickness (ft)
1		Surface Sediments	0.1 – 50	0.5
Miami Limestone	2	First transmissive zone	$\geq 1,000$	15
Fort Thompson	3	Second aquitard	0.1 – 10	1
	4	Second transmissive zone	$\geq 1,000$	29
Tamiami	5	Third aquitard	10 – 100	45
	6	Fourth aquitard	0.1 – 10	85
	7	Third transmissive zone	100 – 1,000	20

Table 6. Summary of historical water levels

	Water Level Gauge (DBHYDRO)	Observed Water Elevation (ft NGVD)		
		Maximum	Average	Minimum
Frog Pond Area (westside)	FROGPD2_G	5.9	3.6	1.8
C-111 Canal	S176_TW	6.5	3.4	1.3
G-864A (east side)	G-864A 2	8.4	2.4	-1.1

Sensitivity Analysis

Parameter sensitivity analysis was performed in a manner consistent with Appendix B. PEST was applied to the model in a predictive analysis mode to identify the parameter values that maximize and minimize the rate of seepage across the levee, and to identify the maximum and minimum seepage rates. PEST determined vertical distributions of hydraulic conductivity (K) derived from the parameter ranges in the conceptual model. The sensitivity analysis was based on model runs in which the joint probability of the K distribution was within the 62% confidence interval (slightly less than one standard deviation away from the mean). The modeled seepage rates and the parameter values that yielded them are shown in Table 7 (below).

Table 7. Seepage Rates Across C-111

	Minimum	Best-fit	Maximum
Seepage rate across levee C-111 between S176-177 [ft ³ /day/ft]	79.4	745	6880
K in layer 1 [ft/d]	0.1	2.24	50.0
K in layer 2 [ft/d]	1660	10000	100000
K in layer 3 [ft/d]	0.88	1.0	2.22
K in layer 4 [ft/d]	1050	10000	50100
K in layer 5 [ft/d]	30.97	31.62	31.65
K in layer 6 [ft/d]	0.95	1.0	1.0
K in layer 7 [ft/d]	314	316	316

Levee seepage coefficients

Levee seepage coefficients for C-111 were computed using the following procedure for each set of hydraulic parameters:

- Develop three sets of water levels for all boundary conditions;
- Run the analytic element model and compute seepage rates for the marsh-to-canal, marsh-to-dry-cell, and dry-cell-to-canal fluxes;
- Use a linear regression procedure, relating each flux term to the head difference (e.g. marsh-to-canal flux versus marsh-to-canal head difference).

The predicted levee seepage coefficients are provided in Table 8.

Table 8. Seepage Coefficients for C-111 Between S-176 and S-177

	K_{ms} (ft/day)	K_{dm} (ft/day)	K_{ds} (ft/day)
MINIMUM	81.96	1.776	83.59
BEST-FIT	769.1	5.025	761.6
MAXIMUM	7098.	14.10	6463.

Using the best-fit ground water parameter values, a more detailed analysis of the seepage coefficient values was carried out as reported in Appendix E. This analysis yielded values similar to those shown in table 8, except that $K_{ds} = 995.8$ ft/day. This latter value should be considered more accurate and the associated minimum/maximum values should be adjusted accordingly.

The C-111 Canal located between S-177 and S-18C

Figure 6 shows the C-111 levee reach located between S-177 and S-18C. The 1966 USACE As-Built drawings, DOQQ aerial images, interpretation of data collected by the USGS at lithologic control well G-3323, and the hydrogeologic conceptualization along the C-111 canal (Fish and Stewart, 1991) provided the information for the development of the conceptual model (Figure 7). The USACE Detail Design Memorandum (USACE, 1963 and 1965) and the Gee & Jenson Frog Pond report (Genereux, 1995) provided additional subsurface information.

The Everglades National Park and Levee 31W lie west of the study area. Control structures S-177 and S-18C bound the levee reach.

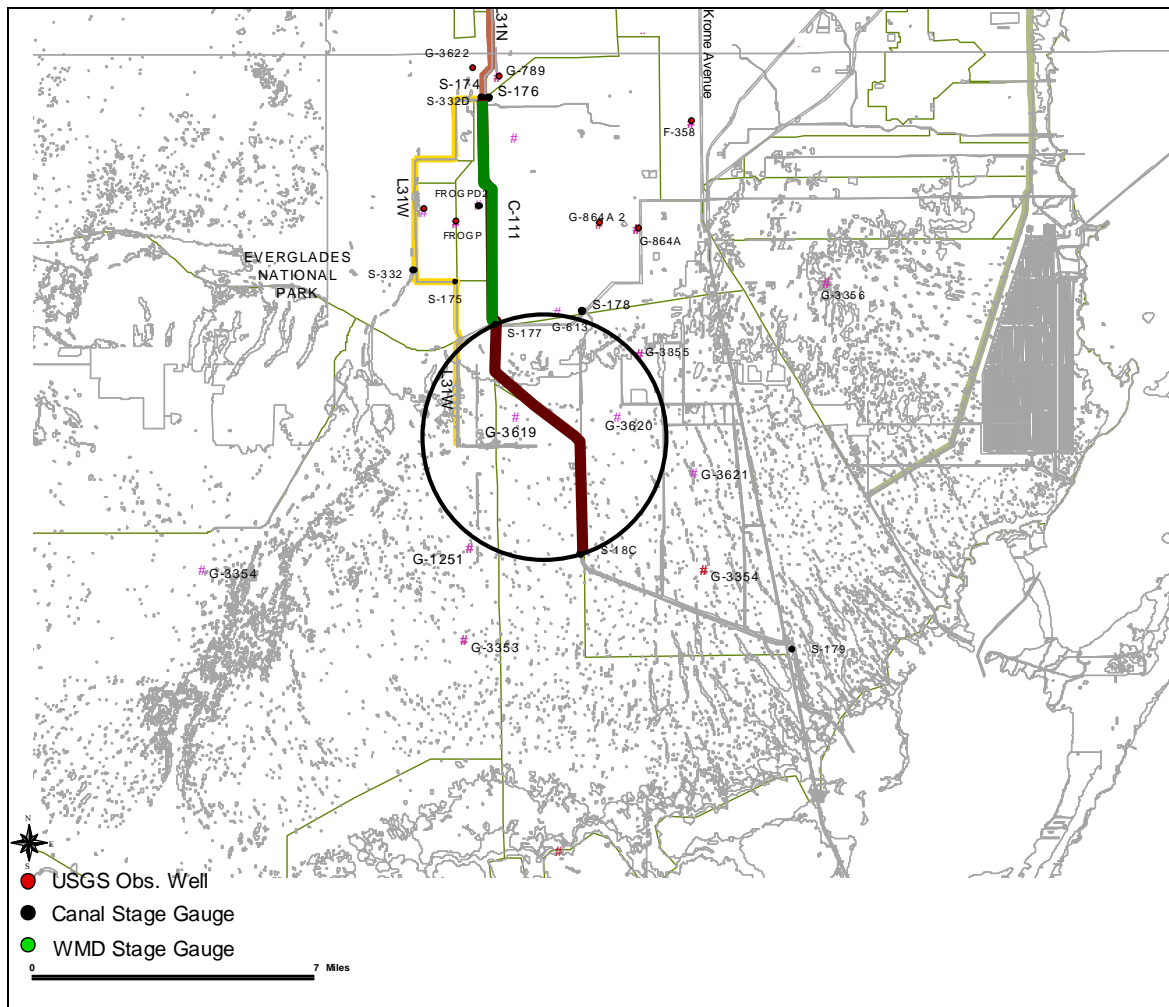


Figure 6. Location of C-111 canal/levee between S-177 and S-18C

Conceptual Model

Existing ground elevations in this area lie approximately between +4.5 ft and 5 ft above mean sea level (MSL). The east and west 10-ft wide levee crests lie at approximately +29 ft MSL. The

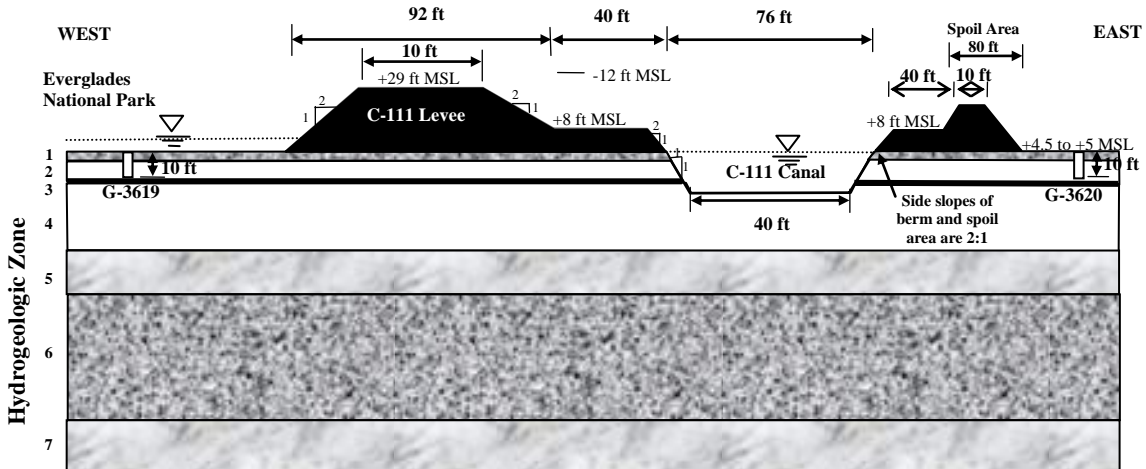


Figure 7. Conceptualization of the levee, canal, and shallow hydrostratigraphy of the C-111 between S-177 and S-18C (NTS)

levee side slopes extend 2:1 (H:V) from the crest and a minimum 40-ft berm (lying at approximately +8 ft MSL) extends between the levee and the C-111 canal. Side slopes of 1:1, a bottom width of 40 ft, and a bottom elevation of approximately -12 ft MSL characterize the C-111 canal. Table 9 summarizes the pertinent hydrogeologic parameters corresponding to the seven zones identified in Figure 7.

Table 9. Hydrogeologic parameters along C-111 between S-177 and S-18C

Zone ID		Feature/Description	Range of Hydraulic Conductivity, K (ft/day)	Thickness (ft)
1		Peat, Muck, Marl	0.1 – 50	2
Miami Oolite	2	First transmissive zone	$\geq 1,000$	10
Fort Thompson	3	Second aquitard	0.1 – 10	1
	4	Second transmissive zone	$\geq 1,000$	30
Tamiami Formation	5	Third transmissive zone	100 – 1,000	20
	6	Third aquitard	0.1 – 10	75
	7	Fourth transmissive zone	100 – 1,000	15

Table 10 summarizes historical extreme and average stages on the C-111 canal reach between structures S-177 and S-18C. This table reflects average stages between S-177_TW and S-18C_HW. Table 10 includes historical water levels obtained at USGS observation well G-3620 at a distance of approximately 6,000 ft east of the C-111 canal reach. Observed stages to the west of the levee come from the USGS well G-3619 located at a distance of about 2,500 ft.

Table 10. Summary of historical water levels

	Water Level Gauge (DBHYDRO)	Observed Water Elevation (ft NGVD)		
		Maximum	Average	Minimum
Everglades National Park (west)	G-3619	4.2	2.5	0.4
C-111 canal	S-177_TW and S- 18C_HW	4.2	2.2	0.2
East of C-111 canal	G-3620	4.3	2.4	0.4

Analytic Element Model

The model domain was truncated 1600 ft north and south of the C-111 levee. The “zero” point in the profile axis was set on the south edge of the C-111 borrow canal. Inhomogeneity domains were extended over the range $-2000 < x < +2000$, for accurate solutions at the ends of the model domain. The use of the truncated domain made it necessary to set GHB conditions at the ends of the model, with resistance computed according to the profile modeling documentation. All strings of inhomogeneity doublets were subdivided as necessary beneath major surface boundary conditions (e.g. at edges of ponded regions) and at the GHB elements that bounded the left and right ends of the model domain.

Sensitivity Analysis

Parameter sensitivity analysis was performed in a manner consistent with Appendix B. PEST was applied to the model in a predictive analysis mode to identify the parameter values that maximize and minimize the rate of seepage across the levee, and to identify the maximum and minimum seepage rates. PEST determined vertical distributions of hydraulic conductivity (K) derived from the parameter ranges in the conceptual model. The sensitivity analysis was based on model runs in which the joint probability of the K distribution was within the 62% confidence interval (slightly less than one standard deviation away from the mean). The modeled seepage rates and the parameter values that yielded them are shown in Table 11 (below).

Levee seepage coefficients for C-111

Levee seepage coefficients for C-111 were computed using the following procedure for each set of hydraulic parameters:

Table 11. Seepage rates, C-111

	Minimum	Best-fit	Maximum
Seepage rate across levee C-111 between S176-18C [ft ³ /day/ft]	-80.1	-807	-7140
K in layer 1 [ft/d]	0.1	2.24	50.0
K in layer 2 [ft/d]	1770	10000.0	100000.0
K in layer 3 [ft/d]	0.54	1.0	2.1
K in layer 4 [ft/d]	1000	10000	51500
K in layer 5 [ft/d]	309	316	317
K in layer 6 [ft/d]	0.99	1.0	1.0
K in layer 7 [ft/d]	314	316	316

hydraulic parameters:

- Develop three sets of water levels for all boundary conditions;
- Run the analytic element model and compute seepage rates for the marsh-to-canal, marsh-to-dry-cell, and dry-cell-to-canal fluxes;
- Use a linear regression procedure, relating each flux term to the head difference (e.g. marsh-to-canal flux versus marsh-to-canal head difference).

The predicted levee seepage coefficients are provided in Table 12.

Table 12. Seepage Coefficients for C-111 Between S-177 and S-18C

	K_{ms} (ft/day)	K_{dm} (ft/day)	K_{ds} (ft/day)
MINIMUM	46.39	0.7967	47.25
BEST-FIT	471.0	2.698	479.8
MAXIMUM	4212.	8.985	4332.

A more detailed evaluation of the seepage coefficients for this levee reach was later carried out as explained in the project report contained in appendix E. Some small, but insignificant, discrepancies may exist between the values contained in the above table and those reported in Appendix E.

The EAA L-6 Levee / Borrow Canal System

Figure 8 indicates the location of the Everglades Agricultural Area (EAA) L-6 levee reach. The USACE 1955 record drawings, DOQQ aerial images, and interpretation of data collected by the USACE (2003 and 2004) and USGS (Judson et. al., 2000) provided the information for the development of the EAA L-6 conceptual model (Figure 9). Compartment B lies northwest of the project study area.

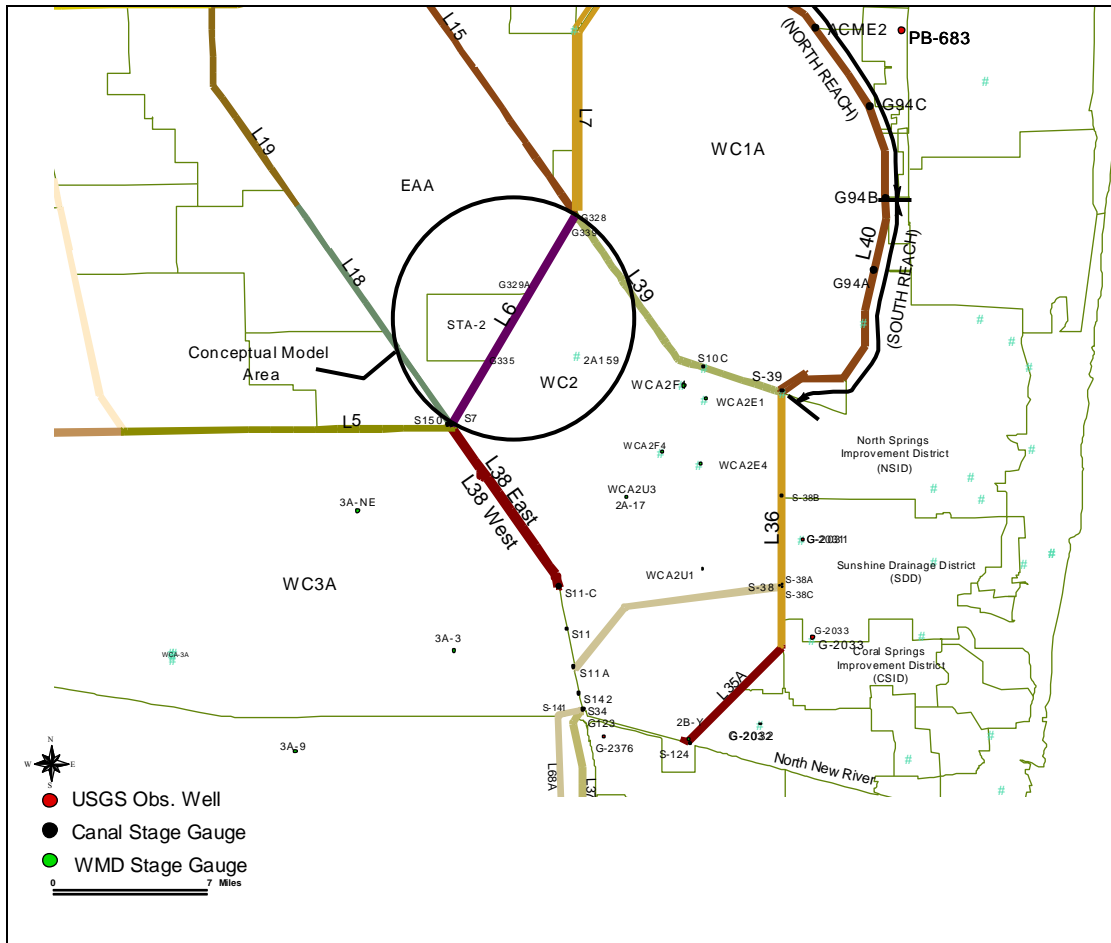


Figure 8. Location of EAA L-6 levee/canal conceptual model

Conceptual Model

As shown in Figure 9, the existing ground elevation in this area averages around +12 ft above mean sea level (MSL). Both the eastern and western EAA L-6 levees contain a 10-ft minimum crest width at approximately +21 ft and +18 ft MSL. The slope of the eastern levee extends 3:1 (H:V) from the crest and a ±70-ft berm extends to the L-6 canal. Similarly, the slope of the western levee extends 2:1 (H:V) from the crest and a ±35-ft berm extends to the canal.

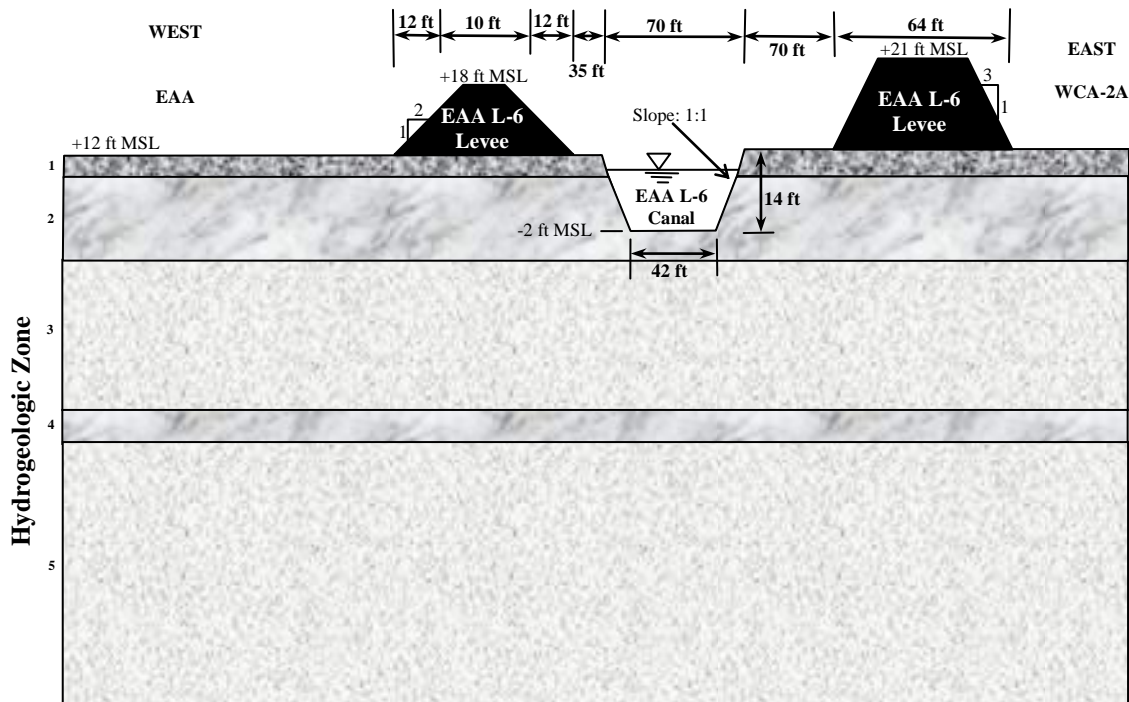


Figure 9. Conceptualization of the levee, canal, and shallow hydrostratigraphy of L-6 (not to scale)

Side slopes of 1:1, a bottom width of about 42 ft, and a bottom elevation of approximately -2 ft MSL characterize the EAA L-6 canal. Table 13 summarizes pertinent hydrogeologic parameters corresponding to the five zones identified in Figure 9.

Table 13. Hydrogeologic parameters along the EAA L-6 corridor

Zone ID	Feature/Description	Range of Hydraulic Conductivity, K(ft/day)	Thickness(ft)
1	Peat, muck, fill	0.1 – 50	5
2	Limestone	50 – 500	12
3	Sand/Sandstone	10 – 100	21
4	Limestone	50 – 500	5
5	Sand/Sandstone	10 – 100	150

For the L-6 levee segment, historical water levels (see Table 14) are available on the east side at gauge CA2A159, on the L-6 canal upstream of structure S-7, and on the west side at several IFAS farm stage gauges within the EAA. Agricultural irrigation practices and structure operations in the interior canals control the water table elevations in the EAA. Typically, the interior canals are maintained around elevation 11.0 ft by drawing water from the primary system canals when there is sufficient water in the primary canals. Water table elevations in the

interior farms of the EAA are maintained typically in the range between 5 and 9 ft depending on the surface elevation of the site. (USCOE and SFWMD, 2004).

Table 14. Summary of historical water levels

	Water Level Gauge (DBHYDRO)	Observed Water Elevation (ft NGVD)		
		Maximum	Average	Minimum
EAA (west)	IFAS farm wells Nos. 00W07FW, 06W02FW, and 09W02FW	9.0	7.5	5.0
L-6 Canal	S7_HW	12.6	10.8	7.8
WCA 2 (east)	CA2A159	15.8	13.9	11.3

Analytic Element Model

The model domain was truncated 1600 ft north and south of the L-6 levee. The “zero” point in the profile axis was set on the south edge of the L-6 borrow canal. Inhomogeneity domains were extended over the range $-2000 < x < +2000$, for accurate solutions at the ends of the model domain. The use of the truncated domain made it necessary to set GHB conditions at the ends of the model, with resistance computed according to the profile modeling documentation. All strings of inhomogeneity doublets were subdivided as necessary beneath major surface boundary conditions (e.g. at edges of ponded regions) and at the GHB elements that bounded the left and right ends of the model domain.

Sensitivity Analysis

Parameter sensitivity analysis was performed in a manner consistent with Appendix B. PEST was applied to the model in a predictive analysis mode to identify the parameter values that maximize and minimize the rate of seepage across the levee, and to identify the maximum and minimum seepage rates. PEST determined vertical distributions of hydraulic conductivity (K) derived from the parameter ranges in the conceptual model. The sensitivity analysis was based on model runs in which the joint probability of the K distribution was within the 62% confidence interval (slightly less than one standard deviation away from the mean). The modeled seepage rates and the parameter values that yielded them are shown in Table 15 (below).

Levee seepage coefficients

Levee seepage coefficients for L-6 were computed using the following procedure for each set of hydraulic parameters:

- Develop three sets of water levels for all boundary conditions;
- Run the analytic element model and compute seepage rates for the marsh-to-canal, marsh-to-dry-cell, and dry-cell-to-canal fluxes;

Table 15. Seepage rates across EAA L6

	Minimum	Best-fit	Maximum
Seepage rate across levee L-6 [ft ³ /day/ft]	16.9	76.0	261
K in layer 1 [ft/d]	0.1	2.24	50.0
K in layer 2 [ft/d]	68.0	158	500
K in layer 3 [ft/d]	18.1	31.6	52.4
K in layer 4 [ft/d]	116	158	193
K in layer 5 [ft/d]	11.3	31.6	65.6

- Use a linear regression procedure, relating each flux term to the head difference (e.g. marsh-to-canal flux versus marsh-to-canal head difference).

The predicted levee seepage coefficients are provided in Table 16.

Table 16. Seepage Coefficients for EAA L-6

	K_{ms} (ft/day)	K_{dm} (ft/day)	K_{ds} (ft/day)
MINIMUM	5.386	0.3120	6.083
BEST-FIT	20.61	2.922	26.57
MAXIMUM	61.72	9.611	91.32

The L-7 Levee / Borrow Canal System

Figure 10 indicates the location of the L-7 levee reach in Palm Beach County, Florida. As shown, Water Conservation Area 1 lies within the interior of the L-7, L-40, and L-39 levee reaches. The USACE (2003), SFWMD (Bennett et. al., 2002 and Rohrer, 1999), and the USGS (Swayze et. al., 1981 and Scott, 1977) provided the information for the development of the L-7 conceptual model (Figure 11). The General and Detail Design Memorandum (USACE, 1972) report provided additional subsurface information.

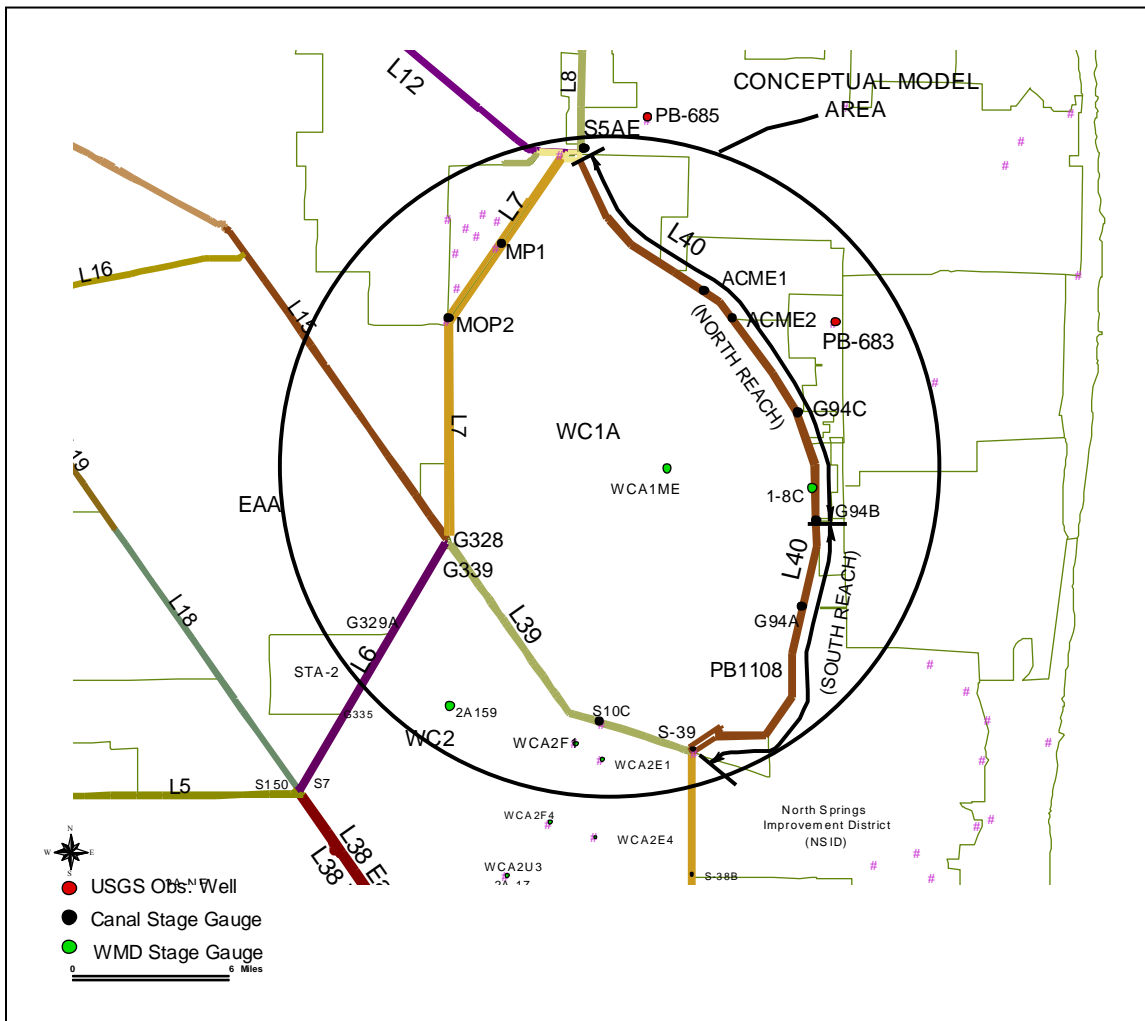


Figure 10. Location of L-7 conceptual model.

Conceptual Model

As shown in Figure 11, existing ground elevations surrounding the L-7 levee lie approximately at +15 ft above mean sea level (MSL) to the southeast (Water Conservation Area 1) and between

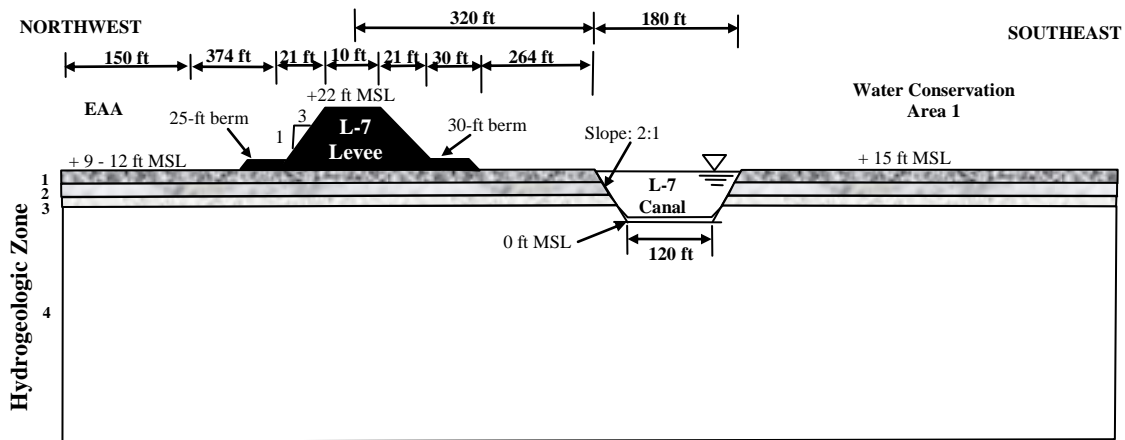


Figure 11. Conceptualization of the levee, canal, and shallow hydrostratigraphy of L-7 (not to scale)

+9 and +12 ft MSL to the northwest (Everglades Agricultural Area [EAA]). The 10-ft wide levee crest lies approximately at +22 ft MSL. Levee side slopes extend 3:1 (H:V) from the crest and a ±25-ft and ±30-ft berm extends from the northwest and southeast sides of the levee. Side slopes of 2:1, a bottom width of approximately 120 ft, and a bottom elevation of approximately 0 ft MSL characterize the L-7 canal. Table 17 summarizes pertinent hydrogeologic parameters corresponding to the four zones identified in Figure 11.

Table 17. Hydrogeologic parameters along the L-7 reach

Zone ID	Feature/Description	Range of Hydraulic Conductivity, K (ft/day)	Thickness (ft)
1	Peat	0.1 – 50	4
2	Hard to medium limestone (cap rock)	0.1– 10	6
3	Quartz sand	10 – 150	2
4	Limestone with inter-bedded sand and shell	≥ 100	60

Table 18 summarizes historical extreme and average water elevations for the area surrounding L-7.

Analytic Element Model

The model domain was truncated 1600 ft southeast and northwest of the L-7 levee. The “zero” point in the profile axis was set on the northwest edge of the L-7 borrow canal. Inhomogeneity domains were extended over the range $-2000 < x < +2000$, for accurate solutions at the ends of the model domain. The use of the truncated domain made it necessary to set GHB conditions at the ends of the model, with resistance computed according to the profile modeling

Table 18. Summary of historical water levels

		Observed Water Elevation (ft NGVD)			
		Water Level Gauge (DBHYDRO)	Maximum	Average	Minimum
L-7 Levee					
WCA-1 (east)	WCA1ME	18.0	16.4	14.5	
L-7 Canal	S5AS_TW	19.0	15.4	9.9	
ENR (west)	G251_HW	13.6	11.1	8.8	
L-40 Levee - Northern Reach					
ACME-Wellington (east)	ACME-2_HW	15.6	12.9	9.4	
L-40 Canal	G94C_HW	17.5	16.2	13.5	
WCA-1 (west)	WCA1ME	18.0	16.4	14.5	
L-40 Levee - Southern Reach					
West Delray Beach/Boca Raton(east)			13.0 ¹		
L-40 Canal	G94C_HW	17.5	16.2	13.5	
WCA-1 (west)	WCA1ME	18.0	16.4	14.5	

¹ Water levels maintained by Lake Worth Drainage District

documentation. All strings of inhomogeneity doublets were subdivided as necessary beneath major surface boundary conditions (e.g. at edges of ponded regions) and at the GHB elements that bounded the left and right ends of the model domain.

Sensitivity Analysis

Parameter sensitivity analysis was performed in a manner consistent with Appendix B. PEST was applied to the model in a predictive analysis mode to identify the parameter values that maximize and minimize the rate of seepage across the levee, and to identify the maximum and minimum seepage rates. PEST determined vertical distributions of hydraulic conductivity (K) derived from the parameter ranges in the conceptual model. The sensitivity analysis was based on model runs in which the joint probability of the K distribution was within the 62% confidence interval (slightly less than one standard deviation away from the mean). The modeled seepage rates and the parameter values that yielded them are shown in Table 19.

Levee seepage coefficients

Levee seepage coefficients for L-7 were computed using the following procedure for each set of hydraulic parameters:

Table 19. Seepage Rates for L-7

	Minimum	Best-fit	Maximum
Seepage rate across levee L-7 [ft ³ /day/ft]	-23.2	-84.3	-299
K in layer 1 [ft/d]	0.23	2.24	21.6
K in layer 2 [ft/d]	0.1	1.0	10.0
K in layer 3 [ft/d]	26.3	38.73	56.6
K in layer 4 [ft/d]	100	316.23	1000

- Develop three sets of water levels for all boundary conditions;
- Run the analytic element model and compute seepage rates for the marsh-to-dry-cell fluxes;
- Use a linear regression procedure, relating each flux term to the head.

The predicted levee seepage coefficients are provided in Table 20.

Table 20. Seepage Coefficients for L-7

	K_{ms} (ft/day)	K_{dm} (ft/day)	K_{ds} (ft/day)
MINIMUM	--	2.676	--
BEST-FIT	--	9.709	--
MAXIMUM	--	34.39	--

The L-8 Levee / Borrow Canal System

Figure 12 indicates the location of the L-8 levee reach. The USACE 1953 drawings, DOQQ aerial images, and interpretation of data collected by the SFWMD (2004) and the USGS (Reese and Memberg, 2000, Miller, 1987, and Scott, 1977) provided the information for the development of the L-8 conceptual model (Figure 13). Water Conservation Area 1 and Lake Okeechobee lie south and west of the study area.

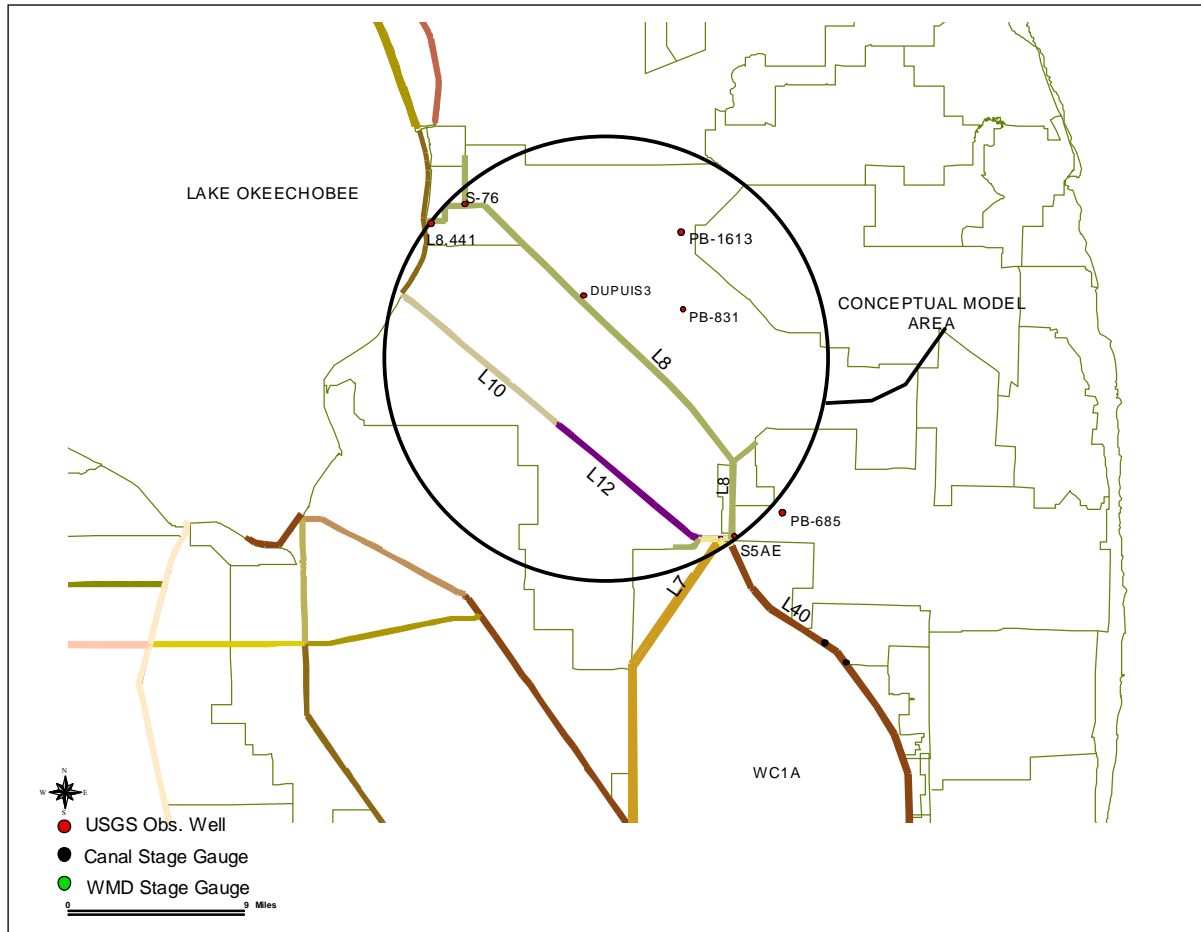


Figure 12. Location of L-8 levee/canal conceptual model

Conceptual Model

Existing ground elevations in this area average around +15 ft above mean sea level (MSL). The L-8 levee contains a 10-ft minimum crest width at approximately +27 ft MSL. Levee side slopes extend 5:1 (H:V) from the crest and a ±40-ft berm extends on both sides of the canal to the levee slope. Excess borrow material extends as much as 85 ft from the centerline of the dike. Side slopes of 1.5:1, a bottom width of about 50 ft, and a bottom elevation of approximately +9 ft MSL characterize the L-8 canal (SFWMD, 2004).

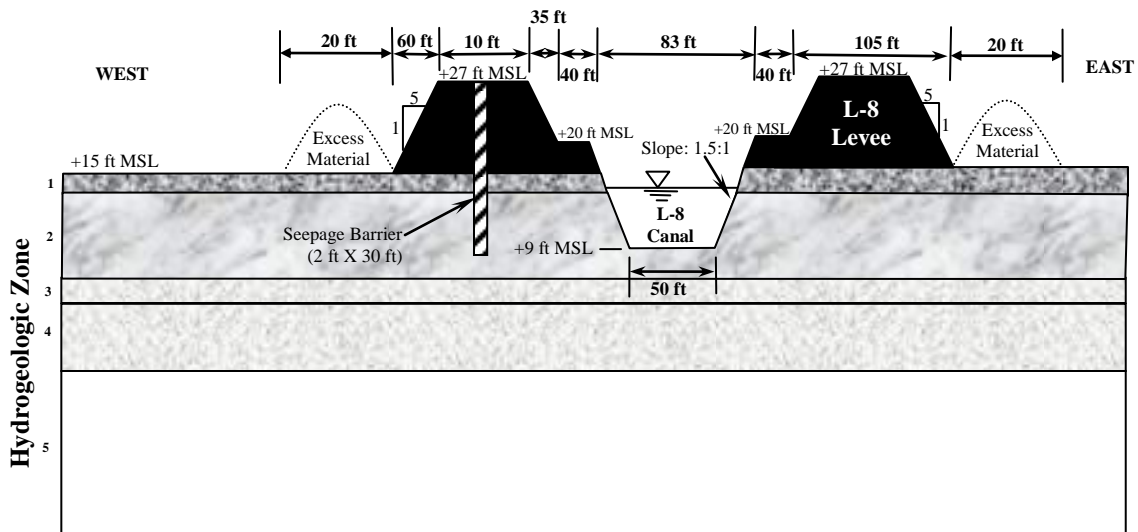


Figure 13. Conceptualization of the levee, canal, and shallow hydrostratigraphy of L-8 (NTS)

Table 21 summarizes pertinent hydrogeologic parameters corresponding to the five zones identified in Figure 10.

Table 21. Hydrogeologic parameters along the L-8 corridor

Zone ID	Feature/Description	Range of Hydraulic Conductivity, K (ft/day)	Thickness (ft)
1	Loose sand	60 – 130	11
2	Dense sand, clays, sit, organic	10 – 60	13
3	Limestone	1 – 10	5
4	Medium dense sand	10 – 60	40
5	Loose sand with shell	60 – 130	100

Historical water levels are available on the east side of the levee at the Dupuis Preserve (DUPUIS3) and in the L-8 canal at control structure S-76 (L8.441_TW) and S-5AS_HW. Stage gauges are not present on the western side of the levee reach. Table 22 summarizes historical extreme and average stages for the area surrounding the L-8 Canal.

Analytic Element Model

The model domain was truncated 1600 ft east and west of the L-8 borrow canal. The “zero” point in the profile axis was set on the west edge of the L-8 borrow canal. Inhomogeneity domains were extended over the range $-2000 < x < +2000$, for accurate solutions at the ends of the model domain. The use of the truncated domain made it necessary to set GHB conditions at the ends of

Table 22. Summary of historical water levels

	Water Level Gauge (DBHYDRO)	Observed Water Elevation (ft NGVD)		
		Maximum	Average	Minimum
East	DUPUIS3	20.9	16.5	11.8
L8 Canal	L8.441_TW/S- 5AS_HW	19.2	13.3	8.5
West	NA	--	--	--

the model, with resistance computed according to the profile modeling documentation. All strings of inhomogeneity doublets were subdivided as necessary beneath major surface boundary conditions (e.g. at edges of ponded regions) and at the GHB elements that bounded the left and right ends of the model domain.

Based on the conceptual model report, we assume that there is not ponded water on either side of levee L-8. During sensitivity runs, it may be necessary to account for ponding on the east side of L-8 (Dupuit Reserve). We will be requesting guidance from SFWMD regarding this issue during the sensitivity analysis modeling.

Sensitivity Analysis

Parameter sensitivity analysis was performed in a manner consistent with Appendix B. PEST was applied to the model in a predictive analysis mode to identify the parameter values that maximize and minimize the rate of seepage across the levee, and to identify the maximum and minimum seepage rates. PEST determined vertical distributions of hydraulic conductivity (K) derived from the parameter ranges in the conceptual model. The sensitivity analysis was based on model runs in which the joint probability of the K distribution was within the 62% confidence interval (slightly less than one standard deviation away from the mean). The modeled seepage rates and the parameter values that yielded them are shown in Table 23 below.

Levee Seepage Coefficients

Levee seepage coefficients for L-8 were computed using the following procedure for each set of hydraulic parameters:

- Develop three sets of water levels for all boundary conditions;
- Run the analytic element model and compute seepage rates for the marsh-to-canal, marsh-to-dry-cell, and dry-cell-to-canal fluxes;
- Use a linear regression procedure, relating each flux term to the head difference (e.g. marsh-to-canal flux versus marsh-to-canal head difference)

Table 23. Seepage Rates for L-8

	Minimum	Best-fit	Maximum
Seepage rate across levee L-8 [ft ³ /day/ft]	-31.5	-47.6	-73.4
K in layer 1 [ft/d]	66.7	88.32	105
K in layer 2 [ft/d]	17.2	24.49	37
K in layer 3 [ft/d]	2.27	3.16	5.4
K in layer 4 [ft/d]	10.7	24.49	60
K in layer 5 [ft/d]	60.0	88.32	130.0

The predicted levee seepage coefficients are provided in Table 24.

Table 24. Seepage Coefficients for L-8

	K_{ms} (ft/day)	K_{dm}(ft/day)	K_{ds} (ft/day)
MINIMUM	15.07	1.357	2.550
BEST-FIT	22.78	2.020	3.900
MAXIMUM	34.82	3.095	6.066

The L-29, Section 1 Levee / Borrow Canal System

Figure 14 indicates the location of the L-29, Section 1 levee reach. The USACE 1962 (stamped 1963) As-Built drawings, DOQQ aerial images, and interpretation of data collected by the USGS at lithologic control well G-3301 (Fish and Stewart, 1991) provided the information for the development of the conceptual model for the western reach of the L-29, Section 1 levee/borrow canal (Figure 15).

Water Conservation Area 3A lies north of the study area. The Everglades National Park lies south and west of the levee reach and across from U.S. 41 and the Tamiami Canal. The SFWMD control structures within this reach of the L-29 Canal include S-14, S-343, and S-343B.

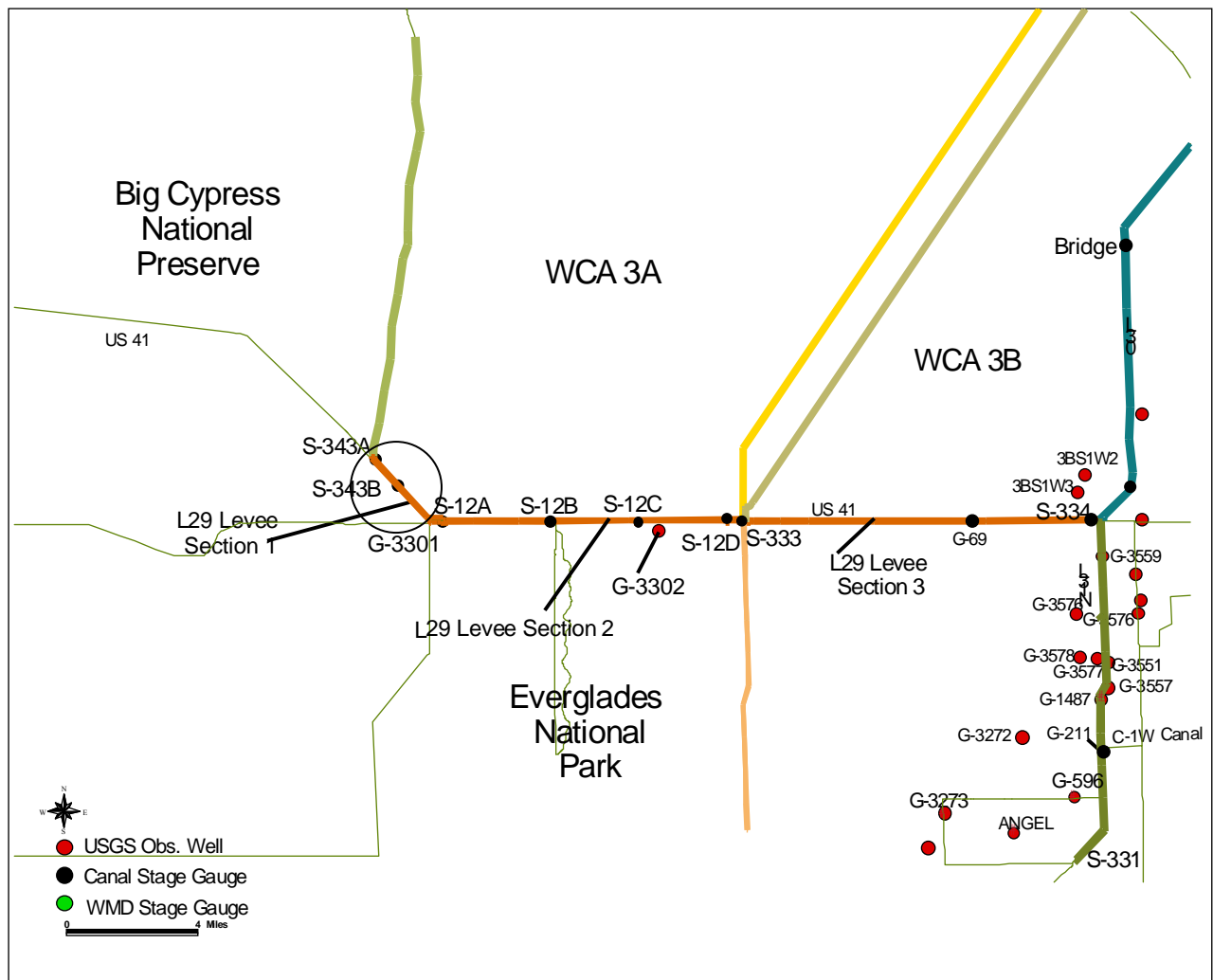


Figure 14. Location of L-29, Section 1 levee/canal conceptual model

Conceptual Model

Existing ground elevations in this area lie approximately between +7 ft and +8 ft NGVD. The 10-ft wide levee crest lies approximately at +17.5 ft MSL. Levee side slopes extend 2:1 (H:V)

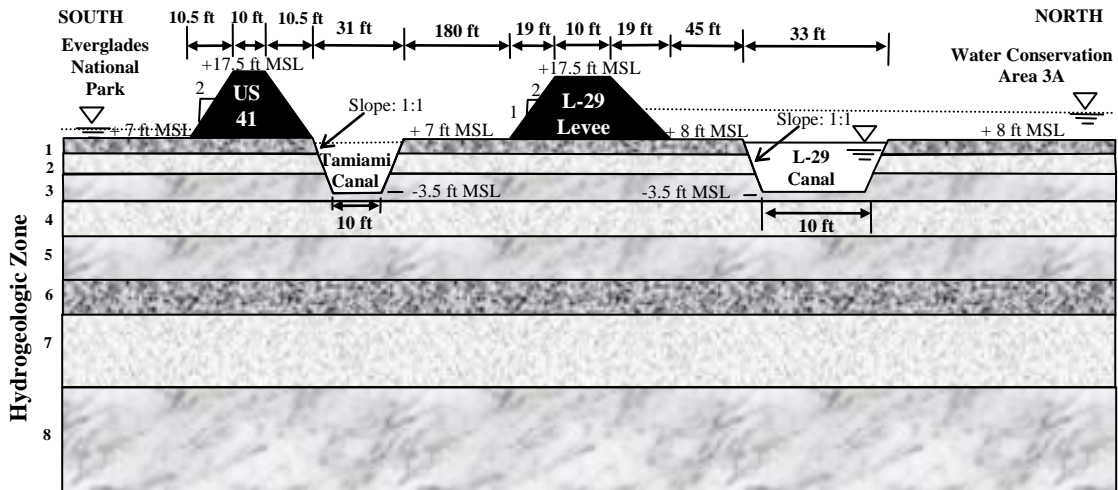


Figure 15. Conceptualization of the levee, canal, and shallow hydrostratigraphy of the L-29, Section 1 reach (NTS)

from the crest and a ±45-ft berm extends between the levee slope and the L-29 canal. Side slopes of 1:1, a bottom width of 10 ft, and a bottom elevation of approximately -3.5 ft MSL characterize this portion of the L-29 canal.

Table 25 summarizes pertinent hydrogeologic parameters corresponding to the eight zones identified in Figure 15.

Table 25. Hydrogeologic parameters along L-29, section 1

Zone ID	Feature/Description	Range of Hydraulic Conductivity, K (ft/day)	Thickness (ft)	
1	Muck, Marl, Dense Limestone	0.10 – 50	5	
Fort Thompson	2	First transmissive zone	100 – 1,000	5
Tamiami	3	Second aquitard	10 – 100	8
	4	Second transmissive zone	100 – 1,000	5
	5	Third aquitard	0.1 – 10	16
	6	Third transmissive zone	100 – 1,000	8
	7	Fourth aquitard	0.1 – 10	24
	8	Fourth transmissive zone	100 – 1,000	68

Long-term historical stages are available upstream and downstream of structure S-12A. The headwater side of the S-12A structure reflects stages in the Water Conservation Area 3 whereas S12A_TW (tail water) represent stage conditions in Everglades National Park. Stages in the Tamiami Canal are represented at the downstream side of structures S-343A and S-343B in Section 1 of the L29 canal. Typically, these two structures are closed and only open when water levels are above the regulation schedule in the WCA3A. The operations of these structures have a minor effect on the average stage in the Tamiami Canal as shown in Table 26.

Table 26. Summary of historical water levels

	Water Level Gauge (DBHYDRO)	Observed Water Elevation (ft NGVD)		
		Maximum	Average	Minimum
WCA3A (north)	S-12A_HW	11.7	9.2	5.2
Tamiami Canal	S-343A_TW	10.1	8.7	6.5
Everglades National Park (south)	S-12A_TW	11.7	8.6	5.2

Analytic Element Model

The model domain was truncated 1600 ft north and south of the L-29 levee. The “zero” point in the profile axis was set on the south edge of the L-29 borrow canal. Inhomogeneity domains were extended over the range $-2000 < x < +2000$, for accurate solutions at the ends of the model domain. The use of the truncated domain made it necessary to set GHB conditions at the ends of the model, with resistance computed according to the profile modeling documentation. All strings of inhomogeneity doublets were subdivided as necessary beneath major surface boundary conditions (e.g. at edges of ponded regions) and at the GHB elements that bounded the left and right ends of the model domain.

Sensitivity Analysis

Parameter sensitivity analysis was performed in a manner consistent with Appendix B. PEST was applied to the model in a predictive analysis mode to identify the parameter values that maximize and minimize the rate of seepage across the levee, and to identify the maximum and minimum seepage rates. PEST determined vertical distributions of hydraulic conductivity (K) derived from the parameter ranges in the conceptual model. The sensitivity analysis was based on model runs in which the joint probability of the K distribution was within the 62% confidence interval (slightly less than one standard deviation away from the mean). The modeled seepage rates and the parameter values that yielded them are shown in Table 27 below.

Levee seepage coefficients

Levee seepage coefficients for L-29, Section 1 were computed using the following procedure for each set of hydraulic parameters:

Table 27. Seepage rates for L-29, Section 1

	Minimum	Best-fit	Maximum
Seepage rate across levee L-29, Section 1 [ft ² /day/ft]	6.78	-28.7	-107
K in layer 1 [ft/d]	0.1	2.24	50.0
K in layer 2 [ft/d]	147	316	1000
K in layer 3 [ft/d]	26.2	31.6	44.7
K in layer 4 [ft/d]	168	316	681
K in layer 5 [ft/d]	0.20	1.0	1.9
K in layer 6 [ft/d]	257	316	335
K in layer 7 [ft/d]	0.68	1.0	1.15
K in layer 8 [ft/d]	172	316	376

- Develop three sets of water levels for all boundary conditions;
- Run the analytic element model and compute seepage rates for the marsh-to-canal, marsh-to-dry-cell, and dry-cell-to-canal fluxes;
- Use a linear regression procedure, relating each flux term to the head difference (e.g. marsh-to-canal flux versus marsh-to-canal head difference).

The predicted levee seepage coefficients are provided in Table 28.

Table 28. Seepage Coefficients for L-29, Section 1

	K_{ms} (ft/day)	K_{dm} (ft/day)	K_{ds} (ft/day)
MINIMUM	8.810	3.105	6.351
BEST-FIT	21.24	9.663	28.50
MAXIMUM	78.23	18.20	113.7

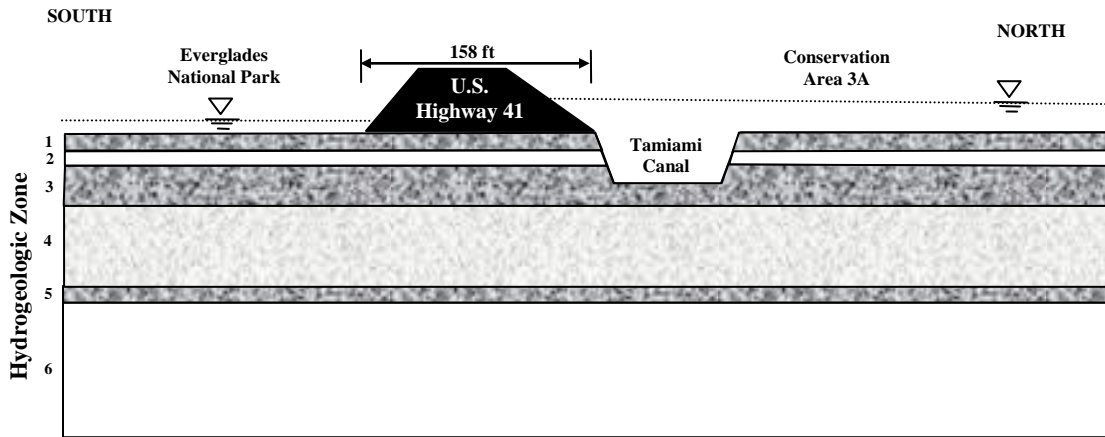


Figure 17. Conceptualization of the levee, canal, and shallow hydrostratigraphy of the L-29, Section 2 corridor (N.T.S.)

Table 29. Hydrogeologic parameters along the eastern reaches of L-29, section 2

Zone ID	Feature/Description	Range of Hydraulic Conductivity, K (ft/day)	Thickness (ft)
1	Wetland bottom	0.1 – 10	8
2	First transmissive zone	100 – 1,000	7
3	First aquitard	0.1 – 10	18
4	Second transmissive zone	10 – 100	30
5	Second aquitard	0.1 – 10	10
6	Third transmissive zone	100 – 1,000	65

canal is comprised of 1:1 side slopes, a bottom width of 20 ft and a bottom elevation of approximately -10 ft NGVD).

Historical extreme and average water elevations on the L-29 Canal and on the north and south sides of the levee are summarized in Table 30.

Analytic Element Model

The model domain was truncated 1600 ft north and south of the L-29 levee. The “zero” point in the profile axis was set on the south edge of the L-29 borrow canal. Inhomogeneity domains were extended over the range $-2000 < x < +2000$, for accurate solutions at the ends of the model domain. The use of the truncated domain made it necessary to set GHB conditions at the ends of

Table 30. Summary of Historical Water Levels

	Water Level Gauge (DBHYDRO)	Observed Water Elevation (ft NGVD)		
		Maximum	Average	Minimum
WCA3A	S12D_HW	11.9	9.4	5.2
Everglades National Park	S12D_TW	11.6	8.5	4.7

the model, with resistance computed according to the profile modeling documentation. All strings of inhomogeneity doublets were subdivided as necessary beneath major surface boundary conditions (e.g. at edges of ponded regions) and at the GHB elements that bounded the left and right ends of the model domain.

Sensitivity Analysis

Parameter sensitivity analysis was performed in a manner consistent with Appendix B. PEST was applied to the model in a predictive analysis mode to identify the parameter values that maximize and minimize the rate of seepage across the levee, and to identify the maximum and minimum seepage rates. PEST determined vertical distributions of hydraulic conductivity (K) derived from the parameter ranges in the conceptual model. The sensitivity analysis was based on model runs in which the joint probability of the K distribution was within the 62% confidence interval (slightly less than one standard deviation away from the mean). The modeled seepage rates and the parameter values that yielded them are shown in Table 31 below.

Levee seepage coefficients

Levee seepage coefficients for L-29, Section 2 were computed using the following procedure for each set of hydraulic parameters:

- Develop three sets of water levels for all boundary conditions;
- Run the analytic element model and compute seepage rates for the marsh-to-dry-cell fluxes;
- Use a linear regression procedure, relating each flux term to the head.

The predicted levee seepage coefficients are provided in Table 32.

Table 31. Seepage Rates for L29, Section 2

	Minimum	Best-fit	Maximum
Seepage rate across levee L-29, Section 2 [ft ³ /day/ft]	-4.85	-16.3	-49.9
K in layer 1 [ft/d]	0.1	1.0	4.99
K in layer 2 [ft/d]	157	316	771
K in layer 3 [ft/d]	0.19	1.0	4.51
K in layer 4 [ft/d]	28.8	31.6	35.6
K in layer 5 [ft/d]	0.88	1.0	2.94
K in layer 6 [ft/d]	120	316	899

Table 32. Seepage Coefficients for L-29, Section 2

	K_{ms} (ft/day)	K_{dm} (ft/day)	K_{ds} (ft/day)
MINIMUM	--	5.391	--
BEST-FIT	--	18.14	--
MAXIMUM	--	55.42	--

The L-29 Levee, Section 3

Figure 18 indicates that the levee reach is located between structures S-333 and S-334. The cross-sectional model includes two levees and a collector canal. The L29 levee parallels highway US 41 and constitutes the southern boundary of water conservation area WCA 3B. The Tamiami Canal (i.e. L-29 borrow canal) is located between the L-29 levee and US 41. In this reach of the Tamiami (L-29) Canal, water enters from the conservation area WCA 3B through three structures: G-69, S-335A and S-335B. Water levels in the Tamiami Canal are controlled through operation of structures S-333 on the west side of the canal reach and S-334 to the east. The Everglades National Park lies south of the levee and receives water from the Tamiami Canal through 19 circular concrete culverts.

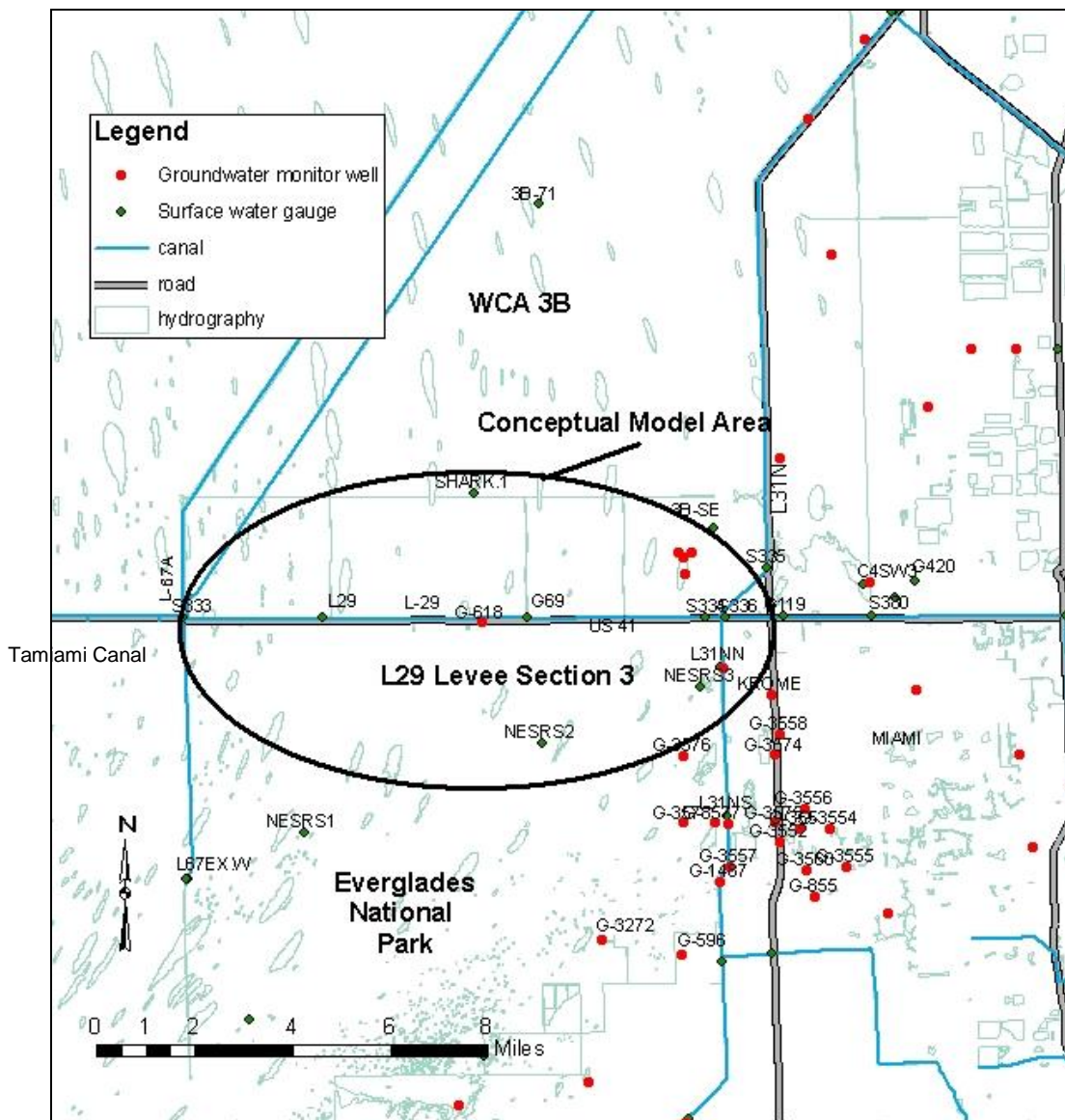


Figure 18. Location of L-29 Levee/Canal Conceptual Model between Structures S333 and S334

Conceptual Model

The USACOE 1960 As-Built drawings, DOQQ aerial images, the interpretation of data collected by the USGS at lithologic control well G-3303, and the hydrogeologic cross-section along the levee reach (Fish and Stewart, 1991) provided the typical section and representative hydrogeologic properties for the conceptual model (Figure 19).

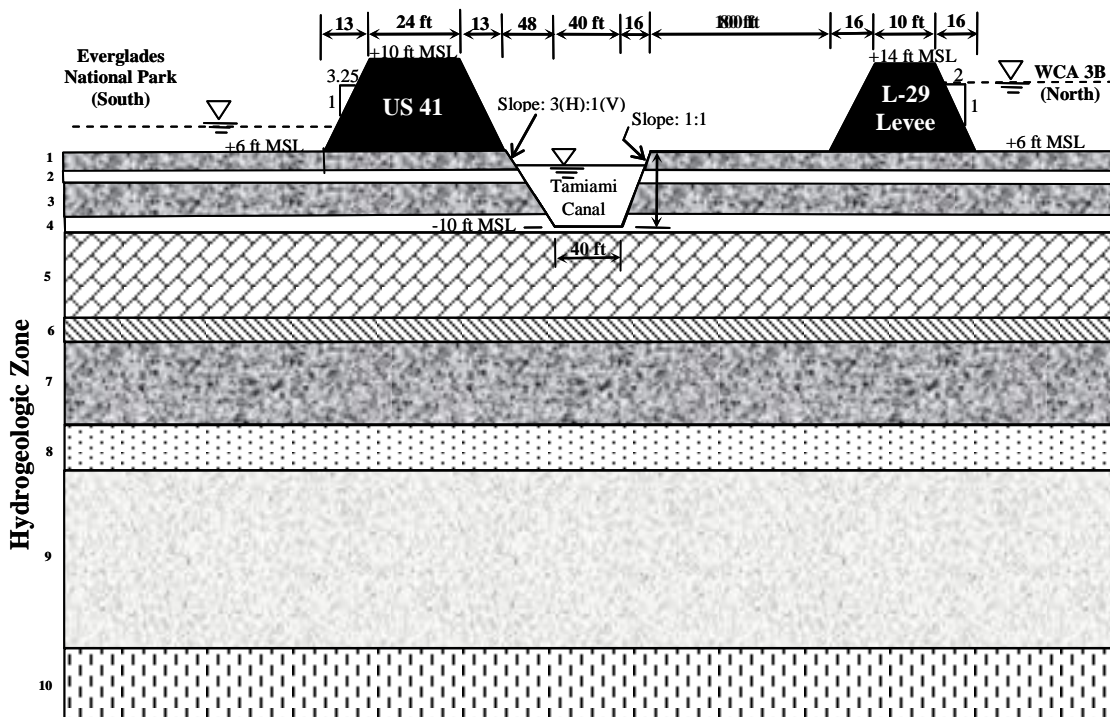


Figure 19. Conceptualization of the levee, canal, and hydrostratigraphy of the L-29 Canal/Levee Section 3 reach located between S-333 and S-334 (N.T.S.)

As shown in the conceptual cross-section in Figure 14, existing ground elevations in this area are about 6 ft above mean sea level (M.S.L.) on both sides of the levee. The L-29 levee has a 10-ft wide crest at elevation +14 ft M.S.L. Levee side slopes extend 2:1 (H:V) from the crest to the levee toe at an approximate elevation of 6.0 ft (M.S.L.). A 100-ft wide berm extends from the toe of the levee to the bank of the Tamiami Canal. The canal cross section is characterized by a 40-ft wide bottom at elevation -10 ft (M.S.L.) along with canal side slopes of 1:1 (north) and 3:1 (south). US Highway 41 located between the Tamiami Canal and the Everglades National Park functions as a levee restricting the flow of water into the park. Water moves across the road via 19 open culverts as mentioned previously.

Regional water-table maps indicate that ground water flows from west to east beneath the Levee 29 (Fish and Stewart, 1991). Table 33 summarizes pertinent hydrogeologic parameters, corresponding to the ten zones identified in Figure 14.

Table 33. Hydrogeologic Parameters of the L-29, Section 3 Levee Conceptual Model

Zone ID		Feature/Description	Range of Hydraulic Conductivity, K (ft/day)	Thickness (ft)
Miami Limestone	1	Oolitic Limestone	$10 < K < 100$	10
	2	First Transmissive Zone – Fort Thompson Formation	$100 < K < 1,000$	4
3	$K > 1000$		17	
4	$100 < K < 1,000$		5	
Upper Tamiami Confining Zone	5	Marine Shells and Sand	$0.1 < K < 10$	17
	6	Marine Shells and Sand	$10 < K < 100$	30
	7	Sand	$0.1 < K < 10$	20
	8	Marine Shells and Sand	$K < 0.1$	10
Gray Limestone Aquifer	9	Second Transmissive Zone – Tamiami Formation	$100 < K < 1,000$	45
Lower Tamiami Confining Zone	10	Claystone or Siltstone – Hawthorne Formation	$10 < K < 100$	17

Historical water levels are available on the north side of the levee at water level gauge SHARK1 and in the L-31N canal at control structures S-333, S-334 and G-69. Water level recorders G-618 and NESRS2 are located in the ENP south of US 41. Historical extreme and average water elevations on the Tamiami Canal at control structure S-334, at gauge Shark1 in Water Conservation Area 3B, and at observation well NESRS2 in the Everglades National Park are summarized in Table 34.

Table 34. Summary of Historical Water Levels

	Water Level Gauge (DBHYDRO)	Observed Water Elevation (ft NGVD)		
		Maximum	Average	Minimum
Everglades National Park	NESRS2	8.5	6.7	3.4
L-29 Canal	S-334_HW	8.6	6.9	3.5
WCA-3B	SHARK1	9.7	7.4	4.0

Analytic Element Model

The model domain was truncated 1600 ft north and south of the L-29 levee. The “zero” point in the profile axis was set at the center of US-41. Inhomogeneity domains were extended over the range $-2000 < x < +2000$, for accurate solutions at the ends of the model domain. The use of the truncated domain made it necessary to set GHB conditions at the ends of the model, with resistance computed according to the profile modeling documentation. All strings of inhomogeneity doublets were subdivided as necessary beneath major surface boundary conditions (e.g. at edges of ponded regions) and at the GHB elements that bounded the left and right ends of the model domain.

Sensitivity Analysis

Parameter sensitivity analysis was performed in a manner consistent with Appendix B. PEST was applied to the model in a predictive analysis mode to identify the parameter values that maximize and minimize the rate of seepage across the levee, and to identify the maximum and minimum seepage rates. PEST determined vertical distributions of hydraulic conductivity (K)

Table 35. Results of sensitivity analysis for L-29, section 3

	<i>Minimum</i>	<i>Best-fit</i>	<i>Maximum</i>
Seepage rate across levee L-29 section 3 [ft ² /day/ft]	-7.42	-38.6	-206.9
K in layer 1 [ft/d]	0.1	1.0	10.0
K in layer 2 [ft/d]	29.45	31.62	65.45
K in layer 3 [ft/d]	276.1	316.2	327.7
K in layer 4 [ft/d]	2373	10000	41842
K in layer 5 [ft/d]	303.1	316.2	317.6
K in layer 6 [ft/d]	3.20	1.0	3.16
K in layer 7 [ft/d]	30.68	31.62	31.7
K in layer 8 [ft/d]	3.13	1.0	3.17
K in layer 9 [ft/d]	0.009	0.07	0.01
K in layer 10 [ft/d]	312.1	316.2	317.0
K in layer 11 [ft/d]	31.56	31.62	31.63

derived from the parameter ranges in the conceptual model. The sensitivity analysis was based on model runs in which the joint probability of the K distribution was within the 62% confidence interval (slightly less than one standard deviation away from the mean). The modeled seepage rates and the parameter values that yielded them are shown in Table 35 (below).

Levee seepage coefficients

Levee seepage coefficients for L-29, Section 3 were computed using the following procedure for each set of hydraulic parameters:

- Develop multiple sets of water levels for all boundary conditions;
- Run the analytic element model and compute seepage rates for the marsh-to-canal, marsh-to-dry-cell, and dry-cell-to-canal fluxes;
- Use a linear regression procedure, relating each flux term to the head difference (e.g. marsh-to-canal flux versus marsh-to-canal head difference).

The predicted levee seepage coefficients are provided in Table 36.

Table 36. Seepage Coefficients for L-29, Section 3

	K_{ms} (ft/day)	K_{dm} (ft/day)	K_{ds} (ft/day)
MINIMUM	32.5	1.26	18.83
BEST-FIT	184.4	1.96	80.05
MAXIMUM	347.9	2.02	1022.

The L-30 Levee / Borrow Canal System Located South of S-335

Figure 20 shows the L-30 reach located south of S-335. The USACE 1951 and 1976 drawings, DOQQ aerial images, and the interpretation of data collected by the USGS (Cunningham, 2004; Sonenshein, 2001; and Fish and Stewart, 1991) provided the information for the development of the southernmost reach of the L-30 levee/borrow canal conceptual model (Figure 21). Water Conservation Area 3B and Pennsuco wetlands lie west and east of the study area. The only SFWMD control structure within this reach of the L-30 canal is S-335 (spillway).

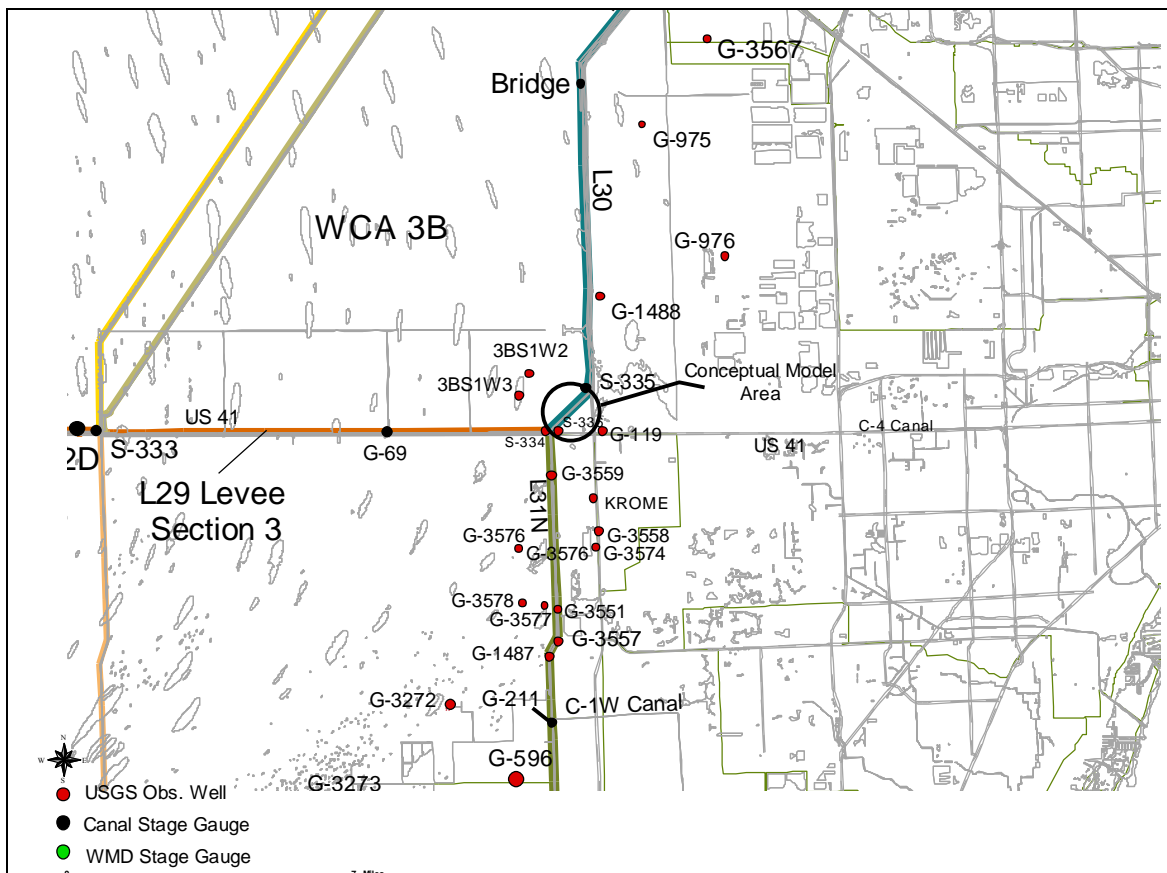


Figure 20. Location of L-30 levee/canal conceptual model located south of S-335

Conceptual Model

As shown in Figure 21, existing ground elevations in this area lie approximately at +8.0 ft MSL. The 10-ft wide levee crest lies approximately at +20.0 ft MSL. The levee side slopes extend 3:1 (H:V) from the west side of the crest and 2.5:1 from the east side of the crest. A 45-ft canal berm exists between the levee toe and the canal. Side slopes of 2:1, a bottom width of 100 ft, and a bottom elevation of approximately -6 ft MSL characterize the L-30 canal.

When the control structure gates are closed, vertical seepage data near L-30 indicate that water

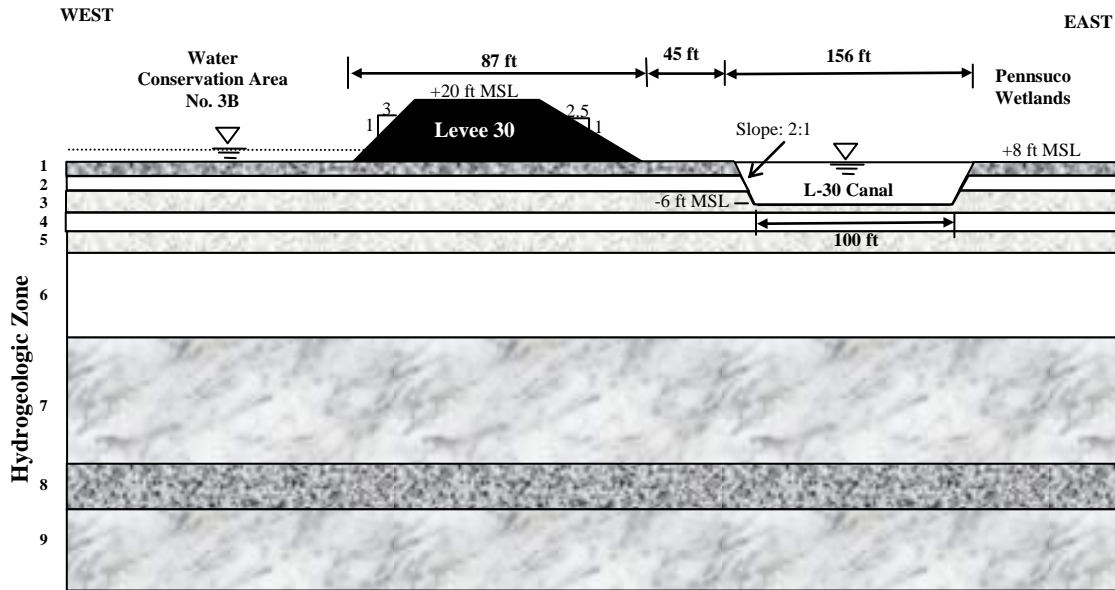


Figure 21. Conceptualization of the levee, canal, and shallow hydrostratigraphy of L-30 levee/canal located south of S-335 (NTS)

from the wetland area infiltrates at a rate between 0.033 and 0.266 ft/day (Sonenshein, 2001). Table 37 summarizes pertinent hydrogeologic parameters, corresponding to the nine zones identified in Figure 21, for the southern reaches of L-30.

Table 38 summarizes historical extreme and average water elevations in the L-30 Canal (Station S-334_TW), to the west in Water Conservation Area 3B (well 3BS1W1_H), and on the east side of the levee. Since no recorded groundwater data were available to the east of the levee, representative stages were estimated using recorded stages at structures S-336 and G-119 located on the L-30 and C-4 canals, respectively.

Analytic Element Model

The model domain was truncated 1600 ft northwest and southeast of the levee. The “zero” point in the profile axis was set on the south edge of the L-30 borrow canal. Inhomogeneity domains were extended over the range $-2000 < x < +2000$, for accurate solutions at the ends of the model domain. The use of the truncated domain made it necessary to set GHB conditions at the ends of the model, with resistance computed according to the profile modeling documentation. All strings of inhomogeneity doublets were subdivided as necessary beneath major surface boundary conditions (e.g. at edges of ponded regions) and at the GHB elements that bounded the left and right ends of the model domain.

Sensitivity Analysis

Parameter sensitivity analysis was performed in a manner consistent with Appendix B. PEST was used to identify the parameter values that maximize and minimize the rate of seepage across the levee, and to identify the maximum and minimum seepage rates. PEST determined vertical distributions of hydraulic conductivity (K) derived from the parameter ranges in the conceptual model. The sensitivity analysis was based on model runs in which the joint probability of the K

Table 37. Hydrogeologic parameters for L-30 south of S-335

Zone ID		Hydrogeologic Framework Characterization		Range of Hydraulic Conductivity, K (ft/day)	Thickness (ft)
		HFC Layer	GWFC Layer		
1		Peat, Muck, Marl	GWFC 1	0.1 – 50	2
Miami Limestone	2	HFC 5, HFC 4, Upper HFC 3b	GWFC 2	> 1,000	10
Fort Thompson Formation	3	Lower HFC 3b, Upper HFC 3a	GWFC 4	10 – 100	4
	4	HFC 3a	GWFC 2	> 1,000	2
	5	HFC 3a, HFC 2	GWFC 3, 4	10 – 100	5
	6	HFC 2	GWFC 2, NA	> 1,000	22
Tamiami Formation	7	NA	NA	100 – 1,000	50
	8	NA	NA	0.1 – 10	15
	9	Gray Limestone Aquifer	NA	100 – 1,000	25

Table 38. Summary of Historical Water Levels

	Water Level Gauge (DBHYDRO)	Observed Water Elevation (ft NGVD)		
		Maximum	Average	Minimum
WCA3B (West)	well 3BS1W_H1	8.5	6.7	4.2
L30 Canal	S-334_TW	7.7	5.9	4.9
East	S-336_TW/G-119_HW	7.6	5.7	3.7

distribution was within the 62% confidence interval (slightly less than one standard deviation away from the mean). The modeled seepage rates and the parameter values that yielded them are shown in Table 39 (below).

Levee seepage coefficients

Levee seepage coefficients for L-30, South of S-335 were computed using the following procedure for each set of hydraulic parameters:

Table 39. Seepage Rates across L-30 south of S-335

	Minimum	Best-fit	Maximum
Seepage rate across levee L-30 south of S-335 [ft ³ /day/ft]	74.7	642	5790
K in layer 1 [ft/d]	0.1	2.24	50.0
K in layer 2 [ft/d]	1497	10000	100000
K in layer 3 [ft/d]	31.3	31.6	33.3
K in layer 4 [ft/d]	5230	10000	10700
K in layer 5 [ft/d]	31.3	31.6	33.9
K in layer 6 [ft/d]	1260	10000	61300
K in layer 7 [ft/d]	247	316	319
K in layer 8 [ft/d]	0.981	1.0	1.0
K in layer 9 [ft/d]	276	316	317

- Develop three sets of water levels for all boundary conditions;
- Run the analytic element model and compute seepage rates for the marsh-to-canal, marsh-to-dry-cell, and dry-cell-to-canal fluxes;
- Use a linear regression procedure, relating each flux term to the head difference (e.g. marsh-to-canal flux versus marsh-to-canal head difference).

The predicted levee seepage coefficients are provided in Table 40.

Table 40. Levee Seepage Coefficients for L-30 south of S-335

	K_{ms} (ft/day)	K_{dm} (ft/day)	K_{ds} (ft/day)
MINIMUM	91.78	15.97	112.9
BEST-FIT	292.5	101.7	337.6
MAXIMUM	1186.	265.4	1234.

Using the best-fit ground water parameter values, a more detailed analysis of the seepage coefficient values was carried out as reported in Appendix E. This analysis yielded values of $K_{dm} = 53.8$ ft/day, $K_{ds} = 465.1$ ft/day and $K_{ms} = 363$ ft/day. These latter values should be considered more accurate and the associated minimum/maximum values should be adjusted accordingly.

The L-30 Levee / Borrow Canal System Located North of the Bridge

Figure 22 shows the L-30 levee reach located north of the bridge. The USACE 1951 and 1976 construction drawings, DOQQ aerial images, and interpretation of data collected by the USGS (Cunningham, 2004 and Fish and Stewart, 1991) and the USACE (USACE, 2004) provided the information for the development of the northern reach of the L-30 levee/borrow canal conceptual model (Figure 23). Water Conservation Area 3B and Pennsuco wetlands lie west and east of the study area. The SFWMD control structures within this reach of the L-30 Canal include S-32A and S-337.

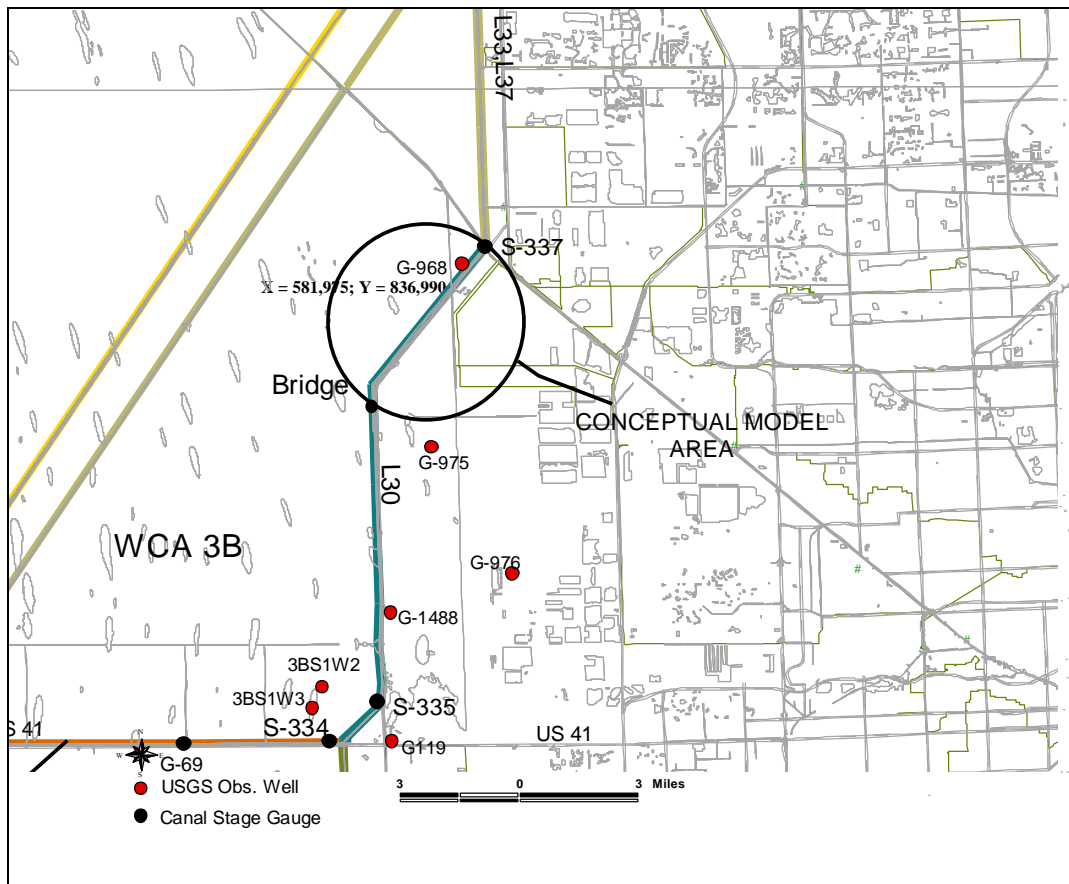


Figure 22. Location of L-30 levee/canal conceptual model located north of the bridge

Conceptual Model

As shown in Figure 23, existing ground elevations in this area lie approximately at +8 ft MSL. The 10-ft wide levee crest lies approximately at +20 ft MSL. The levee side slopes extend 3:1 (H:V) from the west side of the crest and 2.5:1 from the east side of the crest. A 45-ft canal berm exists between the levee toe and the canal. Side slopes of 2:1, a bottom width of 100 ft, and a bottom elevation of approximately -6 ft MSL characterize the L-30 canal. Table 41 summarizes pertinent hydrogeologic parameters corresponding to the fifteen zones identified in Figure 23. Historical extreme and average water elevations on the L30 Canal (S337_T) and on the east (G-

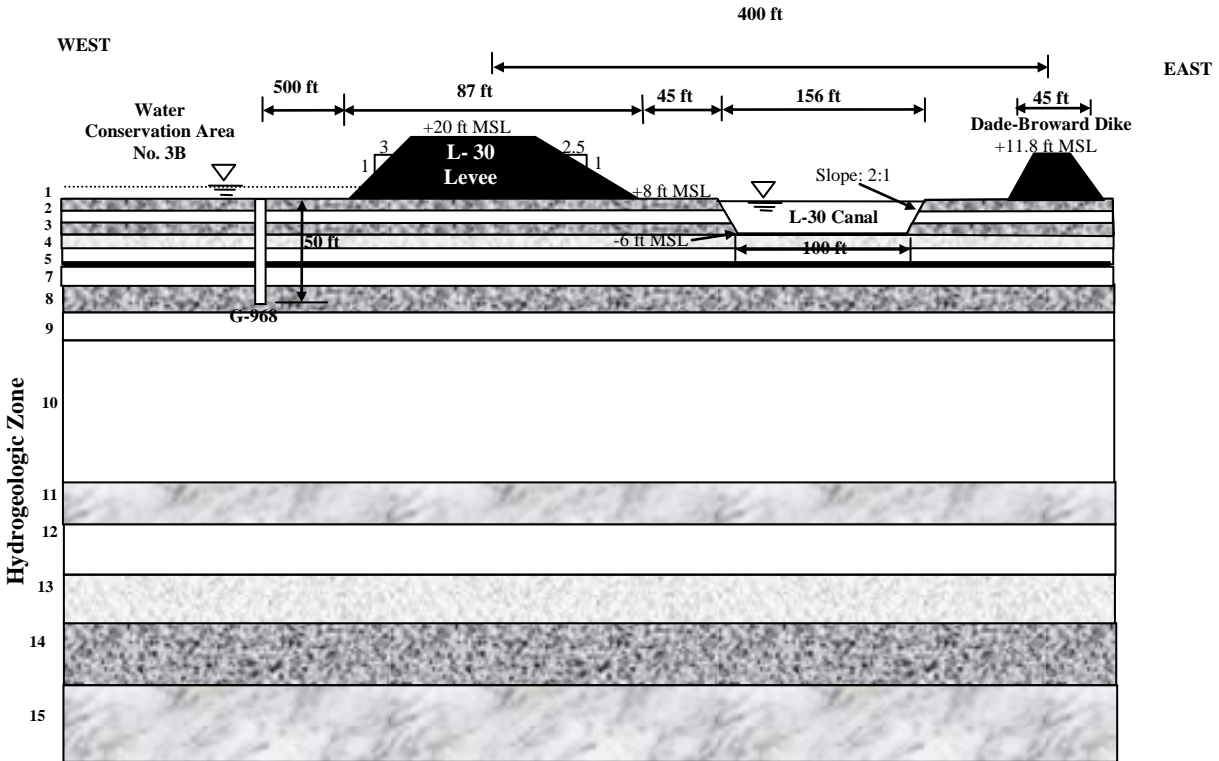


Figure 23. Conceptualization of the levee, canal, and shallow hydrostratigraphy of the L-30 reach located north of the bridge (NTS)

975) and west (G-968) sides of the levee are summarized in Table 42.

Analytic Element Model

The model domain was truncated 1600 ft northwest and southeast of the levee. The “zero” point in the profile axis was set on the south edge of the L-30 borrow canal. Inhomogeneity domains were extended over the range $-2000 < x < +2000$, for accurate solutions at the ends of the model domain. The use of the truncated domain made it necessary to set GHB conditions at the ends of the model, with resistance computed according to the profile modeling documentation. All strings of inhomogeneity doublets were subdivided as necessary beneath major surface boundary conditions (e.g. at edges of ponded regions) and at the GHB elements that bounded the left and right ends of the model domain.

Sensitivity Analysis

Parameter sensitivity analysis was performed in a manner consistent with Appendix B. PEST was used to identify the parameter values that maximize and minimize the rate of seepage across the levee, and to identify the maximum and minimum seepage rates. PEST determined vertical distributions of hydraulic conductivity (K) derived from the parameter ranges in the conceptual model. The sensitivity analysis was based on model runs in which the joint probability of the K distribution was within the 62% confidence interval (slightly less than one standard deviation away from the mean). The modeled seepage rates and the parameter values that yielded them are shown in Table 43 (below).

Table 41. Hydrogeologic parameters along L-30 north of the bridge

Zone ID	Hydrogeologic Framework Characterization		Range of Hydraulic Conductivity, K (ft/day)	Thickness (ft)
	HFC Layer	GWFC Layer		
1	Peat, marl, muck	GWFC 1	0.1 – 50	2
Miami Limestone	2	HFC 5, upper HFC 4	GWFC 2	≥ 1,000
	3	Lower HFC 4, Upper HFC 3b	GWFC 3	0.1 – 10
	4	Lower HFC 3b	GWFC 4	10 – 100
	5	Lower HFC 3b, Upper HFC 3a	GWFC 2	≥ 1,000
	6	HFC 3a	GWFC 4	10 – 100
	7	Lower HFC 3a	GWFC 2	≥ 1,000
	8	Lower HFC 3a, upper HFC 2	GWFC 3, 4	0.1 – 10
Fort Thompson	9	HFC 2	GWFC 2	≥ 1,000
	10	NA	NA	≥ 1,000
	11	NA	NA	100 – 1,000
	12	NA	NA	≥ 1,000
Tamiami	13	NA	NA	10 – 100
	14	NA	NA	0.1 – 10
	15	NA	NA	100 – 1,000

Table 42. Summary of historical water levels

	Water Level Gauge (DBHYDRO)	Observed Water Elevation (ft NGVD)		
		Maximum	Average	Minimum
WCA3A (west)	G-968	8.9	6.5	3.0
L30 Canal	S337_T	8.7	6.5	3.2
East	G-975	8.2	6.0	2.1

Table 43. Seepage Rates, L-30 North of the Bridge

	Minimum	Best-fit	Maximum
Seepage rate across levee L-30 north[ft ³ /day/ft]	150	752	4030
K in layer 1 [ft/d]	0.1	2.24	8.72
K in layer 2 [ft/d]	5910	10000	14700
K in layer 3 [ft/d]	0.811	1.0	4.24
K in layer 4 [ft/d]	31.5	31.6	33.2
K in layer 5 [ft/d]	6260	10000	9610
K in layer 6 [ft/d]	31.6	31.6	32.4
K in layer 7 [ft/d]	6270	10000	9540
K in layer 8 [ft/d]	0.890	1.0	8.65
K in layer 9 [ft/d]	4930	10000	10500
K in layer 10[ft/d]	1096	10000	100000
K in layer 11 [ft/d]	304	316	316
K in layer 12 [ft/d]	2330	10000	24600
K in layer 13 [ft/d]	31.4	31.6	31.6
K in layer 14 [ft/d]	0.974	1.0	1.0
K in layer 15 [ft/d]	290	316	309

Levee seepage coefficients

Levee seepage coefficients for L-30, North of Bridge were computed using the following procedure for each set of hydraulic parameters:

- Develop three sets of water levels for all boundary conditions;
- Run the analytic element model and compute seepage rates for the marsh-to-canal, marsh-to-dry-cell, and dry-cell-to-canal fluxes;
- Use a linear regression procedure, relating each flux term to the head difference (e.g. marsh-to-canal flux versus marsh-to-canal head difference).

The predicted levee seepage coefficients are provided in Table 44.

Table 44. Seepage Coefficients for L-30 North of the Bridge

	K_{ms} (ft/day)	K_{dm} (ft/day)	K_{ds} (ft/day)
MINIMUM	63.44	15.68	62.87
BEST-FIT	185.4	136.6	167.3
MAXIMUM	519.4	939.4	464.1

A more detailed evaluation of the seepage coefficients for this levee reach was later carried out as explained in the project report contained in appendix E. Some small, but insignificant, discrepancies may exist between the values contained in the above table and those reported in Appendix E.

The L-30 Levee / Borrow Canal System Located North of S-335 and South of the Bridge

Figure 24 shows the L-30 levee reach located north of S-335 and south of the bridge. The USACE 1951 and 1976 drawings, DOQQ aerial images, and interpretation of data collected by the USGS (Cunningham, 2004; Sonenshein, 2001; and Fish and Stewart, 1991) provided the information for the development of the central reach of the L-30 levee/borrow canal conceptual model (Figure 25). Water Conservation Area 3B and the Pennsuco wetlands lie west and east of the study area. The only SFWMD control structure within this reach of the L-30 canal is the S-335.

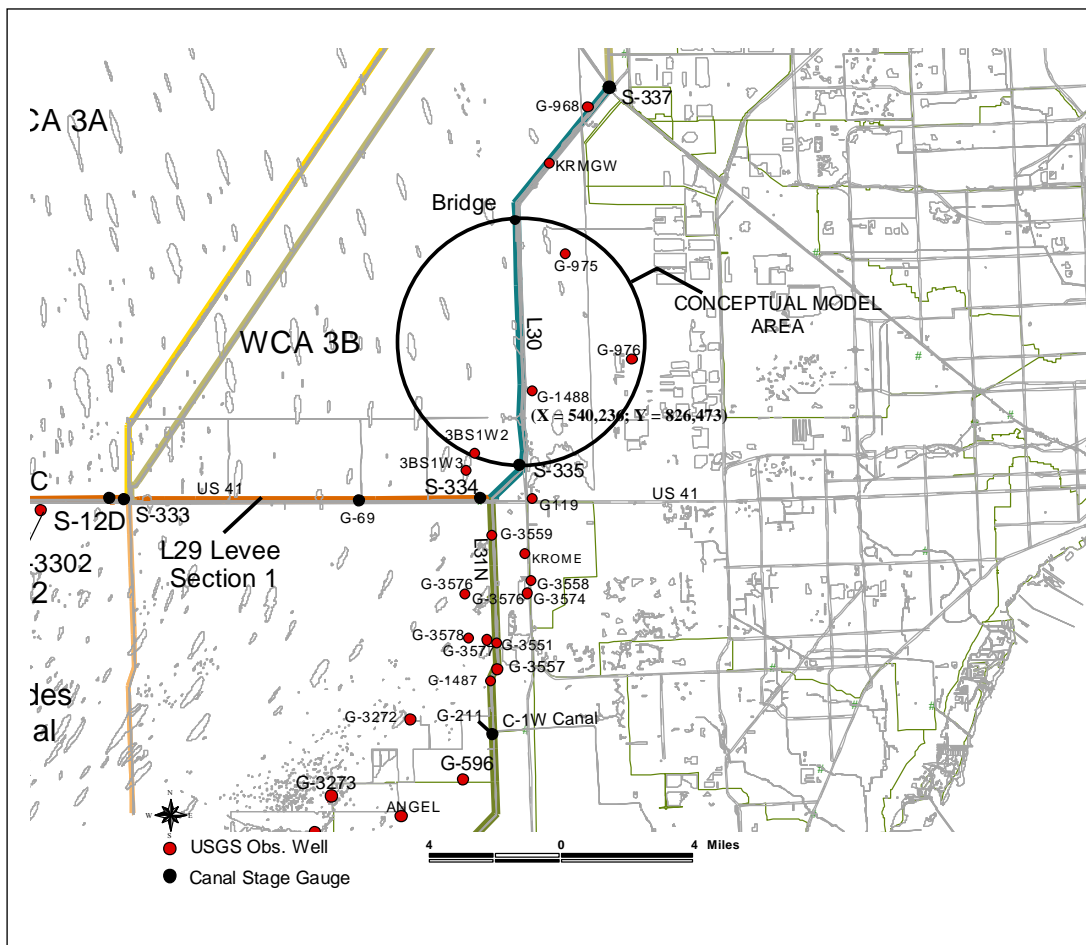


Figure 24. Location of L-30 levee/canal conceptual model located north of S-335 and south of the bridge

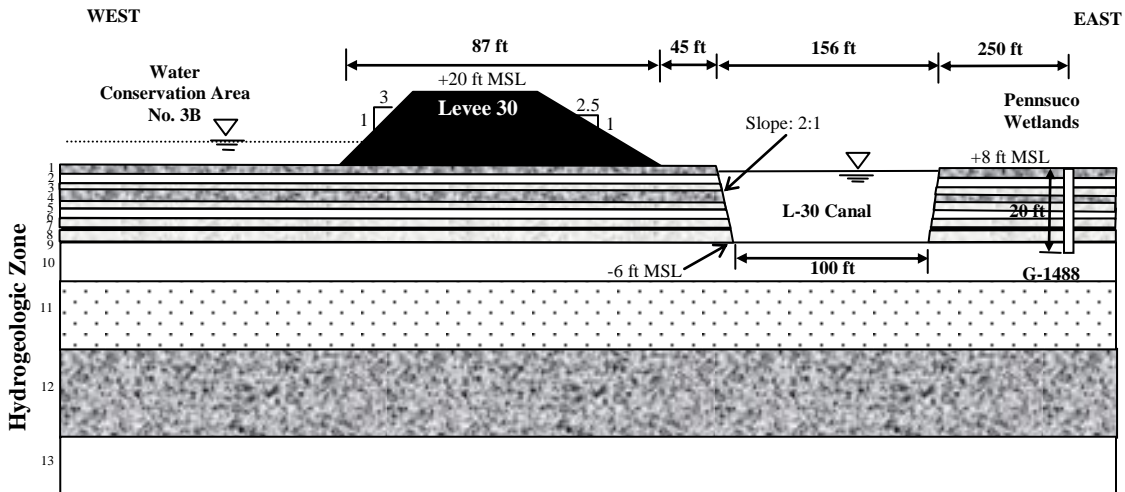


Figure 25. Conceptualization of the levee, canal, and shallow hydrostratigraphy of the L-30 Canal located north of S-335 and south of the bridge (NTS)

Table 45. Hydrogeologic parameters of L-30 north of S-335 and south of the bridge

Zone ID	Hydrogeologic Framework Characterization		Range of Hydraulic Conductivity, K (ft/day)	Thickness (ft)	
	HFC Layer	GWFC Layer			
1	Peat, Muck, Marl	GWFC 1	0.1 – 50	3	
Miami Limestone	2	HFC 5, Upper HFC 4	GWFC 2	> 1,000	2
Fort Thompson	3	Lower HFC 4, HFC 3b	GWFC 4	10 – 100	2
	4	Lower HFC 4, HFC 3b	GWFC 3	0.1 – 10	2
	5	HFC 3b	GWFC 4	10 – 100	2
	6	HFC 3a	GWFC 2	≥ 1,000	2
	7	HFC 3a	GWFC 4	10 – 100	3
	8	HFC 3a	GWFC 2	> 1,000	1
	9	HFC 3a	GWFC 3, 4	10 – 100	4
	10	HFC 2	GWFC 2	≥ 1,000	12
	11	NA	NA	≥ 10,000	30
Tamiami	12	NA	NA	0.1 – 10	35
	13	NA	NA	100 – 1,000	20

Conceptual Model

As shown in Figure 25, existing ground elevations in this area lie approximately at +8.0 ft MSL. The 10-ft wide levee crest lies approximately at +20.0 ft MSL. The levee side slopes extend 3:1 (H:V) from the west side of the crest and 2.5:1 from the east side of the crest. A 45-ft canal berm exists between the levee toe and the canal. Side slopes of 2:1, a bottom width of 100 ft, and a bottom elevation of approximately -6 ft MSL characterize the L-30 canal.

When the control structure gates are closed, vertical seepage data near L-30 indicate that water from the wetland area infiltrates at a rate between 0.033 and 0.266 ft/day (Sonenshein, 2001). Table 45 summarizes pertinent hydrogeologic parameters corresponding to the thirteen zones identified in Figure 25.

Table 46 summarizes historical extreme and average water elevations on the L-30 Canal (S335_H) and on the east (G-1488) and west (3BS1W1_H) sides of the levee.

Table 46. Summary of historical water levels

	Water Level Gauge (DBHYDRO)	Observed Water Elevation (ft NGVD)		
		Maximum	Average	Minimum
WCA3A	3BS1W1_H	8.5	6.7	4.2
L30 Canal	S335_H	8.5	6.3	3.1
East	G-1488	8.3	6.2	2.7

Analytic Element Model

The model domain was truncated 1600 ft north and south of the L-30 levee. The “zero” point in the profile axis was set on the south edge of the L-30 borrow canal. Inhomogeneity domains were extended over the range $-2000 < x < +2000$, for accurate solutions at the ends of the model domain. The use of the truncated domain made it necessary to set GHB conditions at the ends of the model, with resistance computed according to the profile modeling documentation. All strings of inhomogeneity doublets were subdivided as necessary beneath major surface boundary conditions (e.g. at edges of ponded regions) and at the GHB elements that bounded the left and right ends of the model domain.

Sensitivity Analysis

Parameter sensitivity analysis was performed in a manner consistent with Appendix B. PEST was used to identify the parameter values that maximize and minimize the rate of seepage across the levee, and to identify the maximum and minimum seepage rates. PEST determined vertical distributions of hydraulic conductivity (K) derived from the parameter ranges in the conceptual model. The sensitivity analysis was based on model runs in which the joint probability of the K distribution was within the 62% confidence interval (slightly less than one standard deviation away from the mean). The modeled seepage rates and the parameter values that yielded them are shown in Table 47 (below).

Table 47. Seepage Rates, L-30 north of S-335 and south of bridge

	Minimum	Best-fit	Maximum
Seepage rate across levee L-29, Section 1 [ft ² /d]	173	707.89	2545.17
K in layer 1 [ft/d]	0.1	2.24	49.4
K in layer 2 [ft/d]	5050	10000	100000
K in layer 3 [ft/d]	30.9	31.62	32.6
K in layer 4 [ft/d]	0.199	1.0	3.87
K in layer 5 [ft/d]	30.9	31.62	32.6
K in layer 6 [ft/d]	8050	10000	10391
K in layer 7 [ft/d]	32.1	31.62	32.4
K in layer 8 [ft/d]	7710	10000	10481
K in layer 9 [ft/d]	31.4	31.62	33.0
K in layer 10 [ft/d]	2042	2236.07	2270
K in layer 11 [ft/d]	10000	22360	34407
K in layer 12 [ft/d]	0.942	1.0	1.0
K in layer 13 [ft/d]	301	316.23	318

Levee Seepage Coefficients

Levee seepage coefficients for L-30, North of S-335 and South of Bridge were computed using the following procedure for each set of hydraulic parameters:

- Develop three sets of water levels for all boundary conditions;
- Run the analytic element model and compute seepage rates for the marsh-to-canal, marsh-to-dry-cell, and dry-cell-to-canal fluxes;
- Use a linear regression procedure, relating each flux term to the head difference (e.g. marsh-to-canal flux versus marsh-to-canal head difference).

The predicted levee seepage coefficients are provided in Table 48.

Table 48. Seepage Coefficients for L-30 between S-335 and the Bridge

	K_{ms} (ft/day)	K_{dm} (ft/day)	K_{ds} (ft/day)
MINIMUM	91.78	15.97	112.9
BEST-FIT	292.5	101.7	337.6
MAXIMUM	1186.	265.4	1234.

A more detailed evaluation of the seepage coefficients for this levee reach was later carried out as explained in the project report contained in appendix E. Some small, but insignificant, discrepancies may exist between the values contained in the above table and those reported in Appendix E.

The L-31N Levee / Borrow Canal System located between G-211 and S-331

Figure 26 indicates the location of the L-31N levee reach located between G-211 and S-331. The ACOE 1966 As-Built and 1976 construction drawings, DOQQ aerial images, the interpretation of data collected by the USGS at lithologic control well G-3311, and the hydrogeologic cross-section along the L-31N levee reach (Fish and Stewart, 1991) provided typical sections and representative hydrogeologic properties for the conceptual model (Figure 27). The *Draft L-31N Canal Drawdown Test Technical Memorandum* (ACOE, 2004) provided additional subsurface information.

C-1W Canal and Everglades National Park lie north and west of the study area. A combination of agricultural and urban areas lies east of L-31N. Additionally, Lakes RL1 and RL3, originating from mining operations, lie approximately 2.5 miles northeast of the C-1W canal and L-31N canal intersection. Control structures G-211 and S-331 bound this levee reach.

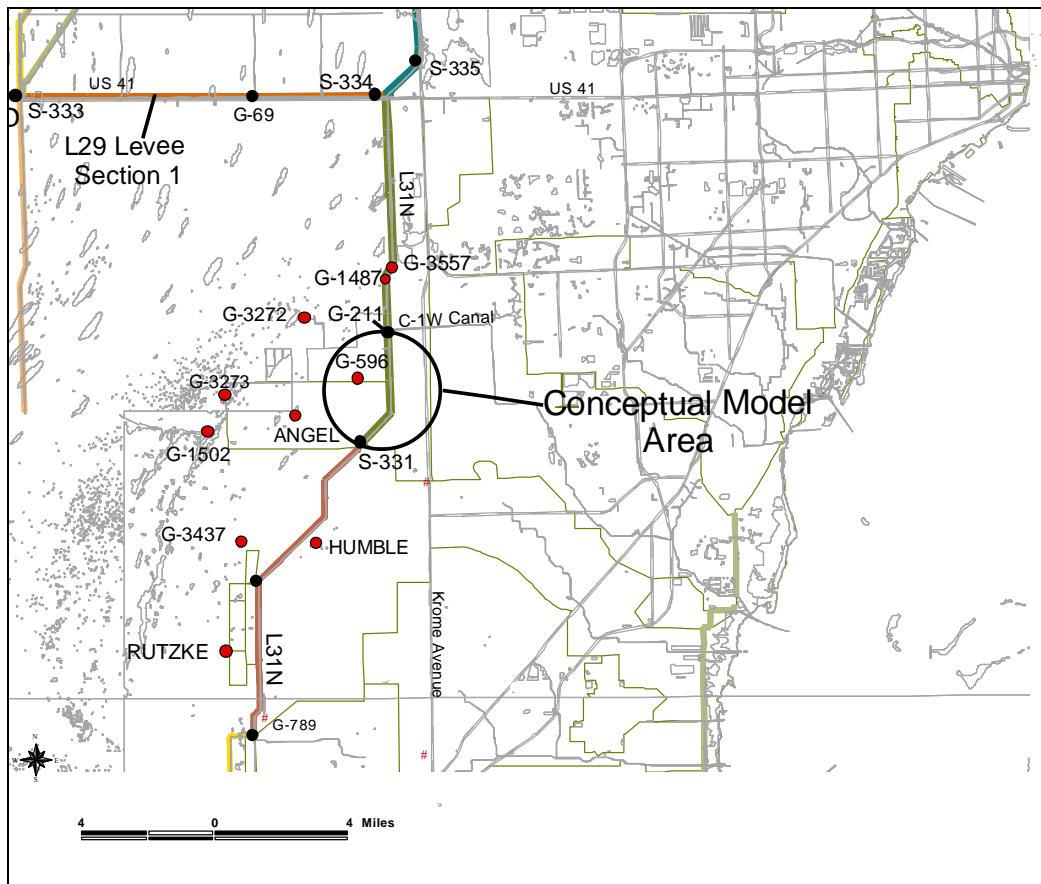


Figure 26. Location of L-31N Levee/Canal Conceptual Model located between G-211 and S-331

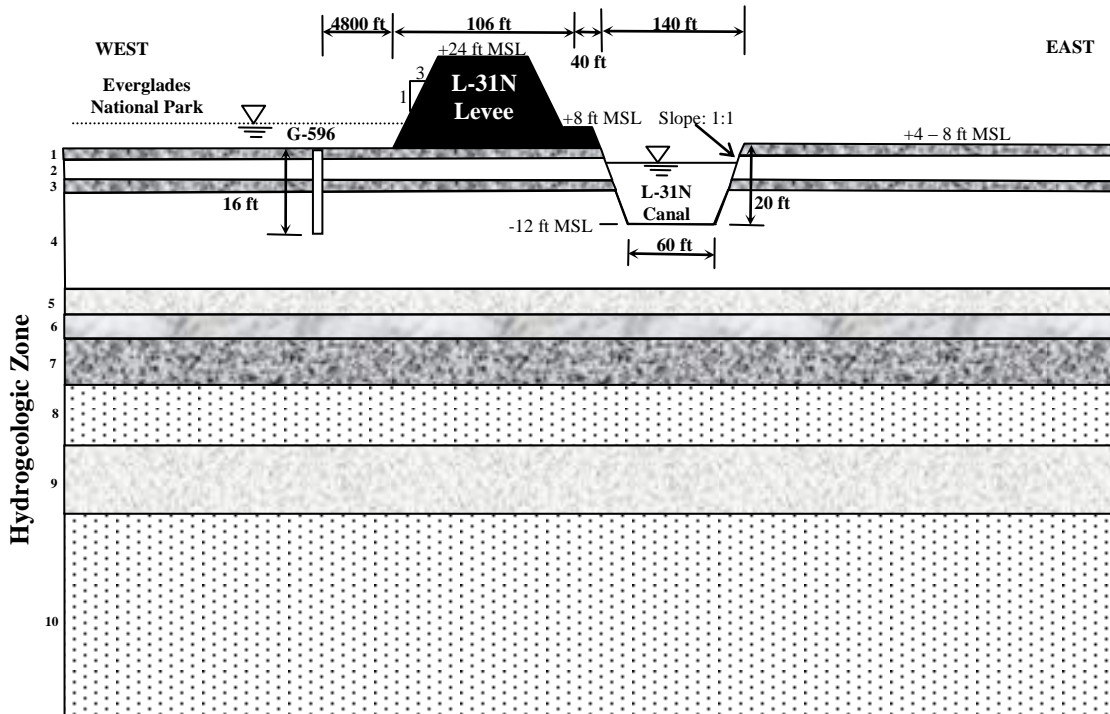


Figure 27. Conceptualization of the levee, canal, and shallow hydrostratigraphy of the L-31N reach located between G-211 and S-331 (N.T.S.)

Conceptual Model

As shown in Figure 27, existing ground elevations in this area range from +4 to 8 ft above mean sea level (M.S.L.). The L-31N levee contains a minimum 10-ft crest width at approximately +24 ft M.S.L. Levee side slopes extend 3:1 (H:V) from the crest and a 40-ft berm (lying at approximately +8.0 M.S.L.) extends between the levee toe and the L-31N canal. The L-31N canal is characterized by 1:1 side slopes, a bottom width of about 60 ft, and a bottom elevation of approximately -12 ft M.S.L.

Regional water-table maps indicate that ground water flows from west to east beneath the Levee 31N (Fish and Stewart, 1991). Table 49 summarizes pertinent hydrogeologic parameters, corresponding to the ten zones identified in Figure 27, for the L-31N reach located between G-211 and S-331.

Historical water levels are available on the west side of the levee at USGS shallow groundwater observation well G-596 and in the L-31N canal at control structure S-331. Observation well G-596 is located about 4,800 ft west of the levee. Historical extreme and average water elevations on the L-31N canal at control structure S-331 and at well G-596 are summarized in Table 50.

Analytic Element Model

The model domain was truncated 1600 ft north and south of the L-31 levee. The “zero” point in the profile axis was set on the south edge of the L-31 borrow canal. Inhomogeneity domains were extended over the range $-2000 < x < +2000$, for accurate solutions at the ends of the model domain. The use of the truncated domain made it necessary to set GHB conditions at the ends of

Table 49. Hydrogeologic parameters along the L-31N reach located between G-211 and S-331

Zone ID		Feature/Description	Range of Hydraulic Conductivity, K (ft/day)	Thickness (ft)
Miami Limestone	1	Peat, Muck, Marl	0.1 – 50	0.5
	2	First transmissive zone	$K \geq 1,000$	10
	3	First aquitard	0.1 – 10	2
Biscayne	4	Second transmissive zone	$K \geq 1,000$	36
Tamiami Formation	5	Second aquitard	10 – 100	10
	6	Third transmissive zone	100 – 1,000	8
	7	Third Aquitard	0.1 – 10	20
	8	Fourth transmissive zone	100 – 1,000	23
	9	Fifth transmissive zone	10 – 100	24
	10	Sixth transmissive zone	100 – 1,000	25

Table 50. Summary of Historical Water Levels

	Water Level Gauge (DBHYDRO)	Observed Water Elevation (ft NGVD)		
		Maximum	Average	Minimum
Everglades National Park	G-596	8.7	5.1	-0.2
L-31N Canal	S-331_HW	8.6	4.7	2.1
East	NA	NA	NA	NA

the model, with resistance computed according to the profile modeling documentation. All strings of inhomogeneity doublets were subdivided as necessary beneath major surface boundary conditions (e.g. at edges of ponded regions) and at the GHB elements that bounded the left and right ends of the model domain.

Sensitivity Analysis

Parameter sensitivity analysis was performed in a manner consistent with Appendix B. PEST was used to identify the parameter values that maximize and minimize the rate of seepage across the levee, and to identify the maximum and minimum seepage rates. PEST determined vertical

distributions of hydraulic conductivity (K) derived from the parameter ranges in the conceptual model. The sensitivity analysis was based on model runs in which the joint probability of the K distribution was within the 62% confidence interval (slightly less than one standard deviation away from the mean). The modeled seepage rates and the parameter values that yielded them are shown in Table 51 (below).

Table 51: Seepage Rates for L-31N, between G-211 and S-331

	Minimum	Best-fit	Maximum
Seepage rate across levee L-31N between G-211 and S-331 [ft ³ /day/ft]	34.5	245	1978
K in layer 1 [ft/d]	0.1	2.24	50.0
K in layer 2 [ft/d]	1670	10000	100000
K in layer 3 [ft/d]	0.502	1.0	2.74
K in layer 4 [ft/d]	1099	10000	44854
K in layer 5 [ft/d]	31.5	31.6	31.6
K in layer 6 [ft/d]	308	316	317
K in layer 7 [ft/d]	0.922	1.0	1.0
K in layer 8 [ft/d]	291	316	317
K in layer 9 [ft/d]	31.3	31.6	31.6
K in layer 10[ft/d]	289	316	317

Levee seepage coefficients

Levee seepage coefficients for L-31 N, between G-211 and S-331 were computed using the following procedure for each set of hydraulic parameters:

- Develop three sets of water levels for all boundary conditions;
- Run the analytic element model and compute seepage rates for the marsh-to-canal, marsh-to-dry-cell, and dry-cell-to-canal fluxes;
- Use a linear regression procedure, relating each flux term to the head difference (e.g. marsh-to-canal flux versus marsh-to-canal head difference).

The predicted levee seepage coefficients are provided in Table 52.

Table 52. Seepage Coefficients for L-31 N, between G-211 and S-331

	K_{ms} (ft/day)	K_{dm} (ft/day)	K_{ds} (ft/day)
MINIMUM	80.89	1.556	68.42
BEST-FIT	637.2	1.550	368.9
MAXIMUM	5197.	1.903	2762.

Using the best-fit ground water parameter values, a more detailed analysis of the seepage coefficient values was carried out as reported in Appendix E. This analysis yielded values of $K_{dm} = 2.3$ ft/day and $K_{ds} = 802.4$ ft/day. These latter values should be considered more accurate and the associated minimum/maximum values should be adjusted accordingly.

The L-31N, North of G-211 Levee / Borrow Canal System

Figure 28 indicates the location of the L-31N (north of G-211) levee reach. The ACOE 1966 As-Built and 1976 construction drawings, DOQQ aerial images, and interpretation of data collected by the USGS provided typical sections and representative hydrogeologic properties for the conceptual model (Figure 29). USGS geologic cores G-3304 (Fish and Stewart, 1991), G-3671 and G-3678 – G-3682 (Cunningham et. al., 2004), and data collected for the *Evaluation of the Use of Reach Transmissivity to Quantify Leakage Beneath Levee 31N, Miami-Dade County, Florida* (Nemeth et. al., 2000), provided additional site-specific subsurface information.

The Tamiami Canal, C-1W Canal, and Everglades National Park lie north, south, and west of the study area. A combination of agricultural and urban areas lies east of L-31N. Additionally, Lakes RL1 and RL3, originating from mining operations, lie approximately 4 to 5 miles south of the L-31N and Tamiami canal intersection, east of L-31N.

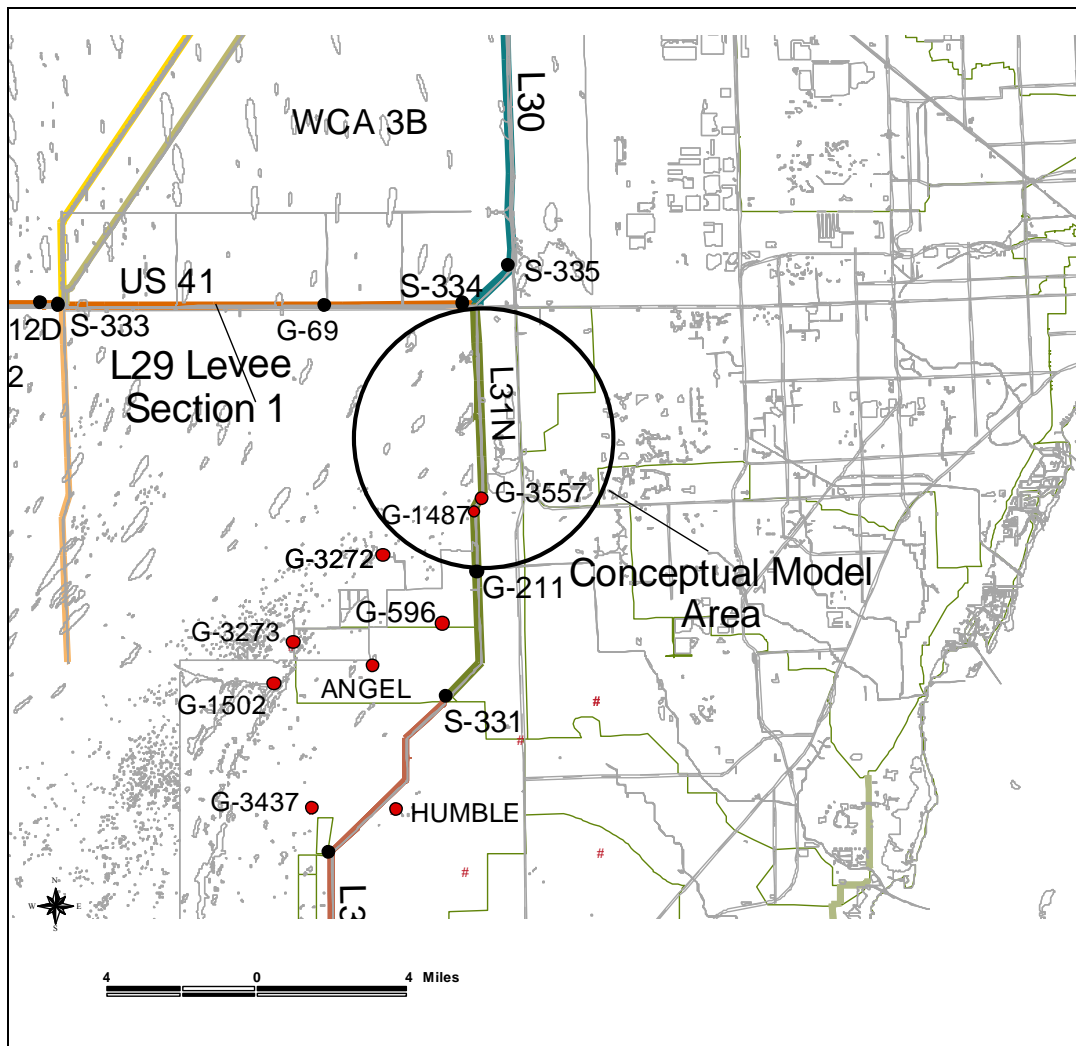


Figure 28. Location of L-31N (north of G-211) Levee/Canal Conceptual Model

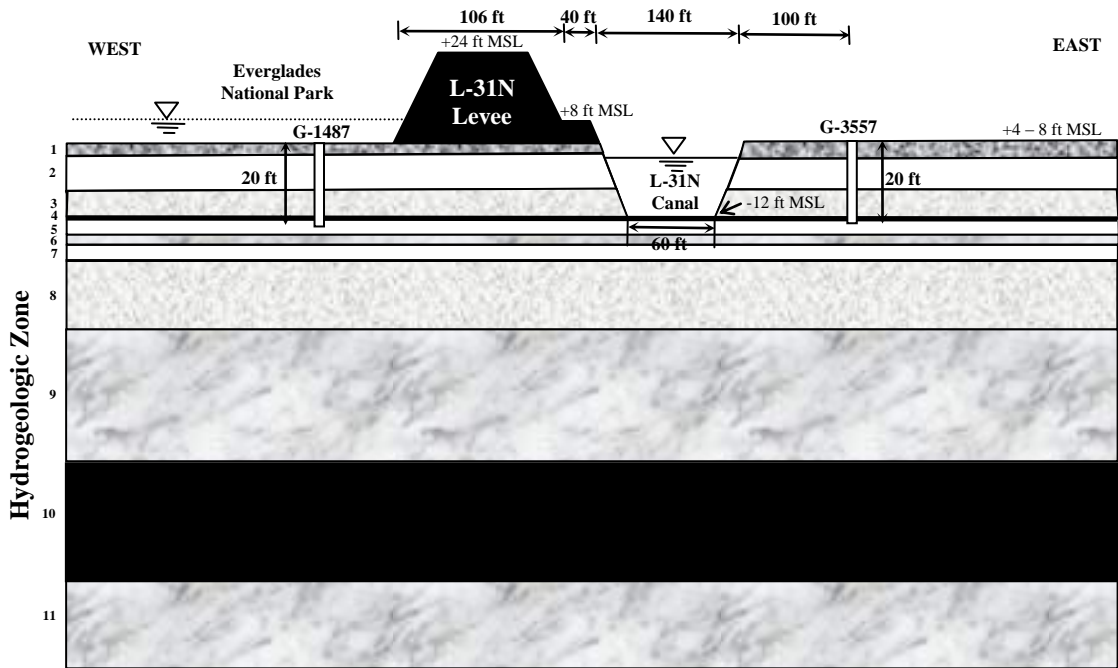


Figure 29. Conceptualization of the levee, canal, and shallow hydrostratigraphy of the L-31N, north of G-211 corridor (N.T.S.)

Conceptual Model

Existing ground elevations in this area range from +4 to 8 ft above mean sea level (M.S.L.). The L-31N levee contains a minimum 10-ft crest width at approximately +24 ft M.S.L. Levee side slopes extend 3:1 (H:V) from the crest and a 40-ft berm (lying at approximately +8.0 M.S.L.) extends between the levee toe and the L-31N canal. The L-31N canal is characterized by 1:1 side slopes, a bottom width of about 60 ft, and a bottom elevation of -12 ft M.S.L.

Regional water-table maps indicate that ground water flows from west to east beneath the Levee 31N (Fish and Stewart, 1991). The canal stage normally does not vary more than 3 ft during the year (Nemeth et. al., 2000). Measured seepage rates were observed to vary seasonally and increase with proximity to the levee (Nemeth et. al., 2000). Table 53 summarizes pertinent hydrogeologic parameters, corresponding to the eleven zones identified in Figure 29, along this reach of L-31N canal. The layers, characterized via cyclostratigraphy and geophysical methods (Cunningham et. al., 2004), consist of quantified GWFC (ground water flow classes) with corresponding HFC (high-frequency cycles) layers.

Historical water levels are available on the east and west sides of the levee/canal for two USGS shallow groundwater observation wells. G-3557 is located 100 ft east of the L-31N canal and G-1487 is located on the west side of the levee about 1 mile west of Krome Avenue. Table 54 summarizes historical extreme and average water levels for both the L-31N Canal and the USGS well recorders.

Table 53. Hydrogeologic parameters along L-31N, north of G-211

Zone ID		Hydrogeologic Framework Characterization		Range of Hydraulic Conductivity, K (ft/day)	Thickness (ft)
		HFC Layer	GWFC Layer		
Miami Limestone	1	Peat, Muck, Marl	GWFC 1	0.1 – 50	2
	2	HFC 5, Upper HFC 4	GWFC 2	> 1,000	10
Fort Thompson Formation	3	Lower HFC 4, HFC 3b, Upper HFC 3a	GWFC 3, 4 (same K)	10 – 100	4
	4	HFC 3a	GWFC 2	> 1,000	0.5
	5	HFC 3a	GWFC 4	10 – 100	4
	6	HFC 3a	GWFC 2	> 1,000	2
	7	HFC 2, Lower HFC 3a	GWFC 3,4	10 – 100	5
	8	HFC 1,2	GWFC 2	> 1,000	20
Tamiami Formation	9	NA	NA	100 – 1,000	45
	10	Semi-Confining Unit	NA	< 0.1	15
	11	Gray Limestone Aquifer	NA	100 – 1,000	30

Table 54. Summary of Historical Water Levels

	Water Level Gauge (DBHYDRO)	Observed Water Elevation (ft NGVD)		
		Maximum	Average	Minimum
Everglades National Park	G-3557	8.2	5.7	3.2
L31N Canal	G211-HW	7.7	5.7	2.9
East	G-1487	7.9	5.6	2.7

Analytic Element Model

The model domain was truncated 1600 ft north and south of the L-31N levee. The “zero” point in the profile axis was set on the south edge of the L-31N borrow canal. Inhomogeneity domains were extended over the range $-2000 < x < +2000$, for accurate solutions at the ends of the model domain. The use of the truncated domain made it necessary to set GHB conditions at the ends of

the model, with resistance computed according to the profile modeling documentation. All strings of inhomogeneity doublets were subdivided as necessary beneath major surface boundary conditions (e.g. at edges of ponded regions) and at the GHB elements that bounded the left and right ends of the model domain.

Sensitivity Analysis

Parameter sensitivity analysis was performed in a manner consistent with Appendix B. PEST was used to identify the parameter values that maximize and minimize the rate of seepage across the levee, and to identify the maximum and minimum seepage rates. PEST determined vertical distributions of hydraulic conductivity (K) derived from the parameter ranges in the conceptual model. The sensitivity analysis was based on model runs in which the joint probability of the K distribution was within the 62% confidence interval (slightly less than one standard deviation away from the mean). The modeled seepage rates and the parameter values that yielded them are shown in Table 55 (below).

Table 55. Seepage rates, L-31N, north of G-211

	Minimum	Best-fit	Maximum
Seepage rate across levee L-31N north of G-211 [ft ³ /day/ft]	49.47	433	3738
K in layer 1 [ft/d]	0.1	2.24	39.0
K in layer 2 [ft/d]	2000	10000	69010
K in layer 3 [ft/d]	32.4	31.6	34.5
K in layer 4 [ft/d]	7609	10000	9990
K in layer 5 [ft/d]	31.8	31.6	34.04
K in layer 6 [ft/d]	4350	10000	10400
K in layer 7 [ft/d]	31.9	31.6	34.8
K in layer 8 [ft/d]	1150	10000	100000
K in layer 9 [ft/d]	240	316	318
K in layer 10[ft/d]	0.071	0.07	0.073
K in layer 11 [ft/d]	263	316	317

Levee seepage coefficients

Levee seepage coefficients for L-31 N, north of G-211 were computed using the following procedure for each set of hydraulic parameters:

- Develop three sets of water levels for all boundary conditions;
- Run the analytic element model and compute seepage rates for the marsh-to-canal, marsh-to-dry-cell, and dry-cell-to-canal fluxes;
- Use a linear regression procedure, relating each flux term to the head difference (e.g. marsh-to-canal flux versus marsh-to-canal head difference).

The predicted levee seepage coefficients are provided in Table 56.

Table 56. Seepage Coefficients for L-31 North of G-211

	K_{ms} (ft/day)	K_{dm} (ft/day)	K_{ds} (ft/day)
MINIMUM	49.70	1.646	52.10
BEST-FIT	345.8	48.44	370.2
MAXIMUM	3090.	425.8	3323.

Using the best-fit ground water parameter values, a more detailed analysis of the seepage coefficient values was carried out as reported in Appendix E. This analysis yielded a value of $K_{ds} = 424.4$ ft/day. This latter value should be considered more accurate and the associated minimum/maximum values should be adjusted accordingly.

The L-31N Levee / Borrow Canal System Located South of S-331

Figure 30 indicates the location of the L-31N levee reach located south of S-331. The USACE 1966 As-Built and 1976 construction drawings, DOQQ aerial images, interpretation of data collected by the USGS at lithologic control well G-3314, and the hydrogeologic conceptualization along the L-31N levee reach (Fish and Stewart, 1991) provided the typical sections and representative hydrogeologic properties for the conceptual model (Figure 31). The *Draft L-31N Canal Drawdown Test Technical Memorandum* (USACE, 2004) and *Hydraulic Conductivity Profiles in Six Frog Pond Boreholes* (Genereux et. al., 1995) report provided additional subsurface information.

The Everglades National Park, the City of Homestead, and L-31W lie west, southeast, and southwest of the study area. Control structures S-331 and S-332D lie at the north and south ends of this levee reach.

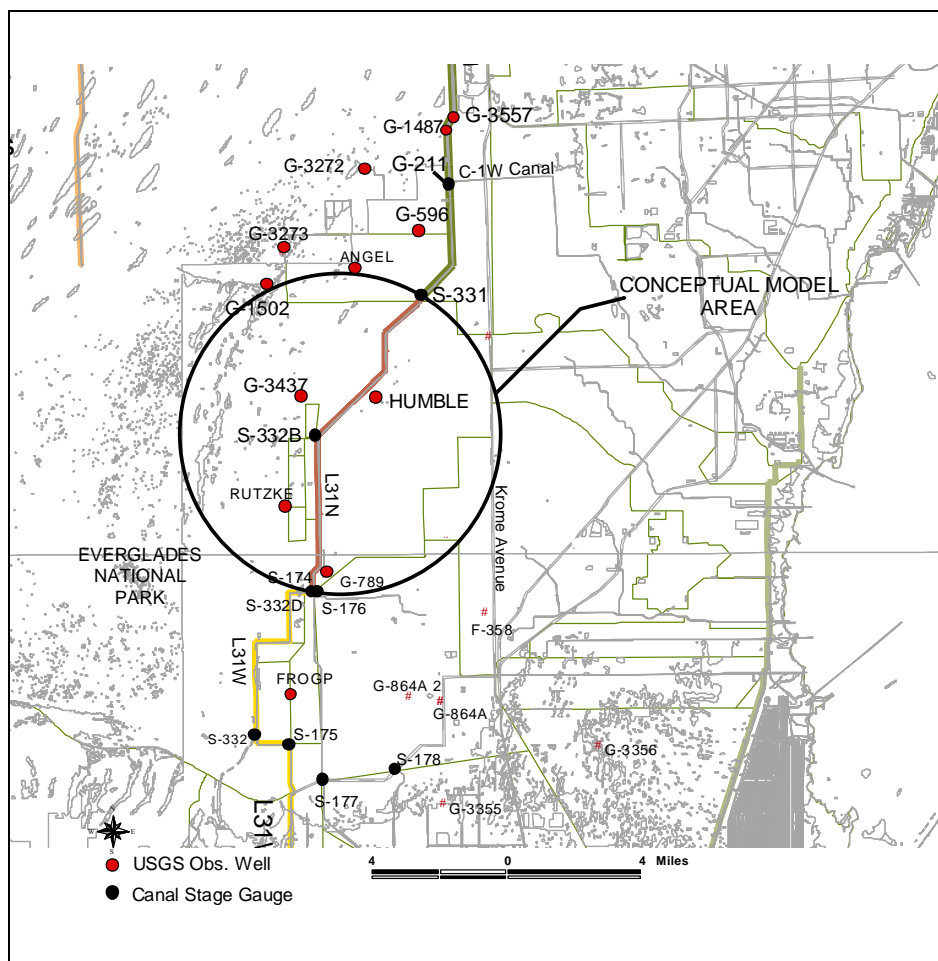


Figure 30. Location of L-31N levee/canal conceptual model located south of S-331

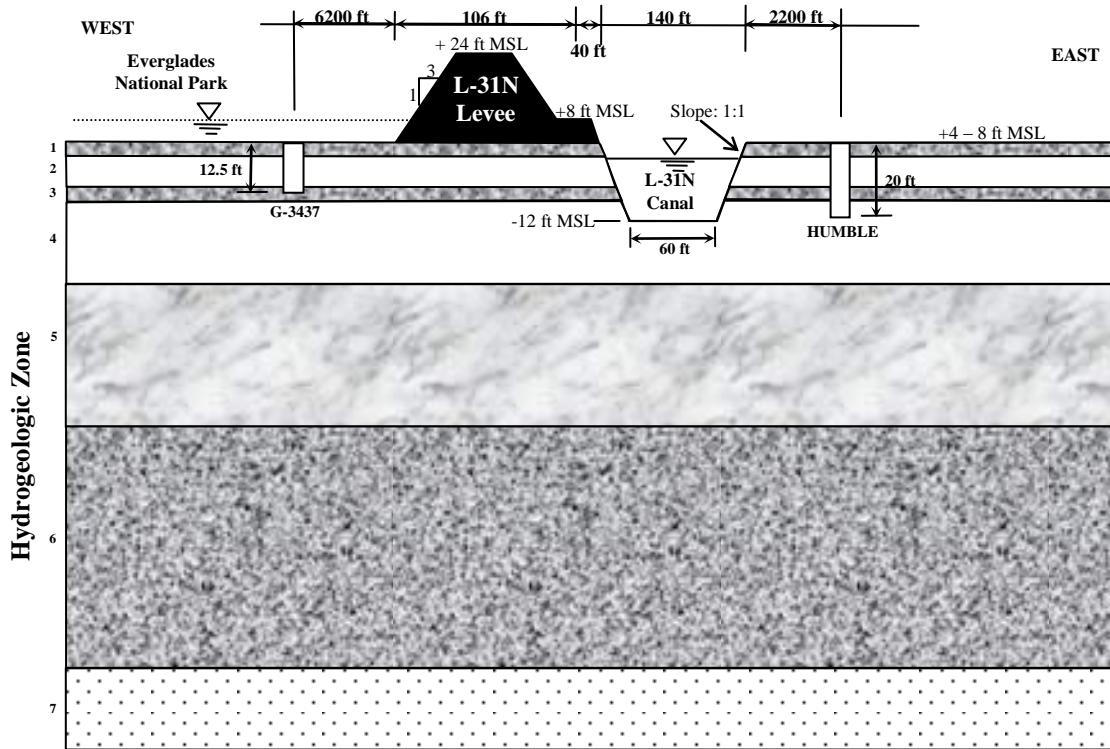


Figure 31. Conceptualization of the levee, canal, and shallow hydrostratigraphy of the L-31N reach located south of S-331 (NTS)

Conceptual Model

As shown in Figure 31, existing ground elevations in this area range from 4 to 8 ft above mean sea level (MSL). The L-31N levee contains a minimum 10-ft crest width at approximately +24 ft MSL. Levee side slopes extend 3:1 (H:V) from the crest and a 40-ft berm (lying at approximately +8.0 MSL) extends between the levee toe and the L-31N canal. Side slopes of 1:1 (H:V), a bottom width of about 60 ft, and a bottom elevation of -12 ft MSL characterize the L-31N canal.

Regional water table maps (Fish and Stewart, 1991) indicate that groundwater flows west to east beneath L-31N. Table 57 summarizes pertinent hydrogeologic parameters, corresponding to the seven zones identified in Figure 31. Historical water levels are available on the east and west sides of the levee/canal for two USGS shallow groundwater observation wells. The HUMBLE observation well is located about 2,200 ft east of the L-31N canal, and well G-3437 is located about 6,200 ft west of the levee. Table 58 summarizes historical extreme and average water elevations for the L-31N Canal and USGS well recorders.

Analytic Element Model

The model domain was truncated 1600 ft north and south of the L-31 levee. The “zero” point in the profile axis was set on the south edge of the L-31 borrow canal. Inhomogeneity domains were extended over the range $-2000 < x < +2000$, for accurate solutions at the ends of the model domain. The use of the truncated domain made it necessary to set GHB conditions at the ends of

Table 57. Hydrogeologic parameters along the L-31N reach located south of S-331

Zone ID		Feature/Description	Range of Hydraulic Conductivity, K (ft/day)	Thickness (ft)
Miami Limestone	1	Peat, muck, marl	0.1 – 50	2
	2	First transmissive layer	≥ 1,000	10
	3	First aquitard	0.1 – 10	2
Biscayne Aquifer	4	Second transmissive layer	≥ 1,000	30
Upper Tamiami	5	Second aquitard	10 – 100	40
	6	Third aquitard	0.1 – 10	90
Gray Limestone	7	Third transmissive layer	100 – 1,000	30

Table 58. Summary of historical water levels

	Water Level Gauge (DBHYDRO)	Observed Water Elevation (ft NGVD)		
		Maximum	Average	Minimum
Everglades National Park	G-3437	7.6	4.4	2.4
L31N Canal	S331-TW	6.5	4.3	1.5
East	HUMBLE	8.3	5.6	2.7

the model, with resistance computed according to the profile modeling documentation. All strings of inhomogeneity doublets were subdivided as necessary beneath major surface boundary conditions (e.g. at edges of ponded regions) and at the GHB elements that bounded the left and right ends of the model domain.

Sensitivity Analysis

Parameter sensitivity analysis was performed in a manner consistent with Appendix B. PEST was used to identify the parameter values that maximize and minimize the rate of seepage across the levee, and to identify the maximum and minimum seepage rates. PEST determined vertical distributions of hydraulic conductivity (K) derived from the parameter ranges in the conceptual model. The sensitivity analysis was based on model runs in which the joint probability of the K

distribution was within the 62% confidence interval (slightly less than one standard deviation away from the mean).

Modeled seepage rates and the parameter values that yielded them are shown in Table 59 (below).

Table 59. Seepage Rates, L-31N, south of S-331

	Minimum	Best-fit	Maximum
Seepage rate L31N, south of S-331 [ft ³ /day/ft]	-28.7	-294	-2720
K in layer 1 [ft/d]	0.1	2.24	50.0
K in layer 2 [ft/d]	1608	10000	100000
K in layer 3 [ft/d]	0.938	1.0	2.52
K in layer 4 [ft/d]	1049	10000	49700
K in layer 5 [ft/d]	30.8	31.6	31.8
K in layer 6 [ft/d]	0.872	1.0	1.002
K in layer 7 [ft/d]	316	316	318

Levee Seepage Coefficients

Levee seepage coefficients for L-31 N, south of S-331 were computed using the following procedure for each set of hydraulic parameters:

- Develop three sets of water levels for all boundary conditions;
- Run the analytic element model and compute seepage rates for the marsh-to-canal, marsh-to-dry-cell, and dry-cell-to-canal fluxes;
- Use a linear regression procedure, relating each flux term to the head difference (e.g. marsh-to-canal flux versus marsh-to-canal head difference).

The predicted levee seepage coefficients are provided in Table 60.

Table 60. Seepage Coefficients for L-31 South of S-331

	K_{ms} (ft/day)	K_{dm} (ft/day)	K_{ds} (ft/day)
MINIMUM	44.40	0.8922	24.00
BEST-FIT	453.7	1.032	192.8
MAXIMUM	4149.	1.028	1277.

Using the best-fit ground water parameter values, a more detailed analysis of the seepage coefficient values was carried out as reported in Appendix E. This analysis yielded values of $K_{dm} = 1.4$ ft/day and $K_{ds} = 475.6$ ft/day. These latter values should be considered more accurate and the associated minimum/maximum values should be adjusted accordingly.

The L-33 Levee / Borrow Canal System

Figure 32 indicates the location of the L-33 levee reach. The USACE 1951 drawings, DOQQ aerial images, interpretation of data collected by the USGS at lithologic control well G-2311, and the hydrogeologic conceptualization of the L-33 levee reach (Fish, 1988) provided the typical section and representative hydrogeologic properties for the conceptual model (Figure 33). Water Conservation Area 3B lies west of the study area. The L-33 levee reach lies between control structures S-32 and S-9X_S.

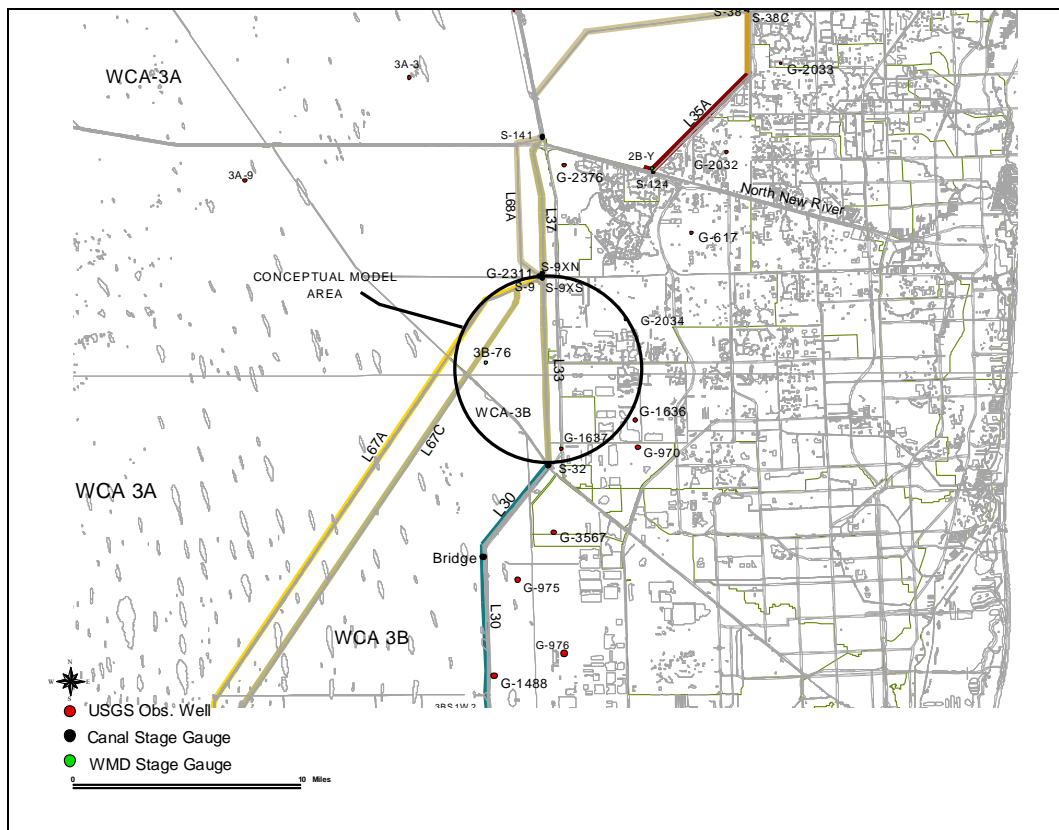


Figure 32. Location of L-33 levee/canal reach conceptual model

Conceptual Model

Existing ground elevations in this area average around +5 to 6.5 ft above mean sea level (MSL). The L-33 levee contains a 10-ft minimum crest width at approximately +20 ft MSL. Levee side slopes extend 3:1 (H:V) from the crest and a ± 45 -ft berm extends between the levee slope and the L-33 canal. The L-33 canal is characterized by 2:1(H:V) side slopes, a bottom width of about 60 ft, and a bottom elevation of approximately -6 ft MSL. Table 61 summarizes pertinent hydrogeologic parameters corresponding to the four zones identified in Figure 33.

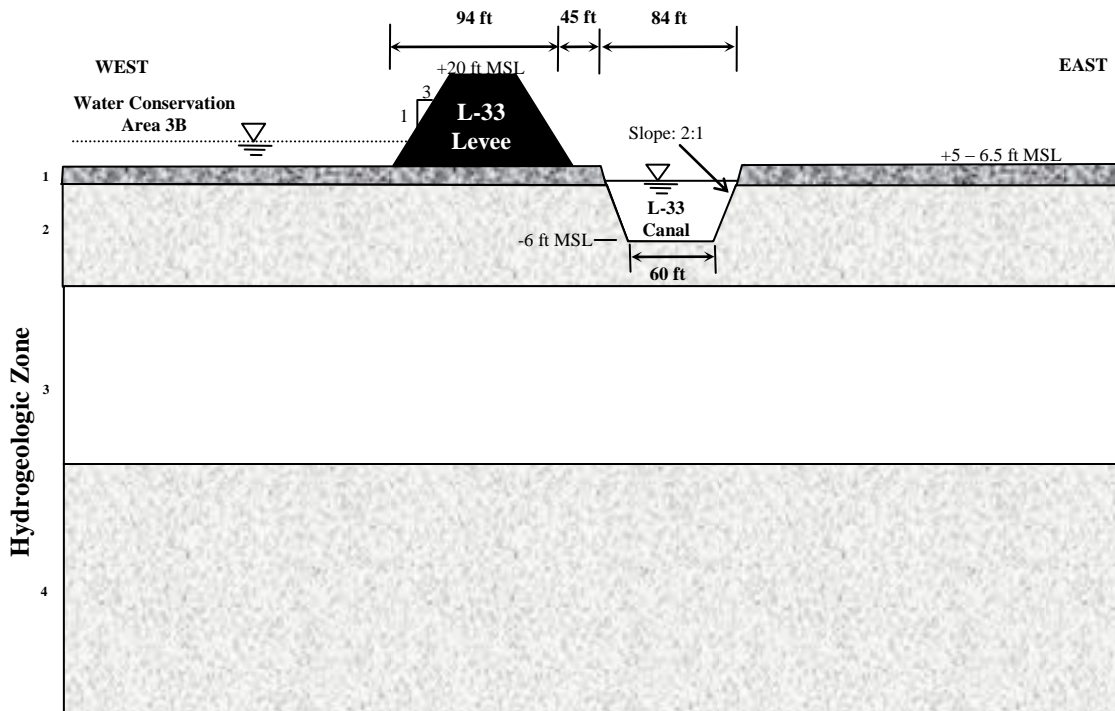


Figure 33. Conceptualization of the levee, canal, and shallow hydrostratigraphy of L-33 (NTS)

Table 61. Hydrogeologic parameters along the L-33 reach

Zone ID	Feature/Description	Range of Hydraulic Conductivity, K (ft/day)	Thickness (ft)
1	Peat, muck, marl	0.1 – 50	2
Fort Thompson	2	First transmissive layer	10 – 100
	3	Second transmissive layer	$\geq 1,000$
Tamiami	4	Second aquitard	0.1– 10

Historical water levels shown in Table 62 are available on the west side of the L-33 levee at WMD stage gauge 3B-76 and to the east at USGS shallow groundwater observation well G-1637. Observed water levels are available in the L-33 Canal at control structure S-32. Observation well G-1637 is located about 3,400 ft west of the levee.

Analytic Element Model

The model domain was truncated 1600 ft north and south of the L-33 levee. The “zero” point in

Table 62. Summary of historical water levels

	Water Level Gauge (DBHYDRO)	Observed Water Elevation (ft NGVD)		
		Maximum	Average	Minimum
WCA-3B	3B-76	9.5	7.8	5.4
L-33 Canal	S-32_HW	8.3	5.8	2.7
East	G-1637	6.2	4.3	2.2

the profile axis was set on the south edge of the L-33 borrow canal. Inhomogeneity domains were extended over the range $-2000 < x < +2000$, for accurate solutions at the ends of the model domain. The use of the truncated domain made it necessary to set GHB conditions at the ends of the model, with resistance computed according to the profile modeling documentation. All strings of inhomogeneity doublets were subdivided as necessary beneath major surface boundary conditions (e.g. at edges of ponded regions) and at the GHB elements that bounded the left and right ends of the model domain.

Sensitivity Analysis

Parameter sensitivity analysis was performed in a manner consistent with Appendix B. PEST was applied to the model in a predictive analysis mode to identify the parameter values that maximize and minimize the rate of seepage across the levee, and to identify the maximum and minimum seepage rates. PEST determined vertical distributions of hydraulic conductivity (K) derived from the parameter ranges in the conceptual model. The sensitivity analysis was based on model runs in which the joint probability of the K distribution was within the 62% confidence interval (slightly less than one standard deviation away from the mean). The modeled seepage rates and the parameter values that yielded them are shown in Table 63 (below).

Table 63. Seepage rates for L-33

	Minimum	Best-fit	Maximum
Seepage rate across levee L-33 [ft ³ /day/ft]	66.2	976	8100
K in layer 1 [ft/d]	0.1	2.24	39.0
K in layer 2 [ft/d]	77.4	31.6	86.5
K in layer 3 [ft/d]	1000	10000	100000
K in layer 4 [ft/d]	0.89	1.0	1.0

Levee seepage coefficients

Levee seepage coefficients for L-33 were computed using the following procedure for each set of hydraulic parameters:

- Develop three sets of water levels for all boundary conditions;
- Run the analytic element model and compute seepage rates for the marsh-to-canal, marsh-to-dry-cell, and dry-cell-to-canal fluxes;
- Use a linear regression procedure, relating each flux term to the head difference (e.g. marsh-to-canal flux versus marsh-to-canal head difference).

The predicted levee seepage coefficients are provided in Table 64.

Table 64. Seepage Coefficients for L-33

	K_{ms} (ft/day)	K_{dm} (ft/day)	K_{ds} (ft/day)
MINIMUM	18.74	5.604	8.526
BEST-FIT	79.53	102.5	31.92
MAXIMUM	273.5	1020.	121.8

The L-35A Levee / Borrow Canal System

Figure 34 indicates the location of the L-35A levee reach. The USACE 1949 drawings, DOQQ aerial images, and interpretation of data collected by the USGS (Swayze, 1988 and Fish, 1988) provided the information for the development of the L-35A conceptual model (Figure 35). Water Conservation Area 2B lies west of the study area. North New River Canal intersects the southernmost extent of L-35A. Control structures along this levee reach include S-124.

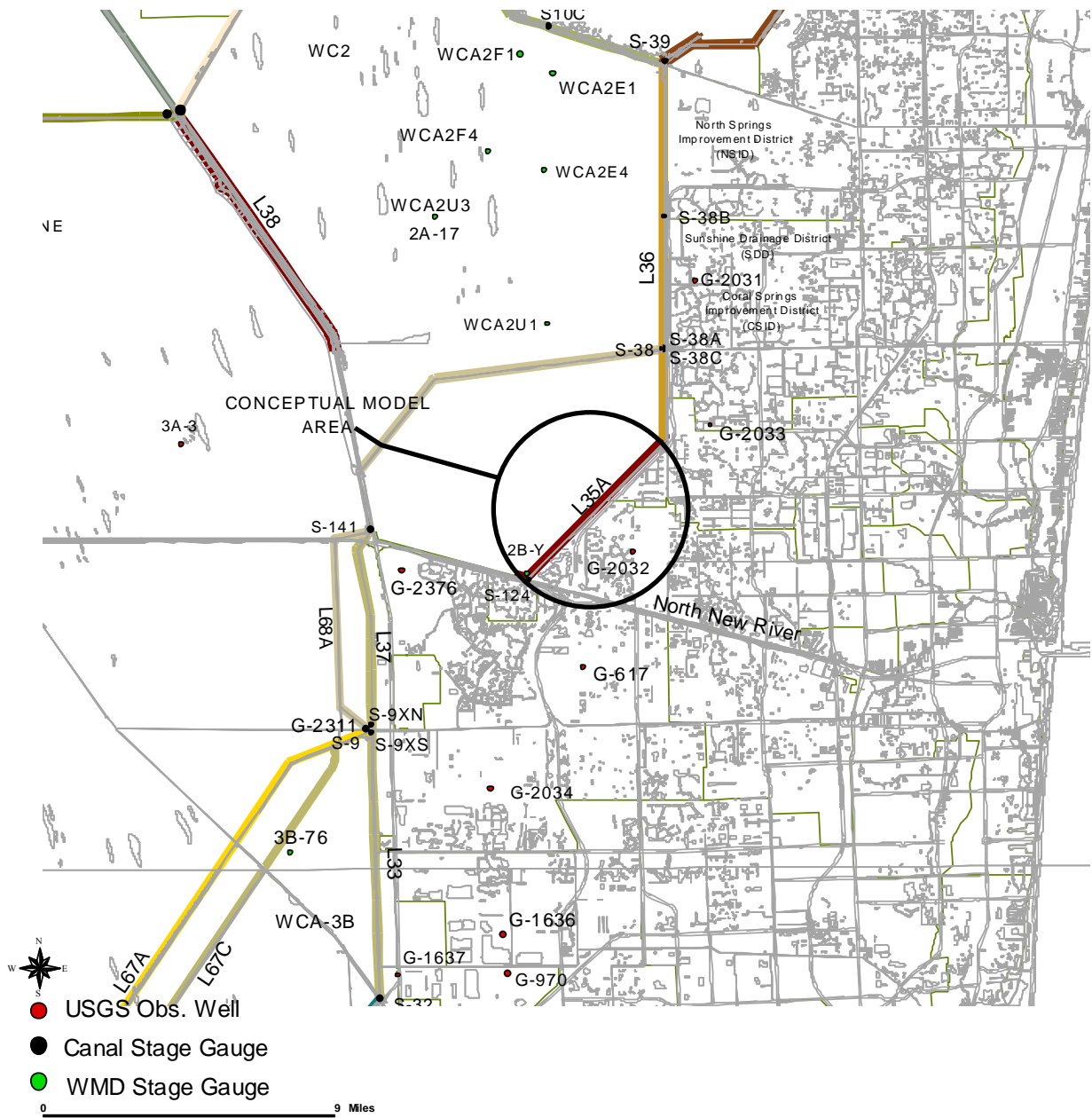


Figure 34. Location of L-35A levee/canal conceptual model

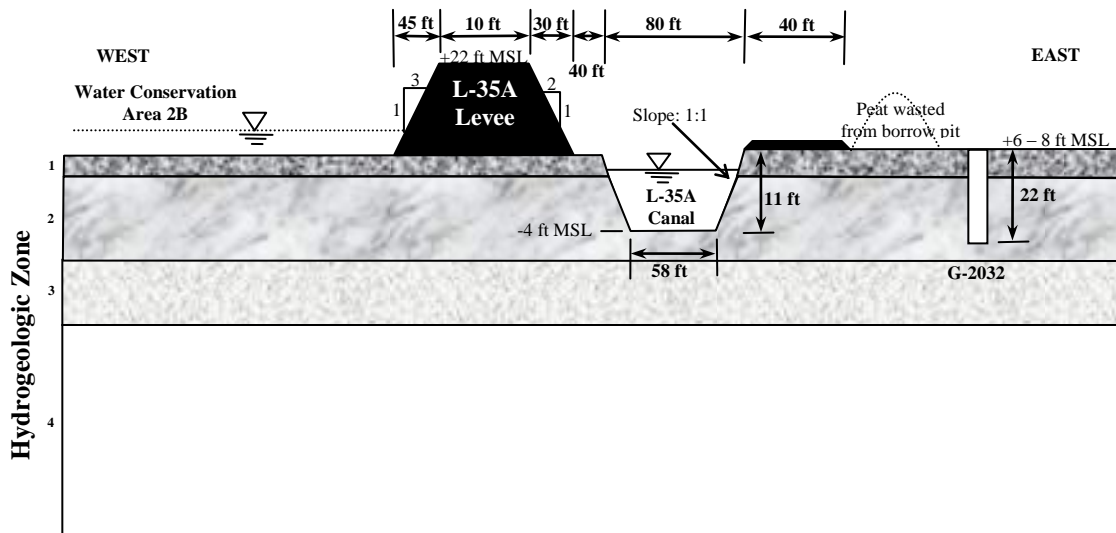


Figure 35. Conceptualization of the levee, canal, and shallow hydrostratigraphy of the L-35A (NTS)

Conceptual Model

Existing ground elevations in this area average around +6 to +8 ft above mean sea level (MSL). The L-35A levee contains a 10-ft minimum crest width at approximately +22 ft MSL. Levee side slopes extend 3:1 (H:V) from the crest on the west side of the levee and 2:1 on the east side of the levee. A minimum 40-ft berm extends between the levee slope and L-35A canal. An additional ± 40 -ft berm lies on the east side of the canal. Side slopes of 1:1, a bottom width of about 58 ft, and a bottom elevation of approximately -4.0 ft MSL characterize the L-35A canal.

An average 5.64-ft head differential exists between water levels in the Water Conservation Area 2B and the L-35A borrow canal (Swayze, 1988). This results in an average loss of 0.013 ft/day of surface water from the conservation area or 2.2×10^{-3} cfs per linear foot of the L-35A canal (Swayze, 1988). Table 65 summarizes pertinent hydrogeologic parameters, corresponding to the four zones identified in Figure 35.

Table 65. Hydrogeologic parameters along the L-35A corridor

Zone ID	Feature/Description	Range of Hydraulic Conductivity, K (ft/day)	Thickness (ft)
1	Peat, muck, marl, sand	0.1 – 50	5
2	First transmissive zone	10 – 100	27
3	First aquitard	0.1 – 10	20
4	Second transmissive zone	$\geq 1,000$	70

Historical water levels are available on the east side of the levee at USGS shallow groundwater observation well G-2032, on the west side of the levee at stage gauge 2B-Y, and in the L-35A canal at control structure S-124. Gauge 2B-Y is located in the Water Catchment Area 2B about 40 ft west of the levee. Observation well G-2032 is located about 9,500 ft east of the levee. The land to the east of L35A consists primarily of an urban development known as Plantation Acres. Water levels in this development are maintained between elevations 3.5 ft and 4.5 ft by a system of pumps that discharge into the North New River Canal (Broward County, DPEP, 2001). Table

66 summarizes historical extreme and average stages in the L-35A Canal, at control structure S-124, and at well G-2032.

Table 66. Summary of historical water levels

	Water Level Gauge (DBHYDRO)	Observed Water Elevation (ft NGVD)		
		Maximum	Average	Minimum
WCA-2B	2B-Y	11.4	8.7	3.4
L35A Canal	S-124_HW	8.1	4.7	3.6
East – USGS Obs. Well	G-2032	7.7	4.4	2.7

Analytic Element Model

The model domain was truncated 1600 ft north and south of the L-35A levee. The “zero” point in the profile axis was set on the south edge of the L-35A borrow canal. Inhomogeneity domains were extended over the range $-2000 < x < +2000$, for accurate solutions at the ends of the model domain. The use of the truncated domain made it necessary to set GHB conditions at the ends of the model, with resistance computed according to the profile modeling documentation. All strings of inhomogeneity doublets were subdivided as necessary beneath major surface boundary conditions (e.g. at edges of ponded regions) and at the GHB elements that bounded the left and right ends of the model domain.

Sensitivity Analysis

Parameter sensitivity analysis was performed in a manner consistent with Appendix B. PEST was applied to the model in a predictive analysis mode to identify the parameter values that maximize and minimize the rate of seepage across the levee, and to identify the maximum and minimum seepage rates. PEST determined vertical distributions of hydraulic conductivity (K) derived from the parameter ranges in the conceptual model. The sensitivity analysis was based on model runs in which the joint probability of the K distribution was within the 62% confidence interval (slightly less than one standard deviation away from the mean). The modeled seepage rates and the parameter values that yielded them are shown in Table 67 below.

Table 67. Seepage rates for L-35A

	Minimum	Best-fit	Maximum
Seepage rate L-35A [ft ³ /day/ft]	50.5	430.7	3780
K in layer 1 [ft/d]	0.311	2.24	17.84
K in layer 2 [ft/d]	18.3	31.6	50.78
K in layer 3 [ft/d]	0.1	1.0	10.0
K in layer 4 [ft/d]	1000	10000	100000

Levee seepage coefficients

Levee seepage coefficients for L-35A were computed using the following procedure for each set of hydraulic parameters:

- Develop three sets of water levels for all boundary conditions;
- Run the analytic element model and compute seepage rates for the marsh-to-canal, marsh-to-dry-cell, and dry-cell-to-canal fluxes;
- Use a linear regression procedure, relating each flux term to the head difference (e.g. marsh-to-canal flux versus marsh-to-canal head difference).

The predicted levee seepage coefficients are provided in Table 68.

Table 68. Seepage Coefficients for L-35A

	K_{ms} (ft/day)	K_{dm} (ft/day)	K_{ds} (ft/day)
MINIMUM	2.601	8.307	3.113
BEST-FIT	9.498	82.01	10.06
MAXIMUM	36.19	752.0	40.16

The L-36 Levee / Borrow Canal System

Figure 36 shows the location of the L-36 levee reach in Broward County, Florida. The USACE 1950 drawings, DOQQ aerial images, and interpretation of data collected at the USGS lithologic control well G-2341 (Fish, 1988) provided the typical section and representative hydrogeologic properties for the L-36 conceptual model (Figure 33).

Water Conservation Area 2A and 2B lie west of the study area. The Hillsboro Canal and North New River Canal lie north and south of L-36. The control structures located along this levee reach include S-39, NSID1, and S-38.

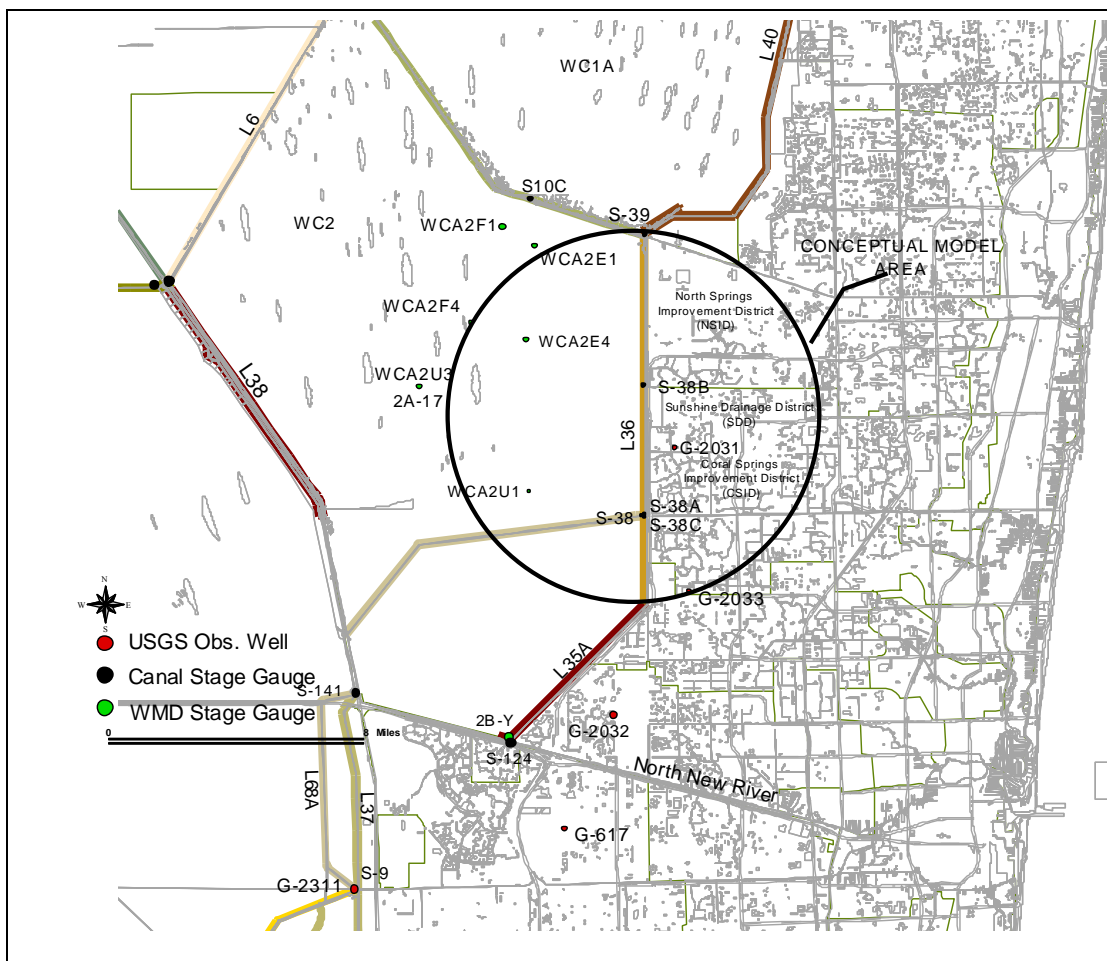


Figure 36. Location of L-36 levee/canal conceptual model

Conceptual Model

As shown in Figure 37, existing ground elevations in this area average between +9 and 11 ft above mean sea level (MSL). The L-36 levee contains a 10-ft crest width at approximately +20 ft MSL. Levee side slopes extend 3:1 (H:V) from the crest on the west side of the levee and 2:1 on

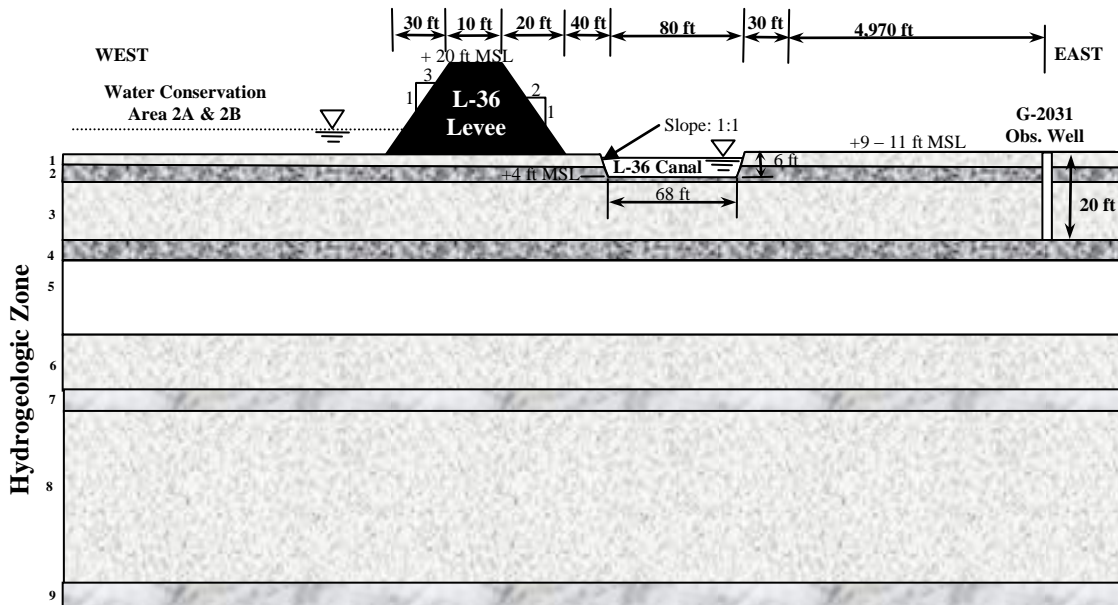


Figure 37. Conceptualization of the levee, canal, and shallow hydrostratigraphy of L-36 (NTS)

the east side of the levee. A minimum 40-ft berm extends between the levee toe and the L-36 canal. Side slopes of 1:1 (H:V), a bottom width of about 68 ft, and a bottom elevation of +4 ft MSL characterize the L-36 canal. A minimum 30-ft berm exists east of the canal.

Table 69 summarizes pertinent hydrogeologic parameters corresponding to the nine zones identified in Figure 37.

Historical extreme and average stages are available on the east side of the levee at USGS shallow groundwater observation well G-2031, on the west side of the levee at stage gauge 2A-17 and in the L-36 canal at control structures S-38C_TW and S-39_TW. Observation well G-2031 is located about 5,000 ft east of the canal. These groundwater stages compare closely with stages recorded within the Sunshine Drainage District canal system which are maintained via pumps at a control elevation of 7.0 ft NGVD (Broward County, 2000). Gauge 2A-17 is located approximately 6.85 miles west of the levee. Table 70 summarizes historical extreme and average water elevations for control structures S-38C_TW/S39_TW, at USGS well G-2031, and the Sunshine Drainage District.

Analytic Element Model

The model domain was truncated 1600 ft east and west of the L-36 levee. The “zero” point in the profile axis was set on the west edge of the L-36 borrow canal. Inhomogeneity domains were extended over the range $-2000 < x < +2000$, for accurate solutions at the ends of the model domain. The use of the truncated domain made it necessary to set GHB conditions at the ends of the model, with resistance computed according to the profile modeling documentation. All strings of inhomogeneity doublets were subdivided as necessary beneath major surface boundary

Table 69. Hydrogeologic parameters along the L-36 reach

Zone ID		Feature/Description	Range of Hydraulic Conductivity, K (ft/day)	Thickness (ft)
Pamlico Sand	1	Sand, fill, muck	10 – 100	4
	2	First aquitard	0.1 – 10	4
Fort Thompson	3	Second aquitard	10 – 100	12
	4	First transmissive zone	≥ 1,000	4
Fort Thompson/ Anastasia	5	Third aquitard	10 – 100	16
Anastasia	6	Fourth aquitard	0.1 – 10	12
	7	Second transmissive zone	100 – 1,000	5
Anastasia/ Tamiami	8	Fifth aquitard	10 – 100	55
Tamiami	9	Third transmissive zone	100 – 1,000	5

Table 70. Summary of historical water levels

	Water Level Gauge (DBHYDRO)	Observed Water Elevation (ft NGVD)		
		Maximum	Average	Minimum
WCA-2	2A-17	11.4	8.7	3.4
L-36 Canal	S-38C_TW/S-39_TW	9.9	6.4	4.6
East – USGS Obs. Well	G-2031	10.9	7.4	4.8
East – Sunshine DD	SDD-W	8.5	7.1	4.4

conditions (e.g. at edges of ponded regions) and at the GHB elements that bounded the left and right ends of the model domain.

Sensitivity Analysis

Parameter sensitivity analysis was performed in a manner consistent with Appendix B. PEST was applied to the model in a predictive analysis mode to identify the parameter values that maximize and minimize the rate of seepage across the levee, and to identify the maximum and minimum seepage rates. PEST determined vertical distributions of hydraulic conductivity (K) derived from the parameter ranges in the conceptual model. The sensitivity analysis was based on model runs in which the joint probability of the K distribution was within the 62% confidence interval (slightly less than one standard deviation away from the mean). The modeled seepage rates and the parameter values that yielded them are shown in Table 71 below

Table 71. Seepage rates for L-36

	Minimum	Best-fit	Maximum
Seepage rate L-36 [ft ³ /day/ft]	-4430	-643	527
K in layer 1 [ft/d]	37.9	31.6	100
K in layer 2 [ft/d]	10	1.0	1.84
K in layer 3 [ft/d]	65.4	31.6	32.5
K in layer 4 [ft/d]	100000	10000	50600
K in layer 5 [ft/d]	32.0	31.6	31.7
K in layer 6 [ft/d]	1.0	1.0	1.0
K in layer 7 [ft/d]	321	316	317.0
K in layer 8 [ft/d]	32.1	31.6	31.8
K in layer 9 [ft/d]	546	316	100

Levee seepage coefficients

Levee seepage coefficients for L-36 were computed using the following procedure for each set of hydraulic parameters:

- Develop three sets of water levels for all boundary conditions;
- Run the analytic element model and compute seepage rates for the marsh-to-canal, marsh-to-dry-cell, and dry-cell-to-canal fluxes;
- Use a linear regression procedure, relating each flux term to the head difference (e.g. marsh-to-canal flux versus marsh-to-canal head difference).

The predicted levee seepage coefficients are provided in Table 72.

Table 72. Seepage Coefficients for L-36

	K_{ms} (ft/day)	K_{dm} (ft/day)	K_{ds} (ft/day)
MINIMUM	2.036	3.023	0.6187
BEST-FIT	9.893	16.39	2.921
MAXIMUM	46.63	140.5	14.69

The L-37 Levee / Borrow Canal System

Figure 38 indicates the location of the L-37 levee reach. The USACE 1951 drawings, DOQQ aerial images, interpretation of data collected by the USGS at lithologic control well G-2311, and the hydrogeologic conceptualization along the L-37 levee reach (Fish, 1988) provided the typical section and representative hydrogeologic properties for the conceptual model (Figure 39). Water Conservation Area 3A lies west of the study area. The L-37 levee reach lies between control structures S-141 and S-9XN.

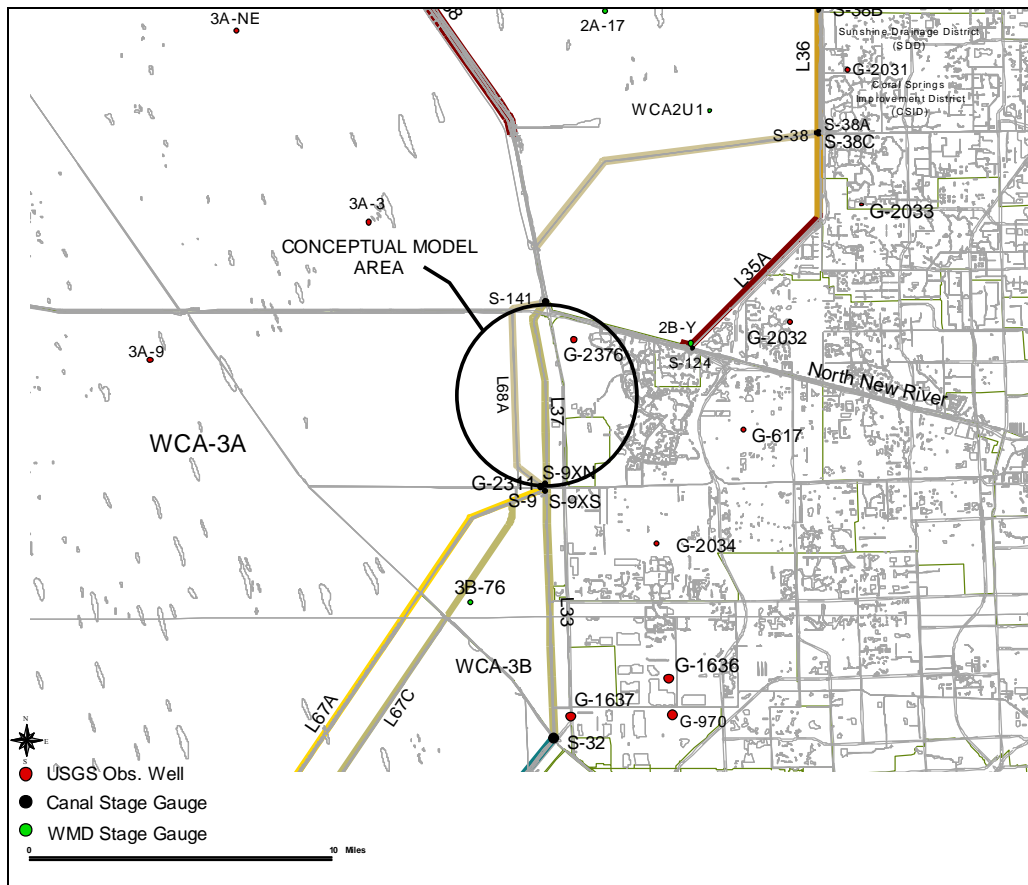


Figure 38. Location of L-37 canal/levee

Conceptual Model

As shown in Figure 39, existing ground elevations in this area average around +5 to +6.5 ft above mean sea level (MSL). The L-37 levee contains a 10-ft minimum crest width at approximately +20 ft MSL. Levee side slopes extend 3:1 (H:V) from the crest and a ±45-ft berm extends between the levee slope and the L-37 canal. Side slopes of 2:1 (H:V), a bottom width of about 60 ft, and a bottom elevation of approximately -6 ft MSL characterize the L-37 canal. Table 73 summarizes pertinent hydrogeologic parameters corresponding to the six zones

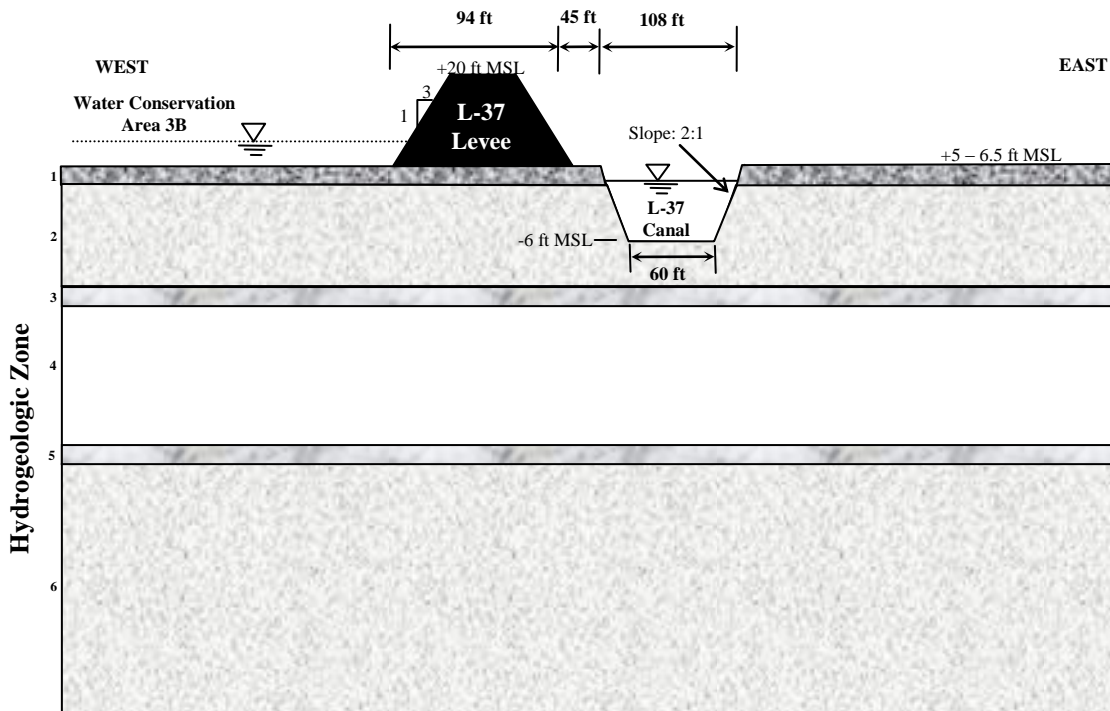


Figure 39. Conceptualization of the levee, canal, and shallow hydrostratigraphy of the L-37 reach (NTS)

identified in Figure 39. Historical stages are available, on the west side of the L-37 levee in the Water Conservation Area 3A, at WMD stage gauge 3A-9. In the L-37 canal, stages are available at gauge S-9XN at the north side of the confluence between L-37 and the S-9 canal. Stage data are available on the east side of the L-37 canal at USGS well G-2376. Table 74 summarizes historical extreme and average stages at the selected gauges

Analytic Element Model

The model domain was truncated 1600 ft east and west of the L-37 levee. The “zero” point in the profile axis was set on the west edge of the L-37 borrow canal. Inhomogeneity domains were extended over the range $-2000 < x < +2000$, for accurate solutions at the ends of the model domain. The use of the truncated domain made it necessary to set GHB conditions at the ends of the model, with resistance computed according to the profile modeling documentation. All strings of inhomogeneity doublets were subdivided as necessary beneath major surface boundary conditions (e.g. at edges of ponded regions) and at the GHB elements that bounded the left and right ends of the model domain.

Sensitivity Analysis

Parameter sensitivity analysis was performed in a manner consistent with Appendix B. PEST was applied to the model in a predictive analysis mode to identify the parameter values that maximize and minimize the rate of seepage across the levee, and to identify the maximum and minimum seepage rates. PEST determined vertical distributions of hydraulic conductivity (K) derived from the parameter ranges in the conceptual model. The sensitivity analysis was based on model runs in which the joint probability of the K distribution was within the 62% confidence

interval (slightly less than one standard deviation away from the mean). The modeled seepage rates and the parameter values that yielded them are shown in Table 75 below.

Table 73. Hydrogeologic parameters along the L-37 reach

Zone ID	Feature/Description	Range of Hydraulic Conductivity, K (ft/day)	Thickness (ft)	
1	Peat, muck, marl	0.1 – 50	4	
Fort Thompson	2	First transmissive layer	10 – 100	
	3	Second transmissive layer	100 – 1,000	
	4	Third transmissive layer	≥ 1,000	
	5	Fourth transmissive layer	100 – 1,000	
Tamiami	6	Second aquitard	0.10 – 10	120

Table 74. Summary of historical water levels

	Water Level Gauge (DBHYDRO)	Observed Water Elevation (ft NGVD)		
		Maximum	Average	Minimum
WCA-3A	3A-9	13.4	10.3	5.4
L37 Canal	S-9XN_HW	8.5	7.5	6.3
East	G-2376	8.0	6.3	4.0

Levee seepage coefficients

Levee seepage coefficients for L-37 were computed using the following procedure for each set of hydraulic parameters:

- Develop three sets of water levels for all boundary conditions;
- Run the analytic element model and compute seepage rates for the marsh-to-canal, marsh-to-dry-cell, and dry-cell-to-canal fluxes;

Table 75. Seepage Rates for L37

	Minimum	Best-fit	Maximum
Seepage rate L-37 [ft ³ /day/ft]	68.96	708.01	5774.26
K in layer 1 [ft/d]	0.1	2.24	37.15
K in layer 2 [ft/d]	14.1	31.62	87.94
K in layer 3 [ft/d]	252.81	316.23	337.68
K in layer 4 [ft/d]	1000	10000.0	100000.0
K in layer 5 [ft/d]	254.63	316.23	314.57
K in layer 6 [ft/d]	0.91	1.0	0.99

- Use a linear regression procedure, relating each flux term to the head difference (e.g. marsh-to-canal flux versus marsh-to-canal head difference).

The predicted levee seepage coefficients are provided in Table 76.

Table 76. Seepage Coefficients for L-37

	K_{ms} (ft/day)	K_{dm} (ft/day)	K_{ds} (ft/day)
MINIMUM	12.51	5.199	12.62
BEST-FIT	48.63	111.1	39.32
MAXIMUM	150.5	1084.	54.93

The L-38E and L-38W Levee / Borrow Canal System

Figure 40 indicates the location of the L-38E and L-38W levee reach in Broward County, Florida. The USACE 1959 and 1965 As-Built drawings, 1978 DDM, DOQQ aerial images, and interpretation of data collected by the USGS (Fish, 1988) provided information for the development of the L-38E and L-38W conceptual models (Figure 341). Review of the USACE (1953) permeability investigation report did not provide adequate stratigraphic information. Water Conservation Area 2 A and 3A lie northeast and southwest of the project study area.

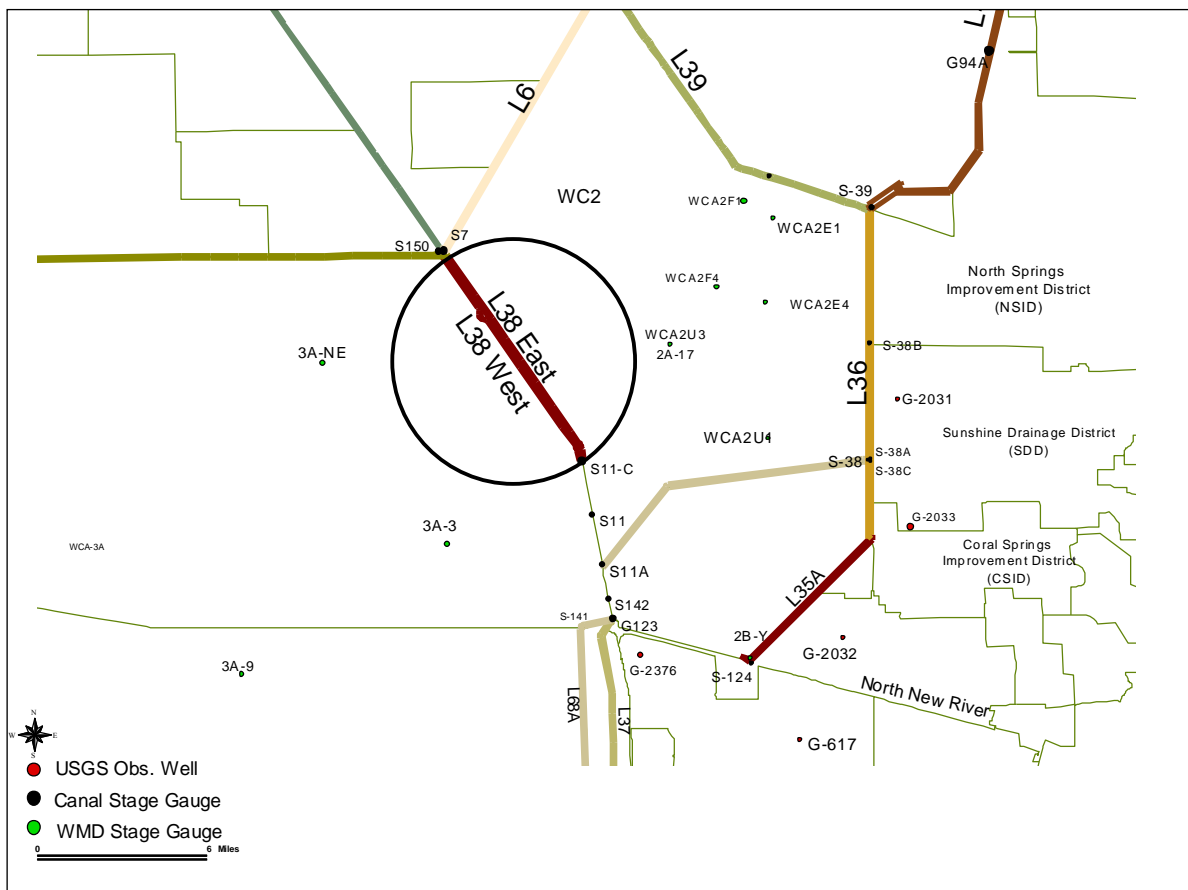


Figure 40. Location of the L-38E and L-38W levee/canal conceptual model

Conceptual Model

As shown in Figure 41, existing ground elevations surrounding the L-38E and L-38W area average between +10 ft and +15 ft above mean sea level (MSL). The L-38E levee contains a 10-ft minimum crest width at approximately +20 ft MSL. Levee side slopes extend 3:1 (H:V) from the crest and a ±40-ft berm extends from the levee slope to the canal. Approximately 525 ft separate the northeast and southwest (U.S. Highway 27) right-of-way lines. Side slopes of 1:1, a bottom width of about 15 ft, and a bottom elevation of approximately -6 ft MSL characterize the L-38E canal. The L-38W levee contains a 10-ft minimum crest width at approximately +17.5 ft

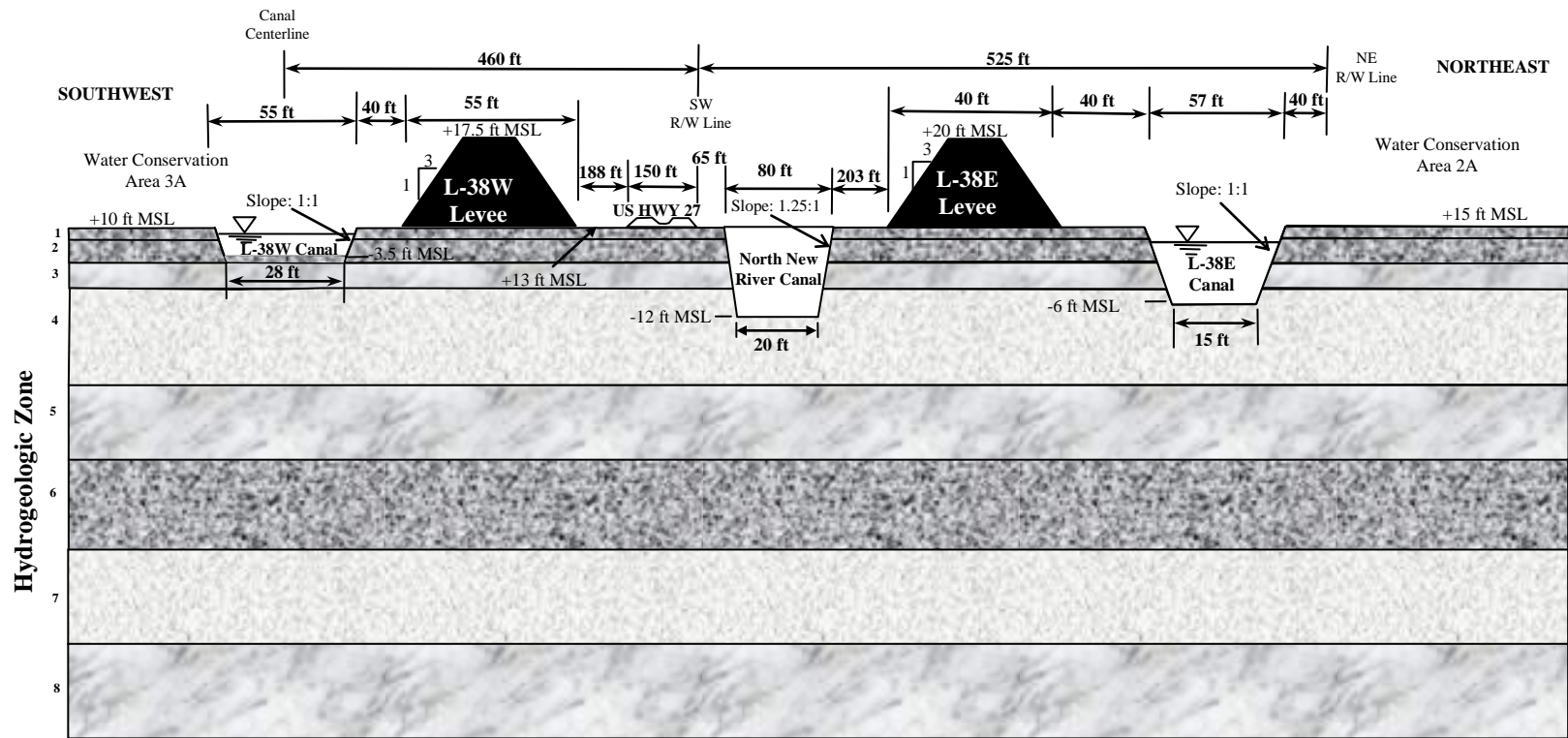


Figure 41. Conceptualization of the levee, canal, and shallow hydrostratigraphy of L-38E and L-38W (NTS)

MSL. Levee side slopes extend 3:1 (H:V) from the crest and a ±40-ft berm extends from the levee slope to the canal. Approximately 450 ft separates the centerline of US Highway 27 from the centerline of the L-38W levee. Side slopes of 1:1, a bottom width of about 15 ft, and a bottom elevation of approximately -3.5 ft MSL characterize the L-38W canal. The North New River Canal, located between U.S. Highway 27 and the L-38E levee, contain side slopes of 1.25:1, a bottom width of about 20 ft, and a bottom elevation of approximately -12 ft MSL.

Table 77 summarizes pertinent hydrogeologic parameters corresponding to the eight zones identified in Figure 41.

Table 77. Hydrogeologic parameters along L-38E and L-38W

Zone ID	Feature/Description	Range of Hydraulic Conductivity, K (ft/day)	Thickness (ft)
1	Peat, Marl	0.1 – 50	4
2	Second aquitard	0.1 – 10	15
3	Third aquitard	10 – 100	30
4	First transmissive zone	100 – 1,000	15
5	Fourth aquitard	10 – 100	15
6	Fifth aquitard	0.1 – 10	30
7	Second transmissive zone	100 – 1,000	25
8	Sixth aquitard	10 – 100	20

Historical water levels are available on the east side of levee L-38E at gauge 2A-17 in Water Conservation Area 2A, in the L-38E and L-38W canals at gauge S-11A, and on the west side of the levee at gauge 3A-3 in Water Conservation Area 3A. Table 78 summarizes historical extreme and average stages.

Table 78. Summary of historical water levels

	Water Level Gauge (DBHYDRO)	Observed Water Elevation (ft NGVD)		
		Maximum	Average	Minimum
WCA-2A	2A-17	15.6	12.6	9.3
L-38E Canal	S-11A_HW	14.8	11.8	9.7
L-38W Canal	S-11A_TW	13.8	10.4	7.6
WCA-3A	3A-3	13.5	10.0	5.8

Analytic Element Model

The model domain was truncated 1600 ft east and west of the L-38E and L-38W levee. The “zero” point in the profile axis was set on the southwestern edge of the North New River Canal. Inhomogeneity domains were extended over the range $-2000 < x < +2000$, for accurate solutions at the ends of the model domain. The use of the truncated domain made it necessary to set GHB conditions at the ends of the model, with resistance computed according to the profile modeling documentation. All strings of inhomogeneity doublets were subdivided as necessary beneath major surface boundary conditions (e.g. at edges of ponded regions) and at the GHB elements that bounded the left and right ends of the model domain.

Sensitivity Analysis

Parameter sensitivity analysis was performed in a manner consistent with Appendix B. PEST was applied to the model in a predictive analysis mode to identify the parameter values that maximize and minimize the rate of seepage across the levee, and to identify the maximum and minimum seepage rates. PEST determined vertical distributions of hydraulic conductivity (K) derived from the parameter ranges in the conceptual model. The sensitivity analysis was based on model runs in which the joint probability of the K distribution was within the 62% confidence interval (slightly less than one standard deviation away from the mean). The modeled seepage rates and the parameter values that yielded them are shown in Table 79 (below).

Table 79. Seepage rates for L-38E and L-38W

	Minimum	Best-fit	Maximum
Seepage rate across levee L-38 [ft ³ /day/ft]	0.35	24.9	80.03
K in layer 1 [ft/d]	2.40	2.24	3.09
K in layer 2 [ft/d]	1.63	1.0	4.45
K in layer 3 [ft/d]	10.0	31.6	100
K in layer 4 [ft/d]	137	316	1000
K in layer 5 [ft/d]	27.3	31.6	33.5
K in layer 6 [ft/d]	0.823	1.0	2.34
K in layer 7 [ft/d]	1000	316	250
K in layer 8 [ft/d]	36.1	31.6	31.0

Levee seepage coefficients

Levee seepage coefficients for L-38 were computed using the following procedure for each set of hydraulic parameters:

- Develop three sets of water levels for all boundary conditions;
- Run the analytic element model and compute seepage rates for the marsh-to-canal, marsh-to-dry-cell, and dry-cell-to-canal fluxes;
- Use a linear regression procedure, relating each flux term to the head difference (e.g. marsh-to-canal flux versus marsh-to-canal head difference).

The predicted levee seepage coefficients are provided in Table 80.

Table 80. Seepage Coefficients for L-38E and L-38W

	K_{ms} (ft/day)	K_{dm} (ft/day)	K_{ds} (ft/day)
MINIMUM	3.075	1.914	2.590
BEST-FIT	9.476	3.616	7.250
MAXIMUM	29.66	7.112	21.14

extend 3:1 from the crest and a ±45-ft berm extends between the levee and the L-40 canal. Side slopes of 1.5:1 and 3:1, a bottom width of approximately 37 ft, and a bottom elevation of approximately +1 ft MSL characterize the L-40 canal. Side slopes of 1.8:1, a bottom width of approximately 20 ft, and a bottom elevation of +1 ft MSL characterize the Lake Worth Drainage District (LDD) Canal E-1WS canal located in the southern portion of the L-40 levee reach. Cross-sectional data for the LDD canal were obtained from a GIS coverage of the canal network developed as part of the South Palm Beach County MODFLOW model (SFWMD, 2004).

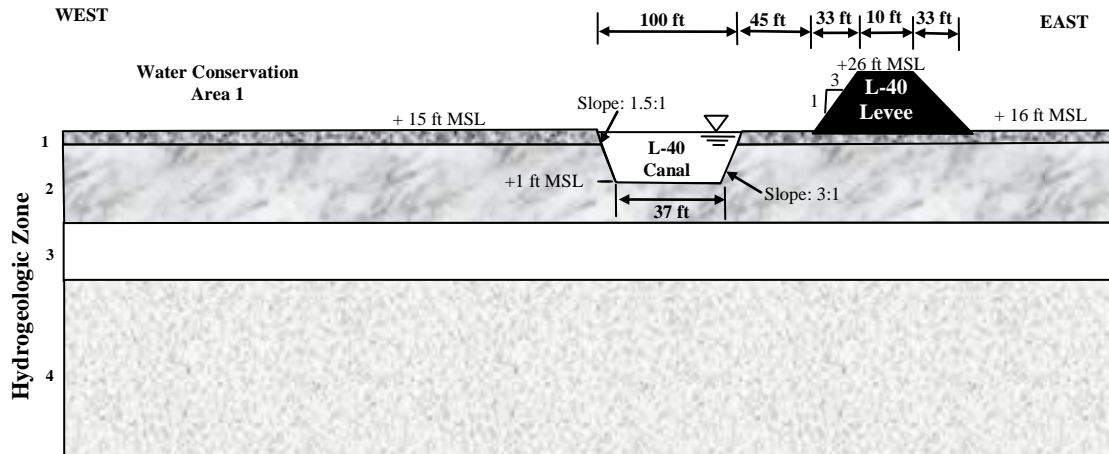


Figure 43. Conceptualization of the levee, canal, and shallow hydrostratigraphy of the L-40 northern reach (NTS)

Table 81 summarizes pertinent hydrogeologic parameters corresponding to the four zones identified in Figures 43 and 44.

Table 81. Hydrogeologic parameters along L-40

Zone ID	Feature/Description	Range of Hydraulic Conductivity, K (ft/day)	Thickness (ft)
1	Peat, muck, marl	0.1 – 50	3
2	Sand, poorly graded, clayey	10 – 150	12
3	Limestone	≥ 100	8
4	Sand, sandstone	10 – 150	45

Table 82 summarizes historical extreme and average water elevations for the area surrounding the L-40 levee reach.

Table 82. Summary of historical water levels

		Observed Water Elevation (ft NGVD)		
Water Level Gauge (DBHYDRO)		Maximum	Average	Minimum
L-7 Levee				
WCA-1 (east)	WCA1ME	18.0	16.4	14.5
L-7 Canal	S5AS_TW	19.0	15.4	9.9
ENR (west)	G251_HW	13.6	11.1	8.8
L-40 Levee - Northern Reach				
ACME-Wellington (east)	ACME-2_HW	15.6	12.9	9.4
L-40 Canal	G94C_HW	17.5	16.2	13.5
WCA-1 (west)	WCA1ME	18.0	16.4	14.5
L-40 Levee - Southern Reach				
West Delray Beach/Boca Raton(east)			13.0 ¹	
L-40 Canal	G94C_HW	17.5	16.2	13.5
WCA-1 (west)	WCA1ME	18.0	16.4	14.5

¹ Water levels maintained by Lake Worth Drainage District

Analytic Element Model (Northern Reach)

The model domain was truncated 1600 ft east and west of the L-40 levee. The “zero” point in the profile axis was set on the west edge of the L-40 borrow canal. Inhomogeneity domains were extended over the range $-2000 < x < +2000$, for accurate solutions at the ends of the model domain. The use of the truncated domain made it necessary to set GHB conditions at the ends of the model, with resistance computed according to the profile modeling documentation. All strings of inhomogeneity doublets were subdivided as necessary beneath major surface boundary conditions (e.g. at edges of ponded regions) and at the GHB elements that bounded the left and right ends of the model domain. Based on the conceptual model report, we assume that water is not ponded east of levee L-40.

Sensitivity Analysis (Northern Reach)

Parameter sensitivity analysis was performed in a manner consistent with Appendix B. PEST was applied to the model in a predictive analysis mode to identify the parameter values that maximize and minimize the rate of seepage across the levee, and to identify the maximum and minimum seepage rates. PEST determined vertical distributions of hydraulic conductivity (K) derived from the parameter ranges in the conceptual model. The sensitivity analysis was based

on model runs in which the joint probability of the K distribution was within the 62% confidence interval (slightly less than one standard deviation away from the mean).

The analysis for this levee differs from the others in that two PEST runs were made for both the maximization and minimization of the seepage estimate. The first run for each was made with an erroneously small gradient (0.01 foot) across the levee. The second run for each case uses a gradient of 1.0 feet. The parameter values from the first run was used as starting values for the next run based on the assumption that the parameter set that either maximizes or minimizes seepage with a small hydraulic gradient would be close to the values that would maximize or minimize seepage with a larger gradient. The PEST utility program parrep was used to make the control files max2.pst and min2.pst using the following commands.

```
parrep          max.par          max.pst          max2.pst
parrep          min.par          min.pst          min2.pst
```

The modeled seepage rates and the parameter values that yielded them are shown in Table 83 below.

Table 83. Seepage rates for L-40 (northern reach)

	Minimum	Best-fit	Maximum
Seepage rate L-40 northern reach [ft ³ /day/ft]	2.021	0.0305	49.6
K in layer 1 [ft/d]	33.5	2.24	5.22
K in layer 2 [ft/d]	40.5	38.7	104
K in layer 3 [ft/d]	100	316	1000
K in layer 4 [ft/d]	11.1	38.7	150

Levee seepage coefficients (Northern Reach)

Levee seepage coefficients were computed using the following procedure for each set of hydraulic parameters:

- Develop three sets of water levels for all boundary conditions;
- Run the analytic element model and compute seepage rates for the marsh-to-dry-cell fluxes;
- Use a linear regression procedure, relating each flux term to the head.

The predicted levee seepage coefficients are provided in Table 84.

Table 84. Seepage Coefficients for L-40 (northern reach)

	Kms	Kdm	Kds
MINIMUM	--	5.022	--
BEST-FIT	--	23.26	--
MAXIMUM	--	86.95	--

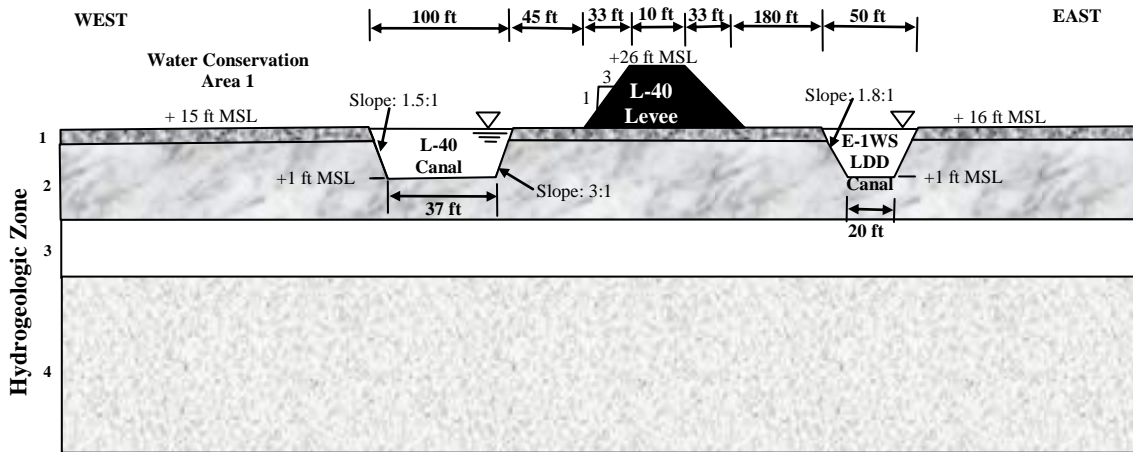


Figure 44. Conceptualization of the levee, canal, and shallow hydrostratigraphy of the L-40 southern reach (NTS)

Analytic Element Model (Southern Reach)

The model domain was truncated 1600 ft east and west of the L-40 levee. The “zero” point in the profile axis was set on the west edge of the L-40 borrow canal. Inhomogeneity domains were extended over the range $-2000 < x < +2000$, for accurate solutions at the ends of the model domain. The use of the truncated domain made it necessary to set GHB conditions at the ends of the model, with resistance computed according to the profile modeling documentation. All strings of inhomogeneity doublets were subdivided as necessary beneath major surface boundary conditions (e.g. at edges of ponded regions) and at the GHB elements that bounded the left and right ends of the model domain. Based on the conceptual model report, we assume that water is not ponded east of levee L-40.

Sensitivity Analysis (Southern Reach)

Parameter sensitivity analysis was performed in a manner consistent with Appendix B. PEST was applied to the model in a predictive analysis mode to identify the parameter values that maximize and minimize the rate of seepage across the levee, and to identify the maximum and minimum seepage rates. PEST determined vertical distributions of hydraulic conductivity (K) derived from the parameter ranges in the conceptual model. The sensitivity analysis was based on model runs in which the joint probability of the K distribution was within the 62% confidence

interval (slightly less than one standard deviation away from the mean). The modeled seepage rates and the parameter values that yielded them are shown in Table 85 below.

Table 85. Seepage rates for L-40 (southern reach)

	Minimum	Best-fit	Maximum
Seepage rate L-40 southern reach [ft ³ /day/ft]	3.92	13.06	43.9
K in layer 1 [ft/d]	2.23	2.24	2.25
K in layer 2 [ft/d]	13.1	38.7	114
K in layer 3 [ft/d]	100	316	1000
K in layer 4 [ft/d]	10.0	38.7	150

Levee seepage coefficients (Southern Reach)

Levee seepage coefficients were computed using the following procedure for each set of hydraulic parameters:

- Develop three sets of water levels for all boundary conditions;
- Run the analytic element model and compute seepage rates for the marsh-to-canal, marsh-to-dry-cell, and dry-cell-to-canal fluxes;
- Use a linear regression procedure, relating each flux term to the head difference (e.g. marsh-to-canal flux versus marsh-to-canal head difference).

The predicted levee seepage coefficients are provided in Table 86.

Table 86. Seepage Coefficients for L-40 (southern reach)

	Kms	Kdm	Kds
MINIMUM	3.63	0.29	0.44
BEST-FIT	12.21	0.85	1.23
MAXIMUM	41.64	2.27	3.01

Summary and Conclusions

Currently, the HSE code utilizes a linear algorithm to move ground water and ponded surface water from the up-gradient (i.e. wetland) side of a levee / borrow canal configuration to the down-gradient side (typically the landward side). This formulation relates total seepage from the wetlands to the wetland water level, the borrow canal stage, the aquifer properties, the geometry of the ground water flow system and borrow canal, and the ambient ground water level on the landward side of the levee (Lal, 2005). In order to utilize such an algorithm as part of an HSE application, the coefficients of this formulation must be obtained *a priori* for each levee reach in question. This may be accomplished by constructing a representative two-dimensional cross section model for each levee reach and measuring ground water flows for typical gradients under saturated conditions.

In support of HSE implementations, cross sectional ground water flow models were constructed under levees C-111, L-31N, L-30, L-29, L-33, L-37, L-38, L-35A, L-36, L-6, L-7, L-8 and L-40. Each of these models was based on the analytic element method for simulating ground water flow. Since, prior to this study, the analytic element method was not used in southern Florida to simulate ground water flow underneath levees in a cross sectional sense, two test models were also implemented to help verify the suitability of the method for the intended purpose. In each case, the results from a cross sectional analytic element model were compared to those obtained from an analytic solution that was also developed as part of this effort.

The levee seepage parameters required by HSE were derived for each of the major levee reaches listed above using the analytic element modeling code ModAem along with automated parameter estimation techniques. The uncertainty inherent to these parameters was also evaluated. These results can be incorporated into implementations of the HSE at regional or subregional scales.

References

Conceptual Model References

C-111 (1)

Fish, Johnnie E. and Mark Stewart. 1991. *Hydrogeology of the Surficial Aquifer System, Dade County, Florida*. U.S. Geological Survey (USGS) in cooperation with the S.F.W.M.D. Water Resources Investigation Report 90-4108. Tallahassee, FL.

Genereux, David and Jose D.A. Guardiario. 1995. *Hydraulic Conductivity Profiles in Six Frog Pond Boreholes*. Florida International University. Miami, FL.

Genereux, David and L.J. Nodarse & Associates. 1995. *Coring and Drilling Operations in the Frog Pond and Everglades National Park along L-31W Canal*. Gee & Jenson. West Palm Beach, FL.

U.S. Army Corps of Engineers (USACE). 1966. *Central and Southern Florida Project for Flood Control and Other Purposes, Canal 111, Sections 2 and 3 and Canal 111 East*. Jacksonville, FL.

U.S. Army Corps of Engineers (USACE). 1965. *Central and Southern Florida Project for Flood Control and Other Purposes, Part V, Coastal Areas South of St. Lucie Canal, Supplement 43 – Detail Design Memorandum Canal 111, Sections 2 and 3; Canal 111 (E); and Control Structures 176, 177, and 178*. Jacksonville, FL.

C-111 (2)

Fish, Johnnie E. and Mark Stewart. 1991. *Hydrogeology of the Surficial Aquifer System, Dade County, Florida*. U.S. Geological Survey (USGS) in cooperation with the S.F.W.M.D. Water Resources Investigation Report 90-4108. Tallahassee, FL.

Genereux, David and Jose D.A. Guardiario. 1995. *Hydraulic Conductivity Profiles in Six Frog Pond Boreholes*. Florida International University. Miami, FL.

Genereux, David and L.J. Nodarse & Associates. 1995. *Coring and Drilling Operations in the Frog Pond and Everglades National Park along L-31W Canal*. Gee & Jenson. West Palm Beach, FL.

U.S. Army Corps of Engineers (USACE). 1966. *Central and Southern Florida Project for Flood Control and Other Purposes, Canal 111, Sections 2 and 3 and Canal 111 East*. Jacksonville, FL.

U.S. Army Corps of Engineers (USACE). 1965. *Central and Southern Florida Project for Flood Control and Other Purposes, Part V, Coastal Areas South of St. Lucie Canal, Supplement 43 – Detail Design Memorandum Canal 111, Sections 2 and 3; Canal 111 (E); and Control Structures 176, 177, and 178*. Jacksonville, FL.

U.S. Army Corps of Engineers (USACE). 1963. *Central and Southern Florida Project for Flood control and other purposes Part V, Coastal Areas South of St. Lucie Canal Supplement 38—Detail Design Memorandum Canal III, Section I and Control Structure 18C*. Jacksonville, FL. Serial No. 10.

L-6

Judson, W.H., Krupa, S.L., Gefvert, C.J., Choi J., Mooney, R.H., and Giddings, J.B. 2000. *Interaction between Ground Water and Surface Water in the Northern Everglades and Relation to Water Budgets and Mercury Cycling: Study Methods and Appendixes*. U.S. Department of the Interior. USGS Open File Report 00-168. Reston, Virginia.

U.S. Army Corps of Engineers (USACE) and South Florida Water Management District. 2004. *Comprehensive Everglades Restoration Plan, Central and Southern Florida Project, B2 Hydraulics, B2.3. Hydrologic Model Calibration and Verification, Everglades Agricultural Area Storage Reservoirs – Phase I*, West Palm Beach, FL.

U.S. Army Corps of Engineers (USACE). 2003. *CERP Everglades Agricultural Area Reservoirs Phase I, Effort 2, Compartment B, Control Borings*. Jacksonville, FL.

U.S. Army Corps of Engineers (USACE). 1955. *Central and Southern Florida Project for Flood Control and Other Purposes Levee L-6*. Jacksonville, FL.

L-7

Bennett, Michael W., Linton, Paul F., Rectenwald, E. Edward. 2002. *Hydrogeologic Investigation of the Floridan Aquifer System Western Hillsboro Basin, Palm Beach County, Florida*. South Florida Water Management District (SFWMD). Technical Publication WS-8. West Palm Beach, FL.

Rohrer, P.R., *Hydrogeologic Characterization and Estimation of Ground Water Seepage in the Everglades Nutrient Removal Project*. 1999. South Florida Water Management District (SFWMD) Technical Publication WRE # 372. West Palm Beach, FL.

Scott, W. B. 1977. *Hydraulic Conductivity and Water Quality of the Shallow Aquifer, Palm Beach County, Florida*. U.S. Geological Survey (USGS). Water Investigations Report 76-119. Tallahassee, FL.

South Florida Water Management District [cited March 2004]. *Geographic Information Systems (GIS) coverages and database for the Water Preserve Areas Feasibility Study using the South Palm Beach Model. 2000-2002*. In GIS and text files [database on server]. West Palm Beach, FL.

Swayze, Leo, McGovern, Michael, and Fischer, John. 1981. *Lithologic Logs and Geophysical Logs from Test Drilling in Palm Beach County, Florida, since 1974*. United States Geological Survey (USGS) in cooperation with Palm Beach County and the S.F.W.M.D. Open-File Report 81-68.

U.S. Army Corps of Engineers (USACE). 2003. North Palm CERP Project. Jacksonville, FL.

U.S. Army Corps of Engineers (USACE). 1972. *Central and Southern Florida Project for Flood Control and other Purposes, Part 1, Agricultural and Conservation Areas Supplement 49 – General and Detail Design Memorandum Modification of Levees 7, 35B, and 38, Section 2 (U.S. Highway 27 – Between Structures 11A and 11C and Deletion of Canal 302)*. Jacksonville, FL.

U.S. Army Corps of Engineers (USACE). 1955. *Central and Southern Florida Project for Flood Control and other Purposes Levee 7*. Jacksonville, FL.

U.S. Army Corps of Engineers (USACE). 1951. *Central and Southern Florida Project for Flood Control and other Purposes First Phase Levee 40*. Jacksonville, FL.

L-8

Miller, Wesley. 1987. *Lithology and base of the surficial aquifer system, Palm Beach County, Florida*. Water-Resources Investigation Report 86-4067. Tallahassee, FL.

Reese, Ronald S. and Member, Steven J. 2000. *Hydrogeology and the Distribution of Salinity in the Floridan Aquifer System, Palm Beach County, Florida*. U.S. Geological Survey (USGS) in cooperation with the S.F.W.M.D. Water-Resources Investigation Report 99-4061, Tallahassee, FL.

Scott, W. B. 1977. *Hydraulic Conductivity and Water Quality of the Shallow Aquifer, Palm Beach County, Florida*. U.S. Geological Survey (USGS). Water Investigations Report 76-119. Tallahassee, FL.

South Florida Water Management District (SFWMD). 2004. *L-8 Seepage Barrier, Palm Beach County, Florida* (RFB CN040124). West Palm Beach, FL.

U.S. Army Corps of Engineers (USACE). 1953. *Central and Southern Florida Project for Flood Control and Other Purposes First Phase Canal and Levee L-8*. Jacksonville, FL

L-29, Section 1

Fish, Johnnie E. and Mark Stewart. 1991. *Hydrogeology of the Surficial Aquifer System, Dade County, Florida*. U.S. Geological Survey (USGS) in cooperation with the S.F.W.M.D. Water Resources Investigation Report 90-4108. Tallahassee, FL

U.S. Army Corps of Engineers (USACE). 1962. Levee 29, Section 1. Jacksonville, FL.

U.S. Army Corps of Engineers (USACE). November 1960. *Central and Southern Florida Project for Flood control and other purposes Part V, Coastal Areas South of St. Lucie Canal Supplement 35 - Detail Memorandum Levee 29, Sections 1 and 2 and Control Structures 12A, B, C, D, E, and 14*. Jacksonville, FL.

L-29, Section 2

Fish, Johnnie E. and Mark Stewart. 1991. *Hydrogeology of the Surficial Aquifer System, Dade County, Florida*. U.S. Geological Survey (Water Resources Investigation Report 90-4108) in cooperation with the S.F.W.M.D. Tallahassee, FL

U.S. Army Corps of Engineers. November 1960. *Central and Southern Florida Project for Flood control and other purposes Part V, Coastal Areas South of St. Lucie Canal Supplement 35 - Detail Memorandum Levee 29, Sections 1 and 2 and Control Structures 12A, B, C, D, E, and 14*. Jacksonville, FL.

U.S. Army Corps of Engineers. 1961. L-29, Section 2 As-Built Drawings. Jacksonville, FL.

L30 (South of S-335)

Cunningham, Kevin J., Carlson, Janine L., Wingard, Lynn G., Robinson, Edward, Wacker, Michael A. U.S. Geological Survey (USGS) In cooperation with S.F.W.M.D. 2004. *Characterization of Aquifer Heterogeneity Using Cyclostratigraphy and Geophysical Methods in the Upper Part of the Karstic Biscayne Aquifer, Southeastern Florida*. Water-Resources Investigations Report 03-4208.

Fish, Johnnie E. and Mark Stewart. 1991. *Hydrogeology of the Surficial Aquifer System, Dade County, Florida*. U.S. Geological Survey (USGS) in cooperation with the S.F.W.M.D. (Water Resources Investigation Report 90-4108) Tallahassee, FL

Sonenshein, Roy S. 2001. U.S. Geological Survey (USGS). *Methods to Quantify Seepage beneath Levee 30, Miami-Dade County, Florida*. Water-Resources Investigations Report 01-4074.

U.S. Army Corps of Engineers (USACE). November 1976. *Central and Southern Florida Project for Flood Control and Other Purposes, Levee 30 Borrow Canal Enlargement, Canal 4 Enlargement, S-32A and S-337*. Jacksonville, FL.

U.S. Army Corps of Engineers (USACE). March 1976. *Central and Southern Florida Project for Flood Control and Other Purposes Part V, Coastal Areas South of St. Lucie Canal Supplement 56 – Detail Design Memorandum Levee 30, Borrow Canal Enlargement, and Control Structures 32A and 337*. Jacksonville, FL.

U.S. Army Corps of Engineers (USACE). February 1951. *Central and Southern Florida Project for Flood Control and Other Purposes, Levee L-30*. Jacksonville, FL.

L-30 (North of Bridge)

Cunningham, Kevin J., Carlson, Janine L., Wingard, Lynn G., Robinson, Edward, Wacker, Michael A. In cooperation with S.F.W.M.D. 2004. U.S. Geological Survey. *Characterization of Aquifer Heterogeneity Using Cyclostratigraphy and Geophysical Methods in the Upper Part of the Karstic Biscayne Aquifer, Southeastern Florida*. Water-Resources Investigations Report 03-4208.

Fish, Johnnie E. and Mark Stewart. 1991. *Hydrogeology of the Surficial Aquifer System, Dade County, Florida*. U.S. Geological Survey (USGS) in cooperation with the S.F.W.M.D. Water Resources Investigation Report 90-4108. Tallahassee, FL

U.S. Army Corps of Engineers (USACE). September 2004. *L-31 North Canal Drawdown Test – L-31 North Canal Dry Season Test: May 24, 2004 to May 28, 2004*. Draft Technical Memorandum. Jacksonville, FL.

U.S. Army Corps of Engineers (USACE). November 1976. *Central and Southern Florida Project for Flood Control and Other Purposes, Levee 30 Borrow Canal Enlargement, Canal 4 Enlargement, S-32A and S-337*. Jacksonville, FL.

U.S. Army Corps of Engineers (USACE). March 1976. *Central and Southern Florida Project for Flood Control and Other Purposes Part V, Coastal Areas South of St. Lucie Canal Supplement 56 – Detail Design Memorandum Levee 30, Borrow Canal Enlargement, and Control Structures 32A and 337*. Jacksonville, FL.

U.S. Army Corps of Engineers (USACE). February 1951. *Central and Southern Florida Project for Flood Control and Other Purposes, Levee L-30*. Jacksonville, FL.

L-30 (North of S-335 and South of Bridge)

Cunningham, Kevin J., Carlson, Janine L., Wingard, Lynn G., Robinson, Edward, Wacker, Michael A. 2004. U.S. Geological Survey (USGS) In cooperation with S.F.W.M.D (Water-Resources Investigations

Report 03-4208). *Characterization of Aquifer Heterogeneity Using Cyclostratigraphy and Geophysical Methods in the Upper Part of the Karstic Biscayne Aquifer, Southeastern Florida.*

Fish, Johnnie E. and Mark Stewart. 1991. *Hydrogeology of the Surficial Aquifer System, Dade County, Florida*. U.S. Geological Survey (USGS) in cooperation with the S.F.W.M.D. (Water Resources Investigation Report 90-4108) Tallahassee, FL

Lukasiewicz, John. 2003. *Floridan Aquifer System Test Well Program L-30N Canal, Miami-Dade, Florida*. S.F.W.M.D. Technical Publication WS-17. West Palm Beach, FL

Sonenshein, Roy S. 2001. U.S. Geological Survey (USGS). *Methods to Quantify Seepage beneath Levee 30, Miami-Dade County, Florida*. Water-Resources Investigations Report 01-4074.

U.S. Army Corps of Engineers (USACE). February 1951. *Central and Southern Florida Project for Flood Control and Other Purposes, Levee L-30*. Jacksonville, FL.

U.S. Army Corps of Engineers. March 1976. *Central and Southern Florida Project for Flood Control and Other Purposes Part V, Coastal Areas South of St. Lucie Canal Supplement 56 – Detail Design Memorandum Levee 30, Borrow Canal Enlargement, and Control Structures 32A and 337*. Jacksonville, FL.

U.S. Army Corps of Engineers. November 1976. *Central and Southern Florida Project for Flood Control and Other Purposes, Levee 30 Borrow Canal Enlargement, Canal 4 Enlargement, S-32A and S-337*. Jacksonville, FL.

L-31N between G-211 and S-331

Fish, Johnnie E. and Mark Stewart. 1991. *Hydrogeology of the Surficial Aquifer System, Dade County, Florida*. U.S. Geological Survey (Water Resources Investigation Report 90-4108) in cooperation with the S.F.W.M.D. Tallahassee, FL

U.S. Army Corps of Engineers. January 1966. *Central and Southern Florida Project for Flood control and other purposes Part V, Coastal Areas South of St. Lucie Canal Supplement 44 - Detail Design Memorandum Levee 31(N), and Control Structures 173*. Jacksonville, FL.

U.S. Army Corps of Engineers. 1966. *Central and Southern Florida Project for Flood control and other purposes. Plans for Construction of L-31(N) Remainder and Canal 111 Section 3 Extension Structures 173 & 176*. Jacksonville, FL.

U.S. Army Corps of Engineers. 1976. *Central and Southern Florida Project for Flood control and other purposes. Plans for Construction of L-31(N) Borrow Canal Enlargement*. Jacksonville, FL.

U.S. Army Corps of Engineers. 2004. *L-31 North Canal Drawdown Test – L-31 North Canal Dry Season Test: May 24, 2004 to May 28, 2004*. Draft Technical Memorandum. Jacksonville, FL.

L-31 North of G-211

Cunningham, Kevin J., Carlson, Janine L., Wingard, Lynn G., Robinson, Edward, Wacker, Michael A. In cooperation with S.F.W.M.D. 2004. U.S. Geological Survey. *Characterization of Aquifer Heterogeneity Using Cyclostratigraphy and Geophysical Methods in the Upper Part of the Karstic Biscayne Aquifer, Southeastern Florida*. Water-Resources Investigations Report 03-4208.

Fish, Johnnie E. and Mark Stewart. 1991. Hydrogeology of the Surficial Aquifer System, Dade County, Florida. U.S. Geological Survey (Water Resources Investigation Report 90-4108) in cooperation with the S.F.W.M.D. Tallahassee, FL

Nemeth, Mark S., Wilcox, Walter M., Solo-Gabriele, Helena M. 2000. . U.S. Geological Survey. *Evaluation of the Use of Reach Transmissivity to Quantify Leakage Beneath Levee 31N, Miami-Dade County, Florida*. Water-Resources Investigations Report 00-4066.

U.S. Army Corps of Engineers. January 1966. *Central and Southern Florida Project for Flood control and other purposes Part V, Coastal Areas South of St. Lucie Canal Supplement 44 - Detail Design Memorandum Levee 31(N), and Control Structures 173*. Jacksonville, FL.

U.S. Army Corps of Engineers. 1966. *Central and Southern Florida Project for Flood control and other purposes. Plans for Construction of L-31(N) Remainder and Canal 111 Section 3 Extension Structures 173 & 176*. Jacksonville, FL

U.S. Army Corps of Engineers. 1976. *Central and Southern Florida Project for Flood control and other purposes. Plans for Construction of L-31(N) Borrow Canal Enlargement*. Jacksonville, FL

U.S. Army Corps of Engineers. 2004. *L-31 North Canal Drawdown Test – L-31 North Canal Dry Season Test: May 24, 2004 to May 28, 2004*. Draft Technical Memorandum. Jacksonville, FL.

L-31N, South of S-331

Fish, Johnnie E. and Mark Stewart. 1991. Hydrogeology of the Surficial Aquifer System, Dade County, Florida. U.S. Geological Survey (Water Resources Investigation Report 90-4108) in cooperation with the S.F.W.M.D. Tallahassee, FL.

Genereux, David and Jose D.A. Guardiario. 1995. *Hydraulic Conductivity Profiles in Six Frog Pond Boreholes*. Florida International University, Miami, FL.

Genereux, David and L.J. Nodarse & Associates. 1995. *Coring and Drilling Operations in the Frog Pond and Everglades National Park along L-31W Canal*. Gee & Jenson. West Palm Beach, FL.

U.S. Army Corps of Engineers (USACE). 1966. *Central and Southern Florida Project for Flood control and other purposes Part V, Coastal Areas South of St. Lucie Canal Supplement 44 - Detail Design Memorandum Levee 31(N), and Control Structures 173*. Jacksonville, FL.

U.S. Army Corps of Engineers (USACE). 1966. *Central and Southern Florida Project for Flood control and other purposes. Plans for Construction of L-31(N) Remainder and Canal 111 Section 3 Extension Structures 173 & 176*. Jacksonville, FL.

U.S. Army Corps of Engineers (USACE). 1976. *Central and Southern Florida Project for Flood control and other purposes. Plans for Construction of L-31(N) Borrow Canal Enlargement*. Jacksonville, FL.

U.S. Army Corps of Engineers (USACE). 2004. *L-31 North Canal Drawdown Test – L-31 North Canal Dry Season Test: May 24, 2004 to May 28, 2004*. Draft Technical Memorandum. Jacksonville, FL.

L-33

Fish, Johnnie. 1988. *Hydrogeology, Aquifer Characteristics, and Ground-Water Flow of the Surficial Aquifer System, Broward County, Florida*. U.S. Geological Survey (Water-Resources Investigation Report 87-4034) in cooperation with S.F.W.M.D. Tallahassee, FL.

U.S. Army Corps of Engineers. January 1951. *Central and Southern Florida Project for Flood Control and Other Purposes First Phase Levee L-33 and L-37*. Jacksonville, FL.

L-35

Broward County, Department of Planning and environmental Protection (DPEP), December 2001. *Modeling Water Management Practices in Central Broward County, Florida. Numerical Model Development and Calibration of the Pilot Area*. Fort Lauderdale, FL.

Fish, Johnnie. 1988. *Hydrogeology, Aquifer Characteristics, and Ground-Water Flow of the Surficial Aquifer System, Broward County, Florida*. U.S. Geological Survey (USGS) in cooperation with S.F.W.M.D. Water-Resources Investigation Report 87-4034. Tallahassee, FL.

Swayze, Leo J. 1988. U.S. Geological Survey (USGS)/S.F.W.M.D. *Ground- Water Flow Beneath Levee 35A From Conservation Area 2B, Broward County, Florida*.

U.S. Army Corps of Engineers (USACE). January 1949. *Central and Southern Florida Project for Flood Control and Other Purposes First Phase Levee L-35A Right-of-Way*. Jacksonville, FL.

L-36

Broward County Department of Planning and Environmental Protection, October, 2000. *Task 4 Report for Contract # C-3126, Component 5: Investigation of Surface Water Management Strategies to Optimize Water Supply Benefits in Northern Broward County, Florida*.

Fish, Johnnie. 1988. *Hydrogeology, Aquifer Characteristics, and Ground-Water Flow of the Surficial Aquifer System, Broward County, Florida*. U.S. Geological Survey (Water-Resources Investigation Report 87-4034) in cooperation with S.F.W.M.D. Tallahassee, FL.

U.S. Army Corps of Engineers (USACE). January 1950. *Central and Southern Florida Project for Flood Control and Other Purposes First Phase Levee 36*. Jacksonville, FL

L-37

Fish, Johnnie. 1988. *Hydrogeology, Aquifer Characteristics, and Ground-Water Flow of the Surficial Aquifer System, Broward County, Florida*. U.S. Geological Survey (USGS) in cooperation with S.F.W.M.D. Water-Resources Investigation Report 87-4034 Tallahassee, FL.

U.S. Army Corps of Engineers (USACE). January 1951. *Central and Southern Florida Project for Flood Control and Other Purposes First Phase Levee L-37 and L-37*. Jacksonville, FL.

L-38

Fish, Johnnie. 1988. *Hydrogeology, Aquifer Characteristics, and Ground-Water Flow of the Surficial Aquifer System, Broward County, Florida*. U.S. Geological Survey (USGS) in cooperation with S.F.W.M.D. Water-Resources Investigation Report 87-4034. Tallahassee, FL.

U.S. Army Corps of Engineers (USACE). 1978. *Central and Southern Florida Project for Flood Control and Other Purposes, Part 1, Agricultural and Conservation Areas, Supplement 51 – General and Detail Design Memorandum, L-18 and L-19 (North New River Canal) L-24 and L-25 (Miami Canal) Hump Removal*. Jacksonville, FL.

U.S. Army Corps of Engineers (USACE). 1965 (As-Built Stamp 1967). *Central and Southern Florida Project for Flood Control and Other Purposes, Levee-38 (West) Section 1*. Jacksonville, FL.

U.S. Army Corps of Engineers (USACE). 1965. *Central and Southern Florida Project for Flood Control and Other Purposes, Part 1, Agricultural and Conservation Areas, Supplement 42 – Detail Design Memorandum, Levee 38 (West), Section 1*. Jacksonville, FL.

U.S. Army Corps of Engineers (USACE). 1959 (As-Built Stamp 1961). *Central and Southern Florida Project for Flood Control and Other Purposes, Levee-38 (East) Section 1*. Jacksonville, FL.

U.S. Army Corps of Engineers (USACE). 1958. *Central and Southern Florida Project for Flood Control and Other Purposes, Part 1, Agricultural and Conservation Areas, Supplement 28 – Detail Design Memorandum, Levee 38 (East), Section 1*. Jacksonville, FL.

U.S. Army Corps of Engineers (USACE). 1953. *Central and Southern Florida Project for Flood Control and Other Purpose, Part I, Agricultural and Conservation Areas, Supplement 7 – Design Memorandum Permeability Investigations by Well – Pumping Tests*. Jacksonville, FL.

L-40 (Northern Reach)

Bennett, Michael W., Linton, Paul F., Rectenwald, E. Edward. 2002. *Hydrogeologic Investigation of the Floridan Aquifer System Western Hillsboro Basin, Palm Beach County, Florida*. South Florida Water Management District (SFWMD). Technical Publication WS-8. West Palm Beach, FL.

Rohrer, P.R., *Hydrogeologic Characterization and Estimation of Ground Water Seepage in the Everglades Nutrient Removal Project*. 1999. South Florida Water Management District (SFWMD) Technical Publication WRE # 372. West Palm Beach, FL.

Scott, W. B. 1977. *Hydraulic Conductivity and Water Quality of the Shallow Aquifer, Palm Beach County, Florida*. U.S. Geological Survey (USGS). Water Investigations Report 76-119. Tallahassee, FL.

South Florida Water Management District [cited March 2004]. *Geographic Information Systems (GIS) coverages and database for the Water Preserve Areas Feasibility Study using the South Palm Beach Model. 2000-2002*. In GIS and text files [database on server]. West Palm Beach, FL.

L-40 (Southern Reach)

Bennett, Michael W., Linton, Paul F., Rectenwald, E. Edward. 2002. *Hydrogeologic Investigation of the Floridan Aquifer System Western Hillsboro Basin, Palm Beach County, Florida*. South Florida Water Management District (SFWMD). Technical Publication WS-8. West Palm Beach, FL.

Rohrer, P.R., *Hydrogeologic Characterization and Estimation of Ground Water Seepage in the Everglades Nutrient Removal Project*. 1999. South Florida Water Management District (SFWMD) Technical Publication WRE # 372. West Palm Beach, FL.

Scott, W. B. 1977. *Hydraulic Conductivity and Water Quality of the Shallow Aquifer, Palm Beach County, Florida*. U.S. Geological Survey (USGS). Water Investigations Report 76-119. Tallahassee, FL.

South Florida Water Management District [cited March 2004]. *Geographic Information Systems (GIS) coverages and database for the Water Preserve Areas Feasibility Study using the South Palm Beach Model. 2000-2002*. In GIS and text files [database on server]. West Palm Beach, FL.

Swayze, Leo, McGovern, Michael, and Fischer, John. 1981. *Lithologic Logs and Geophysical Logs from Test Drilling in Palm Beach County, Florida, since 1974*. United States Geological Survey (USGS) in cooperation with Palm Beach County and the S.F.W.M.D. Open-File Report 81-68.

U.S. Army Corps of Engineers (USACE). 2003. North Palm CERP Project. Jacksonville, FL.

U.S. Army Corps of Engineers (USACE). 1972. *Central and Southern Florida Project for Flood Control and other Purposes, Part 1, Agricultural and Conservation Areas Supplement 49 – General and Detail Design Memorandum Modification of Levees 7, 35B, and 38, Section 2 (U.S. Highway 27 – Between Structures 11A and 11C and Deletion of Canal 302)*. Jacksonville, FL.

U.S. Army Corps of Engineers (USACE). 1955. *Central and Southern Florida Project for Flood Control and other Purposes Levee 7*. Jacksonville, FL.

U.S. Army Corps of Engineers (USACE). 1951. *Central and Southern Florida Project for Flood Control and other Purposes First Phase Levee 40*. Jacksonville, FL.

Other References

Doherty, J. E. 2004. *PEST Model-Independent Parameter Estimation, User's Manual: 5th edition*. Watermark Numerical Computing, Brisbane, Australia, 336 pp.

Kelson, Victor A. 2000. *Practical Advances in Groundwater Flow Modeling with Analytic Elements*. Ph.D Thesis, Indiana University.

Kelson, V. A., M. M. Wilsnack and D. J. Dahlstrom. 2006. Using an Analytic Element Cross-Sectional Model and PEST to Develop Seepage Coefficients for the South Florida Regional Simulation Model. *Proceedings of MODFLOW and More 2006*, Golden, Colorado, pp. 310-314.

Haitjema, H. M. 1995. *Analytic Element Modeling of Groundwater Flow*, ISBN 0-12-316550-4, Academic Press, Inc. San Diego.

Haitjema, H. M. and M. M. Wilsnack. 2006. Truncating Cross Sectional Models Under Wetlands. Proceedings of MODFLOW and More 2006, Golden, Colorado, p. 750.

Lal, A. M. W. 2005. Regional Simulation Model (RSM) User's Manual, Part I of III : Hydrologic Simulation Engine Components. South Florida Water Management District, Office of Modeling, West Palm Beach, Florida, 295 pp.

Shea, P. H. and H. E. Whitsett. 1958. Predicting Seepage Under Dams on Multi-Layered Foundations. Journal of the Soil Mechanics and Foundations Division, Proceedings of the American Society of Civil Engineers, 84(3), pp. 1727.1 – 1727.39.

Strack, Otto D. L. 1989. Groundwater Mechanics. Prentice hall, Englewood Cliffs, NJ.

Appendix A. Development of a Closed-Form Solution to the Initial Test Problem

This appendix presents the derivation of an analytic solution to ground water flow within the system depicted in figure 2. While assuming that flow is strictly horizontal in each of the aquifer layers and strictly vertical through the restrictive layers, Shea and Whitsett (1958) define the hydraulic properties of the ground water flow system as follows:

- K_1 = the vertical hydraulic conductivity of the top blanket underlying the ponded surface water
- K_2 = the horizontal hydraulic conductivity of the upper transmissive zone
- K_3 = the vertical hydraulic conductivity of the middle blanket
- K_4 = the horizontal hydraulic conductivity of the bottom transmissive zone

- Z_1 = the thickness of the top blanket underlying the ponded surface water
- Z_2 = the thickness of the upper transmissive zone
- Z_3 = the thickness of the middle blanket
- Z_4 = the thickness of the bottom transmissive zone

- h_0 = the hydraulic head of the ponded surface water
- h_2 = the hydraulic head within the upper transmissive zone
- h_4 = the hydraulic head within the lower transmissive zone

To facilitate computations, Shea and Whitsett (1958) define the following parameters:

$$C_1 = K_1 / Z_1 \quad C_2 = K_2 Z_2 \quad C_3 = K_3 / Z_3 \quad C_4 = K_4 Z_4$$

$$\alpha_{12} = C_1 / C_2 \quad \alpha_{32} = C_3 / C_2 \quad \alpha_{34} = C_3 / C_4$$

$$a = \alpha_{12} + \alpha_{32} + \alpha_{34} \quad b = \alpha_{12} \alpha_{34}$$

$$f^2 = \frac{a + \sqrt{a^2 - 4b}}{2} \quad g^2 = \frac{a - \sqrt{a^2 - 4b}}{2}$$

$$j = \frac{\alpha_{12} + \alpha_{32} - f^2}{\alpha_{32}} \quad m = \frac{\alpha_{12} + \alpha_{32} - g^2}{\alpha_{32}}$$

$$s = -C_2 / C_4$$

For horizontal ground water flow within a two-layered leaky system that is overlain by surface water, Shea and Whitsett (1958) showed that the governing differential equations are

$$\frac{d^2 h_2}{dx^2} - \alpha_{12} h_2 + \alpha_{32} (h_4 - h_2) = 0 \dots\dots\dots (a1a)$$

$$\frac{d^2 h_4}{dx^2} - \alpha_{34} (h_4 - h_2) = 0 \dots\dots\dots (a1b)$$

The general solution to the system of differential equations given by equations (a1) is (Shea and Whitsett, 1958, p. 19)

$$h_2 = h_o - M_1e^{fx} - M_2e^{-fx} - M_3e^{gx} - M_4e^{-gx} \dots\dots\dots (a2a)$$

$$h_4 = h_o - jM_1e^{fx} - jM_2e^{-fx} - mM_3e^{gx} - mM_4e^{-gx} \dots\dots\dots (a2b)$$

It should be recalled that $x = 0$ at the downstream end of the ground water flow system. It is intuitive that at a large distance from the downstream end, the ground water heads should be nearly equal to the surface water head. Mathematically, this implies that

$$\lim_{x \rightarrow \infty} h_2(x) = \lim_{x \rightarrow \infty} h_4(x) = h_o \dots\dots\dots (a3)$$

Equation (a3) implies that $M_1 = M_3 = 0$ in equations (a2). Hence,

$$h_2 = h_o - M_2e^{-fx} - M_4e^{-gx} \dots\dots\dots (a4)$$

$$h_4 = h_o - jM_2e^{-fx} - mM_4e^{-gx} \dots\dots\dots (a5)$$

In addition, specifying a Dirichlet boundary condition at $x = 0$ allows one to write

$$h_2(0) = h_{2b} \dots\dots\dots (a6)$$

From equations (a4) and (a6) it follows that

$$M_2 + M_4 = h_o - h_{2b} \dots\dots\dots (a7)$$

Applying the same logic to layer 4 results in

$$jM_2 + mM_4 = h_o - h_{4b} \dots\dots\dots (a8)$$

Solving equations (a7) and (a8) yields

$$M_2 = \frac{(m-1)h_o - mh_{2b} + h_{4b}}{(m-j)} \dots\dots\dots (a9)$$

$$M_4 = \frac{(1-j)h_o + jh_{2b} - h_{4b}}{(m-j)} \dots\dots\dots (a10)$$

Appendix B. Methodology for Levee Seepage Sensitivity Analysis

Prepared by
Wittman Hydro Planning Associates, Inc.
Bloomington, Indiana
4th March 2005

Modified by
Mark M Wilsnack, David E Welter
SFWMD
February, 2008

Contents

B1 Introduction	129
B2 Approach	129
B2.1 Inverse modeling	129
B2.2 Predictive analysis	131
B2.2.1 Basis for the method	131
B2.2.2 Levee seepage application	133
B3 Conclusions	134
B4 References	134

B1 Introduction

This report describes the approach used in sensitivity analysis of the ModAEM models of levee seepage. The objective of this study was to determine the range of predicted seepage beneath the levee that could be expected given the specified uncertainty in the model parameters.

B2 Approach

Each conceptual model includes a table of ranges of hydraulic conductivity values for the model layers. Properties such as hydraulic conductivity tend to be log normally distributed in nature so the geometric mean of the range of values was assumed to be the expected value for each layer (see Table B1). In logarithmic space (base 10), the range is assumed to represent the mean plus and minus two standard deviations ($\mu \pm 2\sigma$).

Table B1: Values used in the sensitivity analysis for the L-29 model

Layer	Minimum	Geometric Mean	Maximum	$\log_{10}(\min)$	$\log_{10}(\max)$	$2\log_{10}(\sigma)$	Weight = $1/\log_{10}(\sigma)$
	0.1	1	10	-1	1	1	2
	100	316.2	1000	2	3	0.5	4
	0.1	1	10	-1	1	1	2
	10	31.62	100	1	2	0.5	4
	0.1	1	10	-1	1	1	2
	100	316.2	1000	2	3	0.5	4

B2.1 Inverse modeling

The parameter estimation software package PEST [Doherty, 2004] was applied to this problem. PEST uses a modified Gauss-Marquardt-Levenberg method of nonlinear least squares to determine a parameter set that minimizes the differences between observed and modeled values. These differences (residuals) are summarized as the objective function (Φ) which is a scalar value that PEST seeks to minimize during a typical parameter estimation run; Φ is defined in Equation B1.

$$\Phi = \sum_{i=1}^m [(o_i - c_i)w_i]^2 \quad (\text{B1})$$

where:

m is the number of observations used in the calibration

o_i is an observation consisting of a measured or estimated value the model is being used to simulate

c_i is the corresponding modeled value

$o_i - c_i$ is the error associated with observation i

w_i is the weight associated with observation i .

The current application differs from most hydrologic inverse models in that no measured groundwater levels or fluxes are used in the calibration. Instead, the mean values from the conceptual model are treated as independent estimates of parameter values. In inverse modeling, this is known as *prior information*, which is treated like additional observations. Weighted errors in this case are the difference between the logarithm of the currently modeled parameter value (p_i) and the logarithm of its geometric mean (\underline{x}_i) (Equation B2).

$$w_i (\log_{10}(p_i) - \log_{10}(\underline{x}_i)) \quad (\text{B2})$$

The weight assigned to the article of prior information regarding parameter i is defined by Equation B3.

$$w_i = \log_{10}^{-1}(\sigma_i) \quad (\text{B3})$$

Based on the assumptions described in Section 2, if a parameter is at the either limit of its range as specified in the conceptual model, it is two standard deviations away from its mean value (see Equation B4). Plugging Equation B4 and the definition for the weight in Equation B3 into Equation B2 yields Equation B5, which states that when parameter p_i is at either limit of its range, the contribution to the objective function (Φ) equals 4. If all parameters are at their mean values, the objective function is zero.

$$\log_{10}(p_i) - \log_{10}(\underline{x}_i) = \pm 2 \log_{10}(\sigma_i) \quad (\text{B4})$$

$$(\pm \log_{10}(\sigma_i) / \log_{10}(\sigma_i))^2 = 4 \quad (\text{B5})$$

If an inverse modeling application includes more observations than parameters, which is typically the case, it is referred to as over-determined. Under-determined applications have fewer

observations than parameters. Strategies exist for solving both classes of problems (for example, see [Aster and Thurber, 2004]). PEST is typically applied to over-determined problems. In our application, we have an equal number of observations and parameters. The parameter set that minimizes Φ for this problem has each parameter at its mean value; in this case, $\Phi = 0$. Calibration is unnecessary for this problem.

B2.2 Predictive analysis

In addition to calibration, PEST also performs predictive analysis by which the impact of model parameter uncertainty on model predictions is determined. This technique is more meaningful than standard methods for sensitivity analysis because it accounts for parameter correlation and applies information from the conceptual model and model calibration to determine confidence levels. The general method and its specific application to the levee seepage question are described below.

B2.2.1 Basis for the method

The user typically performs a model calibration to minimize Φ . In our case, the minimum is known by inspection to be $\Phi_{min} = 0$. Figure B1 shows a typical contour plot of the objective function for a two-parameter problem. In general, the surface has a minimum that lies within an

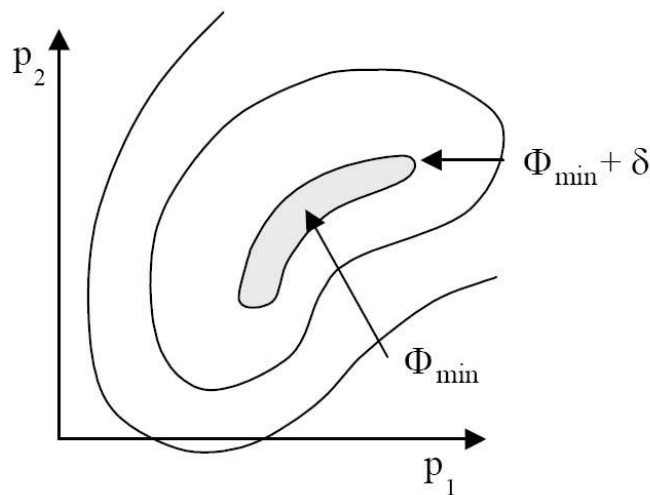


Figure B1: Contours of equal objective function value for a two-parameter model (from Doherty, 2004)

elongated “trough”. The value of Φ typically shows little variation along the axis of this trough. The user specifies an increment to the objective function δ , which is a statistically derived

number based for example on an F test or χ^2 -test. The purpose of this increment is to define a value for the objective function $\Phi_{min} + \delta$ that represents a specific uncertainty associated with the model calibration. The shaded area on Figure 1 is the region of parameter space defined by the Equation B6.

$$\Phi_{min} \leq \Phi \leq \Phi_{min} + \delta \quad (\text{B6})$$

Predictive analysis is performed on a model prediction that is not included in the calculation of Φ . In this example the prediction is the amount of seepage beneath the levee. Contours of values of this independent prediction as a function of parameters p_1 and p_2 are shown conceptually on Figure B2. The analysis consists of finding the combination of parameters that lies within the shaded area of Figure B1 and either maximizes or minimizes the value of an independent model prediction. This point is known as the “critical point”. An example showing maximization of the independent prediction is shown on Figure B3.

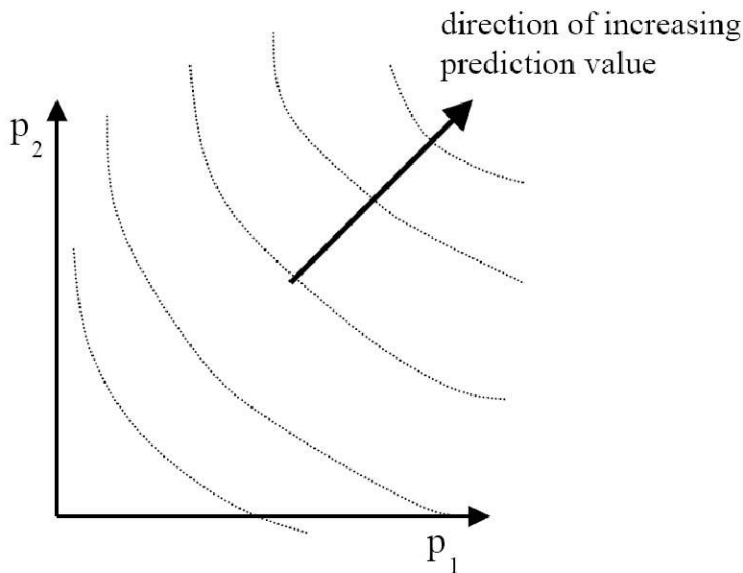


Figure B2: Contours of a model prediction in parameter space (from Doherty, 2004)

This appears simple enough for a two-parameter problem. The conceptual models for this project include 5 to 12 parameters. An infinite number of combinations of parameter values occur within the δ -“contour” for these problems. Without a strategy to actively seek the critical point, thousands of model runs would be required to approximately locate the critical point with any confidence.

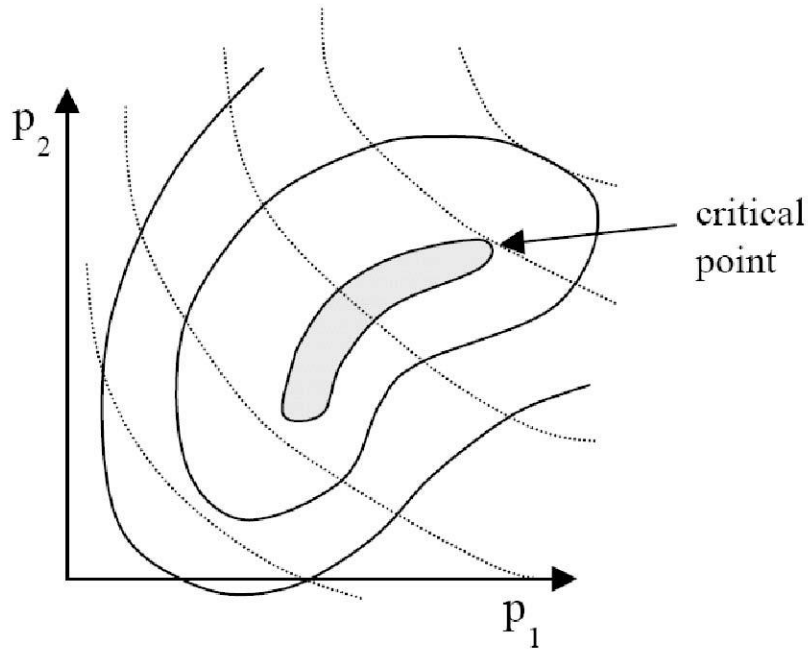


Figure B3: The critical point in parameter space (from Doherty, 2004)

B2.2.2 Levee seepage application

In the predictive analysis based model runs performed by WHPA, it was later discovered that the maximum allowable value of the objective function was set to a value of 2.61 instead of 4.0 as established above. Additionally, the individual weights were set to one half of their correct values. This naturally raises the question as to what confidence interval was actually established for the minimum and maximum seepage rates along with their associated seepage coefficients. This can be addressed as follows.

To apply the concepts discussed above to the analysis performed by WHPA, it is necessary to start with the $\Phi = 2.61$ and back calculate the standard Z-Score and associated confidence interval. From equation (1), it is apparent that a factor of 2 error in the weighting function will translate to a factor of 4 error in the objective function Φ . Thus, before calculating the Z-score and confidence interval associated with $\Phi = 2.61$, this value must first be corrected by dividing it by 4. Applying this correction yields $\Phi = .6525$. Since, by definition, Φ is the square of the standard Z-score, $Z = .808$. Using the normal probability tables we can calculate:

$$P[z > .808] = 1 - .8106 = 0.1894$$

$$P[-.808 \leq z \leq .808] = 1 - 2(0.1894) = .62 = 62\%$$

Hence, a value of $\Phi = 2.61$ along with the incorrect weights used in the predictive analysis simulations results in a 62% confidence interval for the seepage coefficients associated with minimum and maximum seepage rates. So, there is a 42% chance that the levee seepage coefficients will lay outside of this interval. This implies that the limiting values are slightly less

than one standard deviation away from the mean value. Whether or not this is acceptable depends on the intended application of these seepage coefficients. It should be recalled that the confidence interval limits are intended to serve as bounds for these parameters during calibration of the RSM. Allowing them to vary only within a 62% confidence interval instead of within the conventional 95% confidence interval is therefore conservative in regards to avoiding unrealistic parameter values. Consequently, it was decided that the specified ranges for the levee seepage coefficients would be used as bounds for these parameters during calibration of the RSM.

Appendix F provides a comprehensive discussion on predictive confidence limits as implemented in this effort.

B3 Conclusions

Predictive analysis allows one to investigate the effects of parameter correlation on prediction uncertainty in a much more meaningful way than standard sensitivity analyses. Parameter correlation with respect to a given prediction can occur when two parameters can be varied in concert in a way that has little or no net affect on the objective function, but has a relatively large affect on the value of the observation. An elongated trough such as that shown in Figure B3 is a reflection of parameter correlation. An independent observation that varies substantially along the trough on the Φ - surface as shown conceptually on Figure B3 is an observation that will have a large predictive confidence interval.

B4 References

- [Aster and Thurber, 2004] Aster, R., B. B. and Thurber, C. (2004). *Parameter Estimation and Inverse Problems*. Elsevier Academic Press, first edition.
- [Doherty, 2004] Doherty, J. (2004). PEST -model-independent parameter estimation user manual. Software manual.

Appendix C

A Comparison of the Analytic Element Method to an Analytic Solution to Ground Water Flow under L-29, Section 1

Table of Contents

C1. Introduction and Purpose	
C2. Conceptual Model	
C3. Analytic Element Model	
C4. Comparison to an Analytic Solution	

C1. Introduction and Purpose

As a follow-up to the simple verification test presented in sections 2.1 and 2.2 of the report, a more rigorous check of the use of analytic element modeling to simulate ground water flow under levees is presented here. Preliminary conceptual and analytic element models of L-29, Section 1 were constructed for testing purposes. These models were later refined as discussed in Section 3.0 of the report.

C2. Conceptual Model

Figure C1 depicts the conceptual cross section of the levees and borrow canals located along section 1 of the L-29 corridor. Included in the initial conceptual model are the L-29 levee itself along with the U.S. 41 highway embankment, the L-29 borrow canal and the Tamiami canal. The dimensions shown were estimated from as-built drawings or DOQQ images. Also shown in figure C1 is a conceptualization of the hydrostratigraphy within the surficial aquifer. In particular, the hydrogeologic properties were derived from the interpretive information provided by Fish and Stewart (1991) for lithologic control well G-3301. Table C1 lists the properties of each layer that were assigned to the model while table C2 provides the cross sectional properties of the borrow canals. It should be kept in mind that there is considerable uncertainty in the hydraulic conductivity and layer thickness values shown in figure C1. Furthermore, local anomalies are not represented. Nonetheless, the conceptualization is considered to be adequate for the intended purpose.

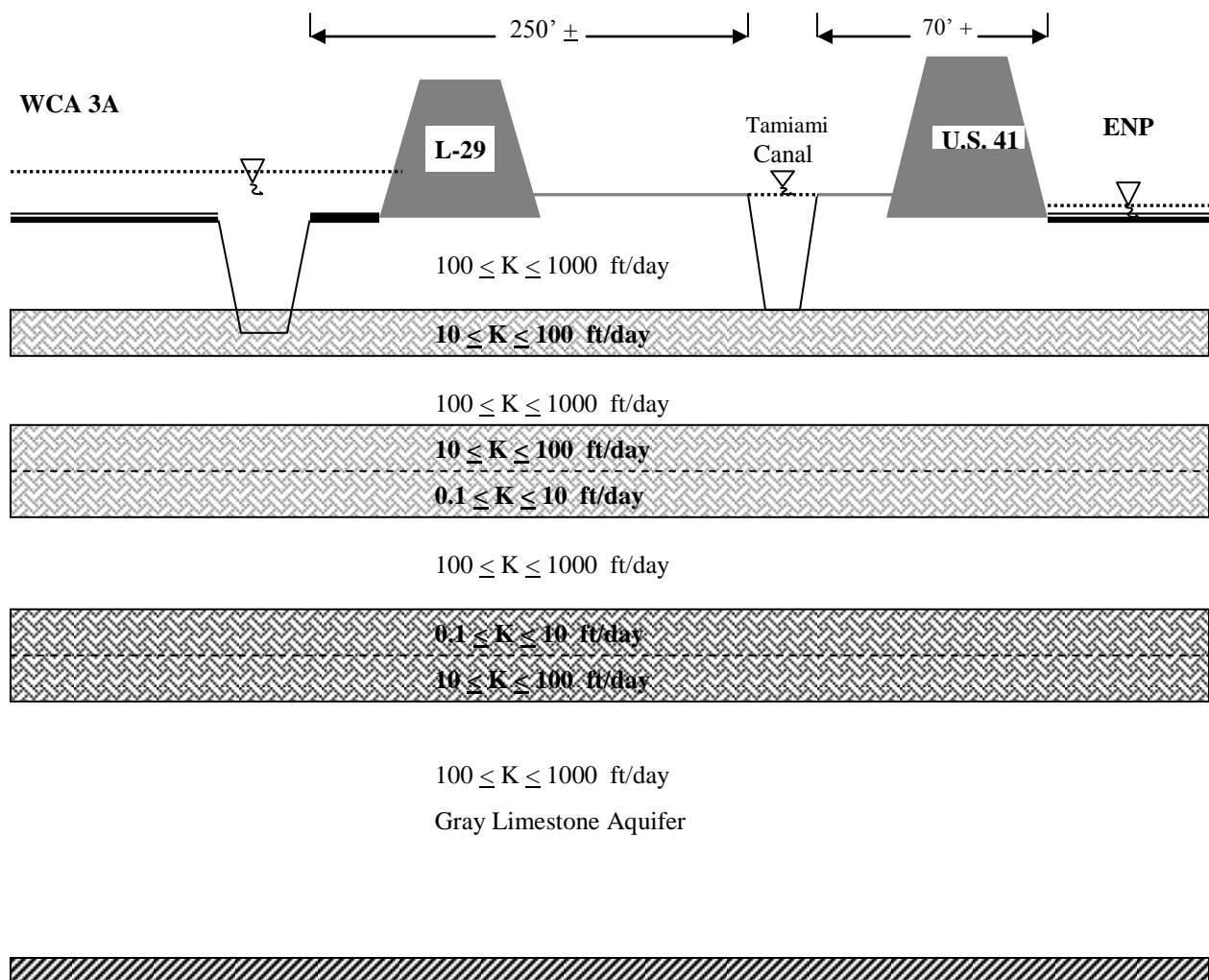


Figure C1. Conceptualization of the levees, canals and shallow hydrostratigraphy along section 1 of the L-29 corridor (N.T.S.)

C3. Analytic Element Model

The conceptual model described above was depicted in an analytic element model by representing the wetland bottoms as horizontal line sinks with appropriate stages and resistance values, the canal side walls as sloped line sinks with specified heads and no resistance, the canal bottoms as impervious flow barriers, and the aquatards as heterogeneities. In each flow zone, the hydraulic conductivity was set to the logarithmic mean of the minimum and maximum values shown. Furthermore, vertical line sinks were placed at the left and right boundaries to account

Table C1. Hydrogeologic parameters along L-29, section 1

Hydrostratigraphic Zone Number	Feature	K (ft/day)	Thickness (ft)
1	wetland bottom	10	4
2	first transmissive zone	300	10
3	first aquatard	30	8
4	second transmissive zone	300	5
5	second aquatard	10	16
6	third transmissive zone	300	8
7	third aquatard	10	24
8	third transmissive zone	300	68

for the inflow of ground water and surface water leakage from the surficial aquifer located outside of the model domain. The resistances of these line sinks were based on values of λ computed for each layer in the manner outlined by Haitjema (2004).

Sensitivity Analysis

The analytic element model of the conceptualized system shown in figure C1 was used to conduct the sensitivity analysis depicted in table C3. The base scenario was simulated using the aquifer parameters presented earlier. In all cases, the surface water stage in WCA-3A was set to 10 feet

Table C2. Canal cross section properties for L-29, section 1

Canal	Bottom Elevation (ft)	Bottom Width (ft)	Side Slope (z:1)
L-29 b.c.	-7	20	1
Tamiami	-7*	10*	1*

*approximate

while the stages in the Tamiami canal and the ENP were set to 9 and 8 feet, respectively. It is interesting to note that *under the specified conditions*, about 40% of the total leakage from WCA-3A originates from the borrow canal and about 54% passes under L-29 through the Gray Limestone aquifer. Furthermore, roughly 17% of the total leakage from WCA 3A is intercepted by the Tamiami canal while this canal supplies additional water to ENP through transmission losses along the southwestern bank. In the other scenarios, one parameter was varied at a time as shown.

Although somewhat simplistic, this sensitivity analysis demonstrates several important aspects of the ground water flow system. First, the relative insensitivity of the total discharge from WCA-3A to order of magnitude changes in hydraulic conductivity of the wetland bottom reflects the

Table C3. Sensitivity of ground water flows (ft²/day) to various parameters for L-29, section 1

Parameter Set	WCA 3A Outflow						Tamiami Canal		ENP Inflow			
	from wetland	Zone				Total	In (left)	Out (right)	Zone			Total
		2	4	6	8				4	6	8	
Base	41.9	17.3	6.3	6.5	37.3	69.4	11.7	35.6	4.2	7.9	44.3	93.4
aquifer K =100	20.4	6.8	2.5	2.7	16.2	30.6	3.7	16.5	1.2	3.1	21.0	43.4
aquifer K = 1000	89.6	50.3	17.7	16.4	83.3	169.5	41.0	83.3	15.0	20.2	91.6	211.7
blanket K = 10(top), 1(mid) 1(bottom)	29.7	15.6	5.4	4.3	18.0	43.7	13.2	34.5	5.7	5.6	18.9	65.0
blanket K = 100(top), 30(mid) 30(bottom)	43.3	17.5	7.1	7.9	47.2	86.7	12.6	40.4	3.1	8.1	58.9	114.6
wetland K = 1	20.5	14.6	6.0	6.0	31.9	60.3	14.7	15.0	2.7	5.5	36.3	60.6
wetland K = 100	63.9	21.5	6.5	6.5	38.7	75.2	11.9	48.6	5.3	9.2	47.1	112.0

previous observation that much of the surface water lost from WCA-3A passes through the borrow canal. In contrast, total inflow to the ENP appears to be sensitive to the hydraulic resistance of the wetland bottom within ENP. Hence, ground water / surface water interactions within ENP may be an important factor in determining total ground water inflow to the ENP along this levee. Total discharges from WCA-3A (and subsequent inflows to ENP) also appear to be sensitive to the hydraulic conductivities of the aquifers and, to a somewhat lesser degree, the aquatards (i.e. the blankets). This suggests that additional hydraulic conductivity data could help to significantly improve the accuracy of leakage estimates derived from the model. Moreover, the fact that the hydraulic conductivity values assigned to the aquatards appear to have a significant influence on leakage rates indicates that ground water flow near the levee / borrow canal configuration is three-dimensional and Dupuit – Forchheimer assumptions are therefore not appropriate.

C4. Comparison to an Analytic Solution

Prior applications of the analytic element method to the types of levee seepage analyses under consideration in this study are almost nonexistent. In contrast, closed-form analytic solutions have been used for decades to analyze seepage under embankments (see, for example, Harr, 1962). Although the application of the analytic element method to the type of seepage problem under consideration here was verified earlier (see Section 2.2) through a simple benchmark test, it would perhaps be appropriate to conduct a more realistic and rigorous test of the analytic element modeling approach prior to implementing it at various levee / aquifer cross sections within the SFWMD. Additionally, it seems natural to question the necessity of constructing analytic element models to analyze seepage under levee reaches if closed-form analytic solutions can be developed and applied. This would seem understandable given such a wide-spread use of closed-form analytic solutions over so many years. Therefore, an analytic solution was developed for the ground water flow system shown in figure C1 except that flow in only the top two transmissive zones was considered in order to keep the solution manageable. This solution, presented in the sections that follow, was used to compute ground water heads and flow rates that were compared to those obtained from an analytic element model constructed for the same reduced system.

C4.1 Derivation of the Analytic Solution

An analytic solution to the ground water flow system depicted in figure C1 was developed with only the top two aquifers and intermediate blanket considered. Hence, in this case the bottom of the ground water flow system is located at the top of hydrostratigraphic layer 5. While this does not reflect the entire ground water flow system in reality, it should be adequate for the purpose of comparing ground water heads and flows obtained by the analytic element method under the field conditions noted to those obtained from a corresponding closed form solution derived under the assumptions stated below. It was necessary to limit the number of horizontal flow zones to two in order to keep the analytic solution manageable.

The procedure applied in this effort required that the system be divided into three separate zones when proceeding from the upstream end to the downstream end. The first zone begins at the location of the southwestern (i.e. right) sidewall of the L-29 borrow canal and ends at the horizontal station of the northeastern (i.e. left) sidewall of the Tamiami canal (figure C2). Similarly, the second section begins at the southwestern sidewall of the Tamiami canal and ends at the downstream toe of the U.S. 41 embankment. Finally, the third zone begins at the U.S. 41 embankment and is assumed to extend infinitely far into the ENP. Additionally, the following assumptions were made:

- Flow within each aquifer is strictly horizontal while flow through the aquatards between the aquifers is strictly vertical.
- The channel side walls are completely open and vertical while leakage through the bottom is negligible
- The levees are impervious
- Within a given aquifer or aquatard, hydraulic conductivity is constant.

- Flow is steady state with specified stages in WCA-3A, each borrow canal and the ENP.

Given these assumptions, analytic solutions for each zone were developed independently using the procedures developed by Shea and Whitsett (1958). These solutions were then combined by considering continuity of head or flow at adjoining boundaries.

The nomenclature used by Shea and Whitsett (1958) to denote the hydraulic properties of the ground water flow system were presented previously in appendix A. For convenience, they are repeated here and are as follows:

K_1 = the vertical hydraulic conductivity of the top blanket underlying the ponded surface water
 K_2 = the horizontal hydraulic conductivity of the upper transmissive zone
 K_3 = the vertical hydraulic conductivity of the middle blanket
 K_4 = the horizontal hydraulic conductivity of the bottom transmissive zone

Z_1 = the thickness of the top blanket underlying the ponded surface water
 Z_2 = the thickness of the upper transmissive zone
 Z_3 = the thickness of the middle blanket
 Z_4 = the thickness of the bottom transmissive zone

h_0 = the hydraulic head of the ponded surface water
 h_2 = the hydraulic head within the upper transmissive zone
 h_4 = the hydraulic head within the lower transmissive zone

$$C_1 = K_1 / Z_1 \quad C_2 = K_2 Z_2 \quad C_3 = K_3 / Z_3 \quad C_4 = K_4 Z_4$$

$$\alpha_{12} = C_1 / C_2 \quad \alpha_{32} = C_3 / C_2 \quad \alpha_{34} = C_3 / C_4$$

$$a = \alpha_{12} + \alpha_{32} + \alpha_{34} \quad b = \alpha_{12} \alpha_{34}$$

$$f^2 = \frac{a + \sqrt{a^2 - 4b}}{2} \quad g^2 = \frac{a - \sqrt{a^2 - 4b}}{2}$$

$$j = \frac{\alpha_{12} + \alpha_{32} - f^2}{\alpha_{32}} \quad m = \frac{\alpha_{12} + \alpha_{32} - g^2}{\alpha_{32}}$$

$$s = -C_2 / C_4 \quad c = \sqrt{\alpha_{32} + \alpha_{34}}$$

Given these definitions along with the assumptions discussed above, the analytic solutions for the three zones underneath the levee / borrow canal configuration are derived in the following manner.

Zone 1 : Beneath the L-29 Levee

As mentioned previously, this portion of the ground water flow system begins at the L-29 borrow canal and ends at the Tamiami canal. Since it was assumed that no leakage occurs from above through the top blanket, leakage from the short strand of wetland located between the borrow canal and the levee (figure C2) was neglected. Under these circumstances, Shea and Whitsett (1958) demonstrate that the governing differential equations can be written as

$$\frac{d^2 h_2}{dx^2} + \alpha_{32}(h_4 - h_2) = 0 \quad \dots\dots\dots (1a)$$

$$\frac{d^2 h_4}{dx^2} - \alpha_{34}(h_4 - h_2) = 0 \quad \dots\dots\dots (1b)$$

where, in this case, x is taken to be 0 at upstream end of the zone. Solving equations (1) simultaneously yields the general solution (Shea and Whitsett, 1958, p. 21)

$$h_2 = R_{1A} + R_{2A}x + R_{3A}e^{cx} + R_{4A}e^{-cx} \quad \dots\dots\dots (2a)$$

$$h_4 = R_{1A} + R_{2A}x + sR_{3A}e^{cx} + sR_{4A}e^{-cx} \quad \dots\dots\dots (2b)$$

At $x = 0$, $h_2 \approx h_4 \approx h_{3A}$, the stage in WCA-3A. In addition, denoting the distance between the L-29 borrow canal and the Tamiami canal as L_{29} , it is readily apparent that at $x = L_{29}$, $h_2 = h_T$, the stage in the Tamiami canal, since it completely penetrates the upper aquifer. The discharge per unit transmissivity that passes under this canal within the lower aquifer can be denoted as q_{4T} . Applying the first three boundary conditions to equations (2) gives

$$h_{3A} = R_{1A} + R_{3A} + R_{4A} \quad \dots\dots\dots (3a)$$

$$h_T = R_{1A} + L_{29}R_{2A} + e^{cL_{29}}R_{3A} + e^{-cL_{29}}R_{4A} \quad \dots\dots\dots (3b)$$

$$h_{3A} = R_{1A} + R_{3A} + R_{4A} \quad \dots\dots\dots (3c)$$

A fourth equation can be written by applying Darcy's law within the bottom aquifer at the right boundary. Here, $q_{4T} = -dh_4 / dx$ at $x = L_{29}$, so

$$-q_{4T} = R_{2A} + scR_{3A}e^{cL_{29}} - scR_{4A}e^{-cL_{29}} \quad \dots\dots\dots (3d)$$

Solving equations (3) for R_{1A} , R_{2A} , R_{3A} , and R_{4A} yields

$$R_{1A} = h_{3A} \quad \dots\dots\dots (4a)$$

$$R_{2A} = \frac{sc(h_T + L_{29}q_{4T} - h_{3A})}{scL_{29} - \tanh(cL_{29})} - q_{4T} \quad \dots\dots\dots (4b)$$

$$R_{3A} = \frac{h_T + L_{29}q_{4T} - h_{3A}}{\sinh(cL_{29}) - scL_{29} \cosh(cL_{29})} \quad \dots\dots\dots (4c)$$

$$R_{4A} = -R_{3A} \dots\dots\dots (4d)$$

Hence,

$$h_2 = h_{3A} + R_{2A}x + R_{3A}\sinh(cx) \dots\dots\dots (5a)$$

$$h_4 = h_{3A} + R_{2A}x + sR_{3A}\sinh(cx) \dots\dots\dots (5b)$$

within zone 1. Equations (5) along with Darcy's law can be used to determine the total ground water discharge from WCA 3A and the portion of the total discharge that is intercepted by the Tamiami canal. The former can be stated as

$$Q_{3A} = -C_2 \frac{dh_2}{dx}(0) - C_4 \frac{dh_4}{dx}(0) = -(C_2 + C_4)R_{2A} - (C_2 + sC_4)cR_{3A} \dots\dots(6)$$

while the latter is

$$Q_{TW} = -C_2 \frac{dh_2}{dx}(L_{29}) = -C_2(R_{2A} + cR_{3A} \cosh(cL_{29})) \dots\dots\dots (7)$$

Similarly, the flow rate passing under the Tamiami canal can be computed from

$$Q_{4T} = -C_4 \frac{dh_4}{dx}(L_{29}) = -C_4(R_{2A} + csR_{3A} \cosh(cL_{29})) \dots\dots\dots (8)$$

Zone 2 : Beneath U.S. 41

Applying the general solution to the system of governing differential equations (1) given by equations (2) yields

$$h_2 = R_{1T} + R_{2T}x + R_{3T}e^{cx} + R_{4T}e^{-cx} \dots\dots\dots (9a)$$

$$h_4 = R_{1T} + R_{2T}x + sR_{3T}e^{cx} + sR_{4T}e^{-cx} \dots\dots\dots (9b)$$

Within this zone, $x = 0$ at the right side of the Tamiami canal. It is apparent that at $x = 0$, $h_2 = h_T$ and $q_{4T} = -dh_4/dx$. At $x = L_{41}$, the width of the U.S. 41 highway embankment, $h_2 = \phi_{2e}$, the unknown value of head within the upper aquifer at the upstream end of ENP. Similarly, in the lower aquifer at this location, $h_4 = \phi_{4e}$. Applying these four boundary conditions to equations (9) results in

$$h_T = R_{1T} + R_{3T} + R_{4T} \dots\dots\dots (10a)$$

$$\phi_{2e} = R_{1T} + L_{41}R_{2T} + e^{cL_{41}}R_{3T} + e^{-cL_{41}}R_{4T} \dots\dots\dots (10b)$$

$$\phi_{4e} = R_{1T} + L_{41}R_{2T} + se^{cL_{41}}R_{3T} + se^{-cL_{41}}R_{4T} \dots\dots\dots(10c)$$

$$-q_{4T} = R_{2T} + scR_{3T} - scR_{4T} \dots\dots\dots (10d)$$

Solving equations (10) yields

$$R_{4T} = \frac{(\phi_{4e} - \phi_{2e})(scL_{41} + 1 - e^{cL_{41}})e^{-cL_{41}} + (s-1)(L_{41}q_{4T} + \phi_{2e} - h_T)}{(s-1)\left\{e^{-2cL_{41}}(scL_{41} + 1 - e^{cL_{41}}) + scL_{41} - 1 + e^{-cL_{41}}\right\}} \dots\dots\dots (11a)$$

$$R_{3T} = \frac{L_{41}q_{4T} + \phi_{2e} - h_T - R_{4T}(e^{-cL_{41}} + scL_{41} - 1)}{e^{cL_{41}} - scL_{41} - 1} \dots\dots\dots (11b)$$

$$R_{2T} = \frac{\phi_{2e} - h_T + (1 - e^{cL_{41}})R_{3T} + (1 - e^{-cL_{41}})R_{4T}}{L_{41}} \dots\dots\dots (11c)$$

$$R_{1T} = h_T - R_{3T} - R_{4T} \dots\dots\dots (11d)$$

From Darcy's law, the leakage from the southwest side of the Tamiami canal is given by

$$Q_{T_{East}} = -C_2 \frac{dh_2}{dx}(0) = C_2 [c(R_{4T} - R_{3T}) - R_{2T}] \dots\dots\dots (12)$$

Zone 3 : Beneath the ENP

For horizontal ground water flow within a two-layered leaky system that is overlain by surface water, Shea and Whitsett (1958) showed that the governing differential equations are the same as equations (1) except that in the upper aquifer equation (1a) becomes

$$\frac{d^2 h_2}{dx^2} - \alpha_{12} h_2 + \alpha_{32} (h_4 - h_2) = 0 \dots\dots\dots (13)$$

in order to account for vertical leakage from surface water. The general solution to the system of differential equations given by (13) and (1b) is (Shea and Whitsett, 1958, p. 19)

$$h_2 = h_e - M_1 e^{fx} - M_2 e^{-fx} - M_3 e^{gx} - M_4 e^{-gx} \dots\dots\dots (14a)$$

$$h_4 = h_e - jM_1 e^{fx} - jM_2 e^{-fx} - mM_3 e^{gx} - mM_4 e^{-gx} \dots\dots\dots (14b)$$

where h_e is the hydraulic head of the ponded surface water. Here, $x = 0$ at the downstream toe of the highway embankment. It is intuitive that at a large distance from the highway, the ground water heads should be nearly equal to the surface water head. Mathematically, this indicates that

$$\lim_{x \rightarrow \infty} h_2(x) = \lim_{x \rightarrow \infty} h_4(x) = h_e \quad \dots\dots\dots (15)$$

Equation (15) implies that $M_1 = M_3 = 0$ in equations (14). In addition, given the downstream boundary conditions for zone 2 it is apparent that $h_2 = \phi_{2e}$ and $h_4 = \phi_{4e}$ at $x = 0$. Incorporating these boundary conditions along with equation (15) into equations (14) gives

$$M_2 + M_4 = h_e - \phi_{2e} \quad \dots\dots\dots (16a)$$

$$jM_2 + mM_4 = h_e - \phi_{4e} \quad \dots\dots\dots (16b)$$

Solving equations (16) for M_2 and M_4 yields

$$M_2 = \frac{(1 - m)h_e + m\phi_{2e} - \phi_{4e}}{j - m} \quad \dots\dots\dots (17a)$$

$$M_4 = \frac{(j - 1)h_e - j\phi_{2e} + \phi_{4e}}{j - m} \quad \dots\dots\dots (17b)$$

Thus, the heads within the aquifer layers within zone 3 are given by

$$h_2 = h_e - M_2e^{-fx} - M_4e^{-gx} \quad \dots\dots\dots (18a)$$

$$h_4 = h_e - jM_2e^{-fx} - mM_4e^{-gx} \quad \dots\dots\dots (18b)$$

Finally, the total ground water discharge into ENP from underneath U.S. 41 is

$$Q_e = -C_2 \frac{dh_2}{dx}(0) - C_4 \frac{dh_4}{dx}(0) = -C_2 (fM_2 + gM_4) - C_4 (jfM_2 + gmM_4) \quad \dots\dots\dots (19)$$

Composite Solution

At this point, the analytic solution to ground water flow within the entire system is not yet complete because the values of q_{4T} , ϕ_{2e} , and ϕ_{4e} are still unknown. These quantities can be determined by considering continuity of flow at the various zone boundaries. For instance, within the upper aquifer at the boundary between zones two and three, the flux out of zone two is the same as the flux into zone 3, so

$$\frac{dh_2}{dx}(L_{41})|_{Zone2} = \frac{dh_2}{dx}(0)|_{Zone3}$$

Substituting equations (9a) and (11) into the above expression and arranging terms leads to

$$\begin{aligned} & \left[\Gamma \left(\frac{s-1-\gamma e^{-cL_{41}}}{\beta} \right) + \frac{1}{L_{41}} - \frac{\tau}{\gamma} + \frac{jg-fm}{j-m} \right] \varphi_{2e} + \left[\frac{\gamma \Gamma e^{-cL_{41}}}{\beta} + \frac{f-g}{j-m} \right] \varphi_{4e} + \left[\frac{\Gamma(s-1)}{\beta} - \frac{\tau}{\gamma} \right] L_{41} q_{4T} \\ & = \left[\frac{1}{L_{41}} - \frac{\tau}{\gamma} + \frac{\Gamma(s-1)}{\beta} \right] h_T + \left[\frac{(1-m)f + (j-1)g}{j-m} \right] h_e \end{aligned} \quad \dots\dots\dots (20)$$

where

$$\gamma = scL_{41} + 1 - e^{cL_{41}} \quad \dots\dots\dots (21a)$$

$$\beta = (s-1)[e^{-2cL_{41}}(scL_{41} + 1 - e^{cL_{41}}) + scL_{41} - 1 + e^{-cL_{41}}] \quad \dots\dots\dots (21b)$$

$$\tau = \frac{(cL_{41} - 1)e^{cL_{41}} + 1}{L_{41}} \quad \dots\dots\dots (21c)$$

$$\Gamma = \frac{1 - (1 + cL_{41})e^{-cL_{41}}}{L_{41}} + \frac{\gamma'}{\gamma} \quad \dots\dots\dots (21d)$$

$$\gamma' = scL_{41} - 1 + e^{-cL_{41}} \quad \dots\dots\dots (21e)$$

Similarly, applying the same logic at the boundary of zones 2 and 3 within the lower aquifer layer and repeating the same steps results in

$$\begin{aligned} & \left[\Gamma_s \left(\frac{s-1-\gamma_s e^{-cL_{41}}}{\beta} \right) + \frac{1}{L_{41}} - \frac{\tau_s}{\gamma} + \frac{jm(g-f)}{j-m} \right] \varphi_{2e} + \left[\frac{\gamma_s \Gamma_s e^{-cL_{41}}}{\beta} + \frac{jf-gm}{j-m} \right] \varphi_{4e} + \left[\frac{\Gamma_s(s-1)}{\beta} - \frac{\tau_s}{\gamma} \right] L_{41} q_{4T} \\ & = \left[\frac{1}{L_{41}} - \frac{\tau_s}{\gamma} + \frac{\Gamma_s(s-1)}{\beta} \right] h_T + \left[\frac{j(1-m)f + m(j-1)g}{j-m} \right] h_e \end{aligned} \quad \dots\dots\dots (22)$$

where

$$\tau_s = \frac{(scL_{41} - 1)e^{cL_{41}} + 1}{L_{41}} \quad \dots\dots\dots (23a)$$

$$\Gamma_s = \frac{1 - (1 + scL_{41})e^{-cL_{41}}}{L_{41}} + \frac{\gamma'}{\gamma} \tau_s \dots\dots\dots (23b)$$

Finally, since it is assumed that there is no interchange between the canal and ground water, q_{4T} has the same value both at the downstream end of zone 1 and the upstream end of zone 2. That is, it remains constant underneath the Tamiami canal. Consequently, it can be quantified by

$$q_{4T} = \frac{h_4(L_{29})|_{zone1} - h_4(0)|_{zone2}}{b_T} \dots\dots\dots (24)$$

where b_T denotes the bottom width of the Tamiami canal and the values of h_4 can be determined by equations (5b) and (9b) for zones 1 and 2, respectively. By substituting the appropriate expressions into (24) and simplifying, one arrives at

$$\{b_T + L_{29}(1 + \xi) - (s-1)L_{41}[\frac{\beta - (s-1)(\gamma' + \gamma)}{\beta\gamma}]\}q_{4T} + \{(1-s)[\frac{1}{\gamma} - (\frac{\gamma'}{\gamma} + 1)(\frac{s-1-\gamma e^{-cL_{41}}}{\beta})]\}\phi_{2e}$$

$$(s-1)(\frac{\gamma'}{\gamma} + 1)(\frac{\gamma e^{-cL_{41}}}{\beta})\phi_{4e} = (1 + \xi)h_{3A} - [\frac{s-1}{\gamma} + \xi + 1 - \frac{(s-1)^2}{\beta}(\frac{\gamma'}{\gamma} + 1)]h_T \dots\dots\dots (25)$$

where

$$\xi = \frac{s[cL_{29} \cosh(cL_{29}) - \sinh(cL_{29})]}{\sinh(cL_{29}) - scL_{29} \cosh(cL_{29})} \dots\dots\dots (26)$$

Equations (20), (22) and (25) provide three equations that can be solved for the three unknowns ϕ_{2e} , ϕ_{4e} , and q_{4T} . This can be followed by the application of equations (6), (7), (12) and (19) to compute the total leakage from WCA-3A, the portion of this leakage intercepted by the Tamiami canal, the transmission losses from the Tamiami canal and the total ground water inflow to ENP.

C4.2 Comparison of the Analytic Element Model with the Analytic Solution

Table C4 provides a comparison of the seepage rates computed by the analytic element model to the corresponding seepage rates determined with the analytic solution. It can be seen that the two methods produce results that are noticeably different, although comparable for practical purposes. These differences in seepage rates are most likely due to certain assumptions that are inherent to the analytic solution but not the analytic element model. For example, the canal side walls are assumed to be vertical in the analytic solution while head losses incurred by ground water flow underneath WCA are neglected. Another reason for the differences between the results derived from the two methodologies is the assumption of quasi-two dimensional flow

used to formulate the analytic solution. That is, it was assumed that flow within the aquifer layers is strictly horizontal while flow through the blankets is strictly vertical. This assumption is not inherent to the analytic element method. Moreover, it is only accurate for layered ground water flow systems where the blankets are very thin in comparison to the aquifer thicknesses and the hydraulic conductivities of the blankets are at least an order of magnitude lower than those of the aquifer layers. It can be seen in table C1 that the former assumption is not met under the stated conditions while the latter assumption is only marginally satisfied. Conversely, the analytic element model solution is only approximate (i.e. not exact) along its boundaries. This will introduce some error into the results.

Despite these limitations, the results in Table C4 serve as a useful reality check of the proposed modeling approach with the analytic element method. Furthermore, it is apparent that the analytic element method is more convenient to use and more readily applicable to complex cross sectional models with numerous layers or internal boundaries. Hence, ground water flow under the various levee reaches of interest in the HSE implementations will be modeled using the analytic element method.

Table C4. Comparison of flow rates (ft²/day) obtained from an analytic element model to corresponding flows computed with an analytic solution.

Solution	WCA-3A Outflow	Tamiami Canal			ENP Inflow
		inflow from left	flow underneath	outflow to right	
analytic element model	17.97	12.04	5.45	32.65	38.78
analytic solution	17.06	11.23	5.82	29.98	35.80
% Difference	5.3	7.2	-6.4	8.9	8.3

Appendix D

Analytic Solutions to Generalized or Proposed Levee / Borrow Canal Configurations

Table of Contents

D1. Introduction and Purpose	
D2. General Case 1: Single Levee with Exterior Borrow Canal and Wetlands on Both Sides ..	
D3. General Case 2: Single Levee with Exterior Borrow Canal and Wetlands on One Side ..	

D1. Introduction and Purpose

As demonstrated previously, AEM based cross section models provide a relatively accurate and efficient means for studying ground water flow beneath existing levee reaches. As expected, however, it is not feasible to conduct this type of modeling effort for every levee reach within the regional model domain. Furthermore, seepage beneath future proposed levees (e.g. those surrounding a new impoundment) may need to be simulated in a regional model. In this case, a design change in the levee / borrow canal system would necessitate modification of the supporting analytic element model. The use of analytic element modeling under these circumstances to develop the required relationships between water levels and seepage rates may prove to be impractical if a large number of designs need to be analyzed.

Given all this, it was felt that analytic solutions to certain generalized levee / borrow canal configurations should be developed to support modeling applications that need to consider seepage under a generic or typical levee and borrow canal system constructed in common subsurface conditions. This could include seepage under future levees or existing levees that have not yet been studied in detail with the analytic element method or other modeling technique. The standard or common types of levee / borrow canal configurations for which solutions have been developed are described below.

D2. General Case 1 : Single Levee with Exterior Borrow Canal and Wetlands on Both Sides

Many impoundments in southern Florida are enclosed by a single levee with an exterior borrow canal. A schematic of such a design is portrayed in figure C1. The surface water within the impoundment is at a stage of h_o , while the borrow canal has a stage of h_c . Additionally, there are wetlands to the right of the borrow canal that have an ambient surface water stage of h_u . It can also be seen that there are two blankets: one separating the ponded surface water behind the levee from the top aquifer layer and another that serves as an aquatard between the top and lower aquifer layer. Following the same convention mentioned in appendices A and B, these blankets are given odd layer numbers while even numbers are assigned to the aquifer layers, where layer numbers increase with depth. Furthermore, layer thickness and hydraulic conductivity are denoted by the parameters K and Z , respectively, with the associated layer number given by the subscript.

In order to develop an analytic solution that relates the surface water stages shown in figure D1 to ground water heads and flow rates, the ground water flow system was divided into the three sections as shown. Within each section, it is assumed that flow within an aquifer layer is strictly horizontal while flow through the blankets is strictly vertical. Consequently, hydraulic conductivities assigned to the aquifer layers are taken to be horizontal hydraulic conductivity while vertical hydraulic conductivity is implied for the blankets. In addition, it is assumed that the impoundment extends infinitely far to the left while the ambient wetland extends infinitely far to the right. The borrow canal is assumed to have a rectangular cross section of width B_c , a depth that results in little or no penetration of the channel into the lower aquifer layer and a bottom that is relatively impervious. Given these assumptions along with the boundary conditions for each section, an analytic solution to ground water flow within each section can be derived using the procedures discussed in Shea and Whitsett (1958). A composite analytic

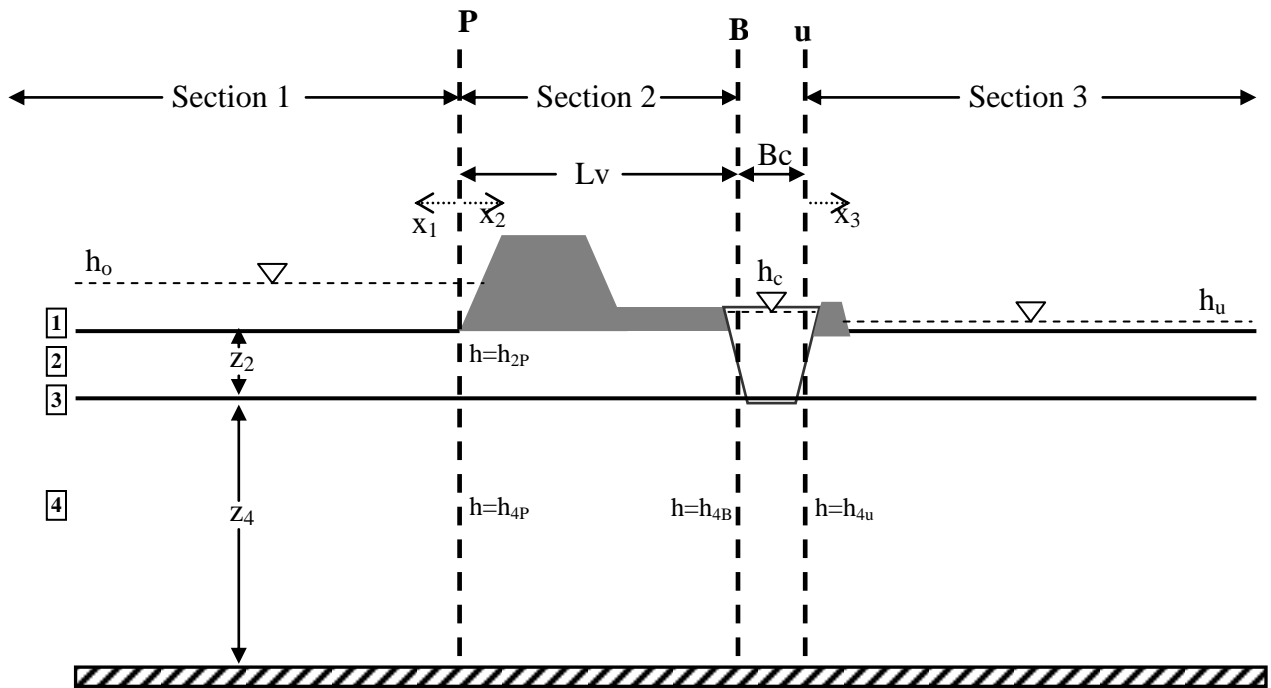


Figure D1. Conceptual cross section of a generalized levee / borrow canal configuration along with the associated ground water flow system

solution covering the entire ground water flow system can subsequently be developed from the three individual solutions by considering continuity of flow between the sections. This is essentially the same methodology that was applied in the analysis presented in appendix C and it was used here as well. Detailed explanations of the solution procedure are given below.

Section 1

The ground water flow system within section 1 is similar to the one used to characterize the surficial aquifer within the ENP, downstream of L-29, section 1. The reader is referred to appendix C for a discussion of that analysis as well as the definitions of variables and notation used here (see also Shea and Whitsett, 1958). For the current situation, equations (18) of appendix C imply that

$$h_2 = h_o - M_2 e^{-fx} - M_4 e^{-gx} \quad \dots \dots \dots (1a)$$

$$h_4 = h_o - jM_2 e^{-fx} - mM_4 e^{-gx} \quad \dots \dots \dots (1b)$$

It should be noted that $x = 0$ at the levee and increases to the left. From figure D1, it is evident that at $x = 0$, $h_2 = h_{2P}$ and $h_4 = h_{4P}$, where h_{2P} and h_{4P} denote the unknown aquifer heads at the boundary between sections 1 and 2. Hence, it follows from equations (1) that

$$h_{2P} = h_o - M_2 - M_4 \quad \dots \dots \dots (2a)$$

$$h_{4P} = h_o - jM_2 - mM_4 \dots\dots\dots (2b)$$

Solving equations (2) for M_2 and M_4 yields

$$M_2 = \frac{(1 - m)h_o + mh_{2P} - h_{4P}}{j - m} \dots\dots\dots (3a)$$

$$M_4 = \frac{(j - 1)h_o - jh_{2P} + h_{4P}}{j - m} \dots\dots\dots (3b)$$

Section 2

The ground water flow system within section 2 is similar to the one used to characterize the surficial aquifer underneath the embankment of L-29, section 1 (appendix C). Therefore, equations (2) of appendix C indicate that the general solution for aquifer heads is given by

$$h_2 = R_1 + R_2x + R_3e^{cx} + R_4e^{-cx} \dots\dots\dots (4a)$$

$$h_4 = R_1 + R_2x + sR_3e^{cx} + sR_4e^{-cx} \dots\dots\dots (4b)$$

At $x = 0$, it is evident from figure D1 that $h_2 = h_{2P}$ and $h_4 = h_{4P}$. From equations (4), it follows that

$$h_{2P} = R_1 + R_3 + R_4 \dots\dots\dots (5a)$$

$$h_{4P} = R_1 + sR_3 + sR_4 \dots\dots\dots (5b)$$

Likewise, at $x = L_v$, $h_2 = h_c$ and $h_4 = h_{4B}$. Hence,

$$h_c = R_1 + L_vR_2 + e^{cL_v}R_3 + e^{-cL_v}R_4 \dots\dots\dots (6a)$$

$$h_{4B} = R_1 + L_vR_2 + se^{cL_v}R_3 + se^{-cL_v}R_4 \dots\dots\dots (6b)$$

Solving equations (5) and (6) for R_1 through R_4 results in

$$R_1 = \frac{sh_{2p} - h_{4p}}{s - 1} \dots\dots\dots (7a)$$

$$R_2 = \frac{s(h_{2p} - h_c) - h_{4p} + h_{4B}}{L_v(1 - s)} \dots\dots\dots (7b)$$

$$R_3 = \frac{h_{2p} - h_{4p}}{1 - s} - R_4 \dots\dots\dots (7c)$$

$$R_4 = \frac{e^{cL_v}(h_{2p} - h_{4p}) + h_{4B} - h_c}{2(1 - s)\sinh(cL_v)} \dots\dots\dots (7d)$$

At this point equations (2) and (6) cannot be used since they are, in their present form, still functions of the unknown heads at the boundaries between the sections. Since a total of four unknown heads were specified at section boundaries, four independent equations will be needed to determine them. These can be obtained by requiring that the flux within each layer be maintained at each of the boundaries. Considering the boundary within layer 4 between sections 2 and 3, it should be recalled that one of the assumptions inherent to this analysis is that no leakage occurs out of the canal bottom. Thus, the unit flux (i.e. the flow rate per unit width of aquifer per unit transmissivity) leaving section 2 through layer 4 is the same as that entering section 3. Denoting this unit flux as q_{4B} , Darcy's law indicates that

$$q_{4B} = \frac{h_{4B} - h_{4u}}{B_c} \dots\dots\dots (8)$$

Also,

$$q_{4B} = -\frac{dh_4}{dx}(L_v) \dots\dots\dots (9)$$

Substituting equations (4b), (7) and (8) into (9) and simplifying yields

$$\left(\xi e^{cL_v} - \gamma - \frac{1}{L_v}\right)h_{2p} + (\gamma - \xi e^{cL_v})h_{4p} + \left(\xi + \frac{1}{B_c}\right)h_{4B} - \frac{h_{4u}}{B_c} = \left(\xi - \frac{1}{L_v}\right)h_c \dots\dots\dots (10)$$

where

$$\xi = \tau [1 - scL_v \coth(cL_v)] \dots\dots\dots (11a)$$

$$\tau = \frac{1}{L_v(1-s)} \dots\dots\dots (11b)$$

$$\gamma = \tau [e^{cL_v}(1 - scL_v) - 1] \dots\dots\dots (11c)$$

Equations (10) and (11) provide one of the four equations needed to determine the unknown boundary head values. Another equation can be formulated by requiring continuity of flow between sections 1 and 2. Referring to figure D1, this can be expressed as

$$\left. \frac{dh_2}{dx}(0) \right|_{\text{section 1}} = - \left. \frac{dh_2}{dx}(0) \right|_{\text{section 2}} \dots\dots\dots (12)$$

Note that the negative sign on the left side of equation (12) was reversed since flow within section 1 is in the negative x direction. Substituting equations (1a), (3), (4a), (7) and (11b) into (12) and rearranging terms results in

$$\begin{aligned} & \{ \tau[s + cL_v(1 - e^{cL_v} \operatorname{csch}(cL_v))] + \frac{fm - jg}{j - m} \} h_{2P} - \{ \tau[1 + cL_v(1 - e^{cL_v} \operatorname{csch}(cL_v))] + \frac{f - g}{j - m} \} h_{4P} \\ & + \tau[1 + cL_v \operatorname{csch}(cL_v)] h_{4B} = \tau[s + cL_v \operatorname{csch}(cL_v)] h_c - \left\{ \frac{f(1 - m) + g(j - 1)}{j - m} \right\} h_o \dots\dots (13) \end{aligned}$$

Similarly, continuity of flow within layer 4 implies that

$$\left. \frac{dh_4}{dx}(0) \right|_{\text{section 1}} = - \left. \frac{dh_4}{dx}(0) \right|_{\text{section 2}} \dots\dots\dots (14)$$

Substituting equations (1b), (3), (4b), (7) and (11b) into (14) and rearranging terms yields

$$\begin{aligned} & \left\{ \sigma\tau[1 + cL_v(1 - e^{cL_v} \operatorname{csch}(cL_v))] + \frac{jm(f - g)}{j - m} \right\} h_{2P} - \left\{ \tau[1 + scL_v(1 - e^{cL_v} \operatorname{csch}(cL_v))] + \frac{jf - gm}{j - m} \right\} h_{4P} \\ & + \tau[1 + scL_v \operatorname{csch}(cL_v)] h_{4B} = \sigma\tau[1 + cL_v \operatorname{csch}(cL_v)] h_c - \left\{ \frac{jf(1 - m) + gm(j - 1)}{j - m} \right\} h_o \quad \dots\dots (15) \end{aligned}$$

Section 3

The same logic used to derive the general solutions for $h_2(x)$ and $h_4(x)$ within section 1 can be applied to section 3 as well. This results in

$$h_2 = h_u - N_2 e^{-fx} - N_4 e^{-gx} \quad \dots\dots\dots (16a)$$

$$h_4 = h_u - jN_2 e^{-fx} - mN_4 e^{-gx} \quad \dots\dots\dots (16b)$$

It should be noted that $x = 0$ at the canal and increases to the right. From figure D1, it is evident that at $x = 0$, $h_2 = h_c$ and $h_4 = h_{4u}$, where h_{4u} denotes the unknown aquifer head within layer 4 at the boundary between sections 2 and 3. Hence, it follows from equations (16) that

$$h_c = h_u - N_2 - N_4 \quad \dots\dots\dots (17a)$$

$$h_{4u} = h_u - jN_2 - mN_4 \quad \dots\dots\dots (17b)$$

Solving equations (17) for N_2 and N_4 yields

$$N_2 = \frac{(1 - m)h_u + mh_c - h_{4u}}{j - m} \quad \dots\dots\dots (18a)$$

$$N_4 = \frac{(j - 1)h_u - jh_c + h_{4u}}{j - m} \quad \dots\dots\dots (18b)$$

Since there is no interchange of water between the canal bottom and the aquifer, the unit flux at $x = 0$ within section 3 is equal to the unit flux at $x = L_v$ within section 2. For section 3, this is written as

$$q_{4B} = -\frac{dh_4}{dx}(0) \quad \dots\dots\dots (19)$$

Putting equations (16b) and (18) into (19) and setting the result equal to the right hand side of equation (8) leads to

$$\left(\frac{j-m}{B_c}\right)h_{4B} + \left[\frac{B_c(gm-jf) - j+m}{B_c}\right]h_{4u} = [jf(m-1) + gm(1-j)]h_u + jm(g-f)h_c \dots\dots (20)$$

At this point, equations (10), (13), (15) and (20) can be solved simultaneously for h_{2P} , h_{4P} , h_{4B} and h_{4u} . With these heads known, the particular solutions for $h_2(x)$ and $h_4(x)$ within each section are complete.

Impoundment Seepage

One of the primary objectives of this effort is to determine the total seepage from the impoundment. The seepage flux at a distance x from the levee can be stated as

$$q_{IM} = -C_1 [h_2(x) - h_o] \dots\dots\dots (21)$$

Since the impoundment is assumed to be semi-infinite in length, the total seepage is then

$$Q_{IM} = \int_0^{\infty} q_{IM}(x) dx \dots\dots\dots (22)$$

By substituting equation (1a) into (21), putting the subsequent result into (22) and carrying out the integration, one obtains

$$Q_{IM} = C_1 \left(\frac{M_2}{f} + \frac{M_4}{g} \right) \dots\dots\dots (23)$$

Equations (3) and (23) can be used to compute the total seepage lost from the reservoir.

Canal – Aquifer Interactions

From figure D1, it is apparent that the ground water flow within section 2 that flows into the borrow canal can be stated as

$$Q_{2B} = -C_2 \frac{dh_2}{dx}(L_v) \dots\dots\dots (24)$$

Substituting equation (4a) into (24) gives

$$Q_{2B} = -C_2 [R_2 + c(R_3e^{cL_v} - R_4e^{-cL_v})] \dots\dots\dots (25)$$

Equations (7) and (25) can be used to determine the amount of impoundment seepage that is intercepted by the borrow canal on its left side. Furthermore, the canal can either leak water to or drain water from the aquifer on its right side. This seepage rate is given by

$$Q_{2u} = -C_2 \frac{dh_2}{dx}(0) \dots\dots\dots (26)$$

Substituting equation (16a) into (26) yields

$$Q_{2u} = -C_2 (f N_2 + g N_4) \dots\dots\dots (27)$$

Equations (18) and (27) can be used to compute the amount of water lost or gained by the canal through its right wall. In addition, the net amount of ground water that flows past the canal towards the right is simply $Q_{IM} - Q_{2B} + Q_{2u}$.

Penetration of the Borrow Canal into Layer 4

Inherent to the analytic solution developed above is the assumption that the borrow canal cuts through layer 2 but extends very little or not at all into layer 4. This assumption may not always be appropriate. Consequently, the case where the borrow canal penetrates well into layer 4 should also be considered. If this is the case, then it is reasonable to assume that $h_{4B} \approx h_c$ and $h_{4u} \approx h_c$. This leaves only h_{2P} and h_{4P} as the unknowns. Also, equations (7b), (7d), (13), (15), and (18) are modified as follows:

$$R_2 = \frac{sh_{2p} - h_{4P} + (1-s)h_c}{L_v(1-s)} \dots\dots\dots (28a)$$

$$R_4 = \frac{e^{cL_v}(h_{2P} - h_{4P})}{2(1-s)\sinh(cL_v)} \dots\dots\dots (28b)$$

$$\begin{aligned} \{ \tau[s + cL_v(1 - e^{cL_v} \operatorname{csc} h(cL_v))] + \frac{fm - jg}{j - m} \} h_{2P} &- \{ \tau[1 + cL_v(1 - e^{cL_v} \operatorname{csc} h(cL_v))] + \frac{f - g}{j - m} \} h_{4P} \\ &= -\frac{h_c}{L_v} - \left\{ \frac{f(1 - m) + g(j - 1)}{j - m} \right\} h_o \dots\dots\dots (29) \end{aligned}$$

$$\begin{aligned} \{s\tau[1 + cL_v(1 - e^{cL_v} \operatorname{csch}(cL_v))]\} + \frac{jm(f - g)}{j - m} \} h_{2P} - \{ \tau[1 + scL_v(1 - e^{cL_v} \operatorname{csch}(cL_v))]\} + \frac{jf - gm}{j - m} \} h_{4P} \\ = -\frac{h_c}{L_v} - \left\{ \frac{jf(1 - m) + gm(j - 1)}{j - m} \right\} h_o \quad \dots\dots (30) \end{aligned}$$

$$N_2 = \frac{(m - 1)(h_c - h_u)}{j - m} \quad \dots\dots\dots (31a)$$

$$N_4 = \frac{(j - 1)(h_u - h_c)}{j - m} \quad \dots\dots\dots (31b)$$

Hence, if the borrow canal penetrates a significant amount of layer 4, equations (29) and (30) can be used to determine h_{2P} and h_{4P} .

D3. General Case 2 : Single Levee with Exterior Borrow Canal and Wetlands on One Side

This scenario is the same as case 1 discussed above except that ponded surface water exists only on the left side of the levee. The aquifer to the right of the borrow canal is assumed to be saturated or nearly saturated with the water table maintained at elevation h_u a distance of L_u from the borrow canal. Under these conditions, equations (16) are replaced by

$$h_2 = P_1 + P_2x + P_3e^{cx} + P_4e^{-cx} \quad \dots\dots\dots (32a)$$

$$h_4 = P_1 + P_2x + sP_3e^{cx} + sP_4e^{-cx} \quad \dots\dots\dots (32b)$$

At $x = 0$,

$$h_c = P_1 + P_3 + P_4 \quad \dots\dots\dots (33a)$$

$$h_{4u} = P_1 + sP_3 + sP_4 \quad \dots\dots\dots (33b)$$

Likewise, at $x = L_u$, $h_2 = h_4 = h_u$. Hence,

$$h_u = P_1 + L_uP_2 + e^{cL_u}P_3 + e^{-cL_u}P_4 \quad \dots\dots\dots (34a)$$

$$h_u = P_1 + L_u P_2 + s e^{cL_u} P_3 + s e^{-cL_u} P_4 \dots\dots\dots (34b)$$

Solving equations (33) and (34) for R_1 through R_4 results in

$$P_1 = \frac{sh_c - h_{4u}}{s - 1} \dots\dots\dots (35a)$$

$$P_2 = \frac{(s - 1)h_u - sh_c + h_{4u}}{(s - 1)L_u} \dots\dots\dots (35b)$$

$$P_3 = \frac{h_c - h_{4u}}{(1 - s)(1 - e^{2cL_u})} \dots\dots\dots (35c)$$

$$P_4 = \frac{-e^{2cL_u}(h_c - h_{4u})}{(1 - s)(1 - e^{2cL_u})} \dots\dots\dots (35d)$$

As in the previous case, continuity of flow between sections 2 and 3 is ensured by applying equation (19). Substituting equations (8), (32b) and (35) into (19) and rearranging terms results in

$$\left(\frac{1}{B_c}\right)h_{4B} + \left[\frac{1 - scL_u \coth(cL_u)}{(s - 1)L_u} - \frac{1}{B_c}\right]h_{4u} = \frac{(1 - s)h_u + s[1 - cL_u \coth(cL_u)]h_c}{(s - 1)L_u} \dots\dots\dots (36)$$

For the current scenario, equation (36) is used in place of equation (20) along with equations (10), (13) and (15) to solve for the unknown values of h_{2P} , h_{4P} , h_{4B} and h_{4u} .

Penetration of the Borrow Canal into Layer 4

As in the case 1 scenario, inherent to the derivation of equations (32) through (36) is the assumption that the borrow canal has little or no protrusion into layer 4. If this assumption is not appropriate, then $h_{4u} \approx h_c$ and it follows from equations (32) and (35) that

$$P_1 = h_c \dots\dots\dots (37a)$$

$$P_2 = \frac{h_u - h_c}{L_u} \dots\dots\dots (37b)$$

$$P_3 = P_4 = 0 \dots\dots\dots (37c)$$

$$h_2(x) = h_4(x) = h_c + \left(\frac{h_u - h_c}{L_u}\right)x \dots\dots\dots (38)$$

while equations (28), (29) and (30) are still applicable to sections 1 and 2. Equations (37) and (38) would be used instead of equations (35) and (32), respectively.

Appendix E

Report on Additional Cross Sectional Modeling of the C-111, L-31N and L-30 Corridors

Detailed Analytic Element Modeling of Levee Seepage Coefficients for HSE

Vic Kelson, Theresa Landewe, and Rhett Moore, WHPA Inc.

August 30, 2006

1. Introduction

In 2004, WHPA completed work that called for the development of cross-sectional analytic element models of seepage at levees and borrow canals in south Florida. That work provided estimated ranges for seepage coefficients for the levee seepage water mover elements in the HSE. At the time that effort was completed, it was found that some levee reaches exhibited flow behavior in which the seepage rate was not linear in the head differences, as is expected in the HSE levee seepage water movers. This report documents a more detailed analysis for eight critical levee reaches, based on many more model runs. This work was conducted under purchase order ST060581-WO02. This document satisfies task 3.4.

We have found that for some levee reaches, the seepage coefficients for flow into and out of the “dry cell” depend upon whether the cell is inundated or dry at the surface. This arises from a change in the boundary condition; when the cell is inundated, there is a reservoir that can move water quickly into the cell. In the model, this changes the type of boundary condition from a “flux-specified” boundary (in this case, no-flow) into a “head-dependent flux” boundary at the ground surface. In cases where the difference in the seepage coefficient is significant (as determined by the modeler) a modified water mover that implements a transition from the “dry” to the “impounded” seepage coefficient is warranted.

2. Methodology

For each cross-section, the analytic element models were built in a manner consistent with the profile models that were developed in 2004. The major difference in this new work was to increase the number of model runs in order to better assess the possibility that the seepage rate is not a linear function of the head difference for some levee seepage processes.

2.1. Construction of the profile models

We built model input files for this analysis by adapting the model designs used in the 2004 work. The models were adjusted to account for differences in the conceptual models, especially ground elevation changes, provided by Mark Wilsnack of SFWMD. In addition, we developed additional preprocessing and post processing scripts that allow the user to easily specify a battery of model runs, using a table of water levels for the marsh, canal segment, and dry cell.

The scope of work for this purchase order called for six model runs at each levee cross-section. The number of required model runs was determined by balancing the benefit of additional model runs versus the effort necessary to build cross-sectional “head-streamline” plots. We found that additional model runs would be helpful for the detailed analysis, and we recommended to Mark Wilsnack (the project manager) that more runs be performed, but omitted from the head-

streamline plots in order to save time. Mark approved this change, and we ran many model runs for each levee cross-section and have included them in this analysis.

2.2. Approach

As recommended by SFWMD, we built three types of model scenarios, each intended to isolate the effects of one boundary condition at a time. For example, “marsh” runs held the canal stage and dry cell stage at equal elevations, but changed the marsh stage in each of a collection of model runs. This procedure allowed us to accurately determine each of the three flux terms (marsh-to-canal, dry-cell-to-canal, and marsh-to-dry-cell) for each set of water-level values.

The model runs were collected as follows:

marsh runs held the canal and dry cell stages equal and raised the marsh stage relative to the dry cell and canal. In all *marsh* runs, the canal and dry cell stages were set 1 ft higher than the ground elevation in the dry cell. In these runs, it was possible to compute marsh-to-canal and marsh-to-dry-cell fluxes.

canal runs held the marsh and dry cell stages equal and both raised and lowered the canal stage relative to the marsh and dry cell. In all *canal* runs, the marsh and dry cell stages were set 1 ft higher than the ground elevation in the dry cell. In these runs, it was possible to compute marsh-to-canal and dry-cell-to-canal fluxes.

dry runs held the marsh and canal stages equal and both raised and lowered the dry cell stage relative to the marsh and canal. In all *dry* runs, the marsh and canal stages were set 1 ft higher than the ground elevation in the dry cell. In these runs, it was possible to compute marsh-to-dry-cell and dry-cell-to-canal fluxes. In addition, when the water level in the dry cell was 1 ft below the water level in the canal (i.e. At ground level), the boundary condition in the dry cell changed to a no-flow condition. These runs were used to determine the “dry” values of the marsh-to-dry-cell and dry-cell-to-canal seepage coefficients.

Measurement of seepage rates in the model

In the model input files, we used the “flux inspection” capability of the ModAEM solver to compute fluxes at three locations:

1. Seepage from the marsh (Q_m) was measured at the center of the levee bounding the marsh;
2. Seepage into or out of the canal (Q_c) was measured at the canal perimeter;
3. Seepage into the dry cell (Q_d) was measured at a convenient location beyond the canal.

This approach is similar to that used in the 2004 analysis, except that in the 2004 analysis we did not explicitly compute the seepage rate into or out of the canal, but computed it as the difference between the marsh and dry cell flux values. The original approach had a potential limitation, because it is possible, especially in reaches that have shallow, highly-conductive layers, for the direction of flow to change in the vertical section. That is, there will be an *a priori* unknown

dividing streamline between the dry cell and the canal. By explicitly measuring the canal flow, we have eliminated this potential source of error.

Computing seepage coefficients

Each of the watermover elements expects a seepage coefficient K_{ij} that is the slope of the curve that relates Q_{ij} to the head difference $H_i - H_j$, where i and j are waterbody elements. In order to compute the three seepage coefficients, we require the water-body-to-water-body seepage rates. Given the seepage rates that were reported by the model solver, we computed the three “waterbody” terms as follows:

For the “marsh” runs,

$$Q_{md} = Q_m - Q_c$$

$$Q_{ms} = Q_c$$

$$Q_{ds} = 0$$

For the “canal” runs,

$$Q_{md} = 0$$

$$Q_{ms} = Q_m$$

$$Q_{ds} = Q_c - Q_m$$

For the “dry” runs,

$$Q_{md} = Q_m$$

$$Q_{ms} = 0$$

$$Q_{ds} = Q_c$$

Where Q_{md} is the marsh-to-dry-cell flux, Q_{ms} is the marsh-to-canal-segment flux, and Q_{ds} is the dry-cell-to-canal-segment flux.

As we will show in Section 3, we found a linear relationship between the flux and head difference in each levee reach. We computed the seepage coefficient as the slope of the line that passes through the data. In some cases, the regression line did not pass exactly through the origin. This appears to be an artifact of the “truncated” models that were used in the analysis. This has been discussed separately, e.g. in the previous levee seepage modeling reports. To summarize, we can safely assume that a Dupuit-Forchheimer condition exists at a distance from the levee that is 3 times the “representative leakage distance” for the layered aquifer. In the levee seepage models, it is computationally impractical to make such large models; we have used the “truncated” model strategy of Haitjema (2004). A truncated model typically provides a good estimate for the cross-sectional problem, but there is a systematic error due to truncation. That error is directly related to the ratio between the model length and the representative leakage length. As a result, we find that some problems, especially problems in which the representative leakage length is large, have non-zero y-intercepts in the regression. For our purposes, we ignore this error and report the slope of the line (the seepage coefficient).

3. Results for Levee Reaches

In this section, we describe the process used to compute seepage coefficients and present results for each of the profile models. The water-level scenarios for all profile models are documented in the previous memorandum of July 10, 2006.

For each profile model, we computed the five linear seepage coefficients by using linear regression of results from the set of model runs as follows:

1. The seepage coefficient for flow from the marsh to the canal segment K_{ms} was computed from the groups of “canal” runs.
2. The seepage coefficient for flow from the marsh to the dry cell K_{md} was computed from the groups of “dry” runs.
3. The seepage coefficient for flow from the dry cell to the canal segment K_{ds} was computed from the groups of “dry” runs.

The linear regression was carried out as described in Section 2.

Effects of dry cell water levels

In every case, we found linear relationships between seepage rates and head differences for the water bodies in the levee seepage problems. However, we found that the linear seepage coefficient is numerically different depending upon whether there is ponded water in the dry cell. This is an important nonlinearity that should be examined more fully in future versions of HSE. The difference arises from the way the boundary condition is treated in the seepage model. When the dry cell is ponded, it is treated as a general-head boundary condition; the dry cell is assumed to be able to provide water or remove water at the land surface. When the dry cell water level is below the ground elevation, it is treated as a no-flow condition.

These two assumptions are approximate; in reality the soil does not dry out precisely when the water level is just below grade, similarly shallowly-ponded water may not efficiently move water to/from the dry cell in a manner consistent with the seepage model. If it will be necessary to construct future HSE models that handle wet and dry conditions in the dry cell, a scheme for making a smooth transition from the “wet” to the “dry” seepage coefficient will be needed.

We have provided five seepage coefficients for each levee reach:

K_{md} (wet) and K_{md} (dry): marsh-to-dry-cell, depending on wet or dry conditions in the dry cell

K_{ms} : marsh-to-canal-segment

K_{ds} (wet) and K_{ds} (dry): marsh-to-dry-cell, depending on wet or dry conditions in the dry cell

In applications, the modeler should consider which coefficient to use, depending upon the typical conditions in the dry cell at each levee reach. It should be noted that at levees where there is a shallow confining unit, the “wet” and “dry” seepage coefficients may only differ slightly.

The remainder of Section 3 describes each levee reach in turn.

3.1. C-111 between S-176 and S-177

Scenarios

Table 1: Reported water levels for C-111 between S-176 and S-177.

Area	Water Level Gauge (DBHYDRO)	Observed Water Elevation (ft NGVD)		
		Maximum	Average	Minimum
Frog Pond Area (west)	FROGPD2_G	5.9	3.6	1.8
C-111 Canal	S176_TW	6.5	3.4	1.3
G-864A (east side)	G-864A 2	8.4	2.4	-1.1

Table 2: Scenarios for C-111 between S-176 and S-177.

Scenario	Frog Pond Area	C-111 Canal	East Side
marsh-1	6.1	6.0	6.0
marsh-2	6.2	6.0	6.0
marsh-3	6.5	6.0	6.0
marsh-4	7.0	6.0	6.0
dry-1	6.0	6.0	2.0
dry-2	6.0	6.0	2.5
dry-3	6.0	6.0	3.0
dry-4	6.0	6.0	3.5
dry-5	6.0	6.0	4.0
dry-6	6.0	6.0	4.5
dry-7	6.0	6.0	5.0
dry-8	6.0	6.0	5.5
dry-9	6.0	6.0	5.8
dry-10	6.0	6.0	5.9
dry-11	6.0	6.0	6.1
dry-12	6.0	6.0	6.2
dry-13	6.0	6.0	6.5
dry-14	6.0	6.0	7.0
canal-1	6.0	5.0	6.0
canal-2	6.0	5.5	6.0
canal-3	6.0	5.8	6.0
canal-4	6.0	5.9	6.0
canal-5	6.0	6.1	6.0
canal-6	6.0	6.2	6.0
canal-7	6.0	6.5	6.0
canal-8	6.0	7.0	6.0

Representative head-streamline plots

Head-streamline plots for C-111 between S-176 and S-177 are shown on the following pages. Heads (in feet MSL) for the model runs in these plots are shown below:

Table 3: Water levels for head-streamline plots.

<i>Marsh runs (Figure 1)</i>			
<i>Run ID</i>	<i>Marsh</i>	<i>Canal</i>	<i>Dry</i>
plot-marsh-1	6.1	6.0	6.0
plot-marsh-4	7.0	6.0	6.0
<i>Dry-cell runs (Figure 2)</i>			
<i>Run ID</i>	<i>Marsh</i>	<i>Canal</i>	<i>Dry</i>
plot-dry-1	6.0	6.0	5.0
plot-dry-14	6.0	6.0	7.0
<i>Canal runs (Figure 3)</i>			
<i>Run ID</i>	<i>Marsh</i>	<i>Canal</i>	<i>Dry</i>
plot-canal-1	6.0	5.0	6.0
plot-canal-8	6.0	7.0	6.0

C-111 between S-176 and S-177

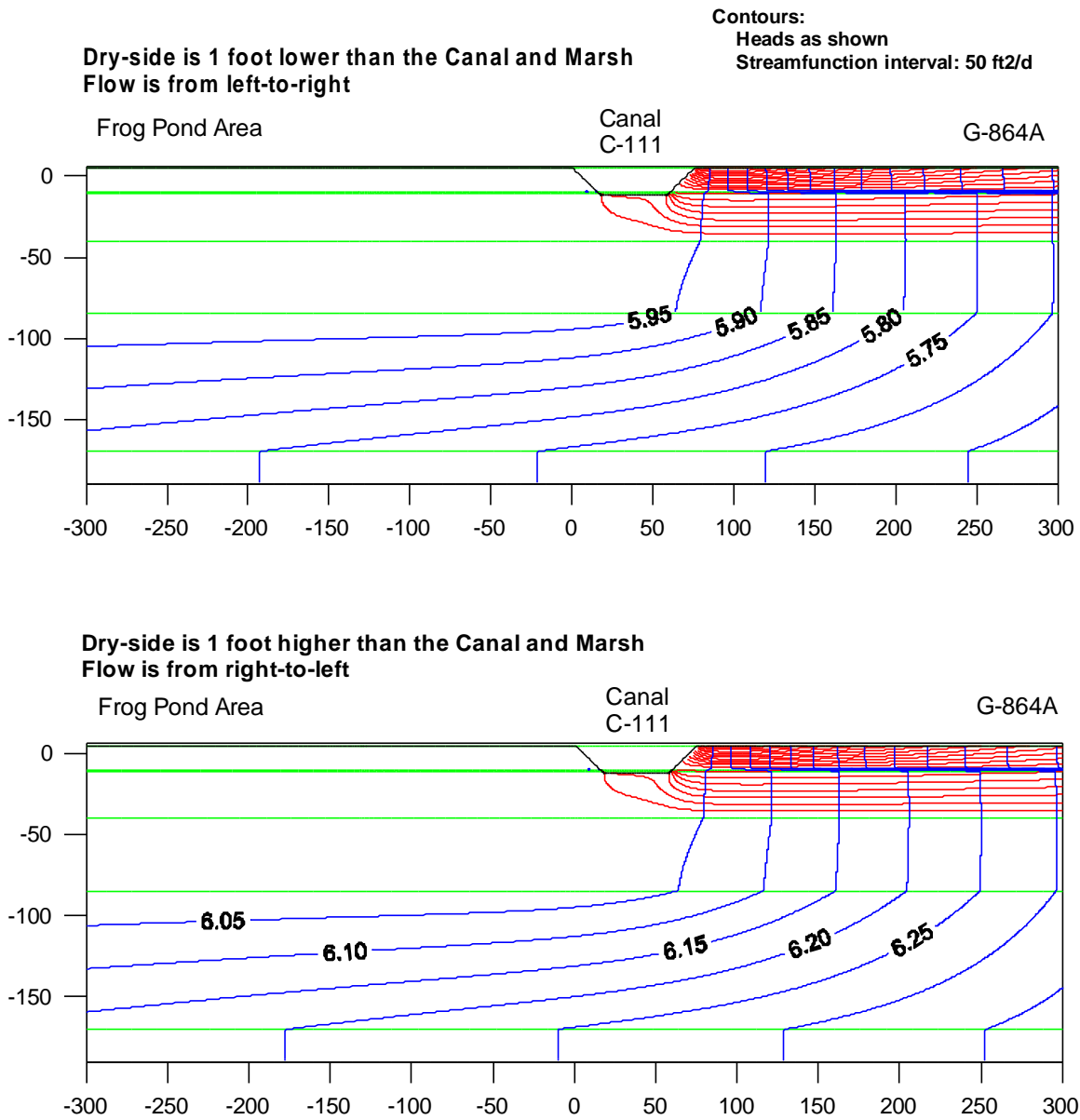


Figure 2: Heads and streamlines for C-111 between S-176 and S-177, for runs in which the dry-side water level was adjusted.

Seepage coefficients

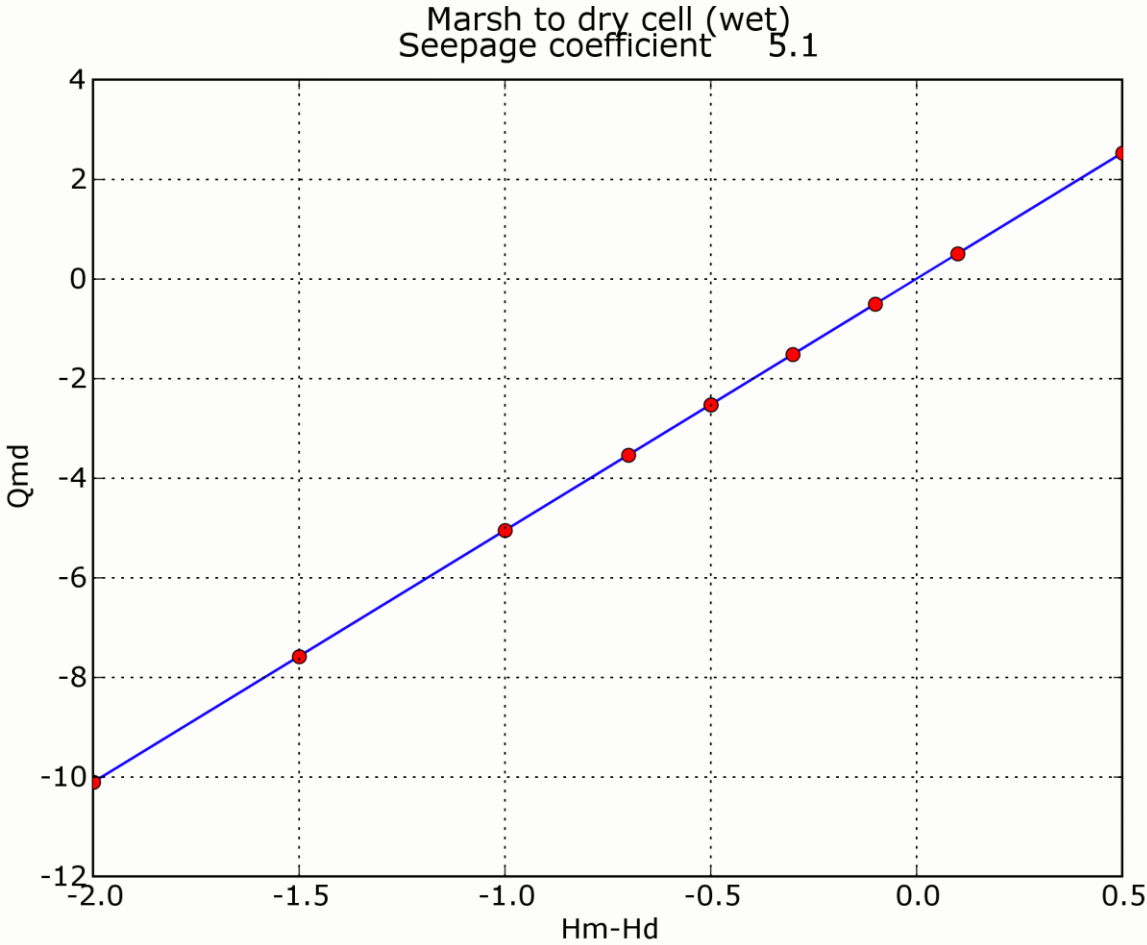


Figure 4: Seepage coefficient for C-111 between S-176 and S-177 from Marsh to Dry Cell (wet).

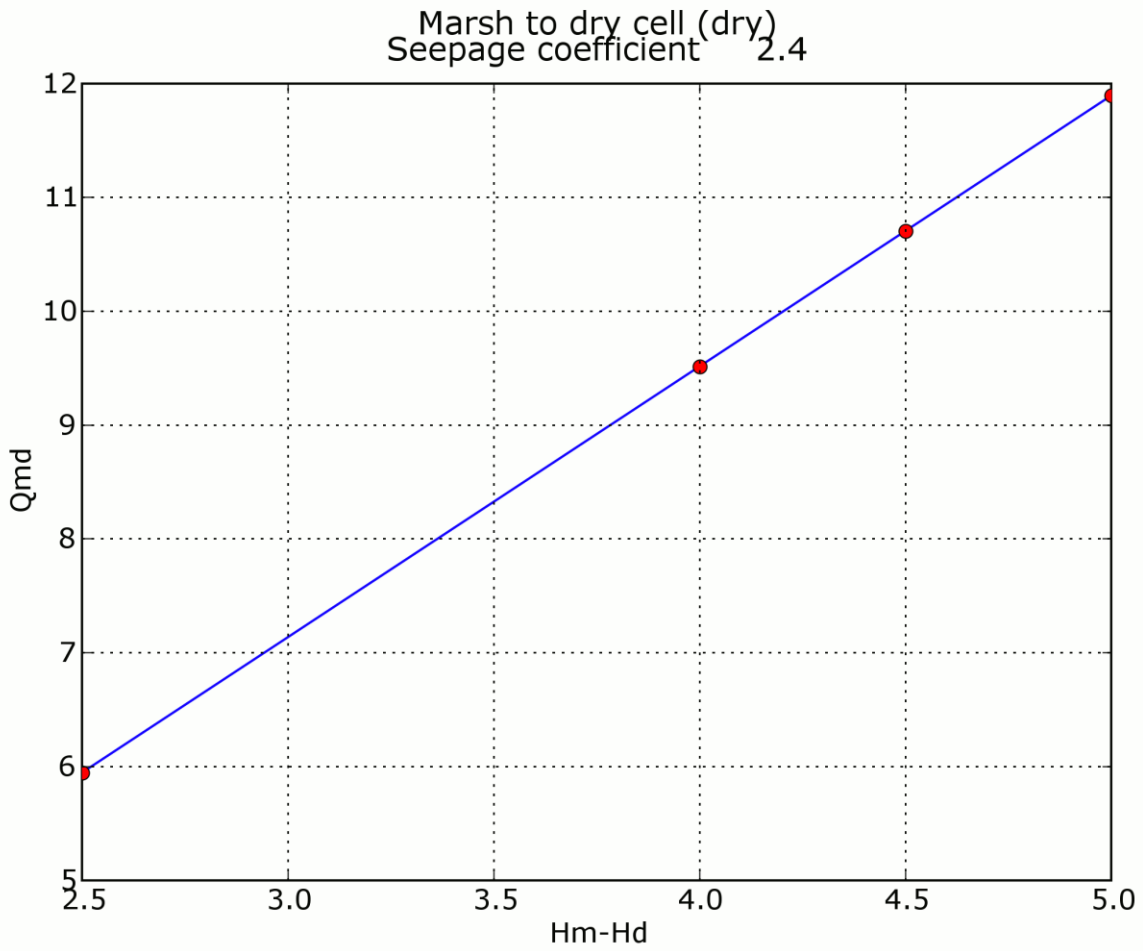


Figure 5: Seepage coefficient for C-111 between S-176 and S-177 from Marsh to Dry-Cell (dry).

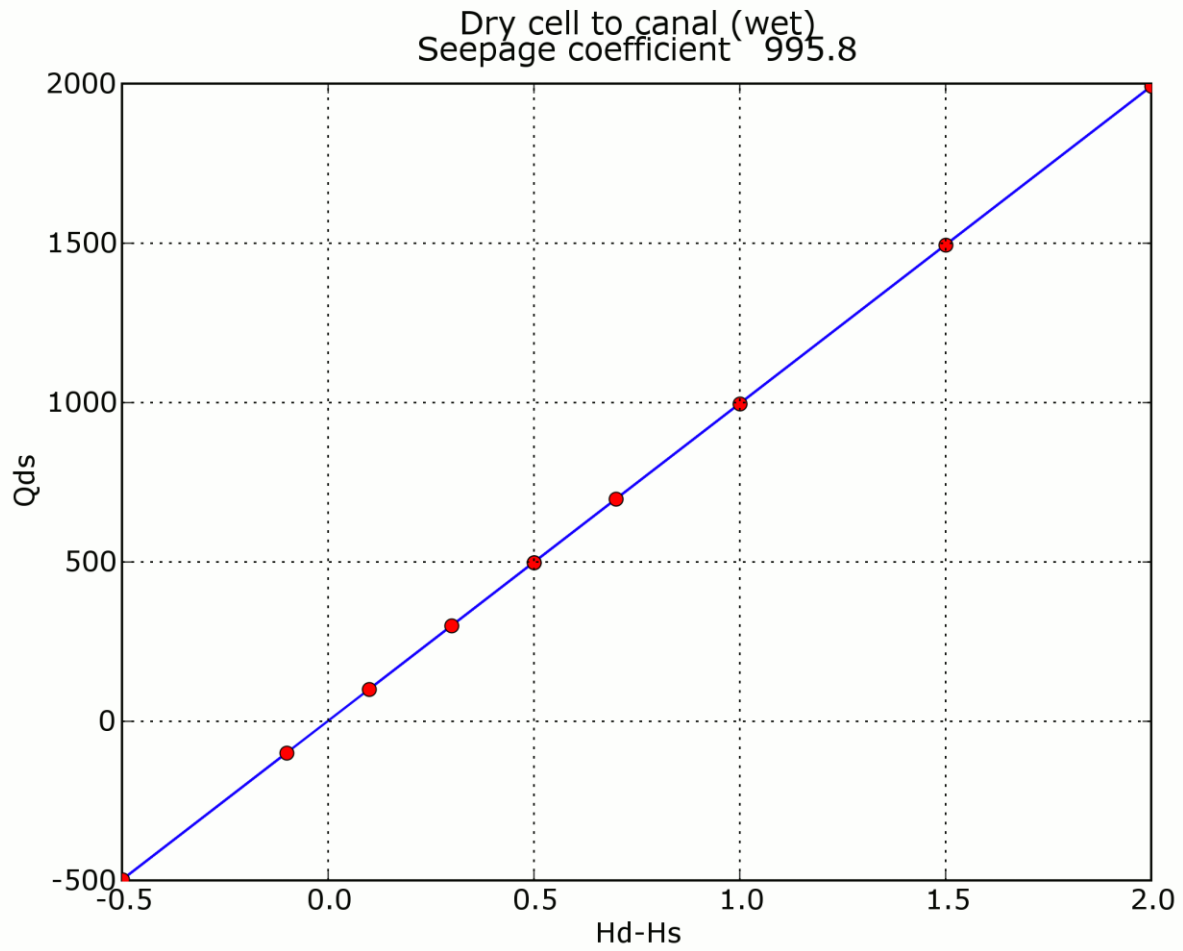


Figure 6: Seepage coefficient for C-111 between S-176 and S-177 from Dry Cell to Canal (wet).

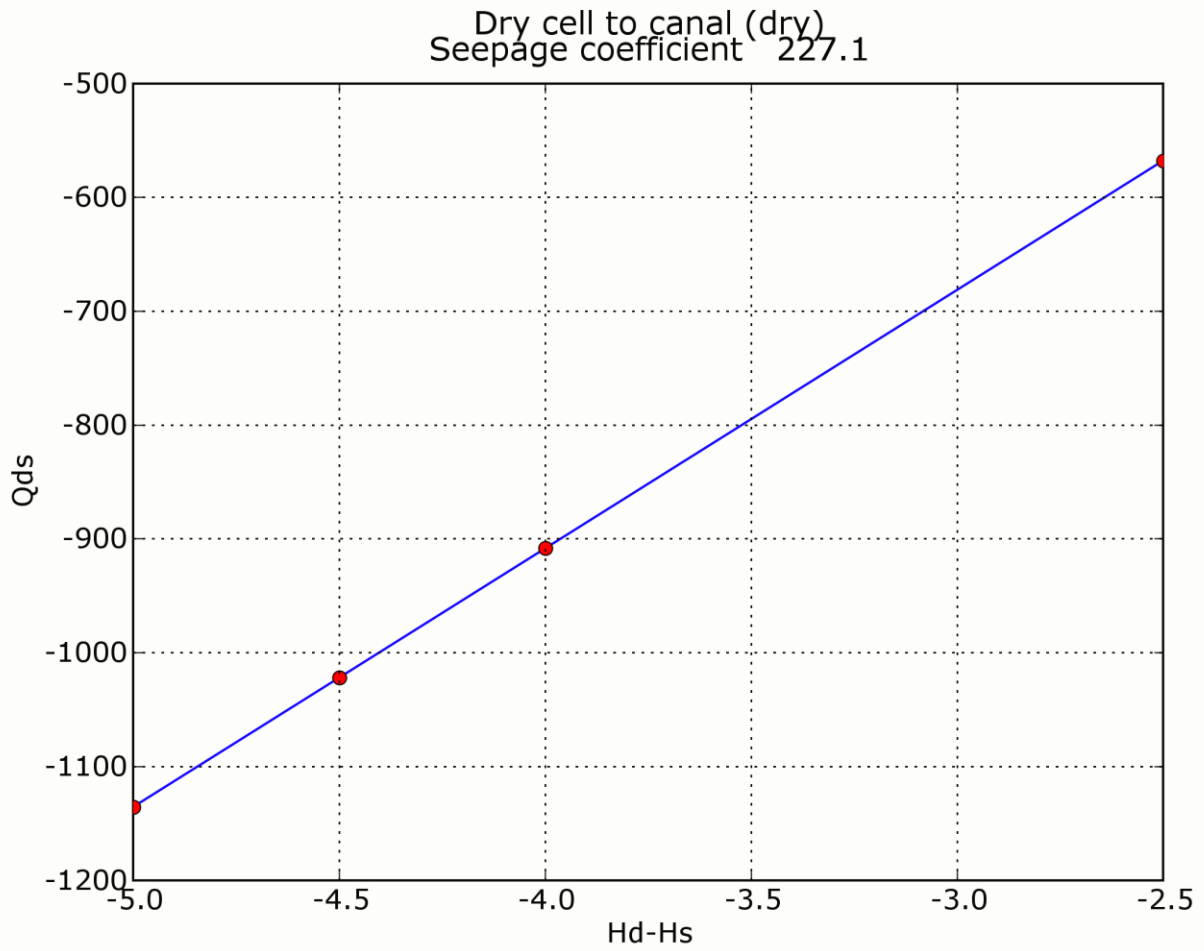


Figure 7: Seepage coefficient for C-111 between S-176 and S-177 from Dry Cell to Canal (dry).

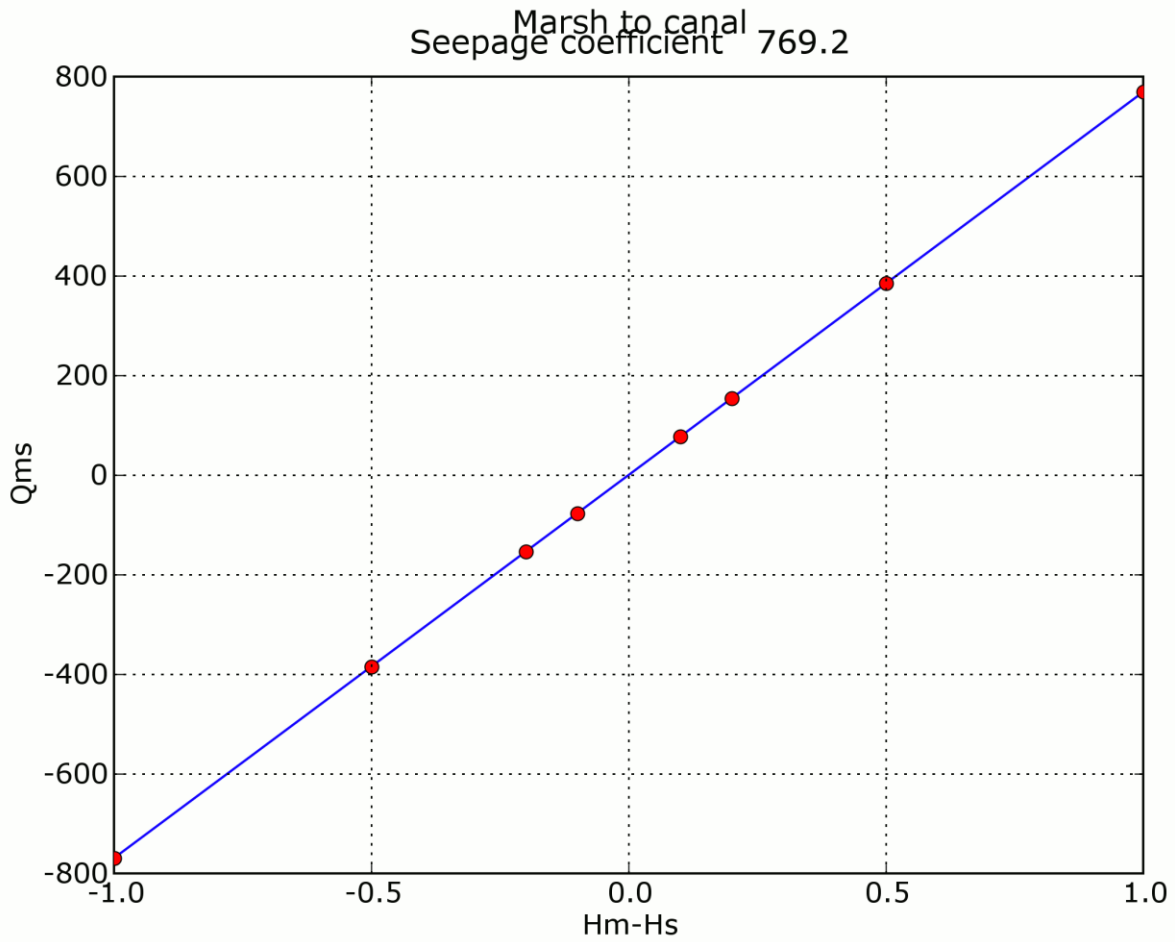


Figure 8: Seepage coefficient for C-111 between S-176 and S-177 from Marsh to Canal.

3.2. C-111 between S-177 and S-18C

Scenarios

Table 4: Reported water levels for C-111 between S-177 and S-18C.

Area	Water Level Gauge (DBHYDRO)	Observed Water Elevation (ft NGVD)		
		Maximum	Average	Minimum
Everglades National Park (west)	G-3619	4.2	2.5	0.4
C-111 Canal	S-177_TW and S-18C_HW	4.2	2.2	0.2
East of C-111 Canal	G-3620	4.3	2.4	0.4

Table 5: Scenarios for C-111 between S-177 and S-18C.

Scenario	ENP (west)	C-111 Canal	East Side
marsh-1	4.6	4.5	4.5
marsh-2	4.7	4.5	4.5
marsh-3	5.0	4.5	4.5
marsh-4	5.5	4.5	4.5
marsh-5	6.0	4.5	4.5
marsh-6	6.5	4.5	4.5
dry-1	4.5	4.5	1.0
dry-2	4.5	4.5	1.5
dry-3	4.5	4.5	2.0
dry-4	4.5	4.5	2.5
dry-5	4.5	4.5	3.0
dry-6	4.5	4.5	3.5
dry-7	4.5	4.5	4.0
dry-8	4.5	4.5	4.3
dry-9	4.5	4.5	4.4
dry-10	4.5	4.5	4.6
dry-11	4.5	4.5	4.7
dry-12	4.5	4.5	5.0
dry-13	4.5	4.5	5.5
dry-14	4.5	4.5	6.0
canal-1	4.5	3.5	4.5
canal-2	4.5	4.0	4.5
canal-3	4.5	4.3	4.5
canal-4	4.5	4.4	4.5
canal-5	4.5	4.6	4.5
canal-6	4.5	4.8	4.5

Scenario	ENP (west)	C-111 Canal	East Side
canal-7	4.5	5.0	4.5
canal-8	4.5	6.0	4.5

Representative head-streamline plots

Head-streamline plots for C-111 between S-177 and S-18C are shown on the following pages. Heads (in feet MSL) for the model runs in these plots are shown below:

Table 6: Water levels for head-streamline plots.

<i>Marsh runs (Figure 9)</i>			
<i>Run ID</i>	<i>Marsh</i>	<i>Canal</i>	<i>Dry</i>
plot-marsh-1	4.6	4.5	4.5
plot-marsh-6	5.5	4.5	4.5
<i>Dry-cell runs (Figure 10)</i>			
<i>Run ID</i>	<i>Marsh</i>	<i>Canal</i>	<i>Dry</i>
plot-dry-1	4.5	4.5	3.5
plot-dry-14	4.5	4.5	5.5
<i>Canal runs (Figure 11)</i>			
<i>Run ID</i>	<i>Marsh</i>	<i>Canal</i>	<i>Dry</i>
plot-canal-1	4.5	3.5	4.5
plot-canal-8	4.5	5.5	4.5

C-111 between S177 and S18C

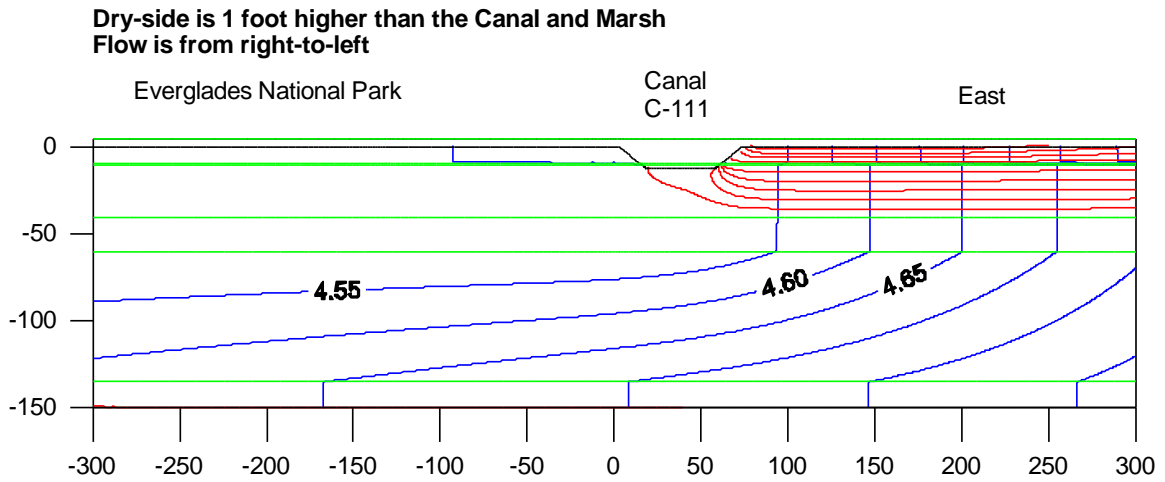
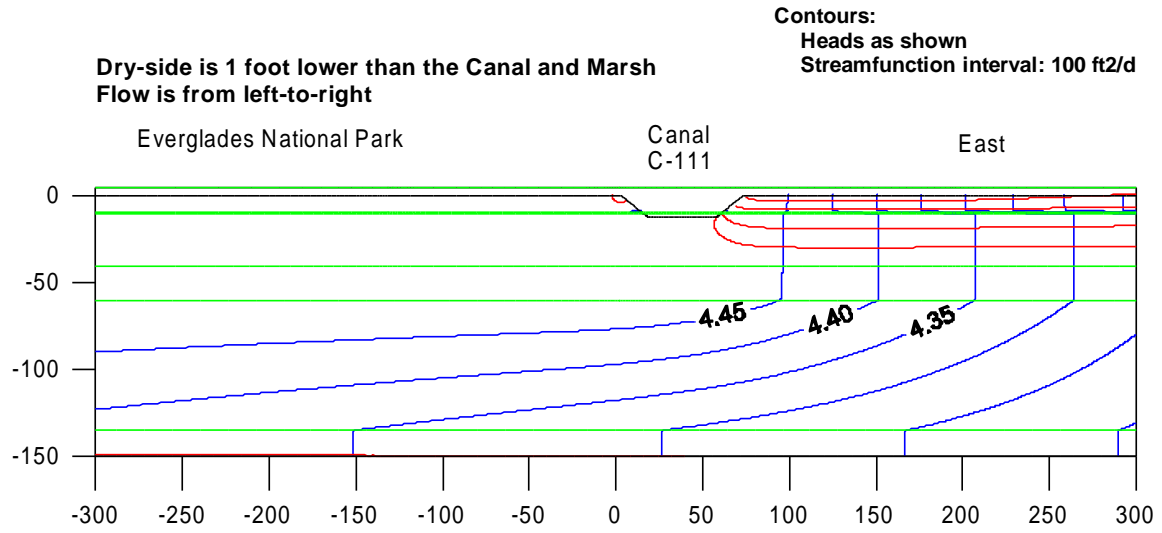


Figure 10: Heads and streamlines for C-111 between S-177 and S18C, for runs in which the dry-side water level was adjusted.

C-111 between S177 and S18C

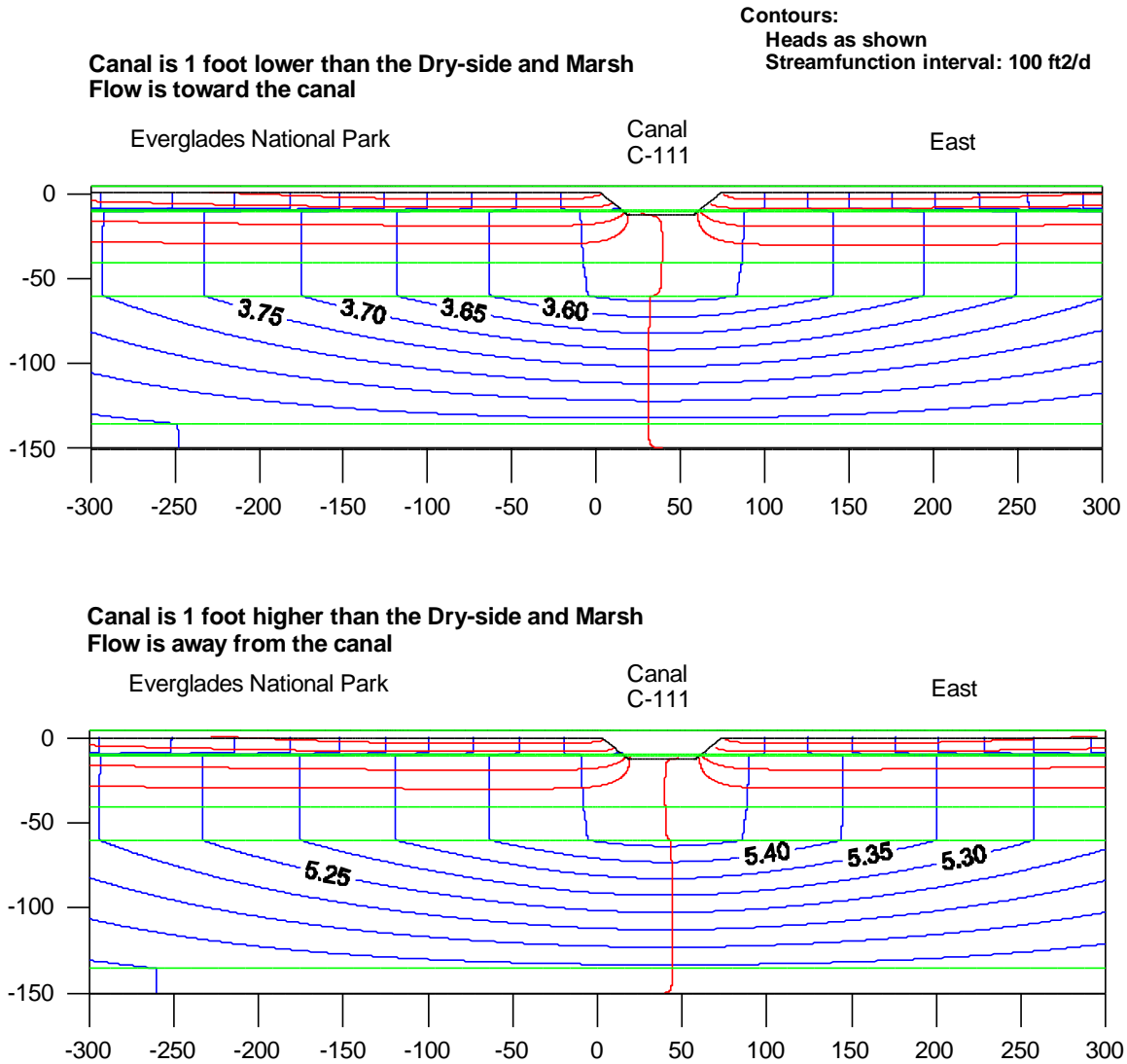


Figure 11: Heads and streamlines for C-111 between S-177 and S18C, for runs in which the canal water level was adjusted.

Seepage coefficients

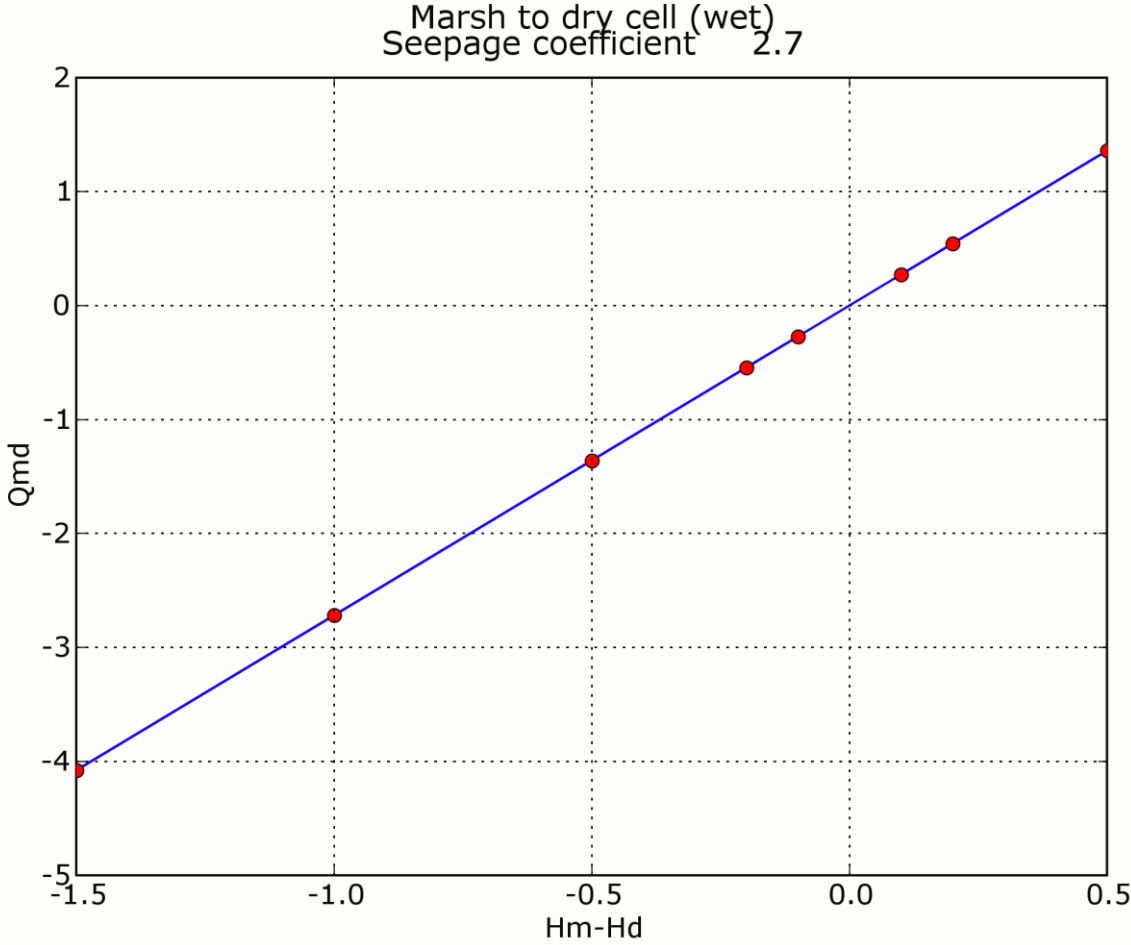


Figure 12: Seepage coefficient for C-111 between S-177 and S18C from Marsh to Dry Cell (wet).

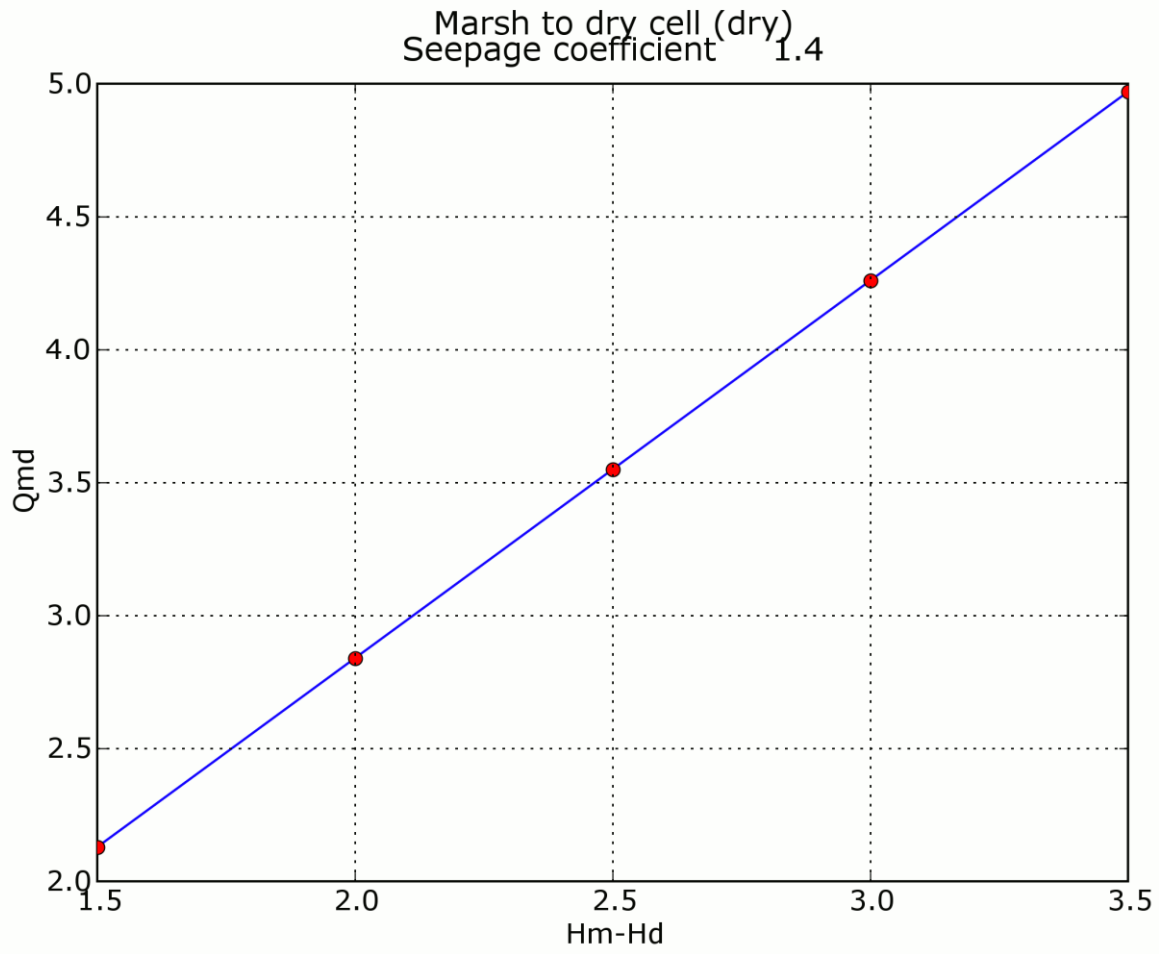


Figure 13: Seepage coefficient for C-111 between S-177 and S18C from Marsh to Dry-Cell (dry).

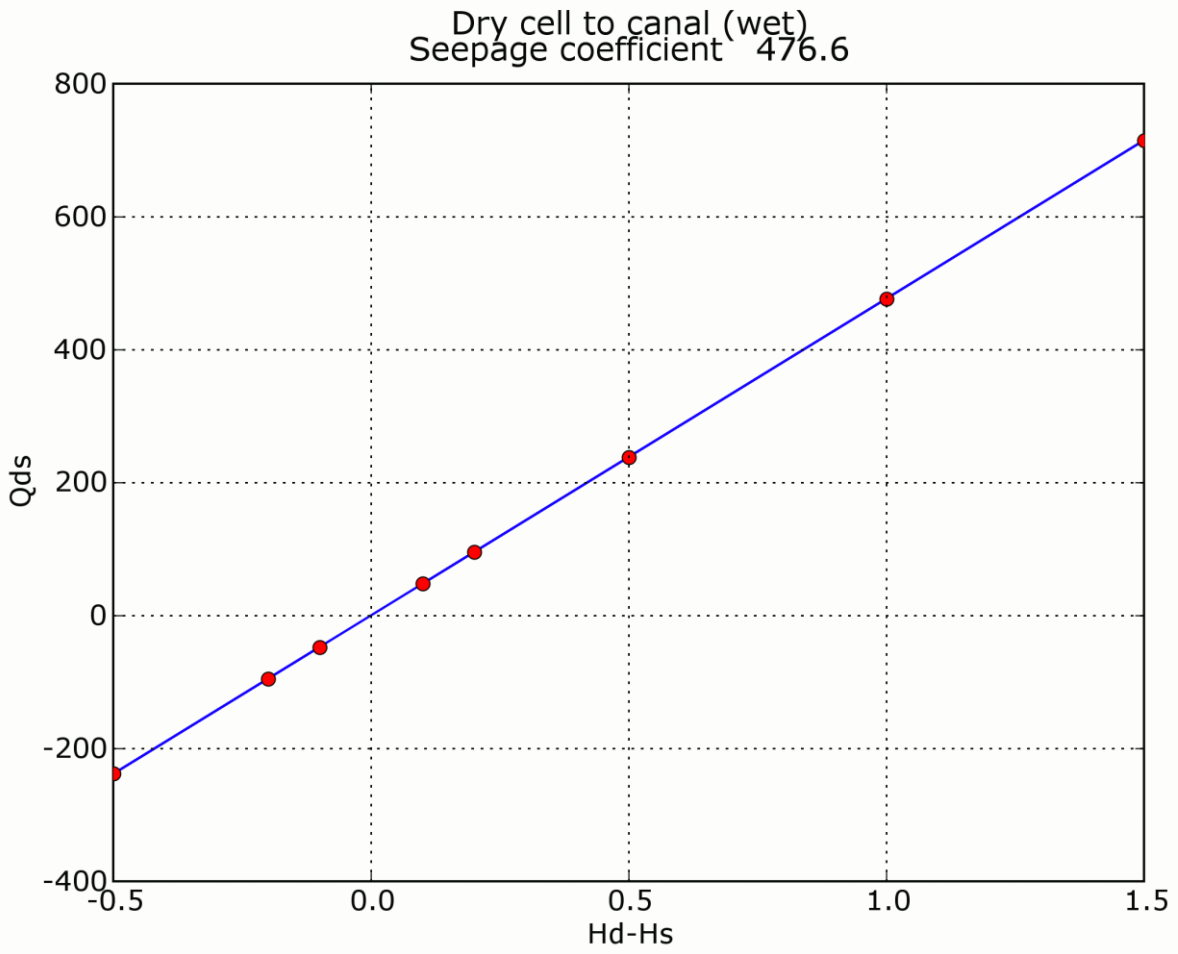


Figure 14: Seepage coefficient for C-111 between S-177 and S18C from Dry Cell to Canal (wet).

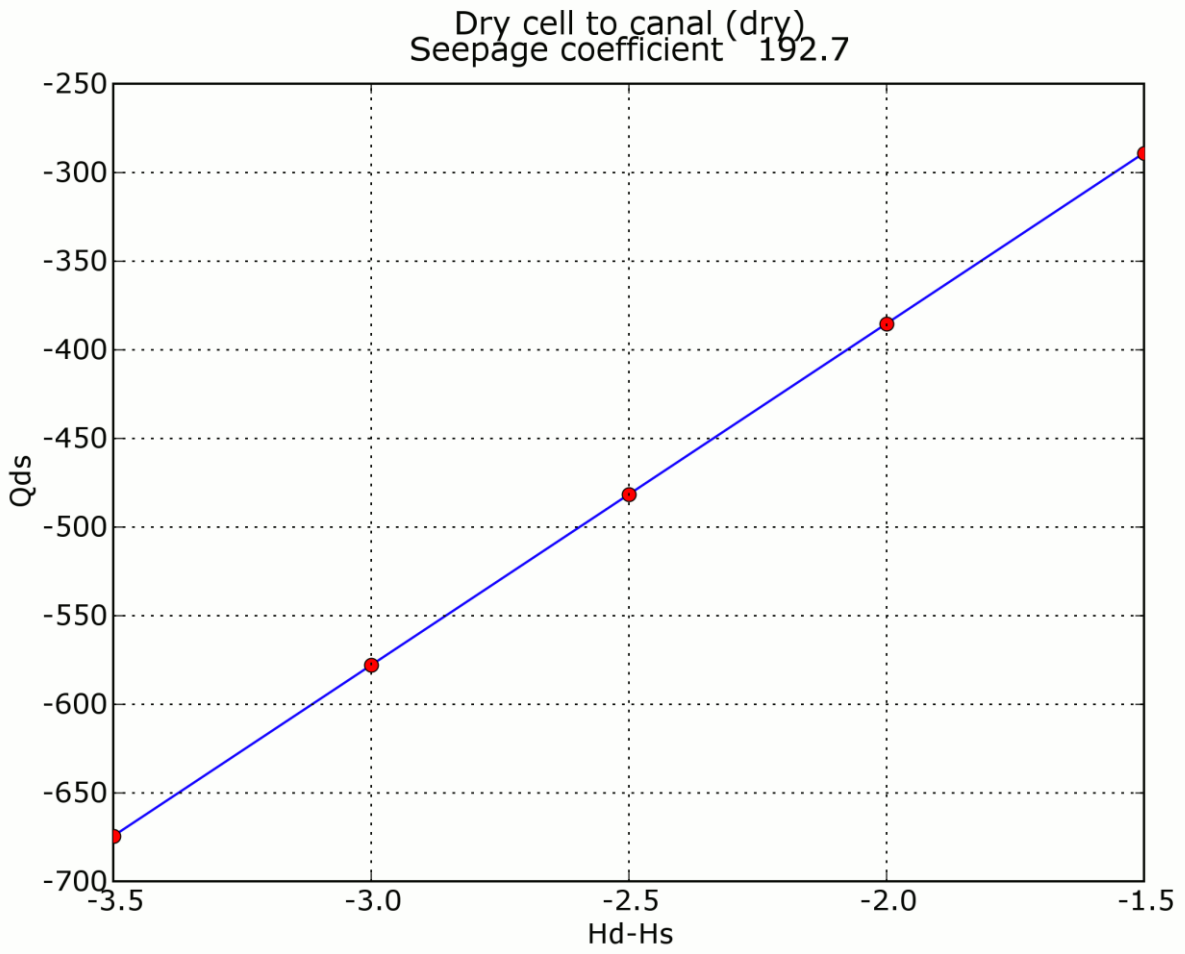


Figure 15: Seepage coefficient for C-111 between S-177 and S18C from Dry Cell to Canal (dry).

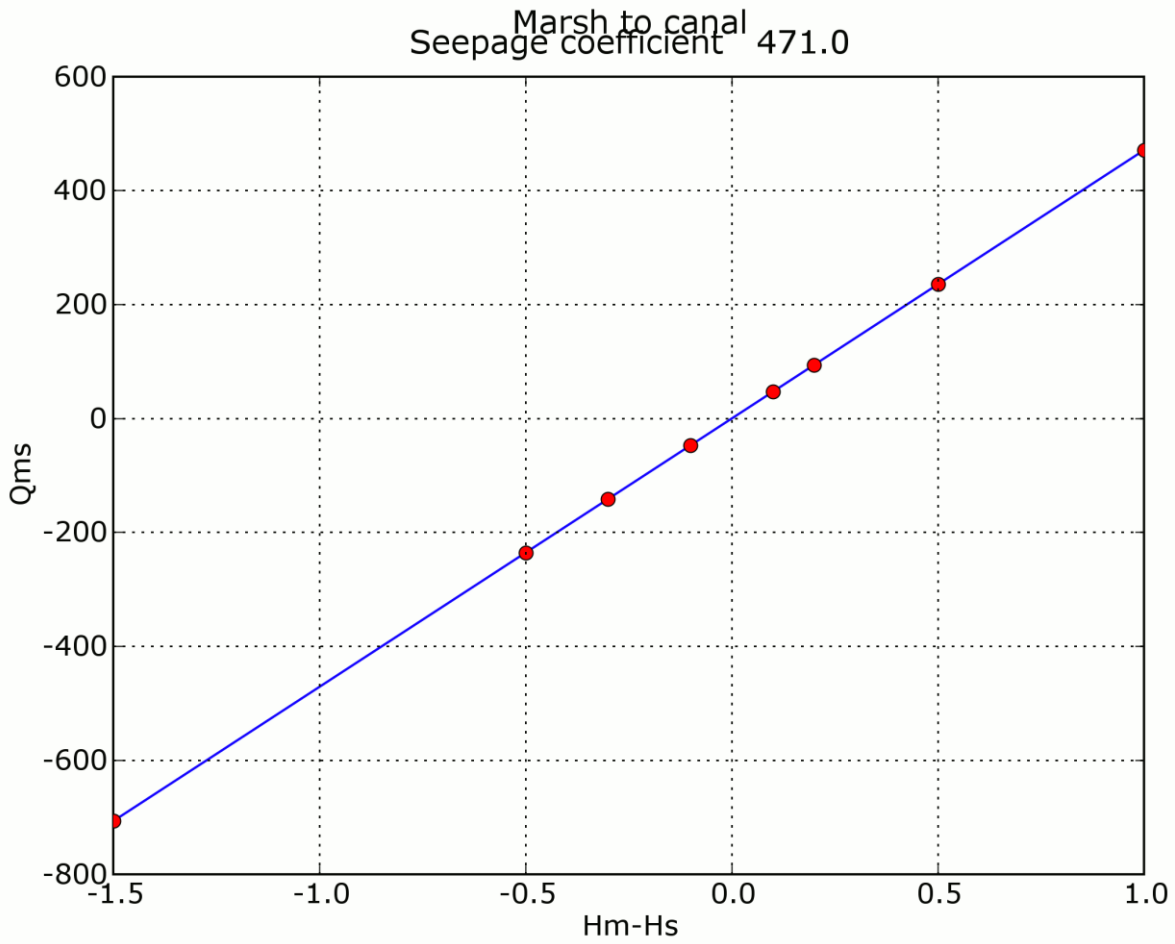


Figure 16: Seepage coefficient for C-111 between S-177 and S18C from Marsh to Canal.

3.3. L-30 south of S-335

Scenarios

Table 7: Reported water levels for L-30 south of S-335.

Area	Water Level Gauge (DBHYDRO)	Observed Water Elevation (ft NGVD)		
		Maximum	Average	Minimum
WCA3B (West)	well 3BS1W_H1	8.5	6.7	4.2
L30 Canal	S-334_TW	7.7	5.9	4.9
East	S-336_TW/G-119_HW	7.6	5.7	3.7

Table 8: Scenarios for L-30 south of S-335.

Scenario	WCA3B (west)	L30 Canal	East Side
marsh-1	5.1	5.0	5.0
marsh-2	5.2	5.0	5.0
marsh-4	5.5	5.0	5.0
marsh-5	6.0	5.0	5.0
marsh-6	6.5	5.0	5.0
marsh-7	7.0	5.0	5.0
marsh-8	8.0	5.0	5.0
dry-1	5.0	5.0	1.0
dry-2	5.0	5.0	1.5
dry-3	5.0	5.0	2.0
dry-4	5.0	5.0	2.5
dry-5	5.0	5.0	3.0
dry-6	5.0	5.0	3.5
dry-7	5.0	5.0	4.0
dry-8	5.0	5.0	4.5
dry-9	5.0	5.0	4.8
dry-10	5.0	5.0	4.9
dry-11	5.0	5.0	5.1
dry-12	5.0	5.0	5.2
dry-13	5.0	5.0	5.5
dry-14	5.0	5.0	6.0
dry-15	5.0	5.0	4.1
dry-16	5.0	5.0	4.2
dry-17	5.0	5.0	4.3
dry-18	5.0	5.0	4.4
canal-1	5.0	4.0	5.0
canal-2	5.0	4.5	5.0
canal-3	5.0	4.8	5.0
canal-4	5.0	4.9	5.0

Scenario	WCA3B (west)	L30 Canal	East Side
canal-5	5.0	5.1	5.0
canal-6	5.0	5.2	5.0
canal-7	5.0	5.5	5.0
canal-8	5.0	6.0	5.0

Representative head-streamline plots

Head-streamline plots for L-30 south of S-335 are shown on the following pages. Heads (in feet MSL) for the model runs in these plots are shown below:

Table 9: Water levels for head-streamline plots.

<i>Marsh runs (Figure 17)</i>			
<i>Run ID</i>	<i>Marsh</i>	<i>Canal</i>	<i>Dry</i>
plot-marsh-1	5.1	5.0	5.0
plot-marsh-8	6.0	5.0	5.0
<i>Dry-cell runs (Figure 18)</i>			
<i>Run ID</i>	<i>Marsh</i>	<i>Canal</i>	<i>Dry</i>
plot-dry-1	5.0	5.0	4.0
plot-dry-18	5.0	5.0	6.0
<i>Canal runs (Figure 19)</i>			
<i>Run ID</i>	<i>Marsh</i>	<i>Canal</i>	<i>Dry</i>
plot-canal-1	5.0	4.0	5.0
plot-canal-8	5.0	6.0	5.0

L-30 south of S335

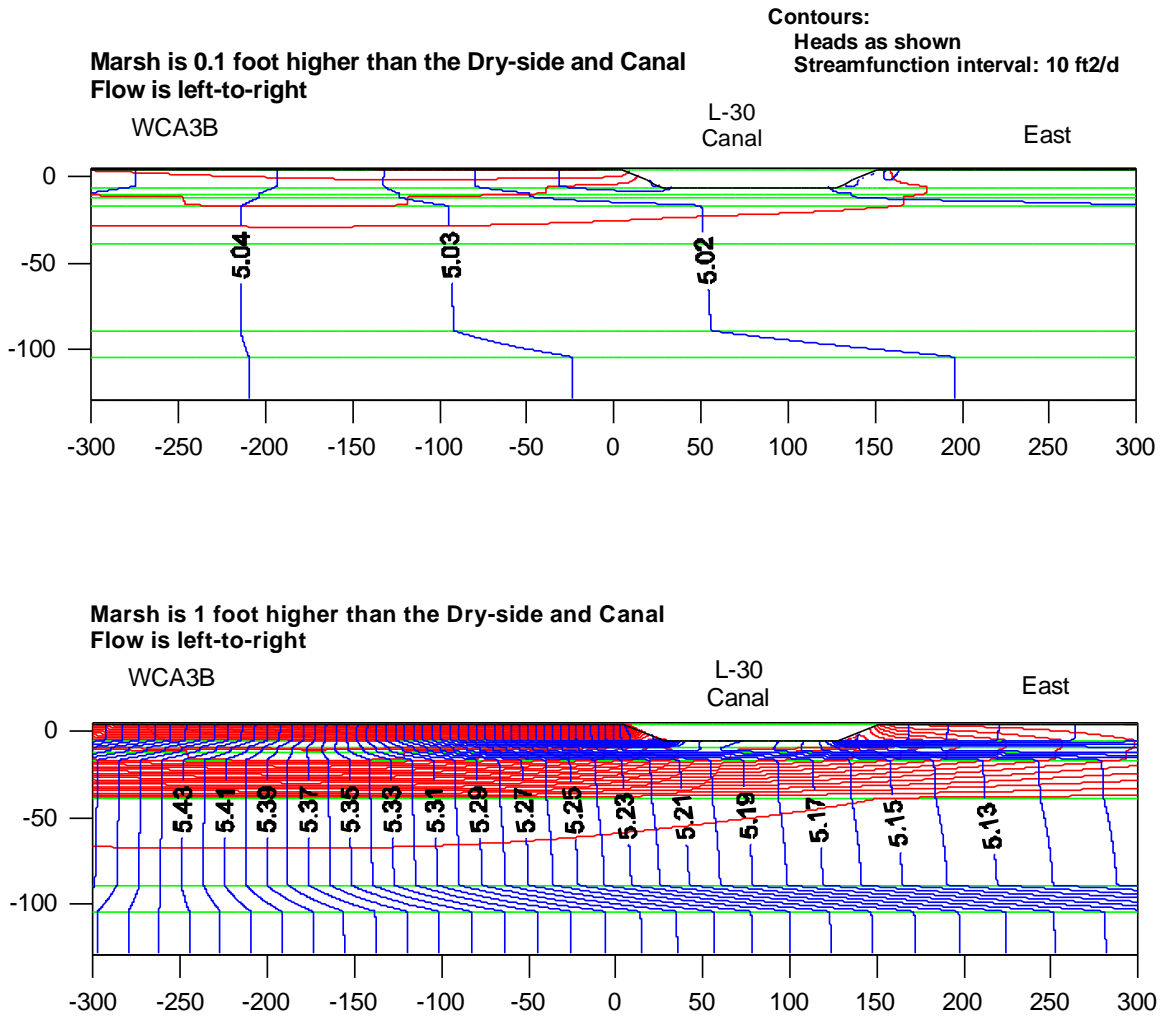


Figure 17: Heads and streamlines for L-30 south of S-335, for runs in which the marsh water level was

L-30 south of S335

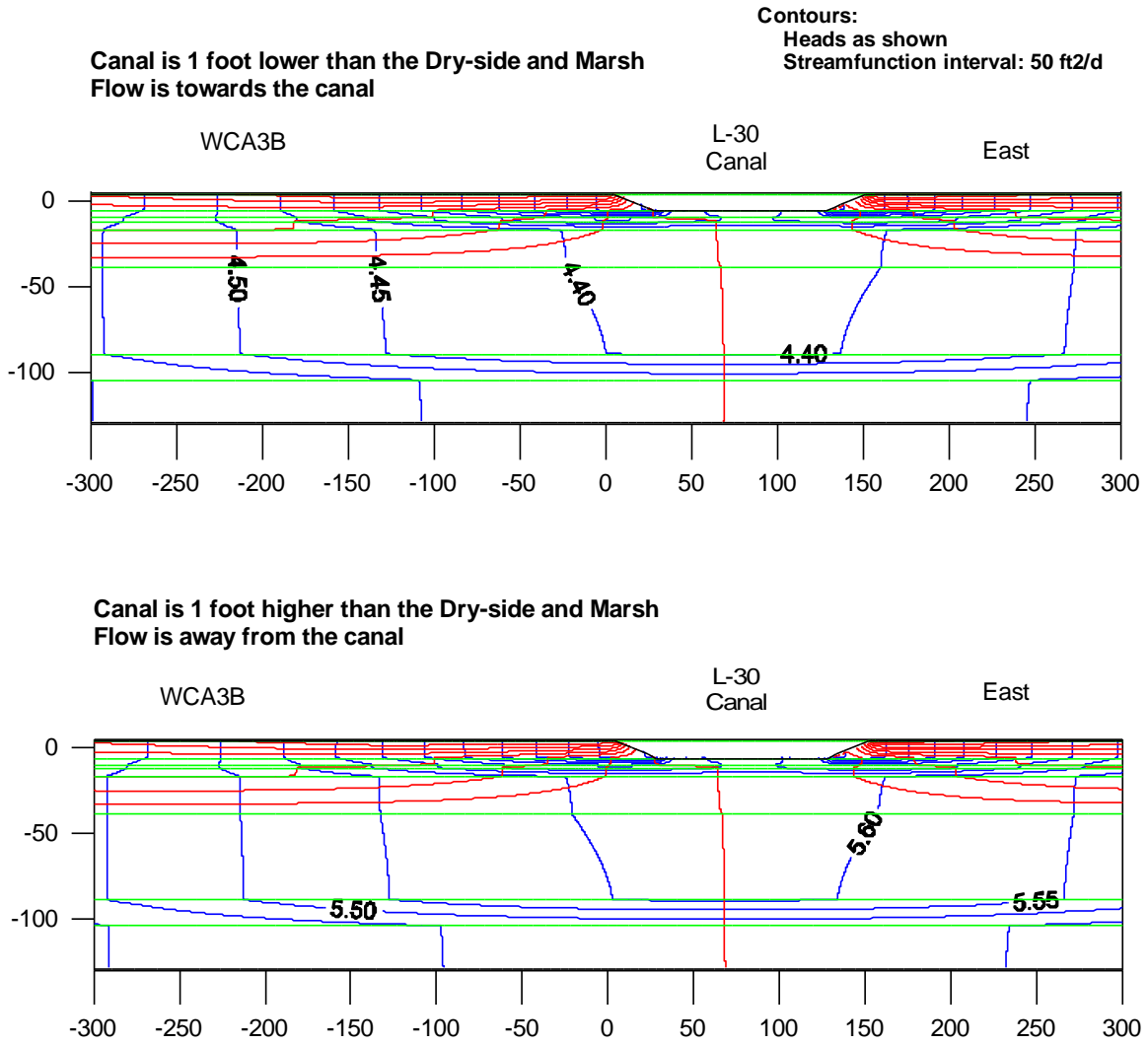


Figure 19: Heads and streamlines for L-30 south of S-335, for runs in which the canal water level was

Seepage coefficients

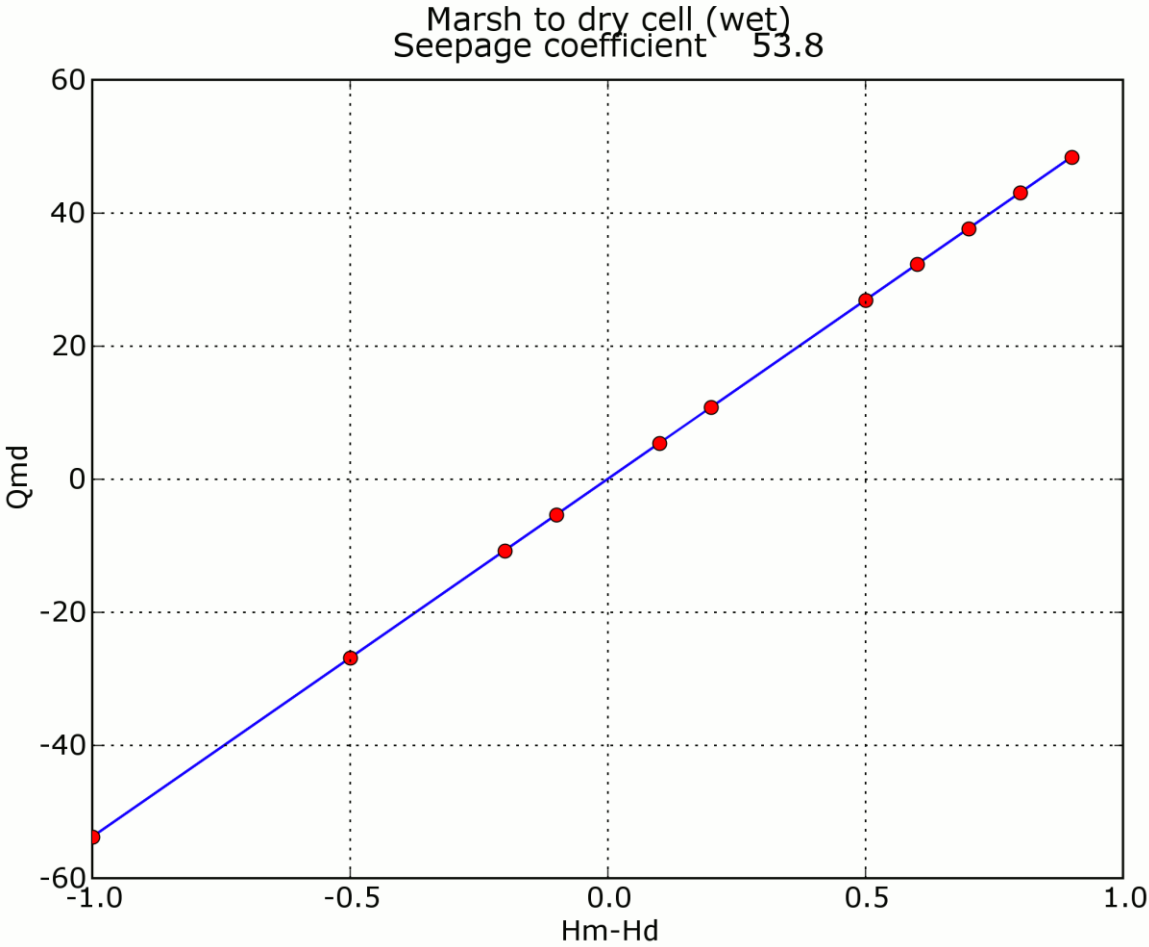


Figure 20: Seepage coefficient for L-30 south of S-335 from Marsh to Dry Cell (wet).

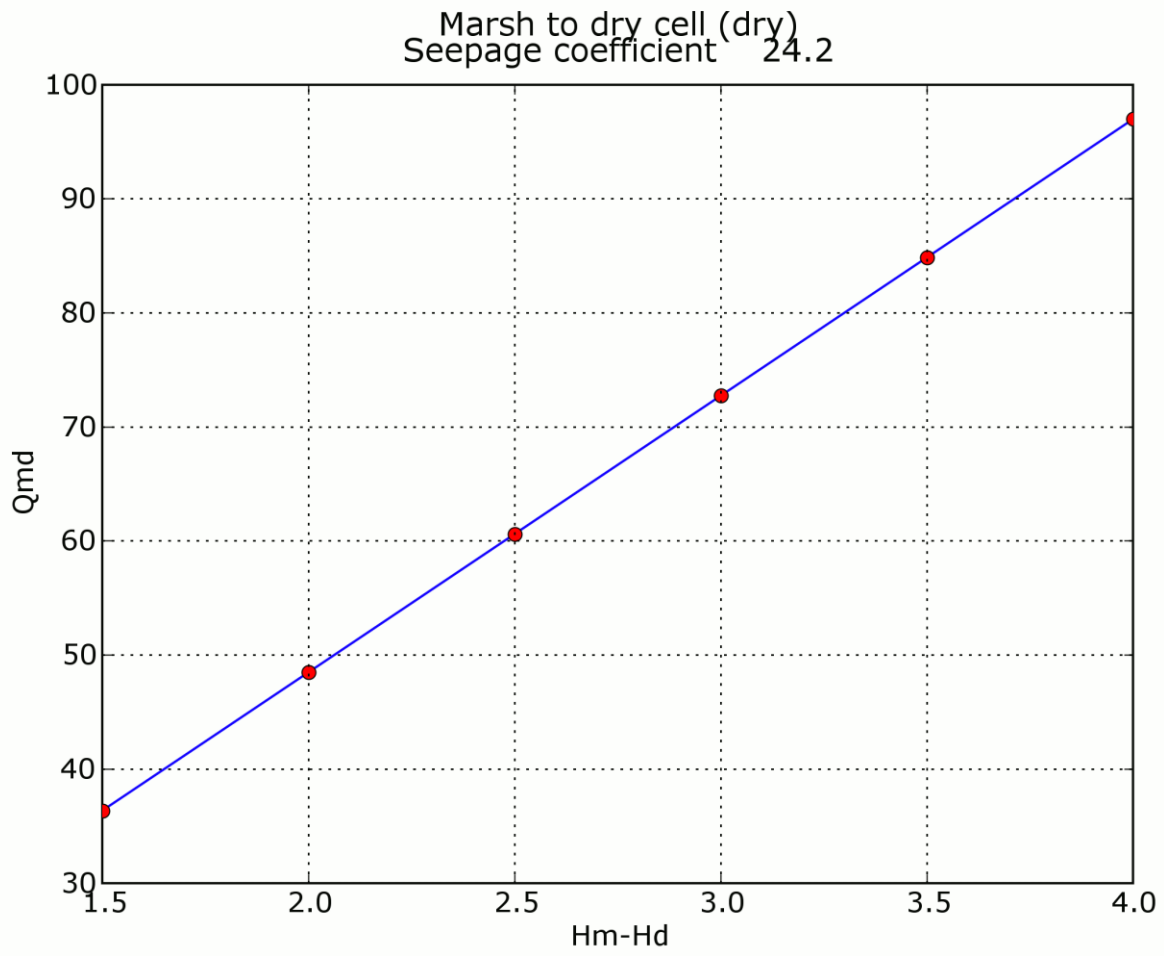


Figure 21: Seepage coefficient for L-30 south of S-335 from Marsh to Dry-Cell (dry).

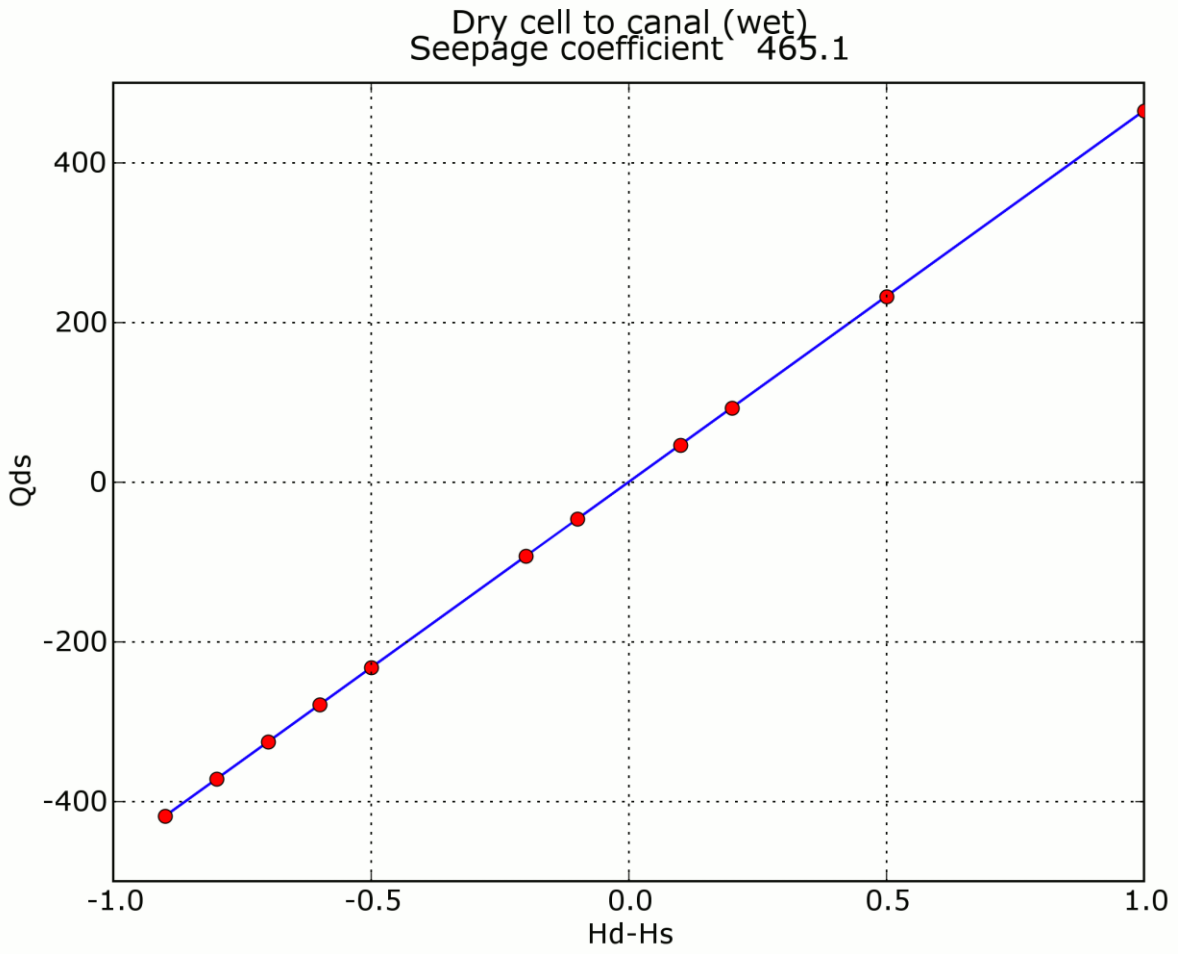


Figure 22: Seepage coefficient for L-30 south of S-335 from Dry Cell to Canal (wet).

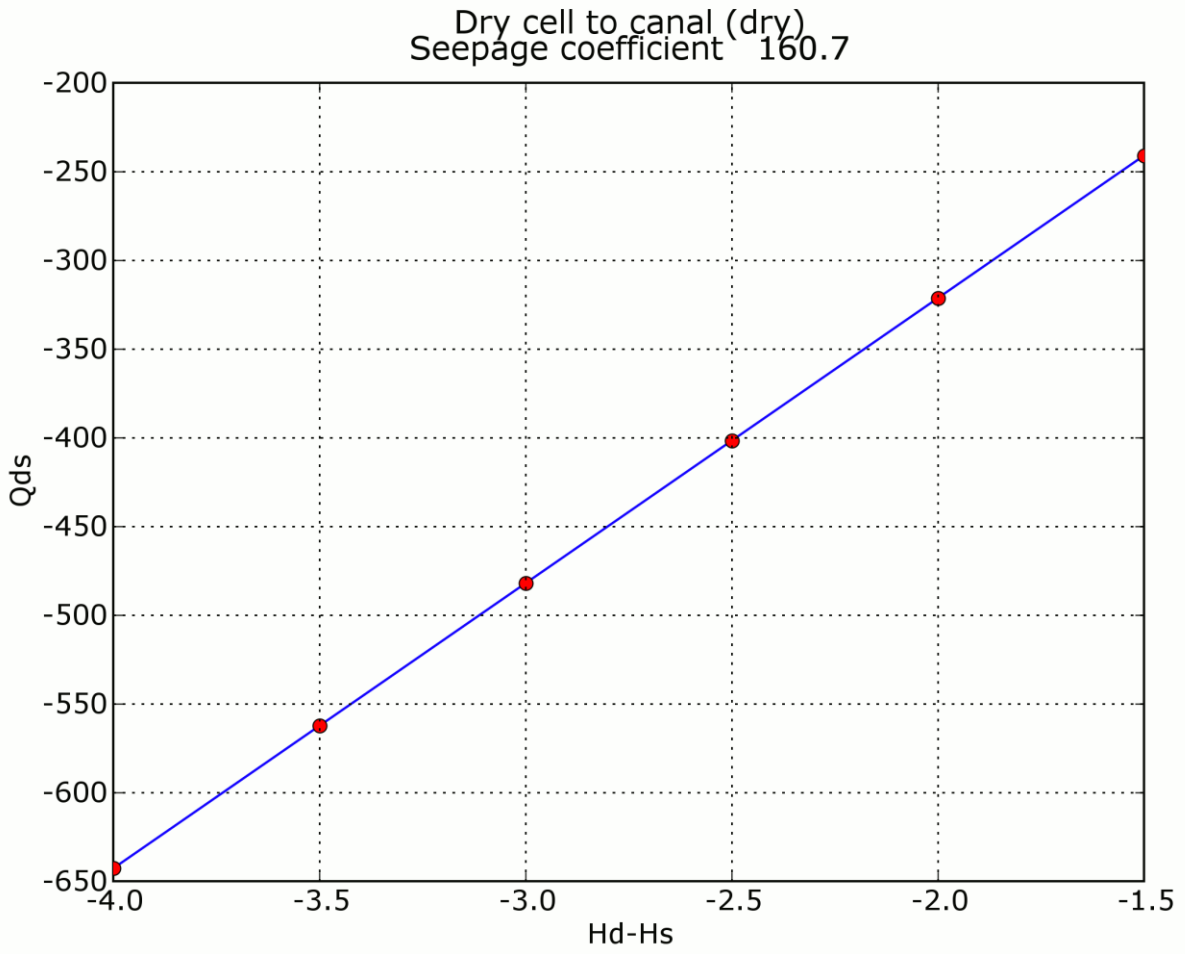


Figure 23: Seepage coefficient for L-30 south of S-335 from Dry Cell to Canal (dry).

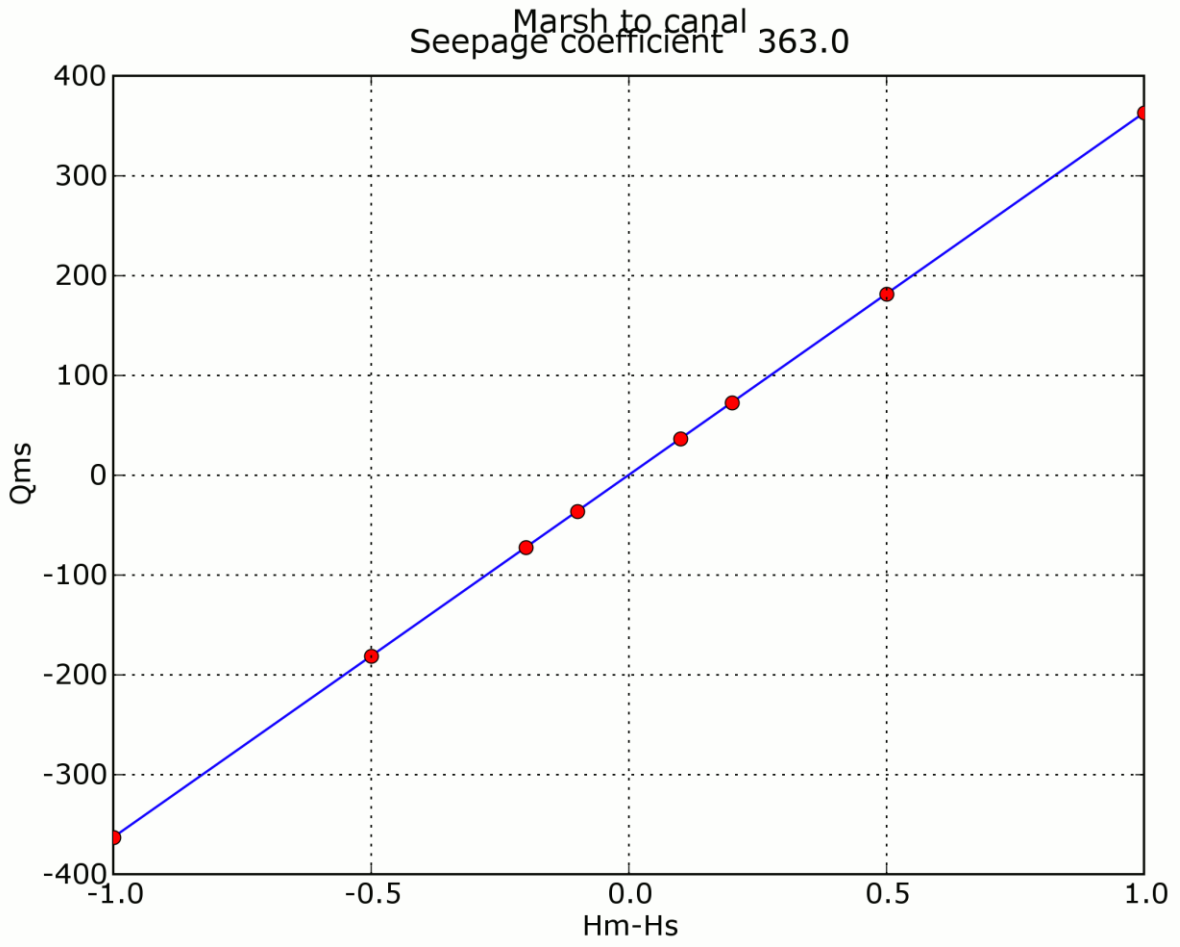


Figure 24: Seepage coefficient for L-30 south of S-335 from Marsh to Canal.

3.4. L-30 north of bridge

Scenarios

Table 10: Reported water levels for L-30 north of the bridge.

Area	Water Level Gauge (DBHYDRO)	Observed Water Elevation (ft NGVD)		
		Maximum	Average	Minimum
WCA3A (West)	G-968	8.9	6.5	3.0
L30 Canal	S337_T	8.7	6.5	3.2
East	G-975	8.2	6.0	2.1

Table 11: Scenarios for L-30 north of the bridge.

Scenario	WCA3A (west)	L30 Canal	East Side
marsh-1	4.6	4.5	4.5
marsh-2	4.7	4.5	4.5
marsh-4	5.0	4.5	4.5
marsh-5	6.5	4.5	4.5
marsh-6	5.5	4.5	4.5
marsh-7	6.0	4.5	4.5
marsh-8	7.0	4.5	4.5
marsh-9	8.0	4.5	4.5
dry-1	4.5	4.5	0.5
dry-2	4.5	4.5	1.0
dry-3	4.5	4.5	1.5
dry-4	4.5	4.5	2.0
dry-5	4.5	4.5	2.5
dry-6	4.5	4.5	3.0
dry-7	4.5	4.5	3.5
dry-8	4.5	4.5	4.0
dry-9	4.5	4.5	4.3
dry-10	4.5	4.5	4.4
dry-11	4.5	4.5	4.6
dry-12	4.5	4.5	4.7
dry-13	4.5	4.5	5
dry-14	4.5	4.5	5.5
dry-15	4.5	4.5	2.6
dry-16	4.5	4.5	2.7
dry-17	4.5	4.5	2.8
dry-18	4.5	4.5	2.9
canal-1	4.5	3.5	4.5
canal-2	4.5	4	4.5
canal-3	4.5	4.3	4.5
canal-4	4.5	4.4	4.5

Scenario	WCA3A (west)	L30 Canal	East Side
canal-5	4.5	4.6	4.5
canal-6	4.5	4.7	4.5
canal-7	4.5	5	4.5
canal-8	4.5	5.5	4.5

Representative head-streamline plots

Head-streamline plots for L-30 north of the bridge are shown on the following pages. Heads (in feet MSL) for the model runs in these plots are shown below:

Table 12: Water levels for head-streamline plots.

<i>Marsh runs (Figure 25)</i>			
<i>Run ID</i>	<i>Marsh</i>	<i>Canal</i>	<i>Dry</i>
plot-marsh-1	4.6	4.5	4.5
plot-marsh-9	5.5	4.5	4.5
<i>Dry-cell runs (Figure 26)</i>			
<i>Run ID</i>	<i>Marsh</i>	<i>Canal</i>	<i>Dry</i>
plot-dry-1	4.5	4.5	3.5
plot-dry-18	4.5	4.5	5.5
<i>Canal runs (Figure 27)</i>			
<i>Run ID</i>	<i>Marsh</i>	<i>Canal</i>	<i>Dry</i>
plot-canal-1	4.5	3.5	4.5
plot-canal-8	4.5	5.5	4.5

L-30 north of bridge

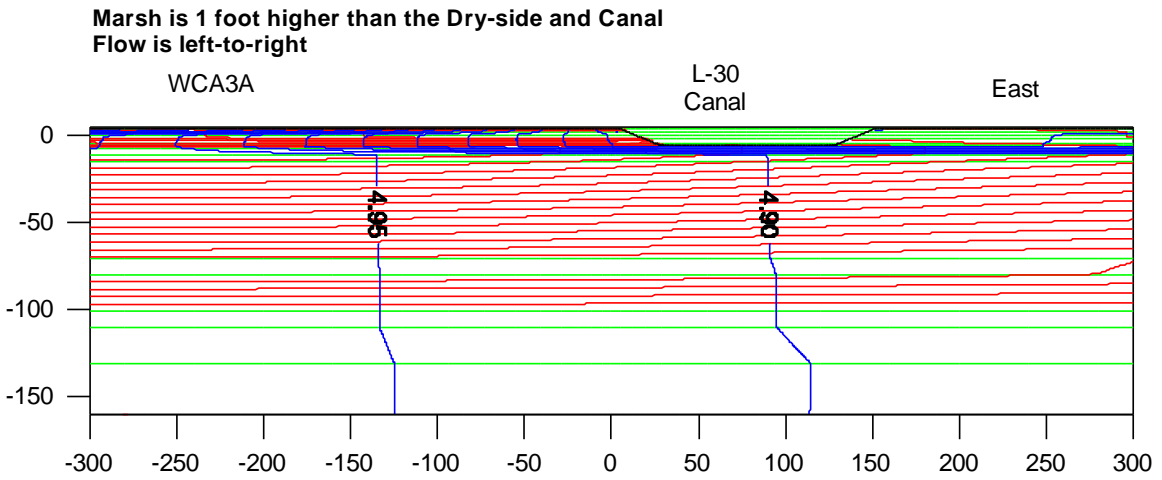
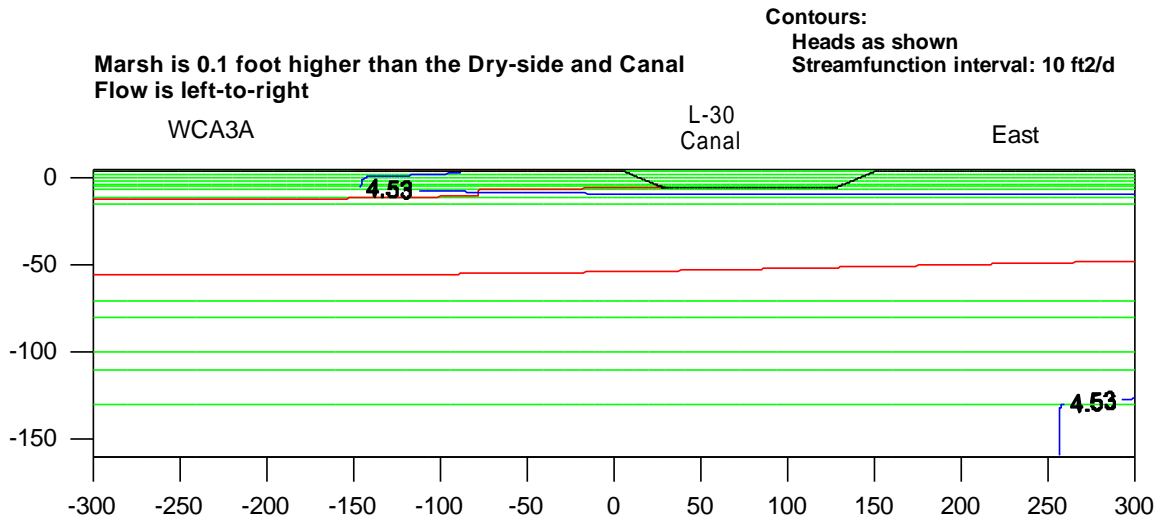


Figure 25: Heads and streamlines for L-30 north of the bridge, for runs in which the marsh water level was adjusted.

L-30 north of bridge

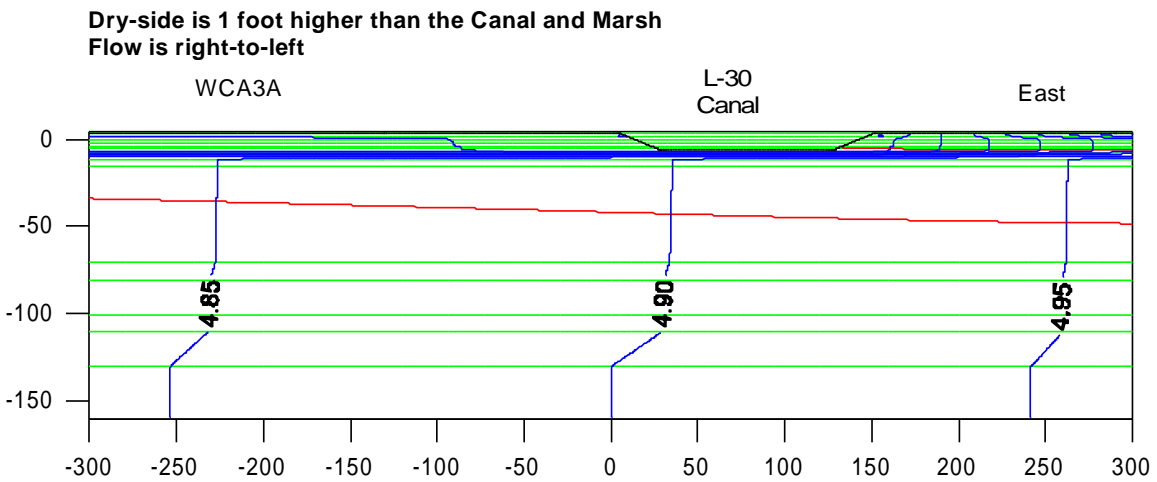
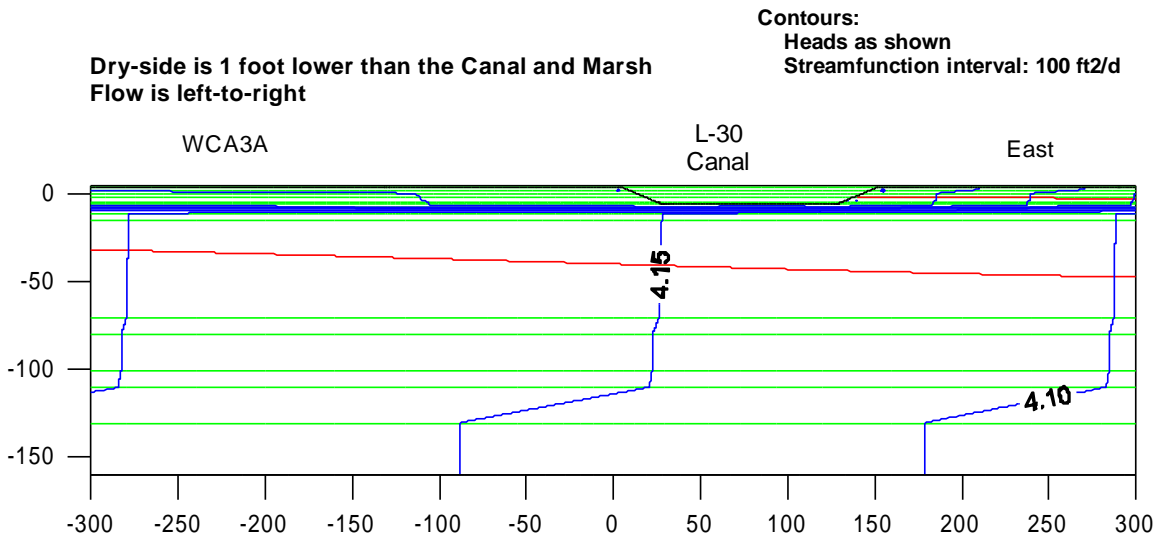


Figure 26: Heads and streamlines for L-30 north of the bridge, for runs in which the dry-side water level was adjusted.

L-30 north of bridge

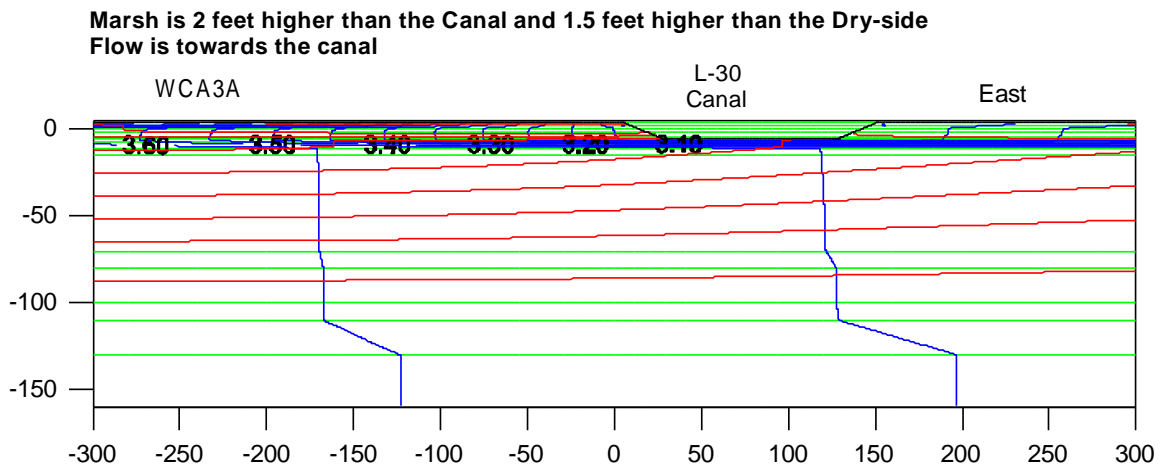
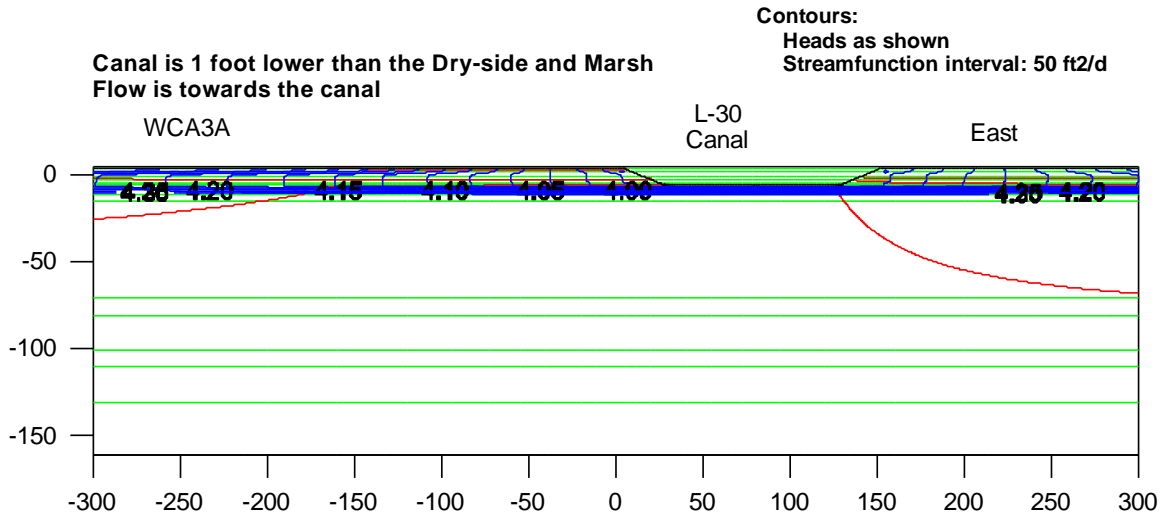


Figure 27: Heads and streamlines for L-30 north of the bridge, for runs in which the canal water level was adjusted.

Seepage coefficients

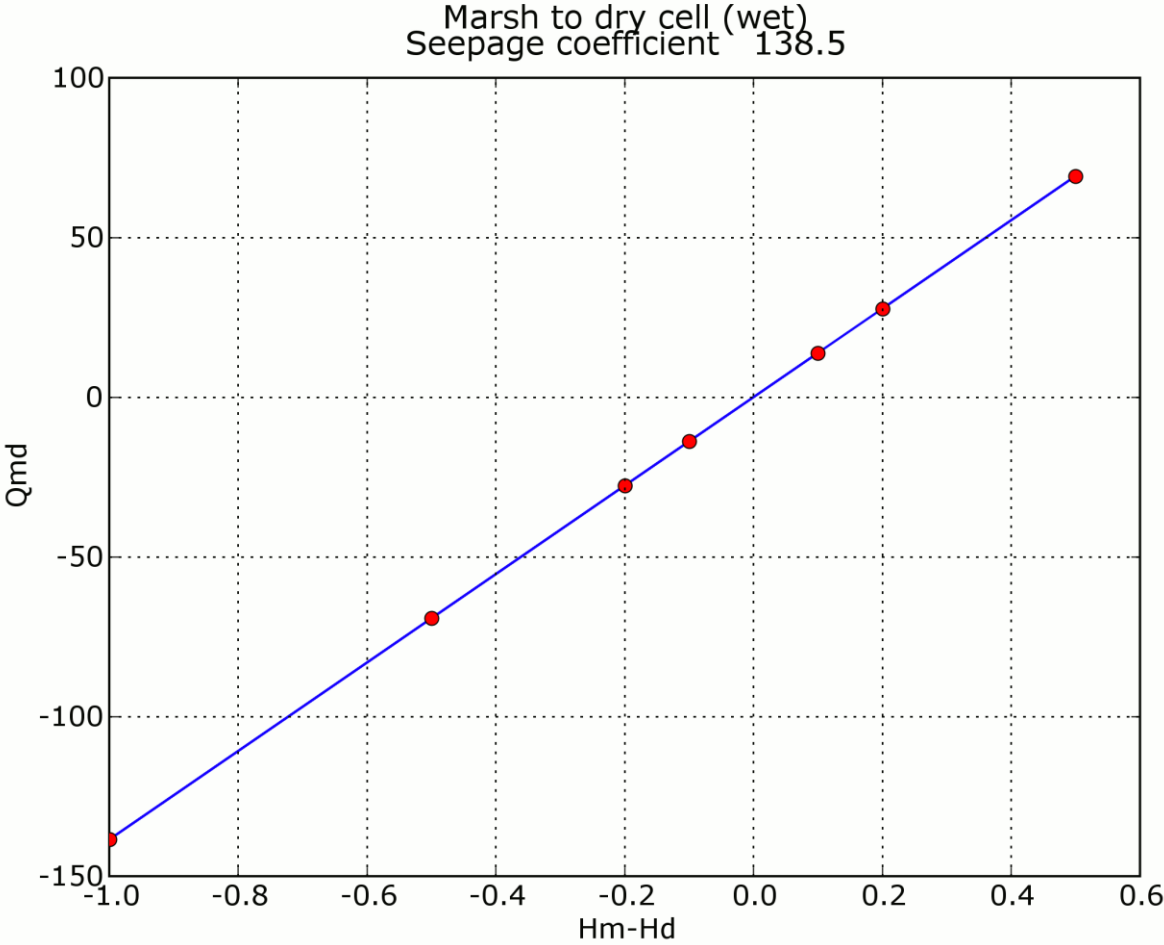


Figure 28: Seepage coefficient for L-30 north of the bridge from Marsh to Dry Cell (wet).

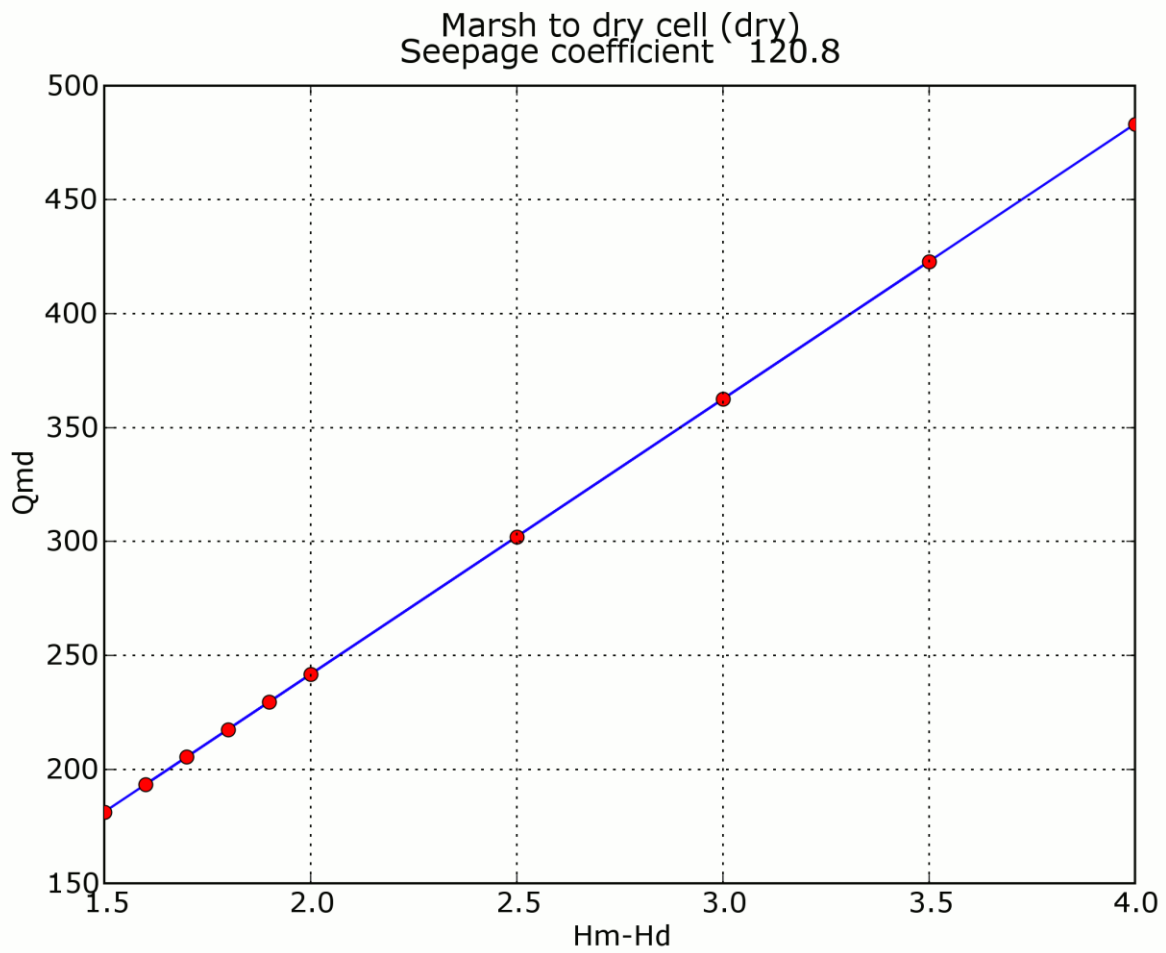


Figure 29: Seepage coefficient for L-30 north of the bridge from Marsh to Dry-Cell (dry).

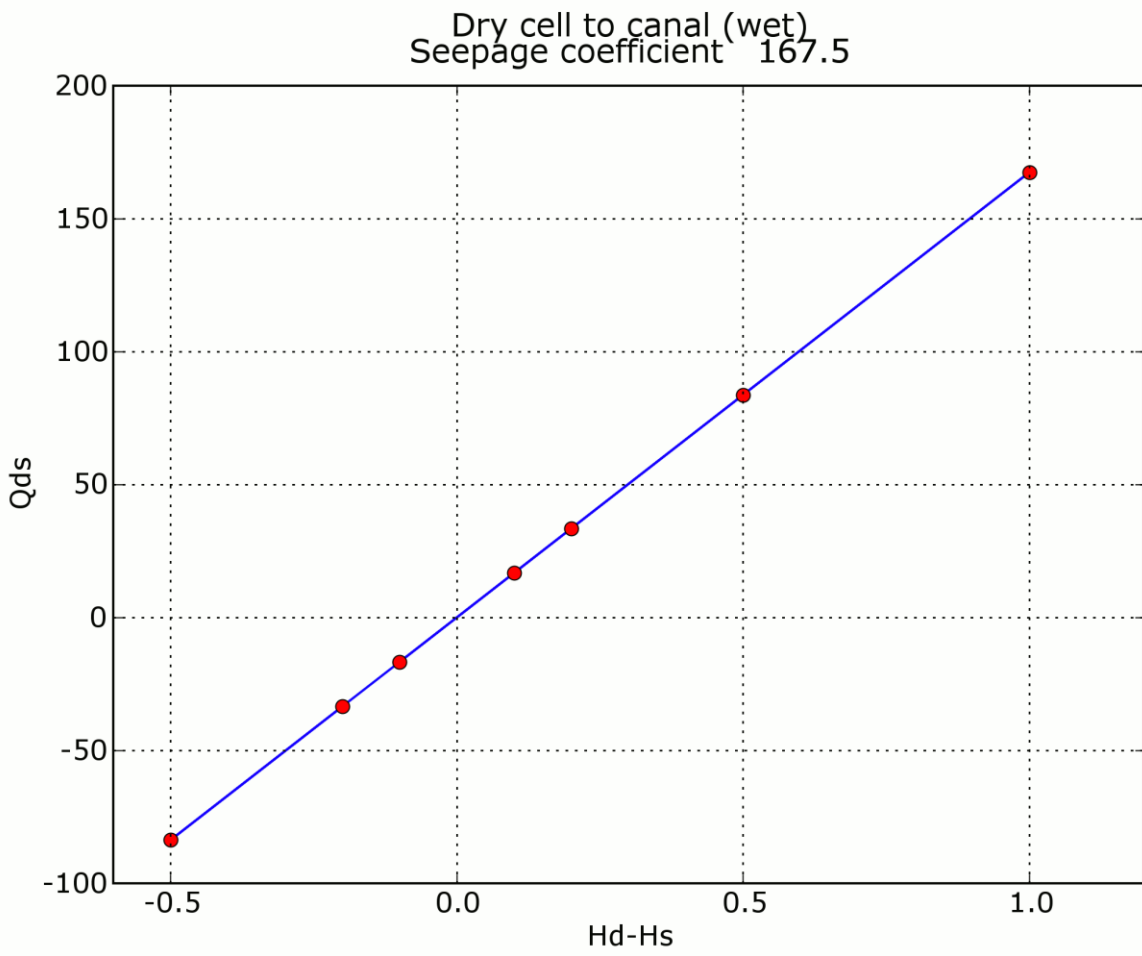


Figure 30: Seepage coefficient for L-30 north of the bridge from Dry Cell to Canal (wet).

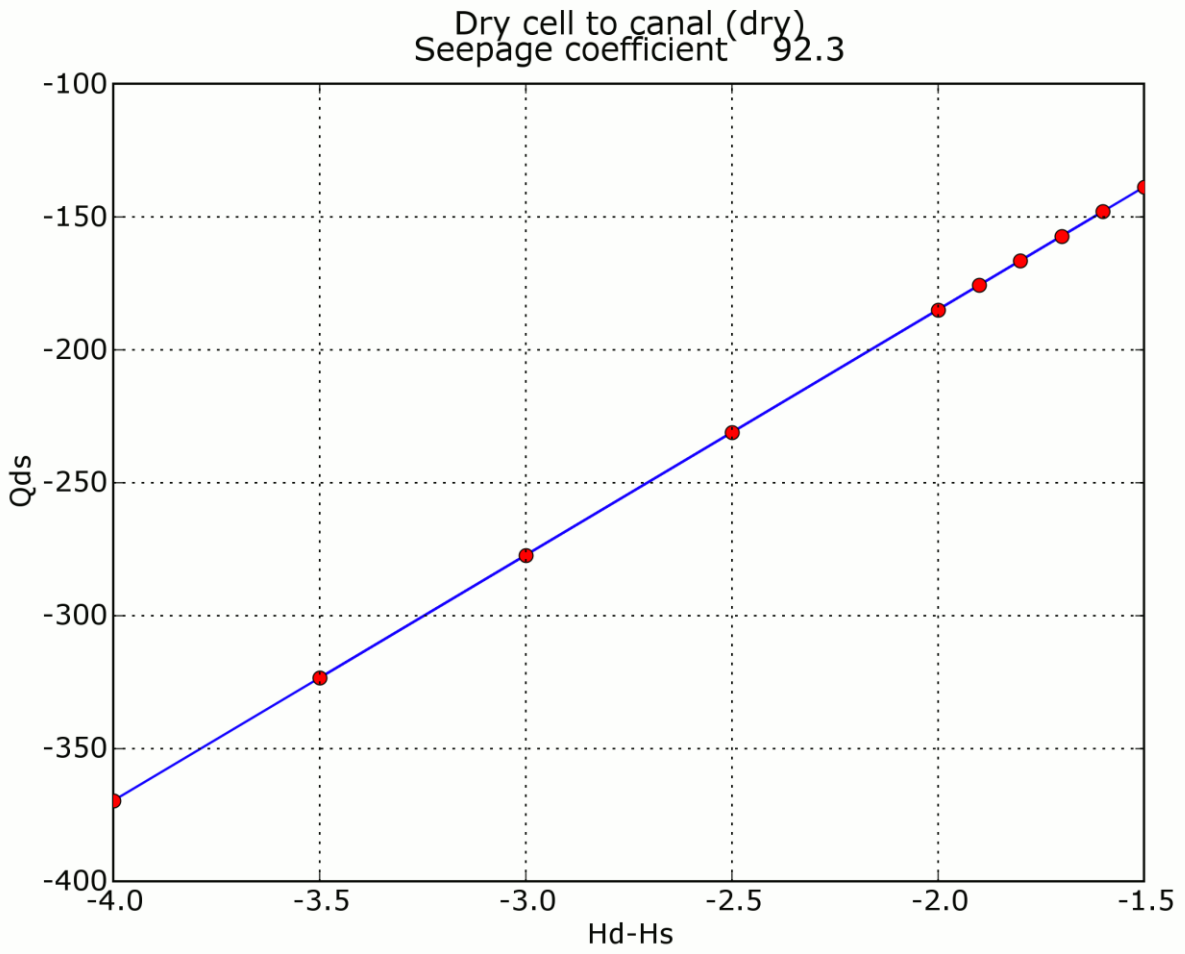


Figure 31: Seepage coefficient for L-30 north of the bridge from Dry Cell to Canal (dry).

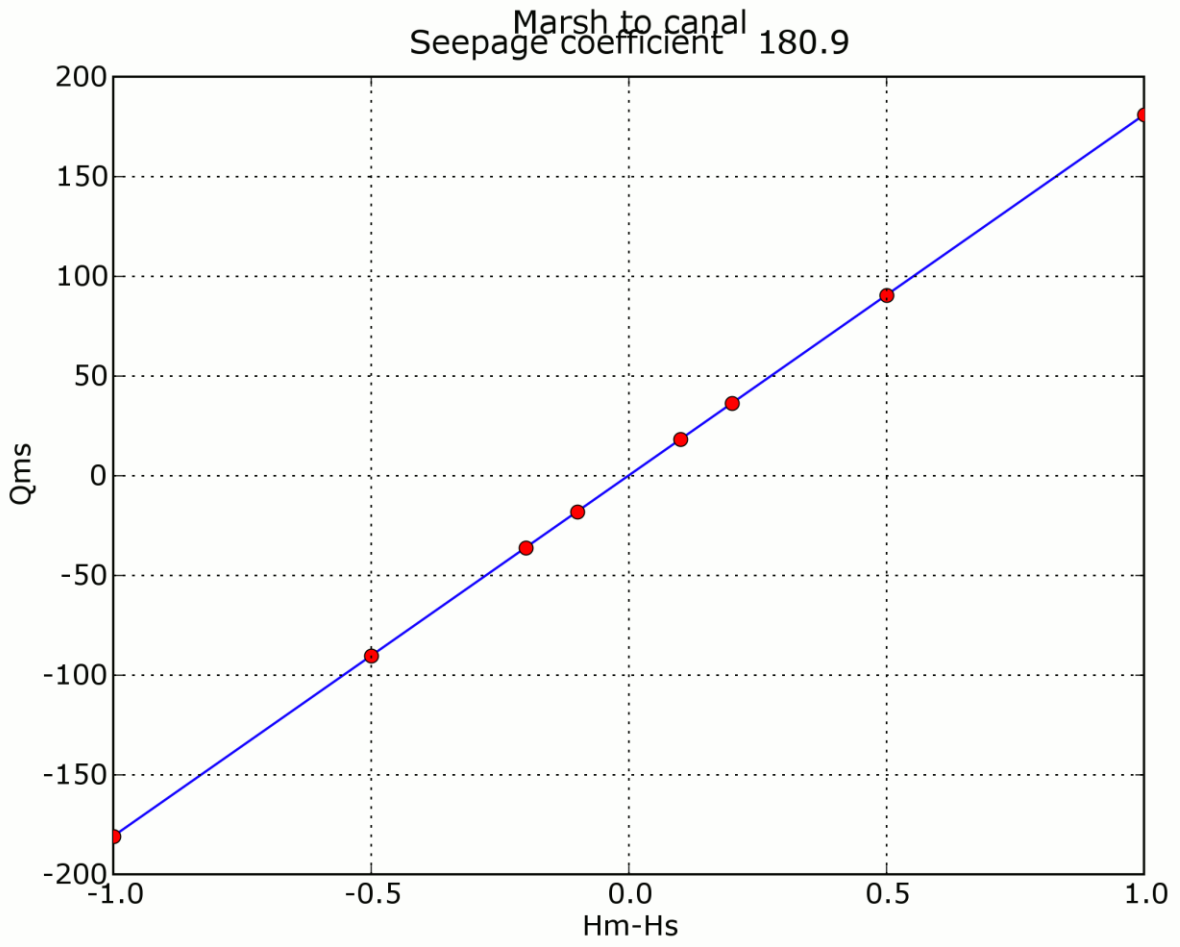


Figure 32: Seepage coefficient for L-30 north of the bridge from Marsh to Canal.

3.5. L-30 north of S-335 and south of bridge

Scenarios

Table 13: Reported water levels for L-30 north of S-335 and south of the bridge.

Area	Water Level Gauge (DBHYDRO)	Observed Water Elevation (ft NGVD)		
		Maximum	Average	Minimum
WCA3A (West)	3BS1W1_H	8.5	6.7	4.2
L30 Canal	S335_H	8.5	6.3	3.1
East	G-1488	8.3	6.2	2.7

Table 14: Scenarios for L-30 north of S-335 and south of the bridge.

Scenario	WCA3A (west)	L30 Canal	East Side
marsh-1	5.1	5.0	5.0
marsh-2	5.2	5.0	5.0
marsh-4	5.5	5.0	5.0
marsh-5	6.0	5.0	5.0
marsh-6	6.5	5.0	5.0
marsh-7	7.0	5.0	5.0
marsh-8	8.0	5.0	5.0
dry-1	5.0	5.0	1.0
dry-2	5.0	5.0	1.5
dry-3	5.0	5.0	2.0
dry-4	5.0	5.0	2.5
dry-5	5.0	5.0	3.0
dry-6	5.0	5.0	3.5
dry-7	5.0	5.0	4.0
dry-8	5.0	5.0	4.5
dry-9	5.0	5.0	4.8
dry-10	5.0	5.0	4.9
dry-11	5.0	5.0	5.1
dry-12	5.0	5.0	5.2
dry-13	5.0	5.0	5.5
dry-14	5.0	5.0	6.0
dry-15	5.0	5.0	3.1
dry-16	5.0	5.0	3.2
dry-17	5.0	5.0	3.3
dry-18	5.0	5.0	3.4
canal-1	5.0	4.0	5.0
canal-2	5.0	4.5	5.0
canal-3	5.0	4.8	5.0
canal-4	5.0	4.9	5.0
canal-5	5.0	5.1	5.0

Scenario	WCA3A (west)	L30 Canal	East Side
canal-6	5.0	5.2	5.0
canal-7	5.0	5.5	5.0
canal-8	5.0	6.0	5.0

Representative head-streamline plots

Head-streamline plots for L-30 north of S-335 and south of the bridge are shown on the following pages. Heads (in feet MSL) for the model runs in these plots are shown below:

Table 15: Water levels for head-streamline plots.

<i>Marsh runs (Figure 33)</i>			
<i>Run ID</i>	<i>Marsh</i>	<i>Canal</i>	<i>Dry</i>
plot-marsh-1	5.1	5.0	5.0
plot-marsh-6	6.0	5.0	5.0
<i>Dry-cell runs (Figure 34)</i>			
<i>Run ID</i>	<i>Marsh</i>	<i>Canal</i>	<i>Dry</i>
plot-dry-1	5.0	5.0	4.0
plot-dry-14	5.0	5.0	6.0
<i>Canal runs (Figure 35)</i>			
<i>Run ID</i>	<i>Marsh</i>	<i>Canal</i>	<i>Dry</i>
plot-canal-1	5.0	4.0	5.0
plot-canal-8	5.0	6.0	5.0

L-30 north of S-335 and south of the bridge

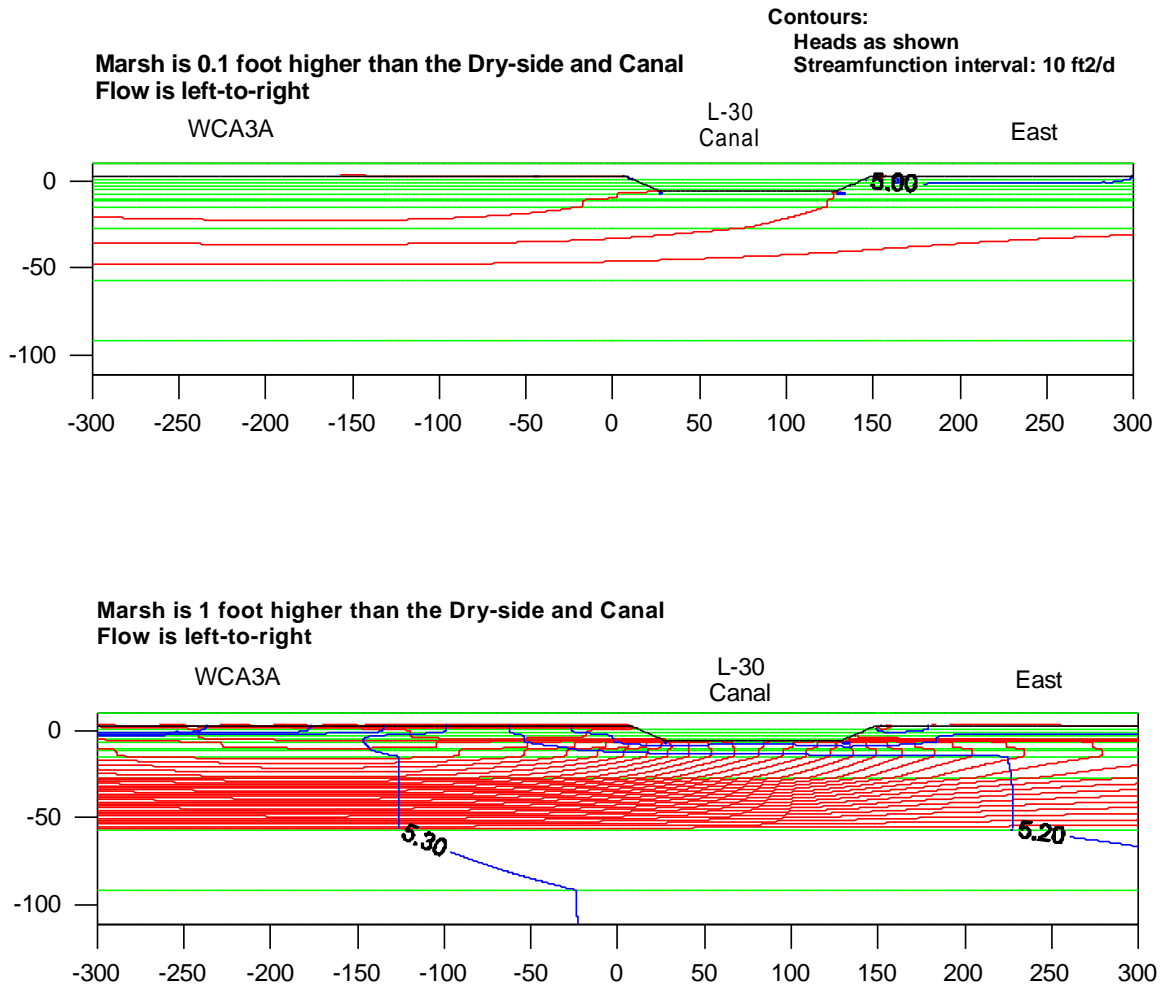


Figure 33: Heads and streamlines for L-30 north of S-335 and south of the bridge, for runs in which the marsh water level was adjusted.

L-30 north of S-335 and south of the bridge

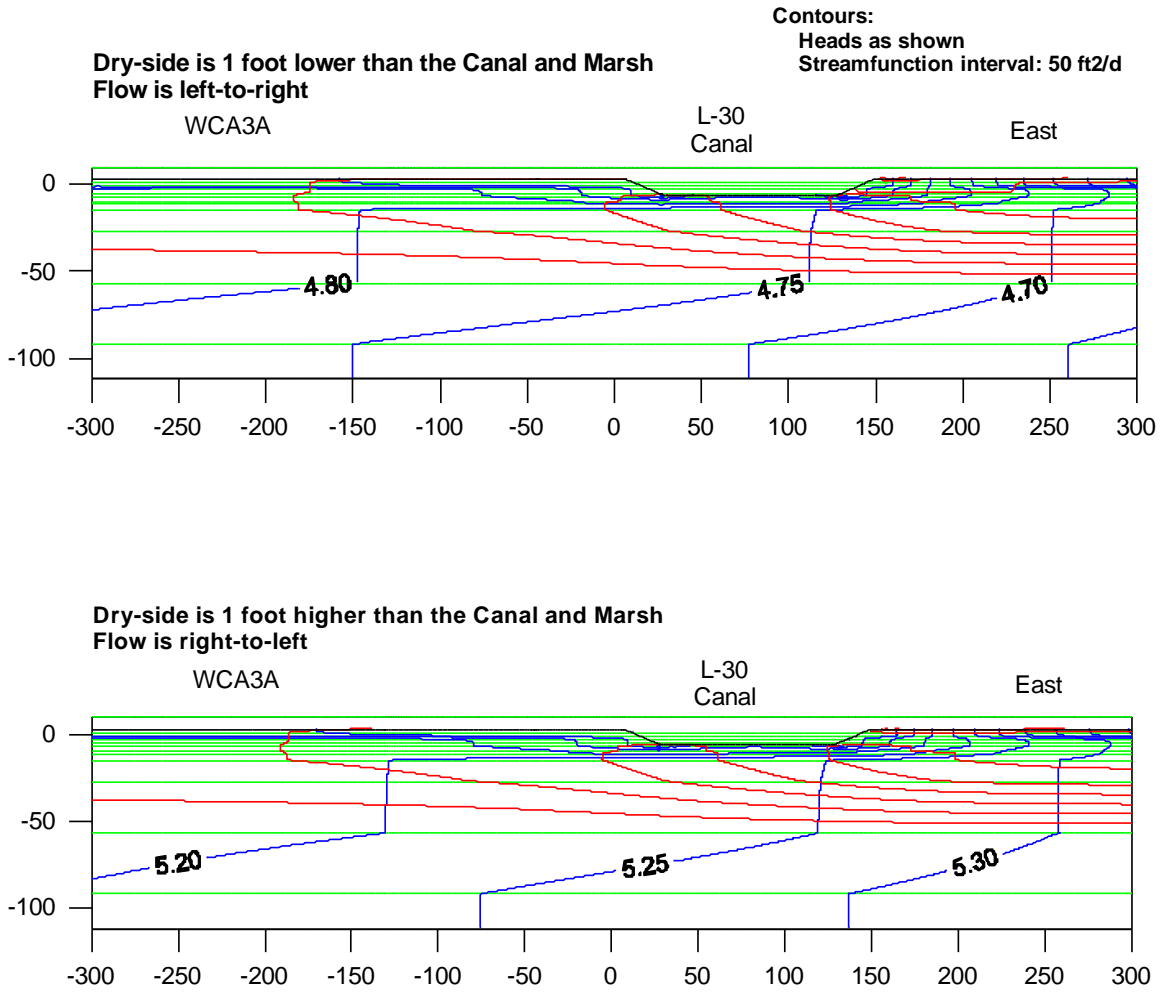


Figure 34: Heads and streamlines for L-30 north of S-335 and south of the bridge, for runs in which the dry-side water level was adjusted.

Seepage coefficients

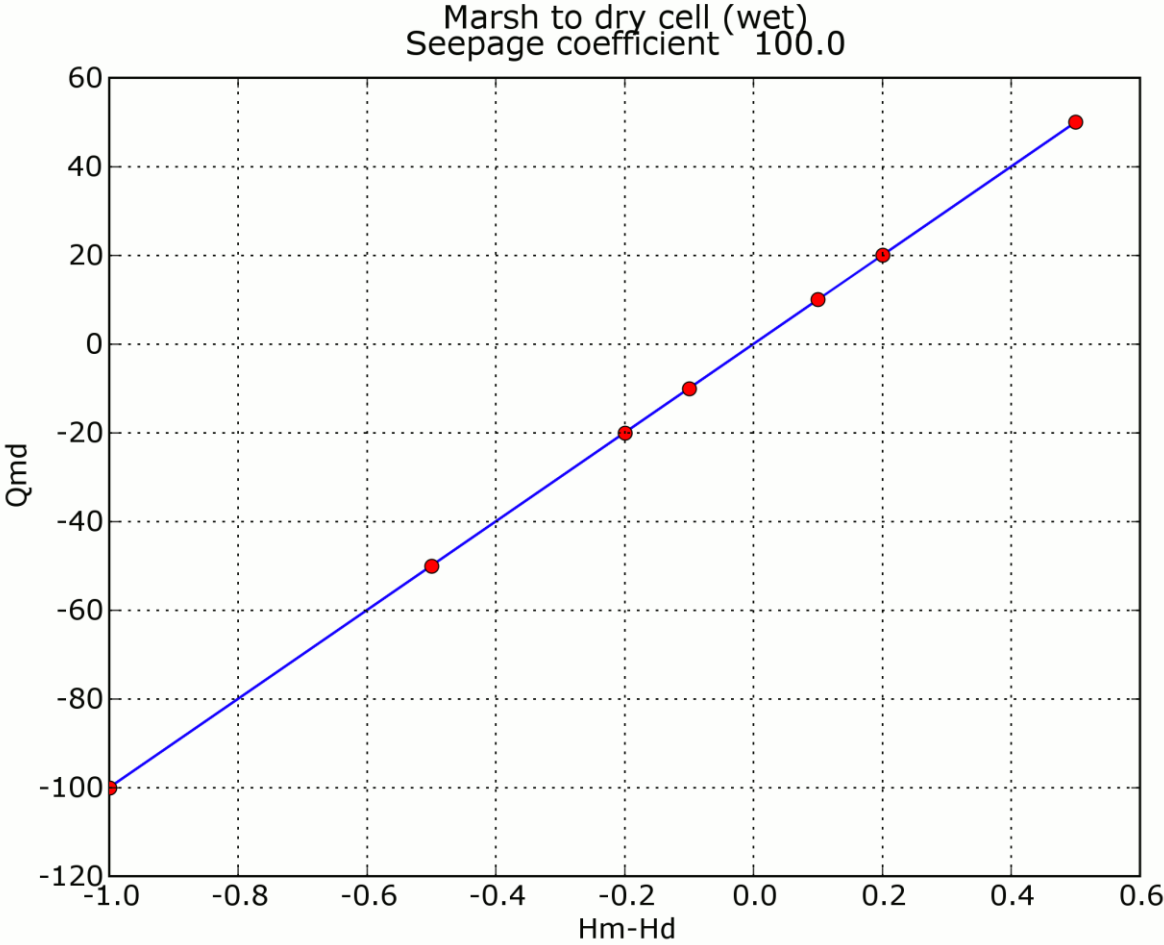


Figure 36: Seepage coefficient for L-30 north of S-335 and south of the bridge from Marsh to Dry Cell (wet).

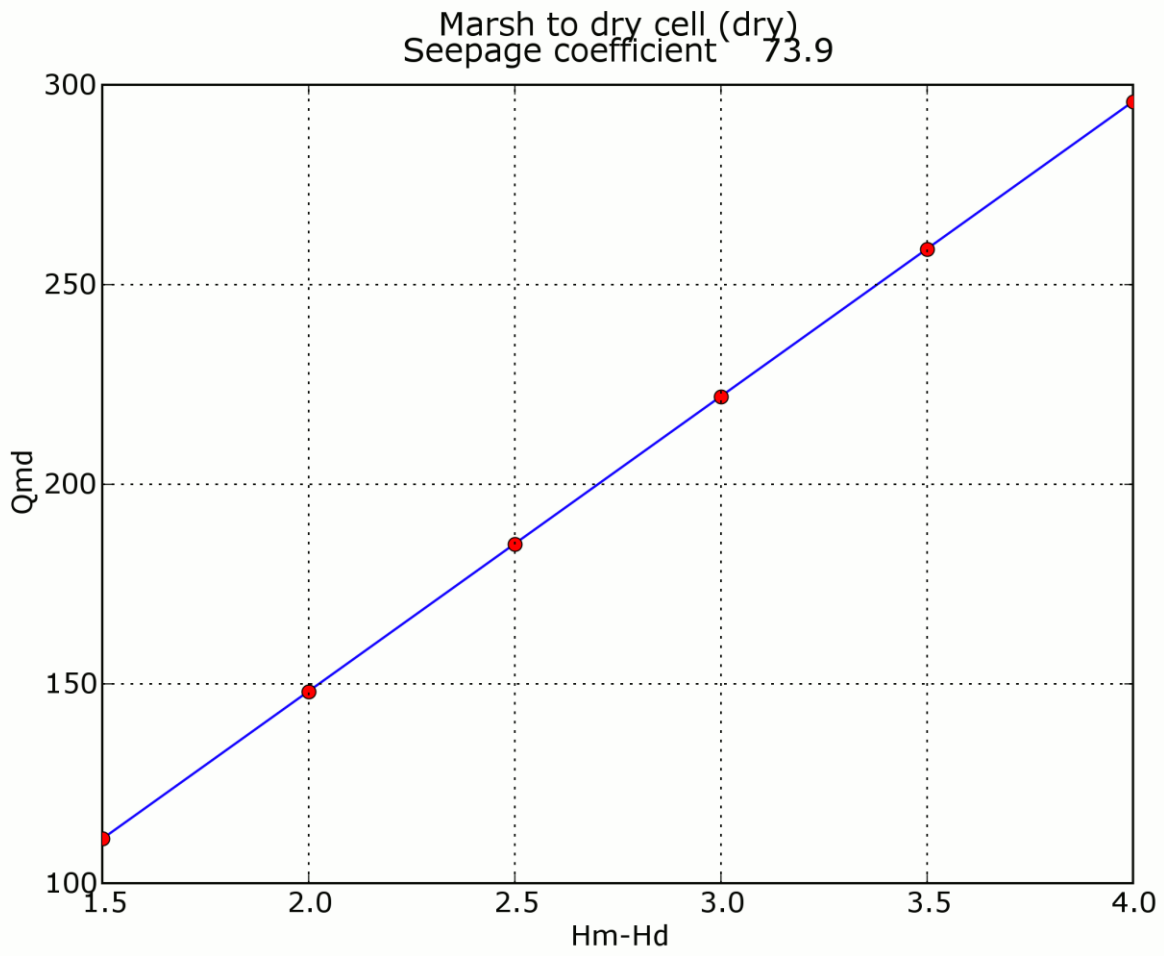


Figure 37: Seepage coefficient for L-30 north of S-335 and south of the bridge from Marsh to Dry-Cell (dry).

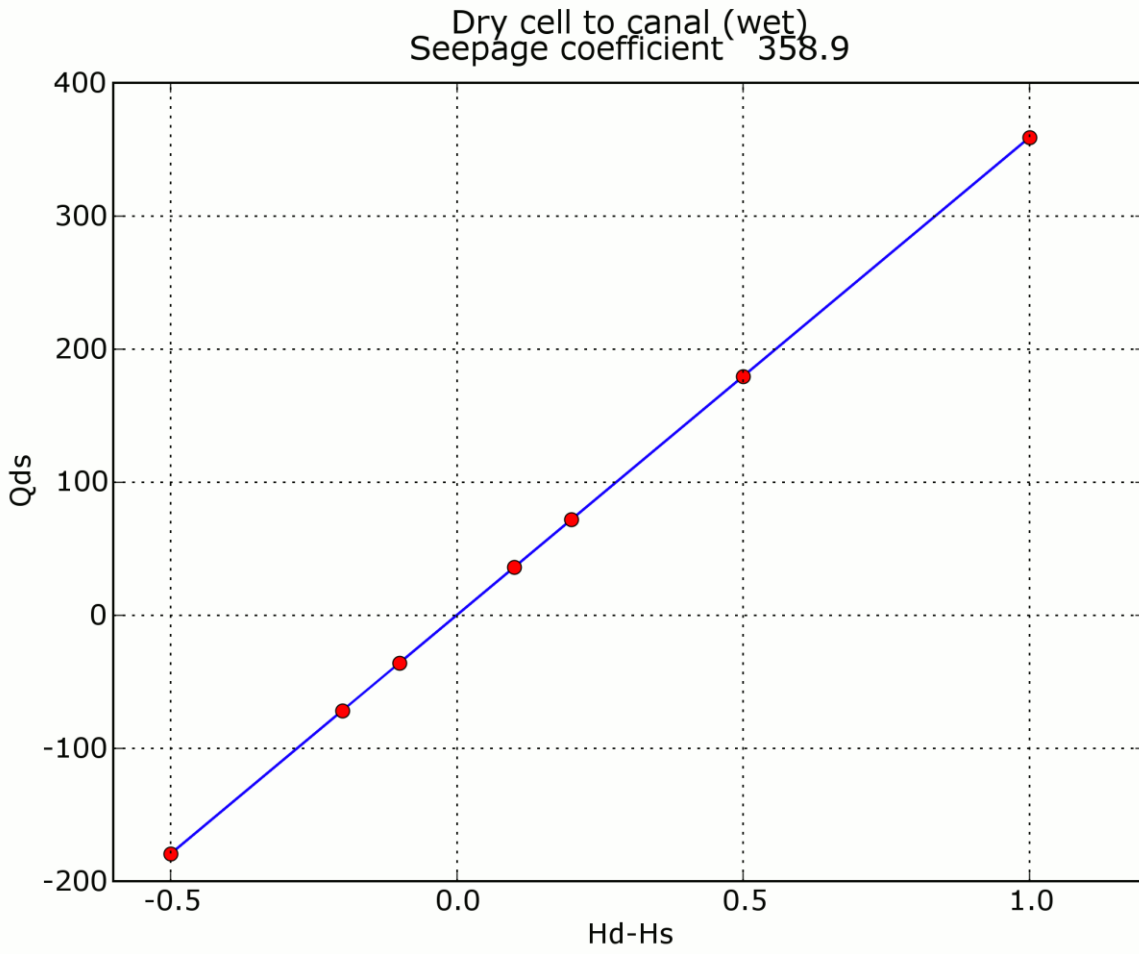


Figure 38: Seepage coefficient for L-30 north of S-335 and south of the bridge from Dry Cell to Canal (wet).

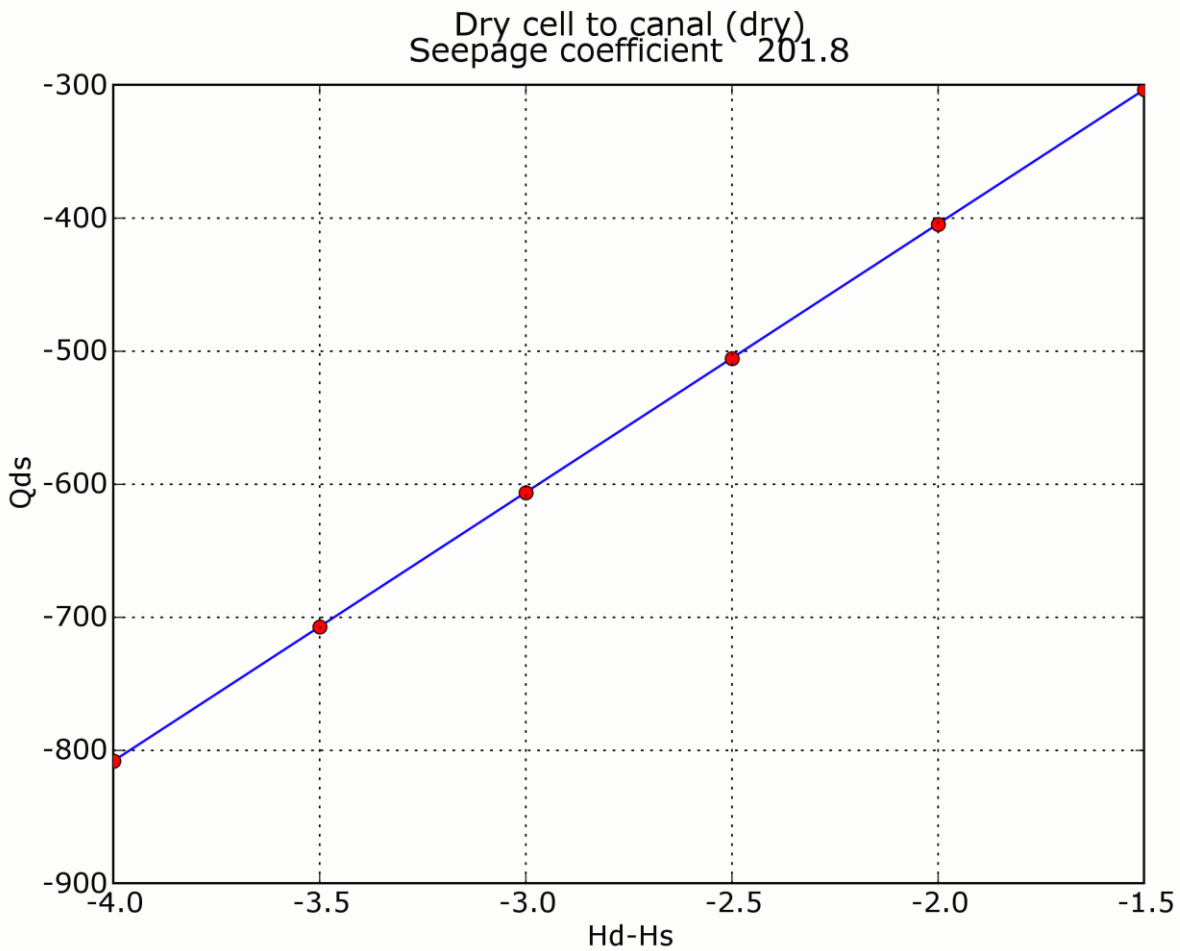


Figure 39: Seepage coefficient for L-30 north of S-335 and south of the bridge from Dry Cell to Canal (dry).

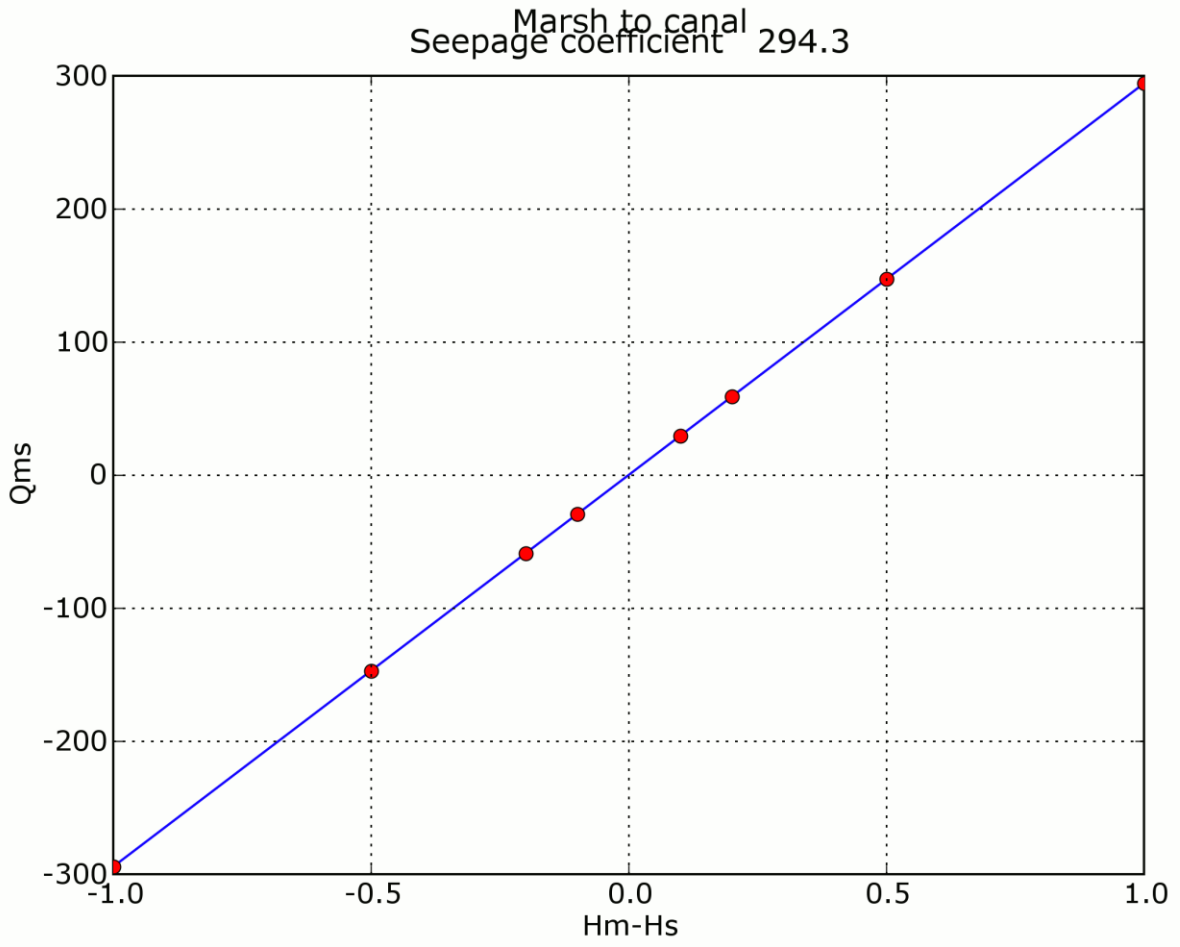


Figure 40: Seepage coefficient for L-30 north of S-335 and south of the bridge from Marsh to Canal.

3.6. L-31 between G-211 and S-331

Scenarios

Table 16: Reported water levels for L-31 between G-211 and S-331.

Area	Water Level Gauge (DBHYDRO)	Observed Water Elevation (ft NGVD)		
		Maximum	Average	Minimum
Everglades National Park	G-596	8.7	5.1	-0.2
L-31N Canal	S-331_HW	8.6	4.7	2.1
East	NA	NA	NA	NA

Table 17: Scenarios for L-31 between G-211 and S-331.

Scenario	ENP	L-31N	East Side
marsh-1	7.1	7.0	7.0
marsh-2	7.2	7.0	7.0
marsh-3	7.5	7.0	7.0
marsh-4	8.0	7.0	7.0
dry-1	7.0	7.0	3.0
dry-2	7.0	7.0	3.5
dry-3	7.0	7.0	4.0
dry-4	7.0	7.0	4.5
dry-5	7.0	7.0	5.0
dry-6	7.0	7.0	5.5
dry-7	7.0	7.0	6.0
dry-8	7.0	7.0	6.5
dry-9	7.0	7.0	6.8
dry-10	7.0	7.0	6.9
dry-11	7.0	7.0	7.1
dry-12	7.0	7.0	7.2
dry-13	7.0	7.0	7.5
dry-14	7.0	7.0	8.0
canal-1	7.0	6.0	7.0
canal-2	7.0	6.5	7.0
canal-3	7.0	6.8	7.0
canal-4	7.0	6.9	7.0
canal-5	7.0	7.1	7.0
canal-6	7.0	7.2	7.0
canal-7	7.0	7.5	7.0
canal-8	7.0	8.0	7.0

Representative head-streamline plots

Head-streamline plots for L-31N between G211 and S331 are shown on the following pages. Heads (in feet MSL) for the model runs in these plots are shown below:

Table 18: Water levels for head-streamline plots.

<i>Marsh runs (Figure 41)</i>			
<i>Run ID</i>	<i>Marsh</i>	<i>Canal</i>	<i>Dry</i>
plot-marsh-1	7.1	7.0	7.0
plot-marsh-4	8.0	7.0	7.0
<i>Dry-cell runs (Figure 42)</i>			
<i>Run ID</i>	<i>Marsh</i>	<i>Canal</i>	<i>Dry</i>
plot-dry-1	7.0	7.0	6.0
plot-dry-14	7.0	7.0	8.0
<i>Canal runs (Figure 43)</i>			
<i>Run ID</i>	<i>Marsh</i>	<i>Canal</i>	<i>Dry</i>
plot-canal-1	7.0	6.0	7.0
plot-canal-8	7.0	8.0	7.0

L-31N between G211 and S331

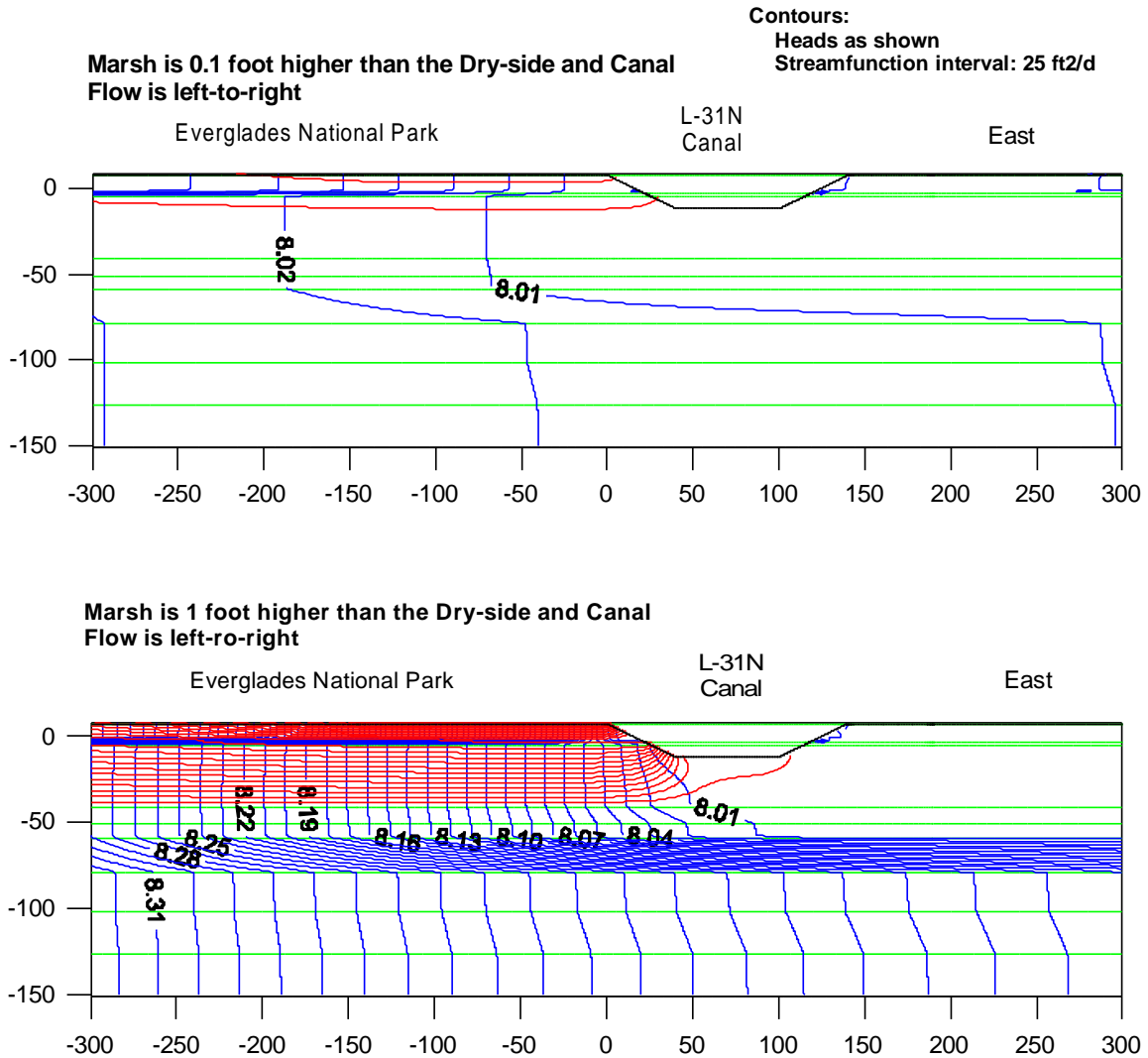


Figure 41: Heads and streamlines for L-31N between G211 and S331, for runs in which the marsh water level was adjusted.

L-31N between G211 and S331

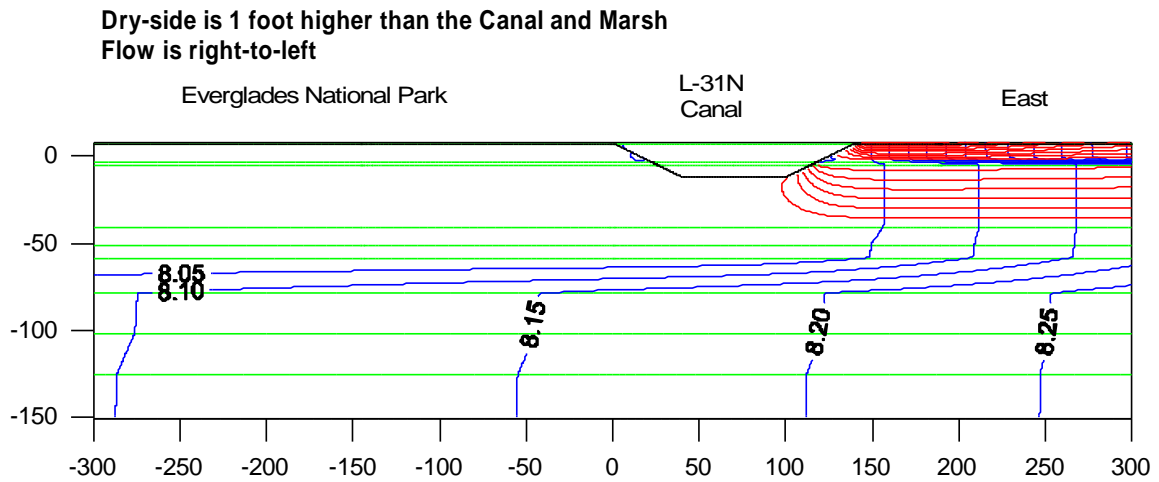
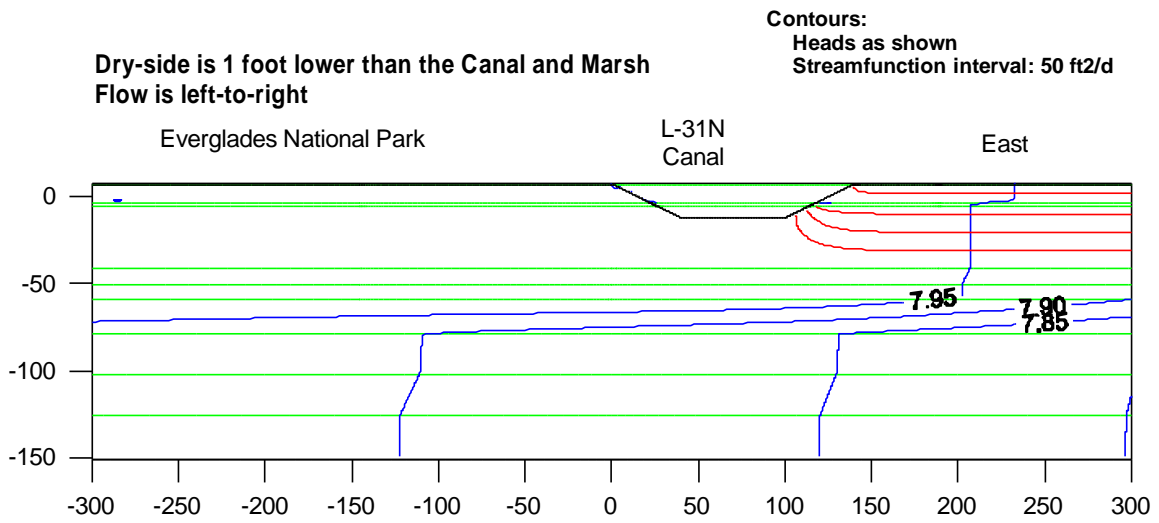


Figure 42: Heads and streamlines for L-31N between G211 and S331, for runs in which the dry-side water level was adjusted.

L-31N between G211 and S331

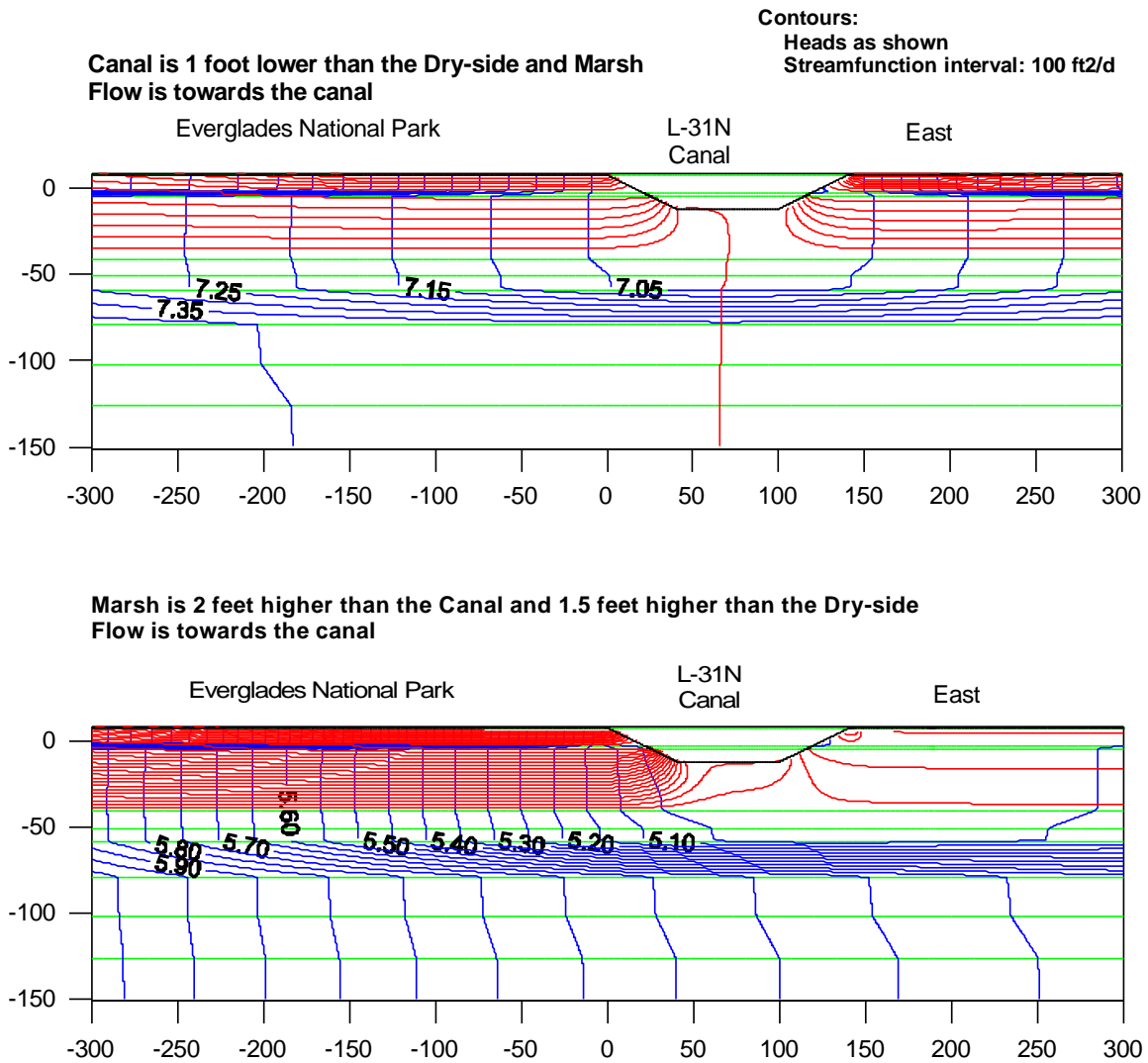


Figure 43: Heads and streamlines for L-31N between G211 and S331, for runs in which the canal water level was adjusted.

Seepage coefficients

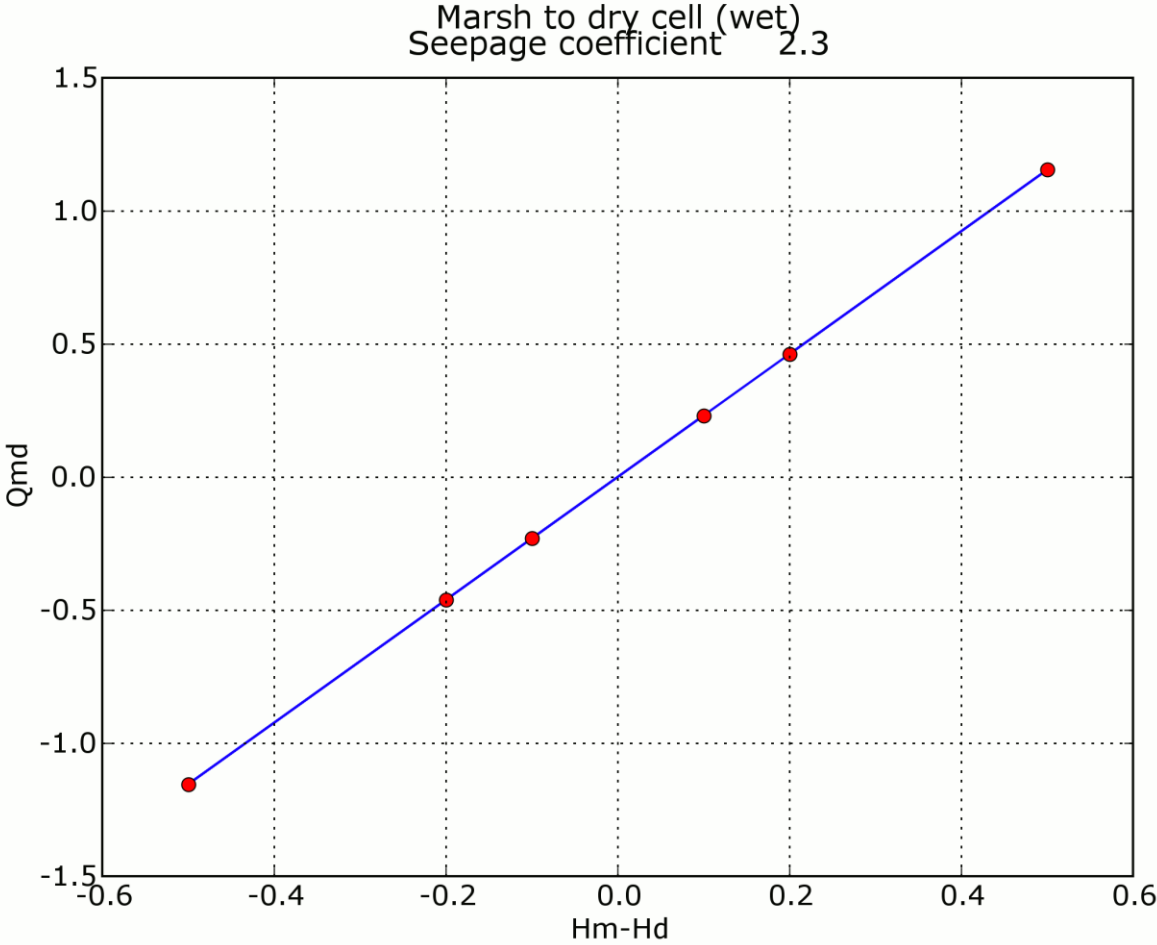


Figure 44: Seepage coefficient for L-31N between G211 and S331 from Marsh to Dry Cell (wet).

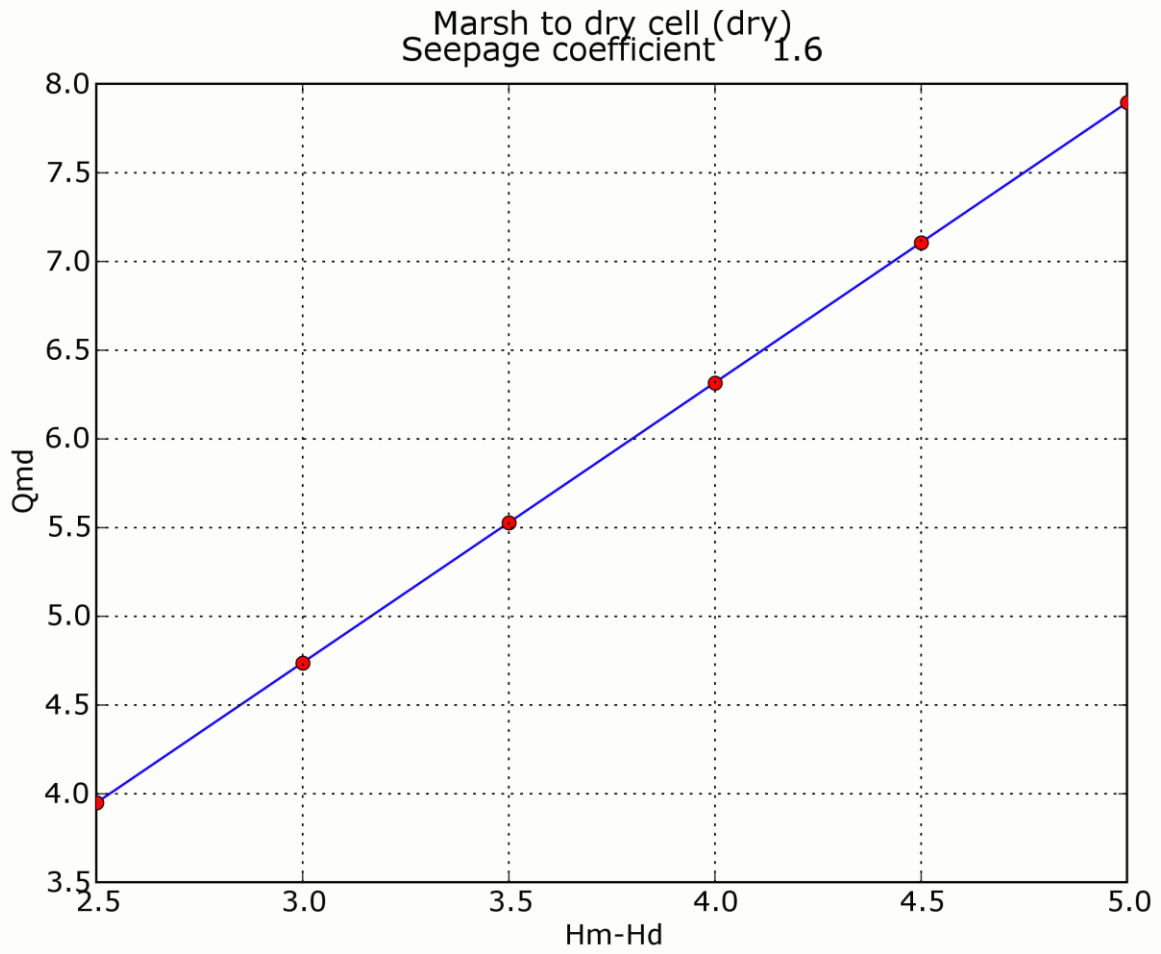


Figure 45: Seepage coefficient for L-31N between G211 and S331 from Marsh to Dry-Cell (dry).

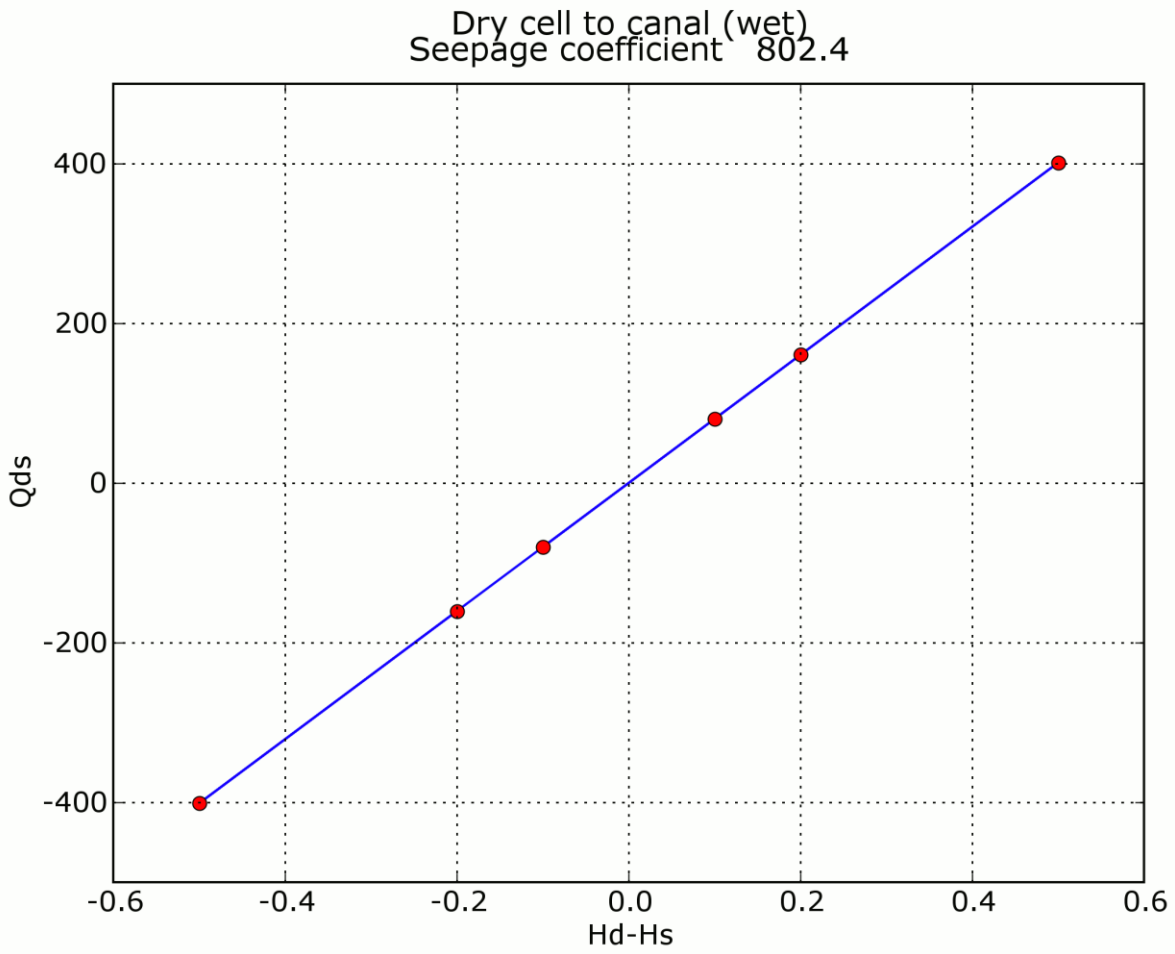


Figure 46: Seepage coefficient for L-31N between G211 and S331 from Dry Cell to Canal (wet).

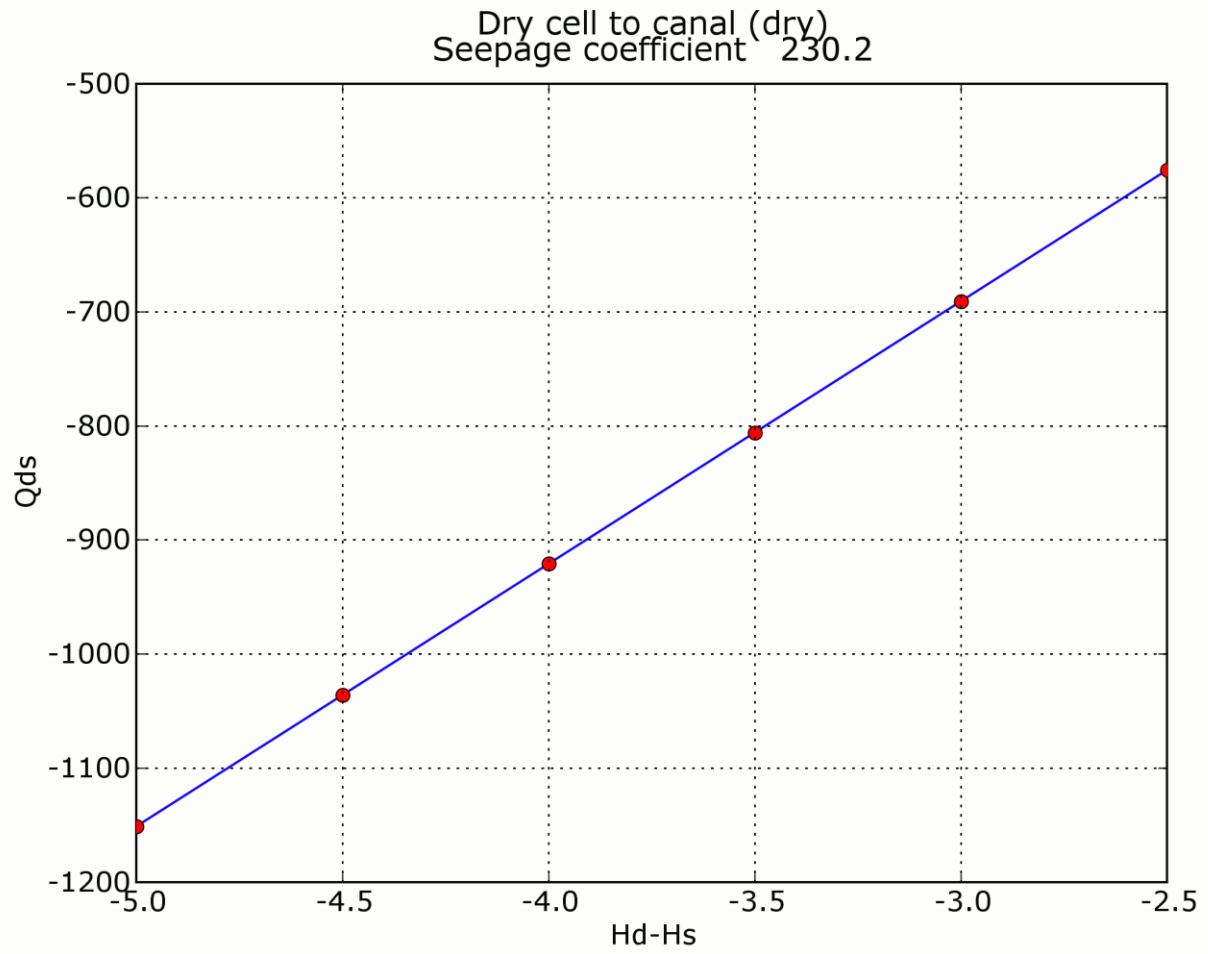


Figure 47: Seepage coefficient for L-31N between G211 and S331 from Dry Cell to Canal (dry).

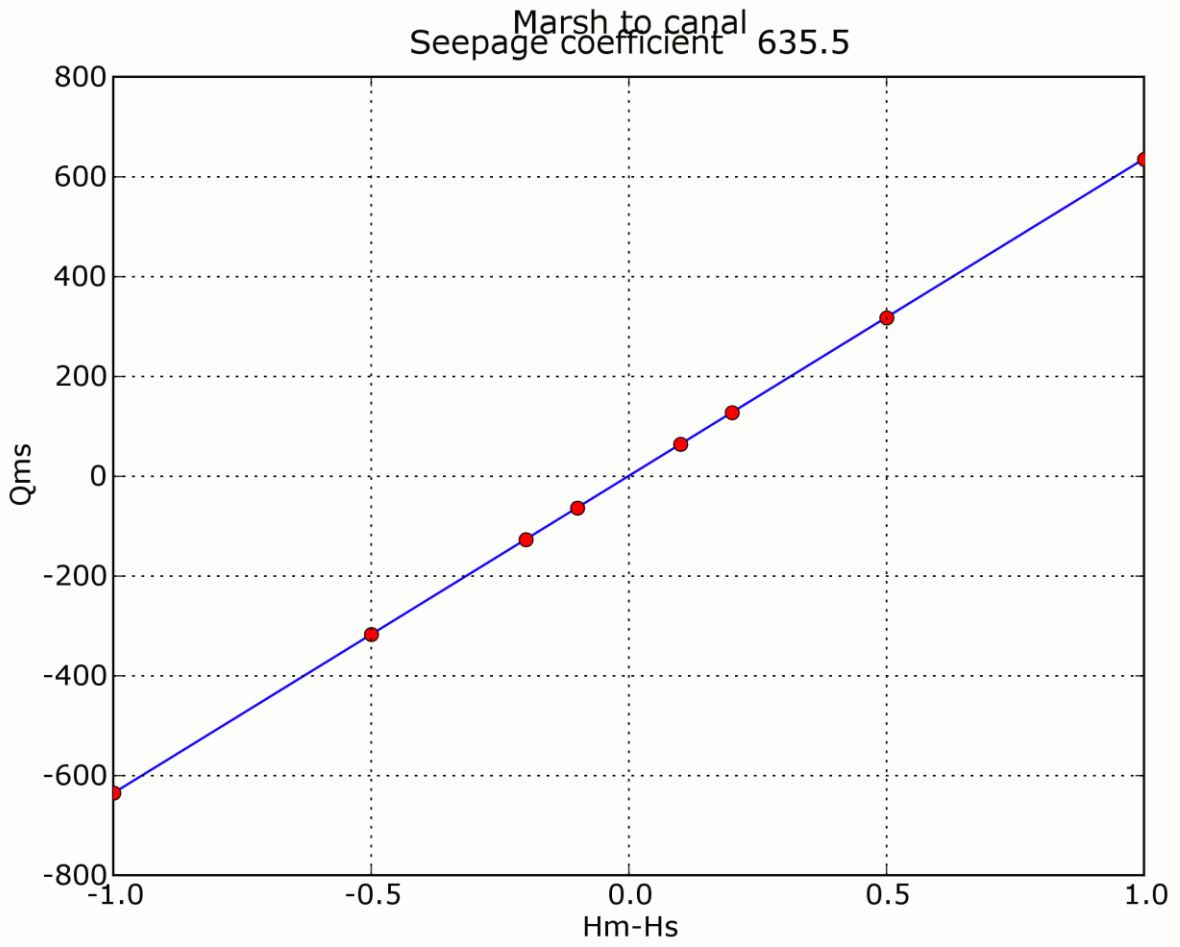


Figure 48: Seepage coefficient for L-31N between G211 and S331 from Marsh to Canal.

3.7. L-31 north of G-211

Scenarios

Table 19: Reported water levels for L-31 north of G-211.

Area	Water Level Gauge (DBHYDRO)	Observed Water Elevation (ft NGVD)		
		Maximum	Average	Minimum
Everglades National Park	G-3557	8.2	5.7	3.2
L-31N Canal	G211-HW	7.7	5.7	2.9
East	G-1487	7.9	5.6	2.7

Table 20: Scenarios for L-31 north of G-211.

Scenario	ENP	L-31N	East Side
marsh-1	5.1	5.0	5.0
marsh-2	5.2	5.0	5.0
marsh-4	5.5	5.0	5.0
marsh-5	6.0	5.0	5.0
marsh-6	6.5	5.0	5.0
marsh-7	7.0	5.0	5.0
marsh-8	8.0	5.0	5.0
dry-1	5.0	5.0	1.0
dry-2	5.0	5.0	1.5
dry-3	5.0	5.0	2.0
dry-4	5.0	5.0	2.5
dry-5	5.0	5.0	3.0
dry-6	5.0	5.0	3.5
dry-7	5.0	5.0	4.0
dry-8	5.0	5.0	4.5
dry-9	5.0	5.0	4.8
dry-10	5.0	5.0	4.9
dry-11	5.0	5.0	5.1
dry-12	5.0	5.0	5.2
dry-13	5.0	5.0	5.5
dry-14	5.0	5.0	6.0
dry-15	5.0	5.0	4.1
dry-16	5.0	5.0	4.2
dry-17	5.0	5.0	4.3
dry-18	5.0	5.0	4.4
canal-1	5.0	4.0	5.0
canal-2	5.0	4.5	5.0
canal-3	5.0	4.8	5.0
canal-4	5.0	4.9	5.0

Scenario	ENP	L-31N	East Side
canal-5	5.0	5.1	5.0
canal-6	5.0	5.2	5.0
canal-7	5.0	5.5	5.0
canal-8	5.0	6.0	5.0

Representative head-streamline plots

Head-streamline plots for L-31N north of G211 are shown on the following pages. Heads (in feet MSL) for the model runs in these plots are shown below:

<i>Marsh runs (Figure 49)</i>			
<i>Run ID</i>	<i>Marsh</i>	<i>Canal</i>	<i>Dry</i>
plot-marsh-1	5.1	5.0	5.0
plot-marsh-8	6.0	5.0	5.0
<i>Dry-cell runs (Figure 50)</i>			
<i>Run ID</i>	<i>Marsh</i>	<i>Canal</i>	<i>Dry</i>
plot-dry-1	5.0	5.0	4.0
plot-dry-18	5.0	5.0	6.0
<i>Canal runs (Figure 51)</i>			
<i>Run ID</i>	<i>Marsh</i>	<i>Canal</i>	<i>Dry</i>
plot-canal-1	5.0	4.0	5.0
plot-canal-8	5.0	6.0	5.0

L-31N north of G-211

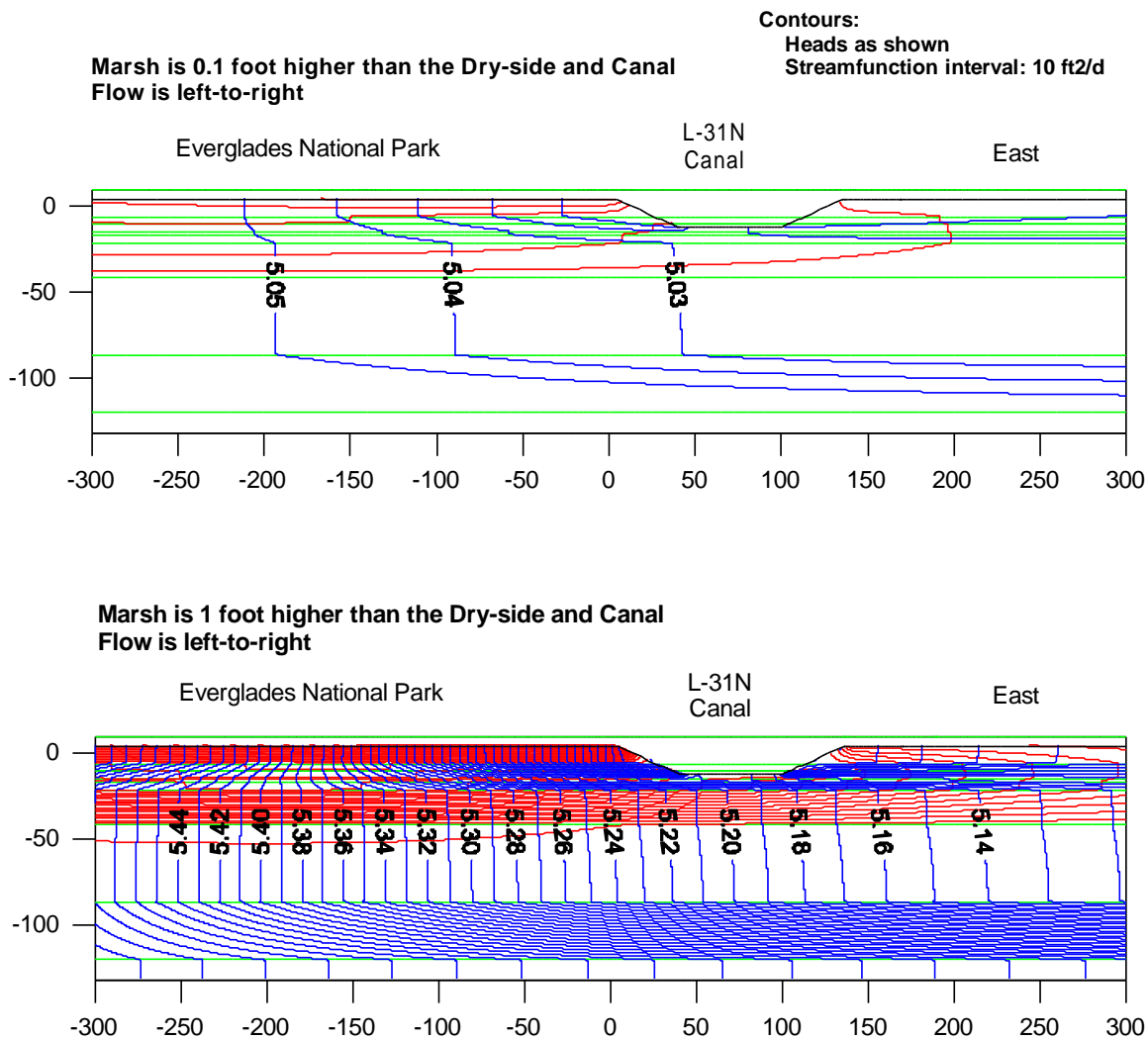


Figure 49: Heads and streamlines for L-31N north of G211, for runs in which the marsh water level

L-31N north of G-211

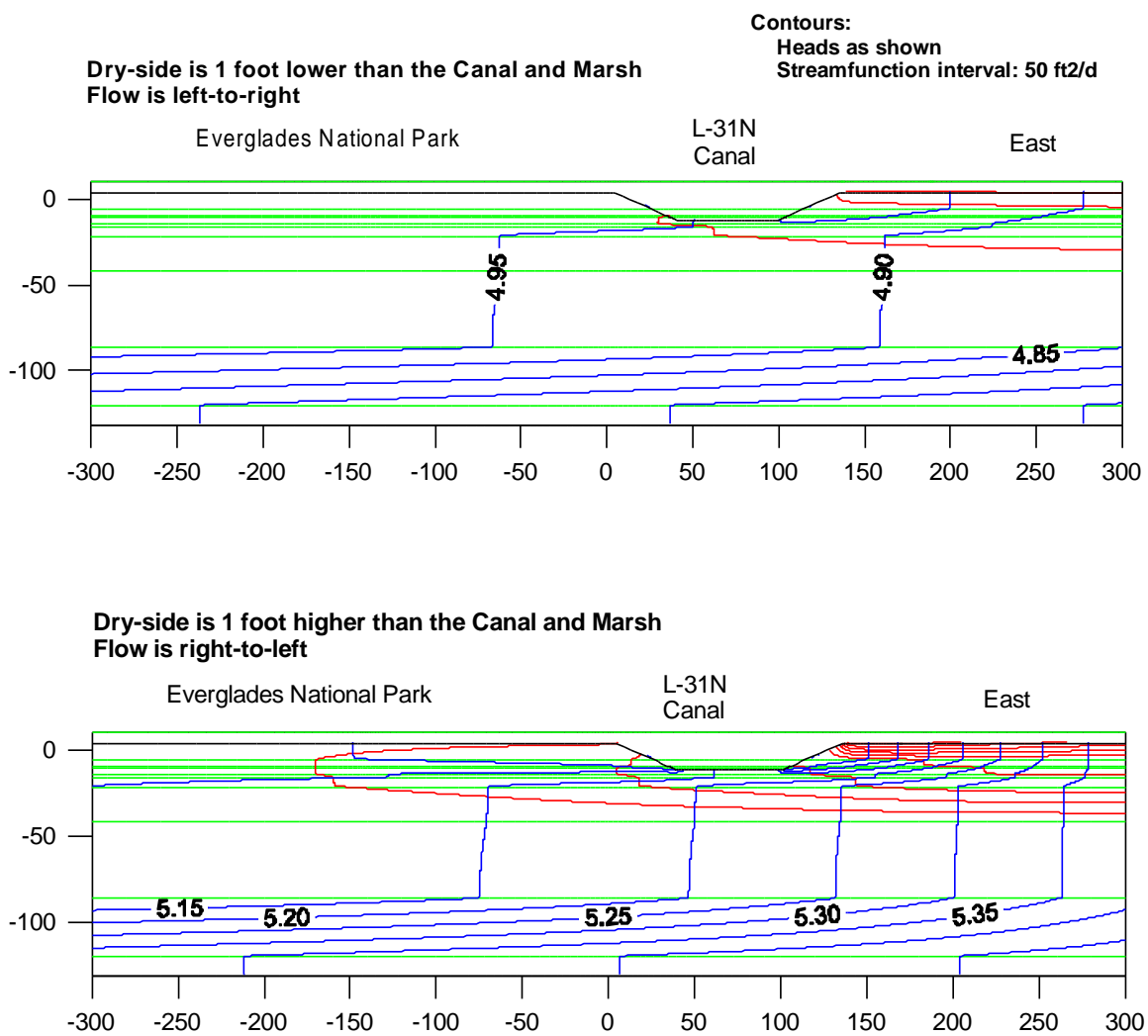


Figure 50: Heads and streamlines for L-31N north of G211, for runs in which the dry-side water level was adjusted.

L-31N north of G-211

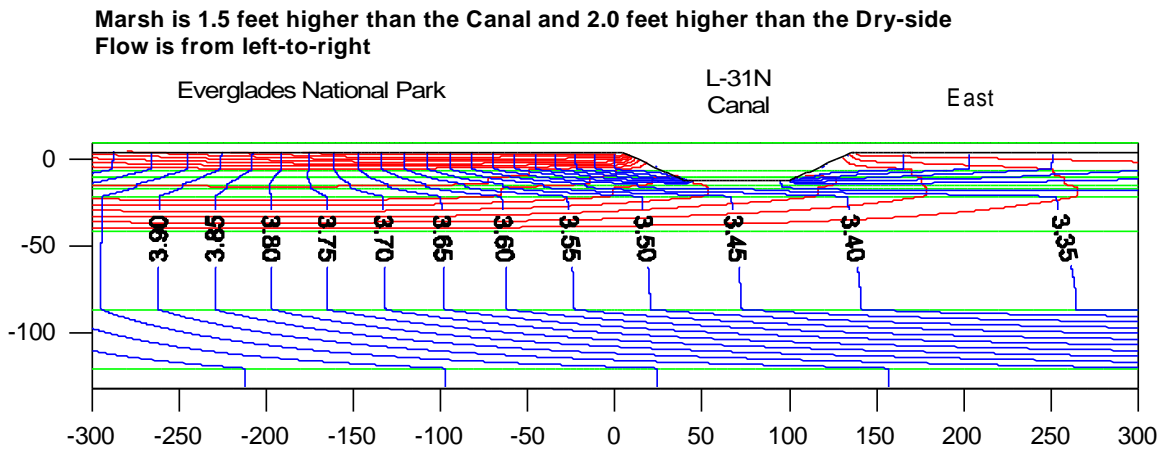
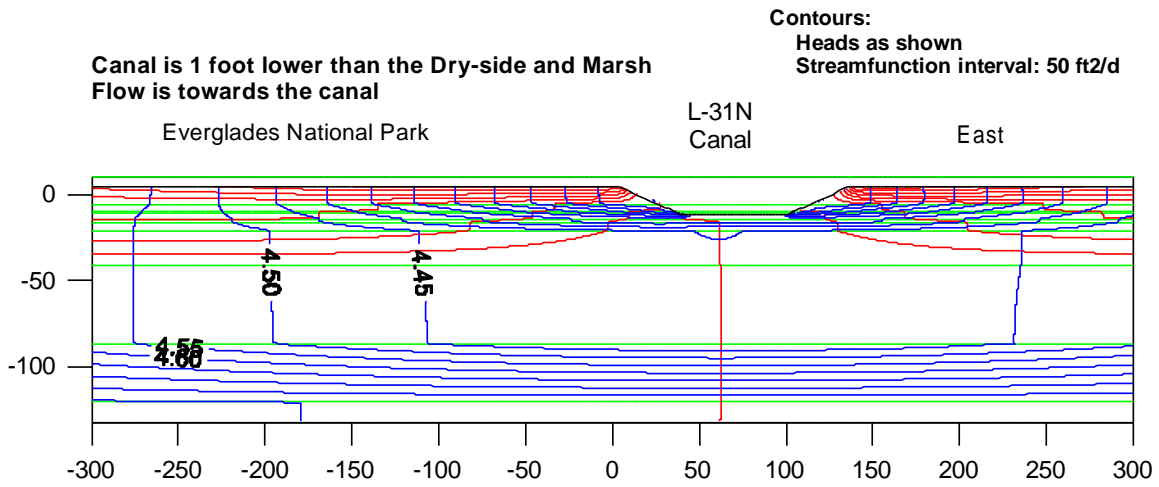


Figure 51: Heads and streamlines for L-31N north of G211, for runs in which the canal water level was

Seepage coefficients

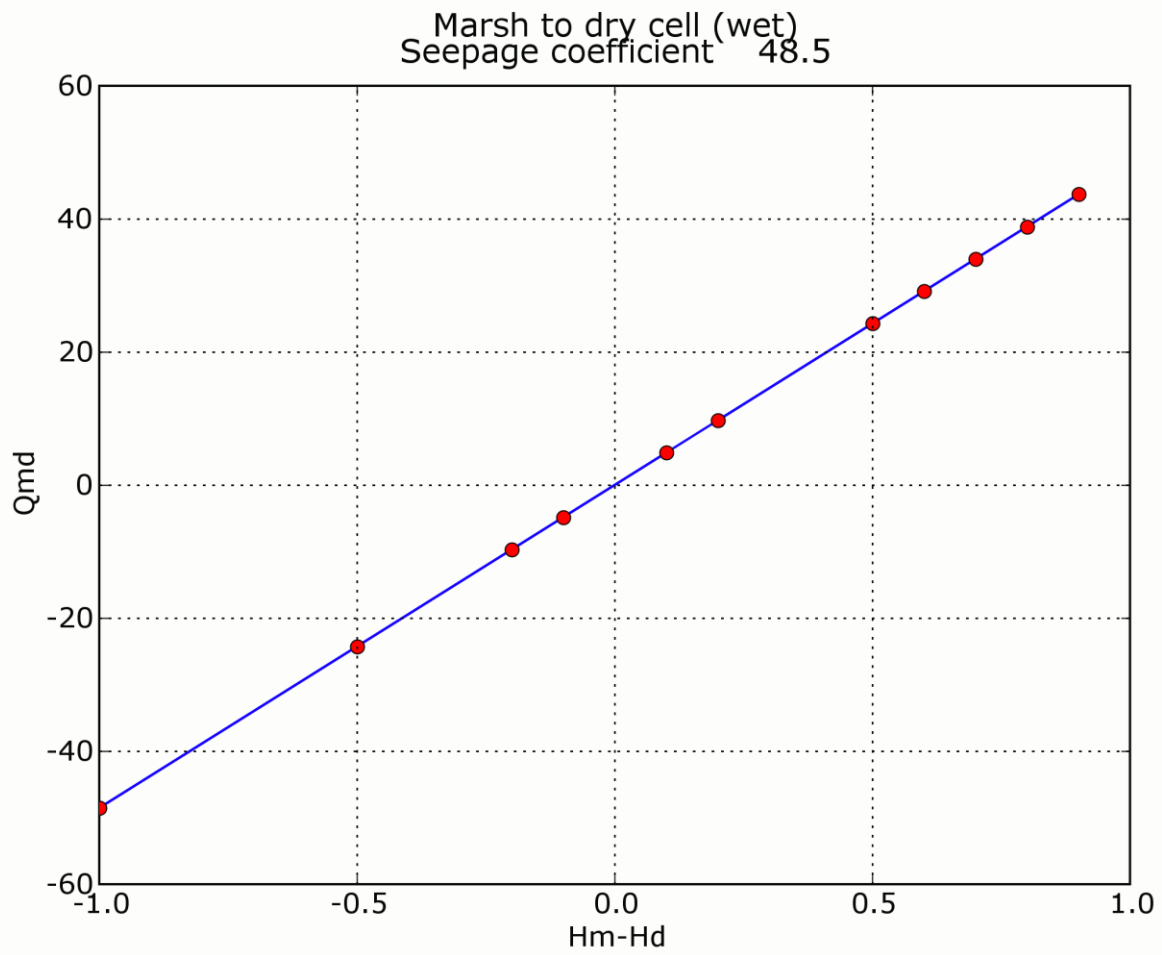


Figure 52: Seepage coefficient for L-31N north of G211 from Marsh to Dry Cell (wet).

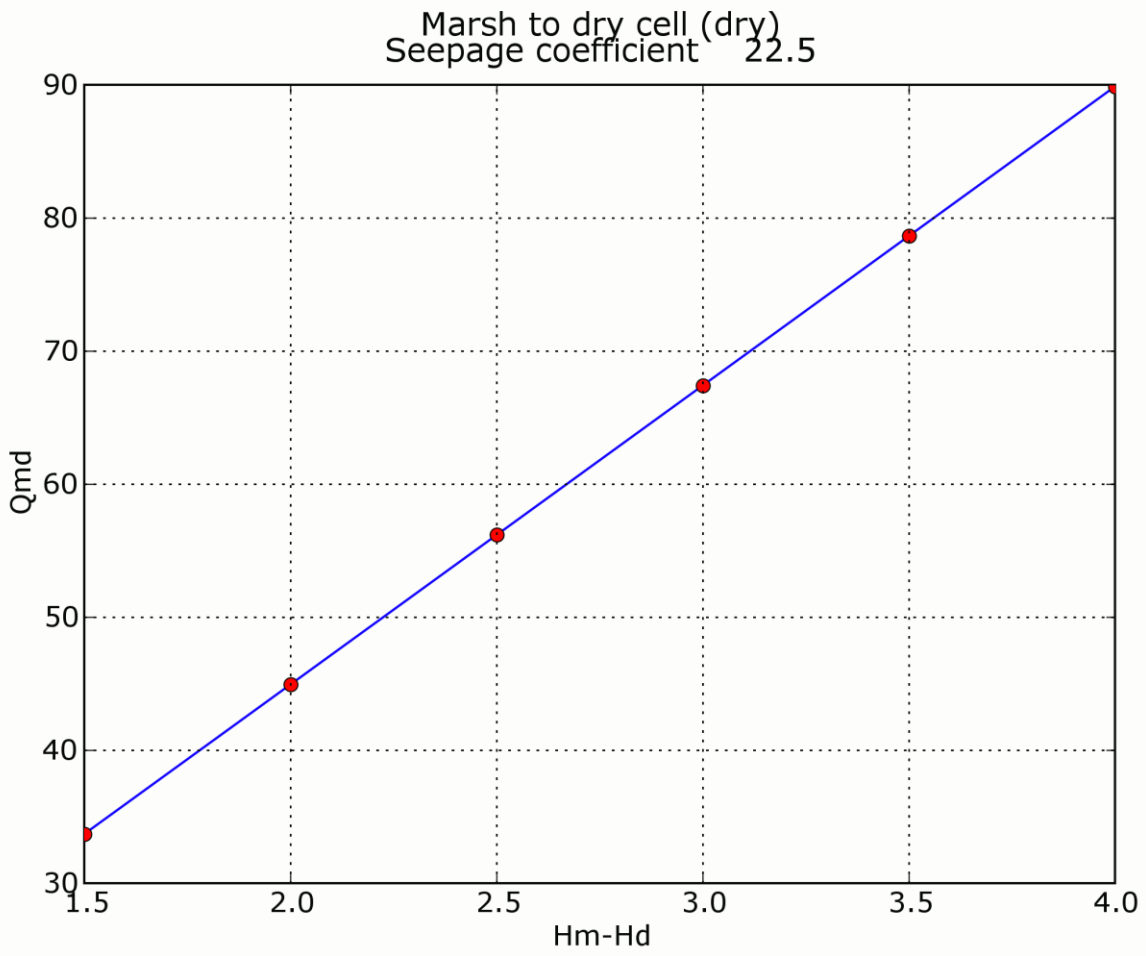


Figure 53: Seepage coefficient for L-31N north of G211 from Marsh to Dry-Cell (dry).

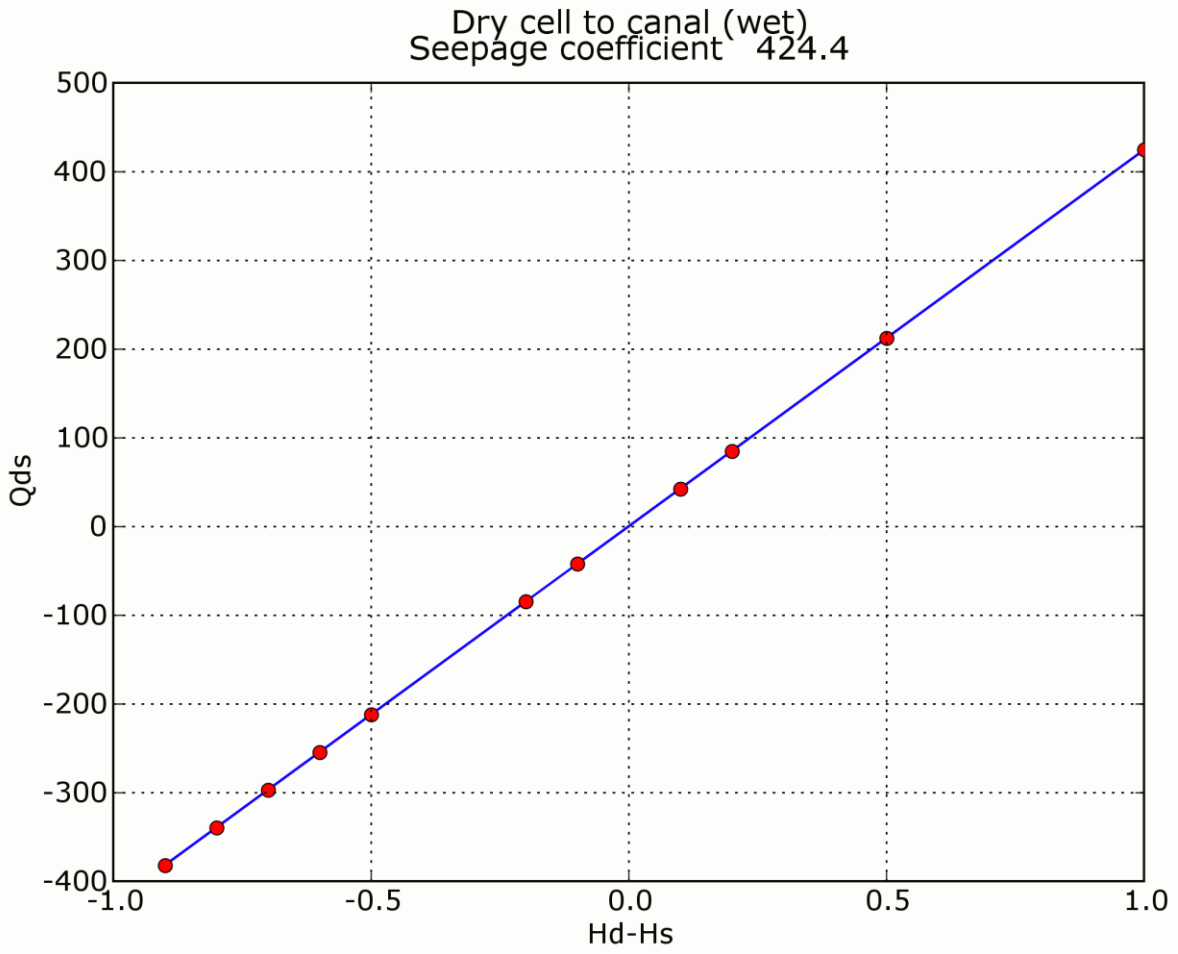


Figure 54: Seepage coefficient for L-31N north of G211 from Dry Cell to Canal (wet).

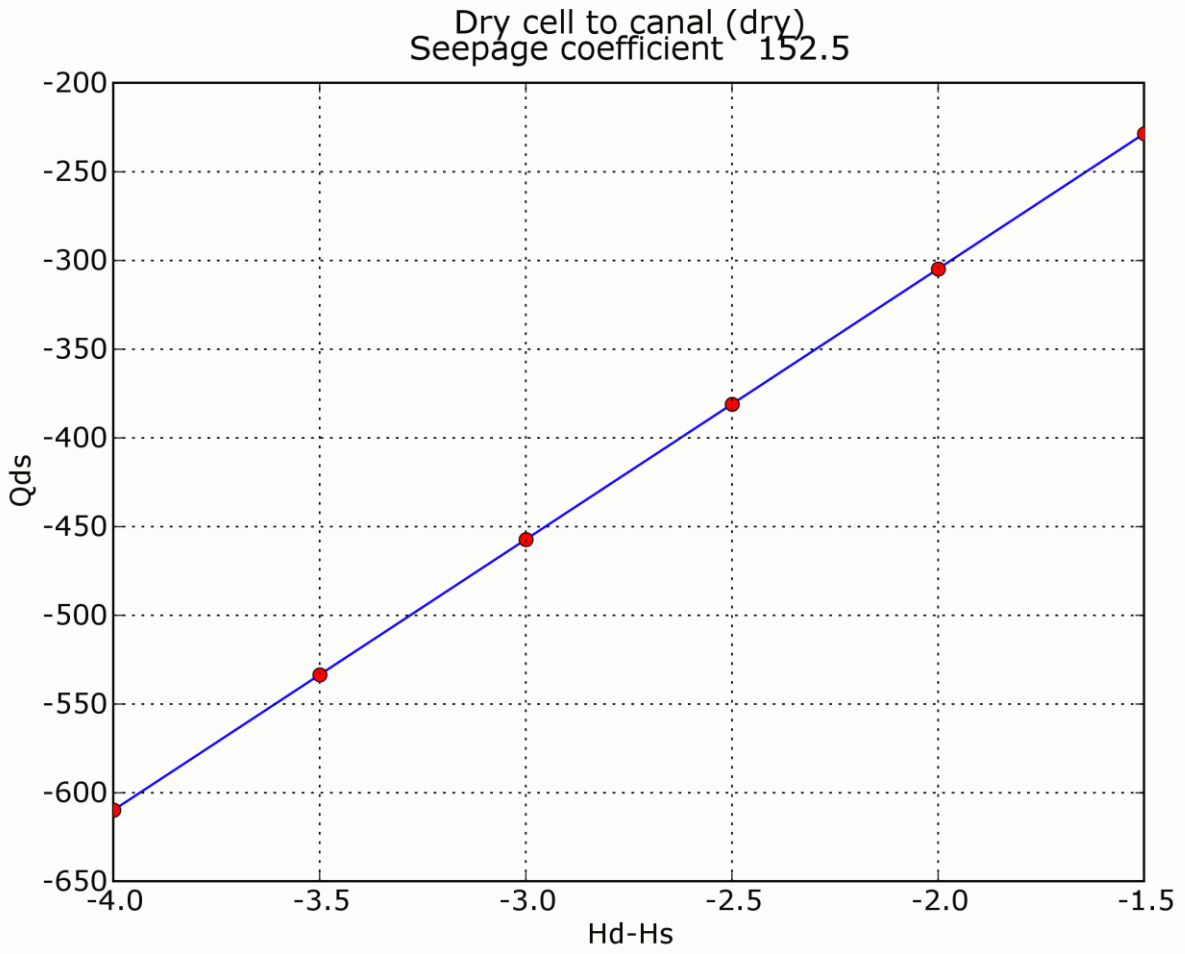


Figure 55: Seepage coefficient for L-31N north of G211 from Dry Cell to Canal (dry).

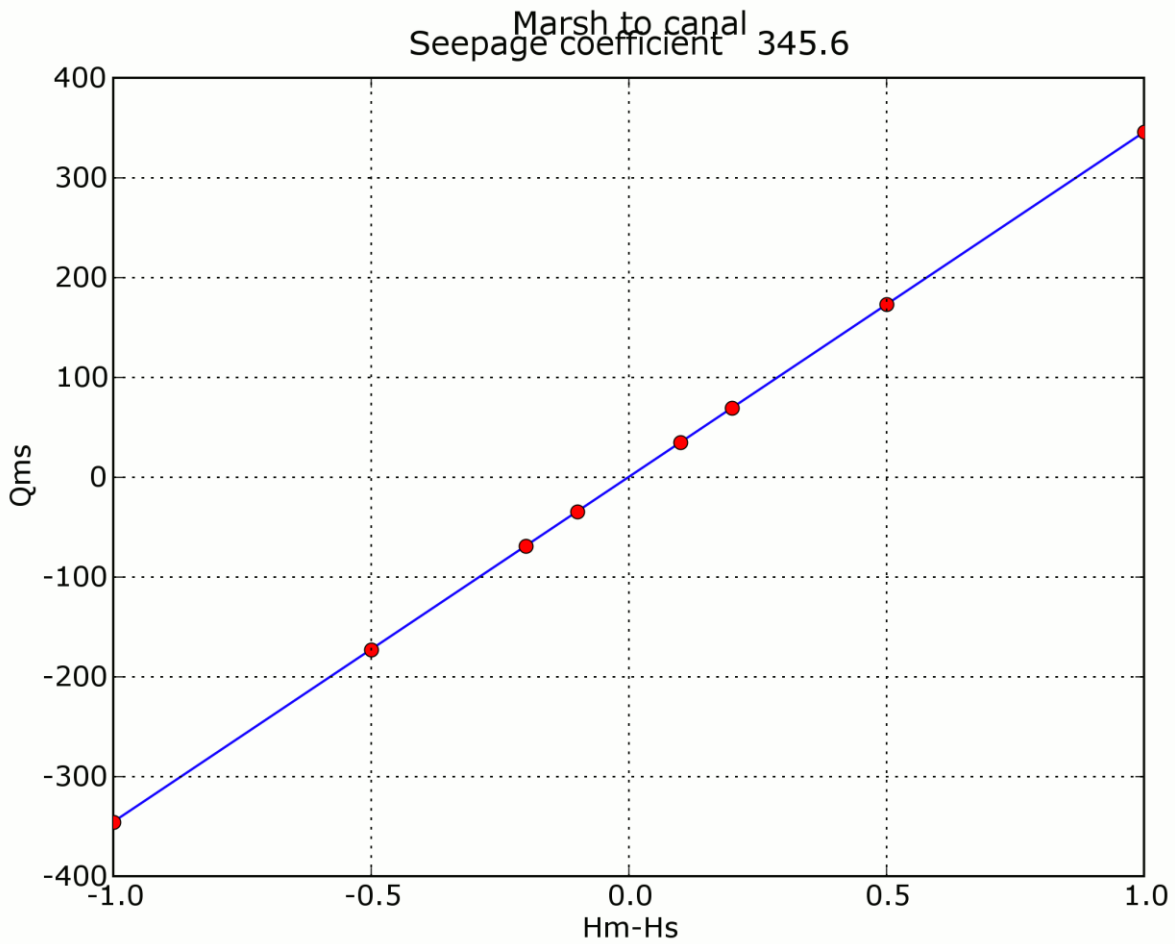


Figure 56: Seepage coefficient for L-31N north of G211 from Marsh to Canal.

3.8. L-31N south of S-331

Scenarios

Table 21: Water levels for L-31 south of S-331.

	<i>Water Level Gauge (DBHYDRO)</i>	<i>Observed Water Elevation (ft NGVD)</i>		
		<i>Maximum</i>	<i>Average</i>	<i>Minimum</i>
Everglades National Park	G-3437	7.6	4.4	2.4
L31N Canal	S331-TW	6.5	4.3	1.5
East	HUMBLE	8.3	5.6	2.7

Table 22: Scenarios for L-31 north of G-211.

Scenario	ENP	L-31N	East Side
marsh-1	5.1	5.0	5.0
marsh-2	5.2	5.0	5.0
marsh-4	5.5	5.0	5.0
marsh-5	6.0	5.0	5.0
marsh-6	6.5	5.0	5.0
marsh-7	7.0	5.0	5.0
marsh-8	8.0	5.0	5.0
dry-1	5.0	5.0	1.0
dry-2	5.0	5.0	1.5
dry-3	5.0	5.0	2.0
dry-4	5.0	5.0	2.5
dry-5	5.0	5.0	3.0
dry-6	5.0	5.0	3.5
dry-7	5.0	5.0	4.0
dry-8	5.0	5.0	4.5
dry-9	5.0	5.0	4.8
dry-10	5.0	5.0	4.9
dry-11	5.0	5.0	5.1
dry-12	5.0	5.0	5.2
dry-13	5.0	5.0	5.5
dry-14	5.0	5.0	6.0
dry-15	5.0	5.0	4.1
dry-16	5.0	5.0	4.2
dry-17	5.0	5.0	4.3
dry-18	5.0	5.0	4.4

Scenario	ENP	L-31N	East Side
canal-1	5.0	4.0	5.0
canal-2	5.0	4.5	5.0
canal-3	5.0	4.8	5.0
canal-4	5.0	4.9	5.0
canal-5	5.0	5.1	5.0
canal-6	5.0	5.2	5.0
canal-7	5.0	5.5	5.0
canal-8	5.0	6.0	5.0

Representative head-streamline plots

Head-streamline plots for L-31N south of S331 are shown on the following pages. Heads (in feet MSL) for the model runs in these plots are shown below:

Table 23: Water levels for head-streamline plots.

Marsh runs (Figure 57)			
Run ID	Marsh	Canal	Dry
plot-marsh-1	5.1	5.0	5.0
plot-marsh-4	6.0	5.0	5.0
Dry-cell runs (Figure 58)			
Run ID	Marsh	Canal	Dry
plot-dry-1	5.0	5.0	4.0
plot-dry-14	5.0	5.0	6.0
Canal runs (Figure 59)			
Run ID	Marsh	Canal	Dry
plot-canal-1	5.0	4.0	5.0
plot-canal-8	5.0	6.0	5.0

L-31N south of S331

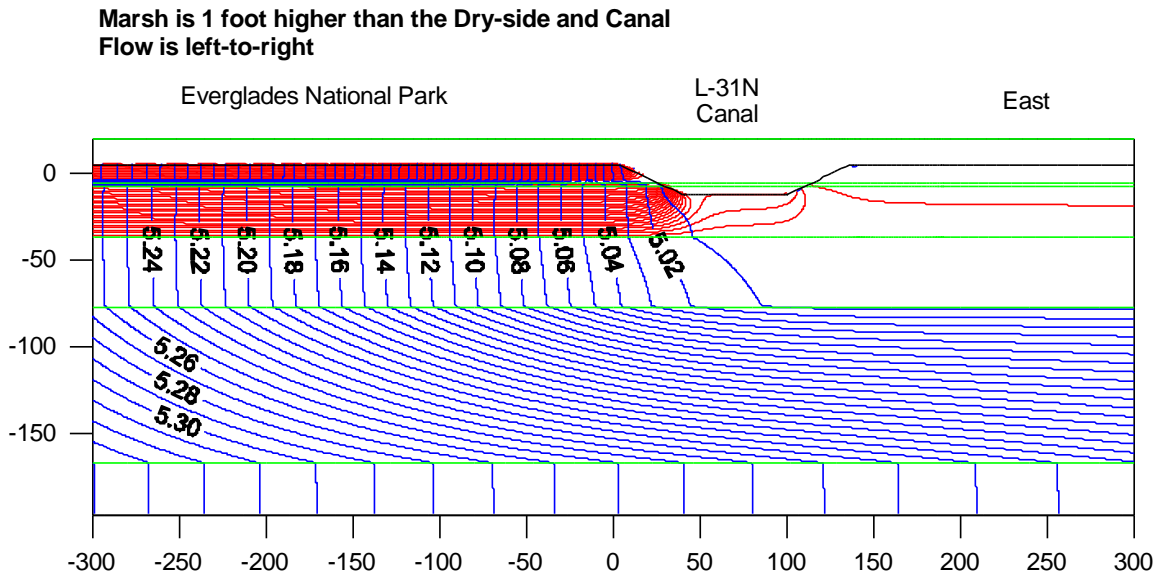
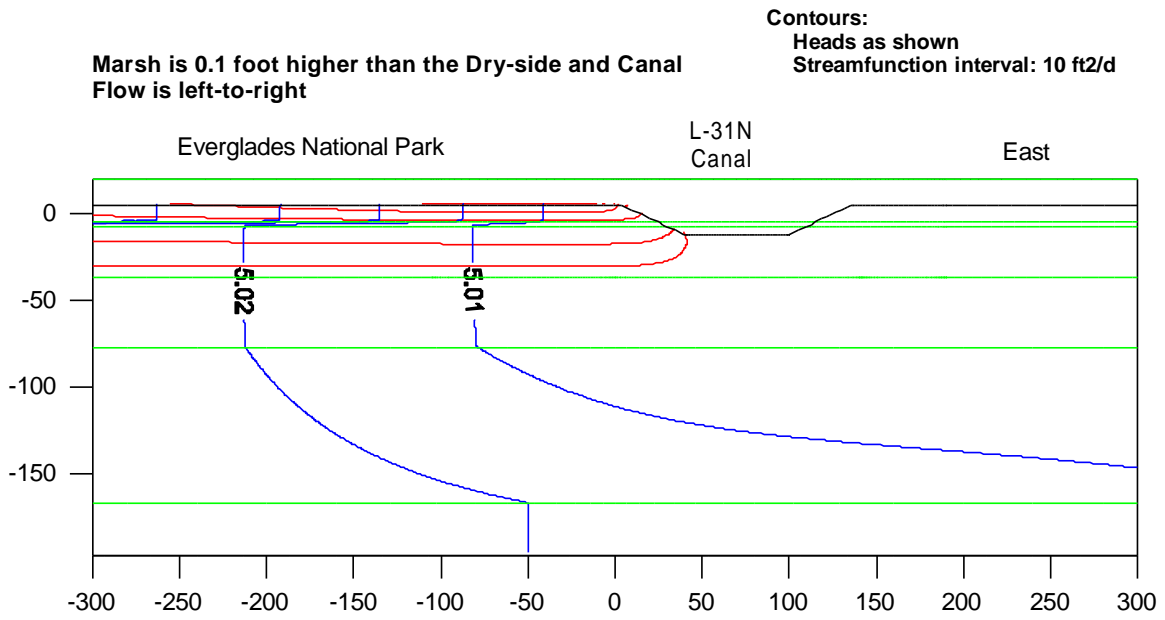


Figure 57: Heads and streamlines for L-31N south of S331, for runs in which the marsh water level was

L-31N south of S331

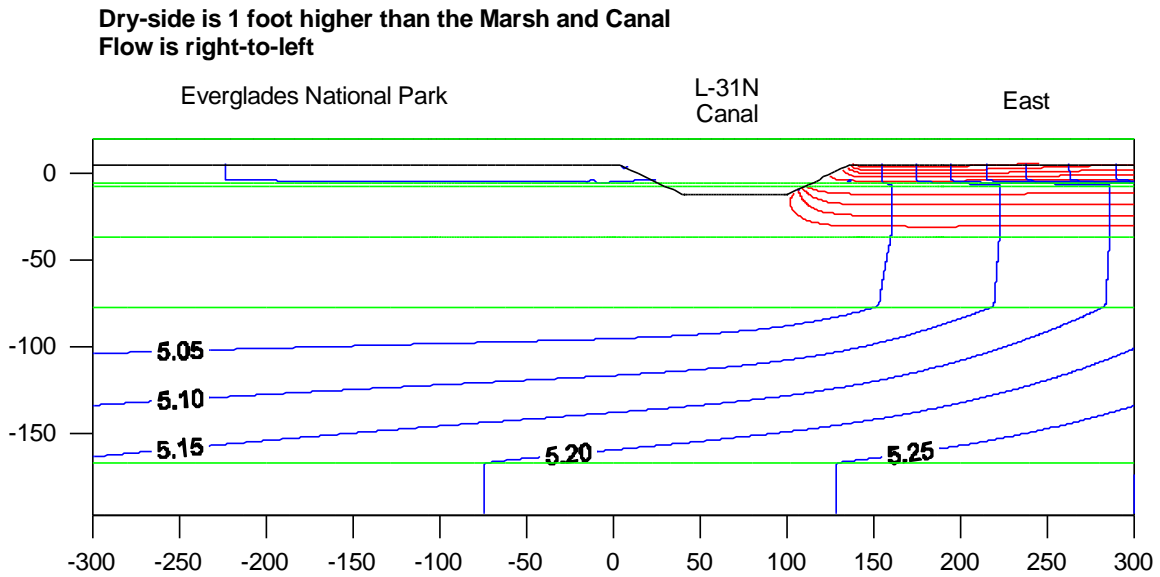
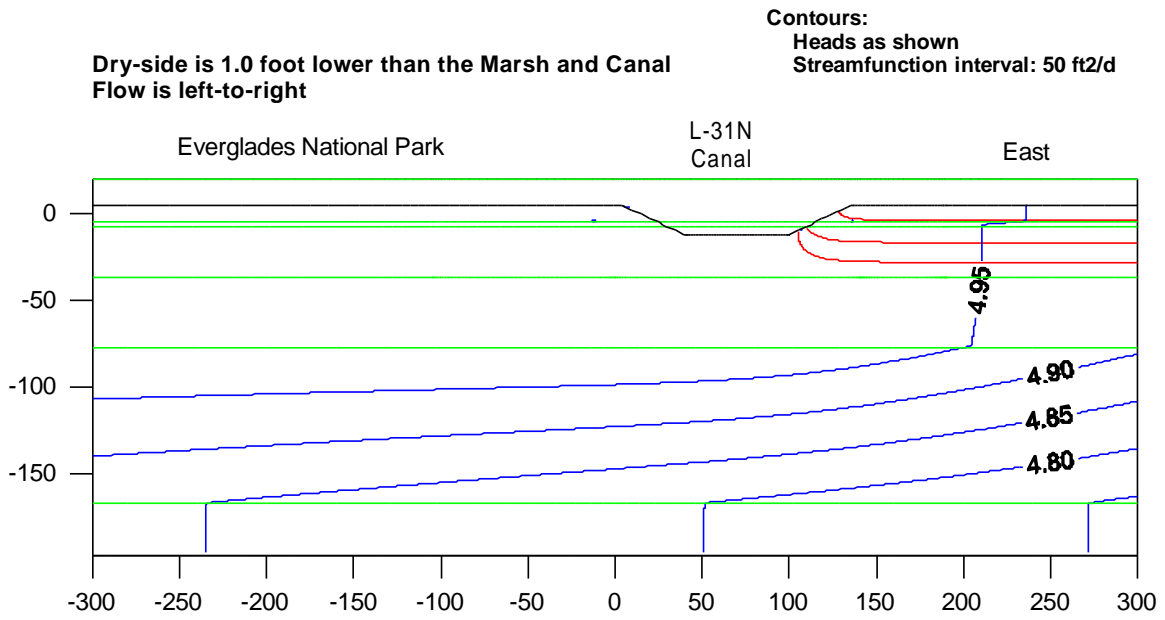


Figure 58: Heads and streamlines for L-31N south of S331, for runs in which the dry-side water level was adjusted.

L-31N south of S331

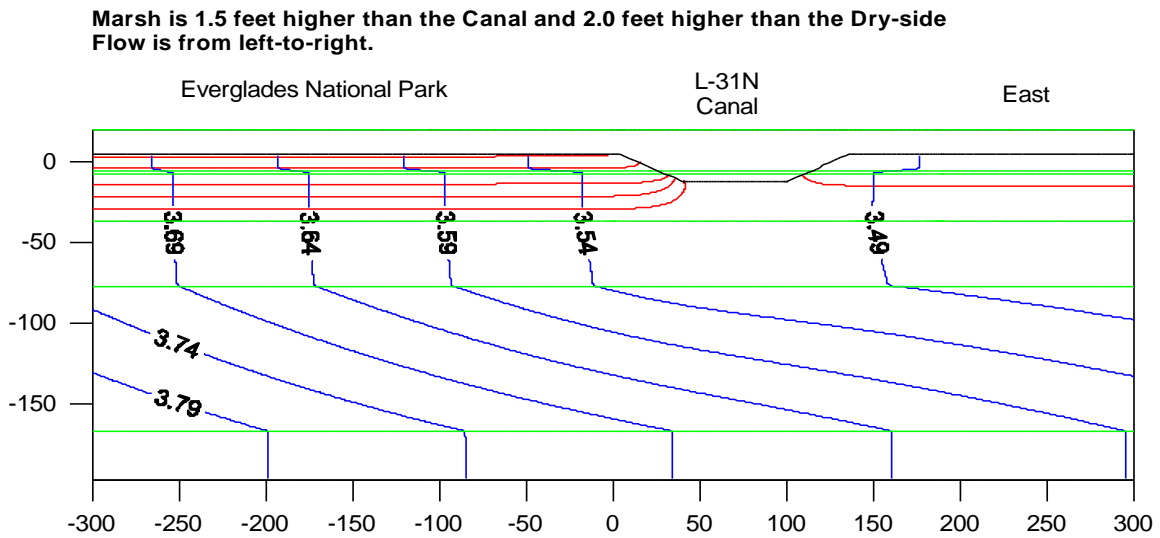
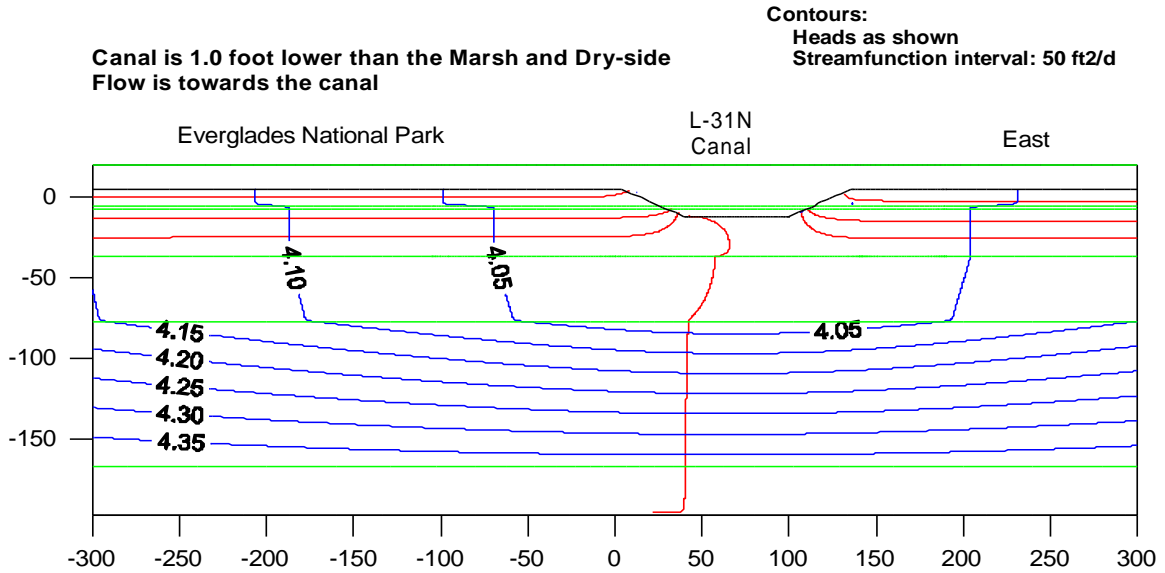


Figure 59: Heads and streamlines for L-31N south of S331, for runs in which the canal water level was adjusted.

Seepage coefficients

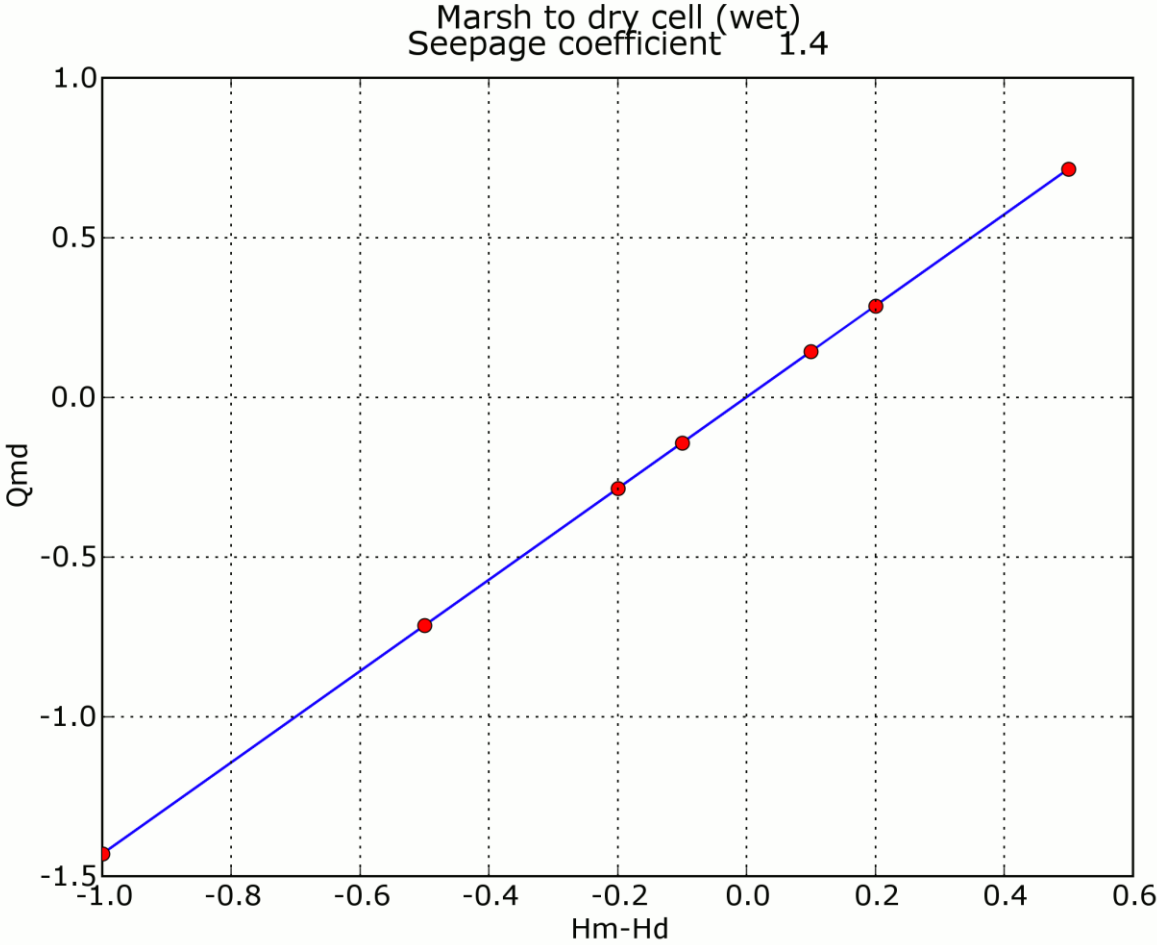


Figure 60: Seepage coefficient for L-31N south of S331 from Marsh to Dry Cell (wet).

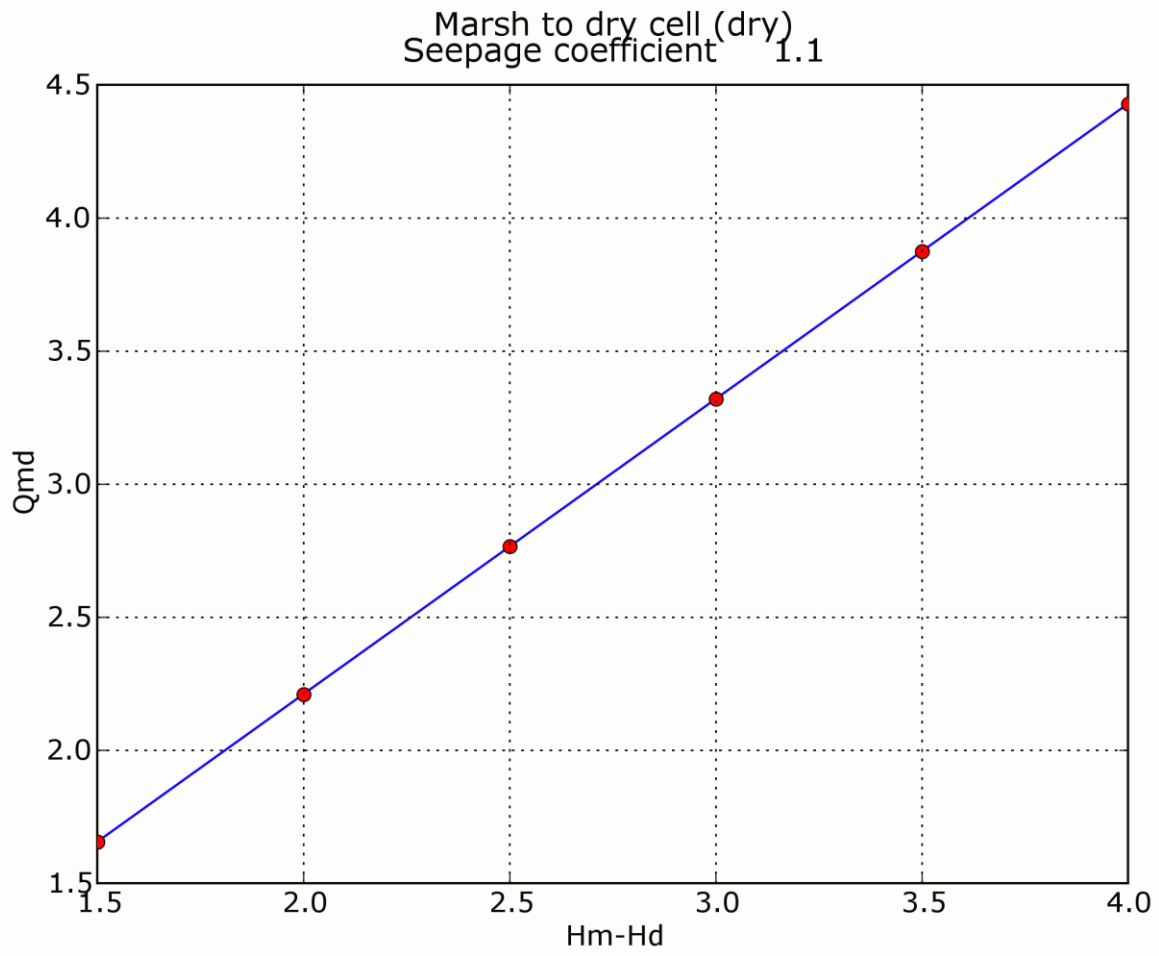


Figure 61: Seepage coefficient for L-31N south of S331 from Marsh to Dry-Cell (dry).

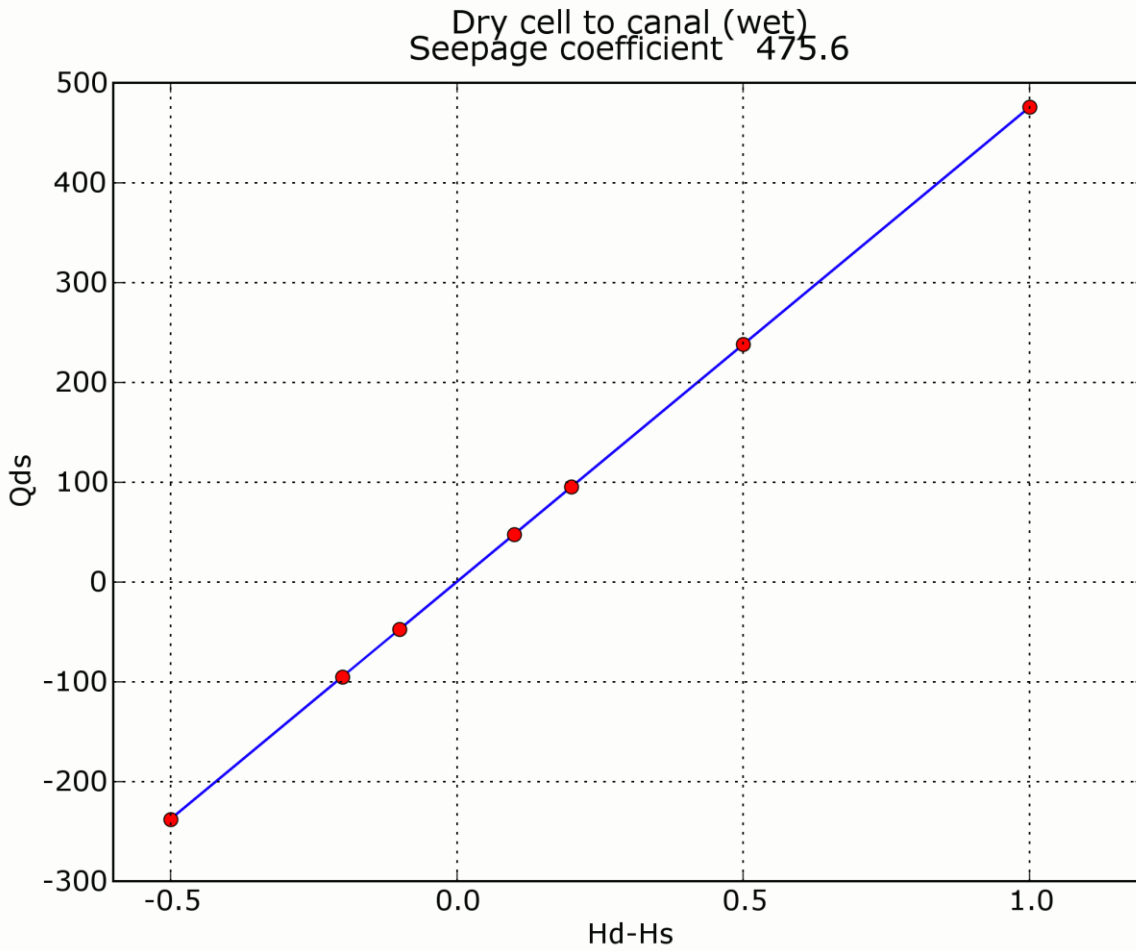


Figure 62: Seepage coefficient for L-31N south of S331 from Dry Cell to Canal (wet).

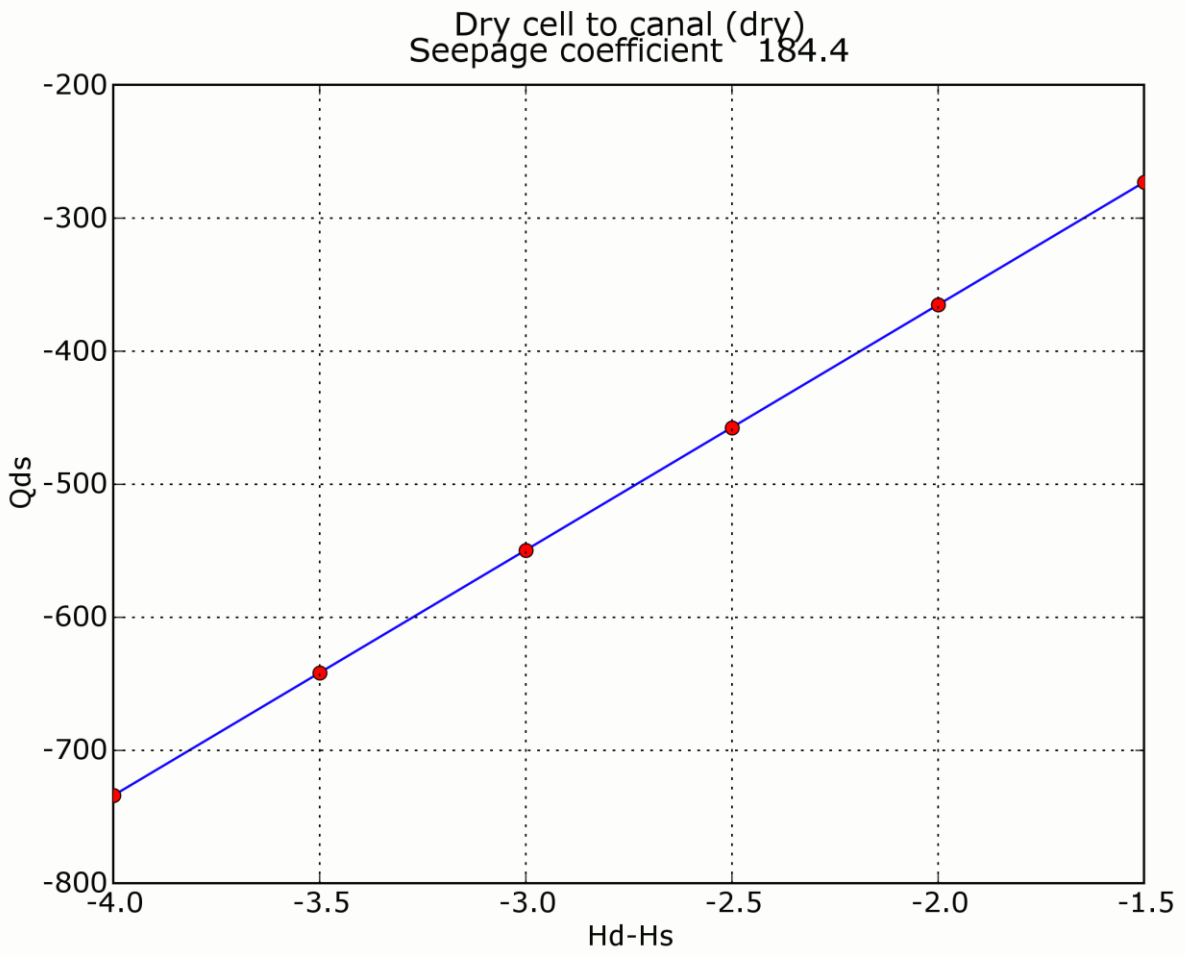


Figure 63: Seepage coefficient for L-31N south of S331 from Dry Cell to Canal (dry).

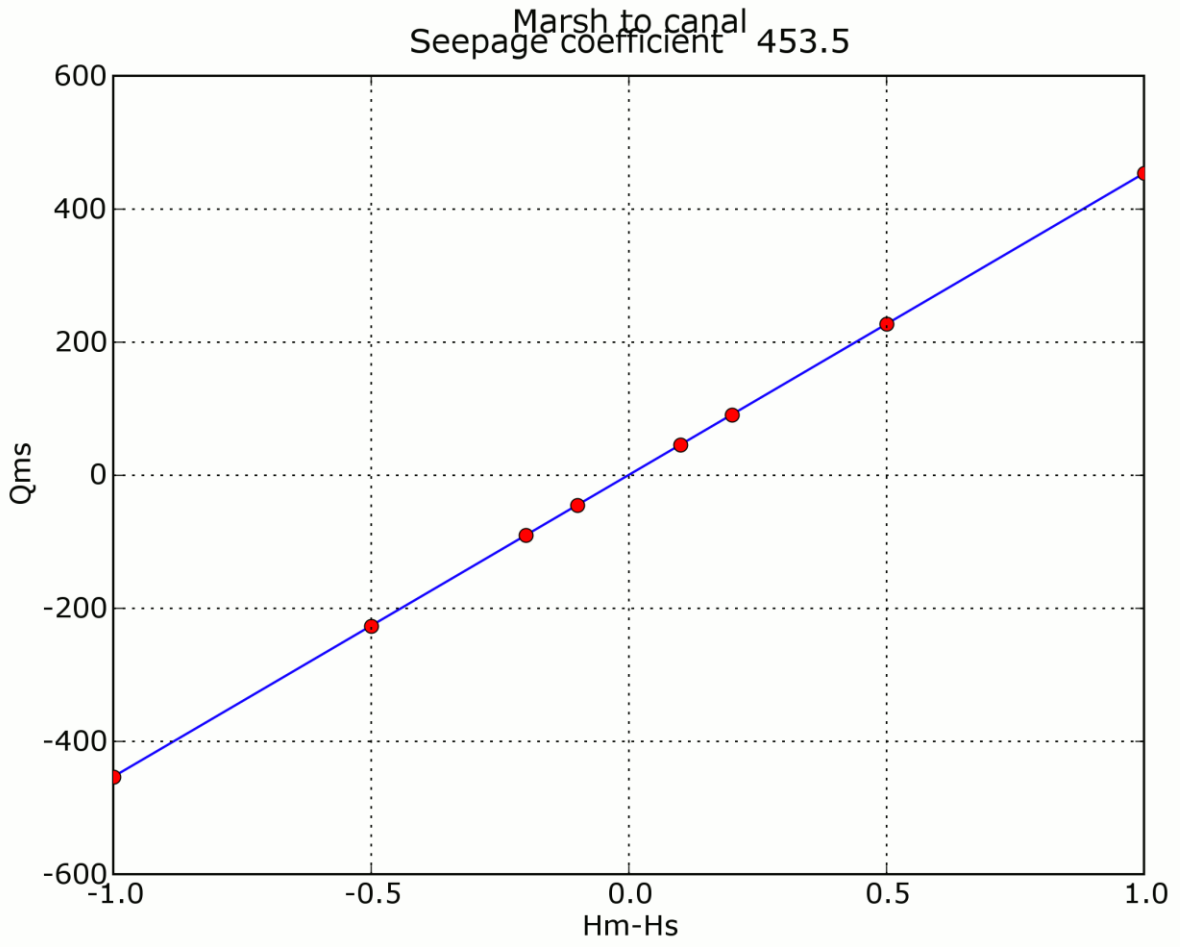


Figure 64: Seepage coefficient for L-31N south of S331 from Marsh to Canal.

4. Conclusions

WHPA has used detailed analytic element models of levee seepage to compute seepage coefficients to be used in HSE for eight levee reaches in South Florida. Several hundred different model realizations were used in the analysis, and coefficients that are based on the “best estimate” aquifer properties are provided in Table 24.

We found that seepage coefficients that are related to the dry cell can be very different depending on whether the dry cell is ponded or dry. If it will be necessary to construct future HSE models that handle wet and dry conditions in the dry cell, a scheme for making a smooth transition from the “wet” to the “dry” seepage coefficient will be needed.

We have provided five seepage coefficients for each levee reach:

K_{md} (wet) and K_{md} (dry): marsh-to-dry-cell, depending on wet or dry conditions in the dry cell

K_{ms} : marsh-to-canal-segment

K_{ds} (wet) and K_{ds} (dry): marsh-to-dry-cell, depending on wet or dry conditions in the dry cell

In applications, the modeler should consider which coefficient to use, depending upon the typical conditions in the dry cell at each levee reach.

<i>Reach</i>	K_{md} (dry)	K_{md} (wet)	K_{ms}	K_{ds} (dry)	K_{ds} (wet)
C-111 between S-176 and S-177	2.4	5.1	769.2	227.1	995.8
C-111 between S-177 and S-18C	1.4	2.7	471.0	192.7	476.6
L-30 south of S-335	24.2	53.8	363.0	160.7	465.1
L-30 between S-335 and the bridge	73.9	100.0	294.3	201.8	358.9
L-30 north of the bridge	120.8	138.5	180.9	92.3	167.5
L-31 south of S-331	1.1	1.4	453.5	184.4	475.6
L-31N between S-331 and G-211	1.6	2.3	635.5	230.2	802.4
L-31N north of G-211	22.5	48.5	345.6	152.5	424.4

Table 24: Summary of seepage coefficients.

Appendix F

A Discussion of Predictive Confidence Limits by John Doherty

Predictive Confidence Limits

General

This document considers calculation of confidence intervals of predictions made by a model. The following is assumed.

1. The model provides a correct representation of physical processes on which the prediction is dependent.
2. Spatial/temporal variability of model parameters is represented on the same scale as spatial/temporal variability of hydraulic properties; hence no artificial “parameter lumping” has taken place.
3. No historical measurements of system state are available by which to constrain parameter values; in other words, the model is not “calibrated”.

As an outcome of these conditions, predictive uncertainty is solely a function of *a priori* parameter uncertainty. Also, “predictive noise” (incurred through model inadequacy or through parameter lumping) need not be included in the analysis. In practice the first two of the above conditions are always violated. However as compensatory predictive noise is very difficult to calculate, it is mostly ignored; hence model-based uncertainty analysis can only ever be approximate. Nevertheless the approximation can be good, especially where predictions depend on broad-scale processes and parameterisation, rather than on process and parameterisation detail.

Linear Analysis

Let model parameters p_1, p_2 etc. comprise the elements of the vector \mathbf{p} . Let a prediction s be calculable from \mathbf{p} using the formula:-

$$s = \mathbf{y}^t \mathbf{p} \quad (1)$$

where \mathbf{y} is a vector which encapsulates the sensitivities of the prediction to parameters employed by the model. Let the innate variability of parameters be expressed by the covariance matrix $\mathbf{C}(\mathbf{p})$. Note that off-diagonal elements within this matrix can be used to express the fact that spatial/temporal variability of one parameter is not statistically independent of that of another. From equation (1), the variance (square of standard deviation) of the prediction s (referred to herein as σ_s^2) becomes:-

$$\sigma_s^2 = \mathbf{y}^t \mathbf{C}(\mathbf{p}) \mathbf{y} \quad (2)$$

Define the matrix \mathbf{Q} through the equation:-

$$\mathbf{Q} = \mathbf{C}^{-1}(\mathbf{p}) \quad (3)$$

Then (recalling that $\mathbf{C}(\mathbf{p})$ is a positive definite matrix):-

$$\mathbf{Q}^{1/2} \mathbf{C}(\mathbf{p}) \mathbf{Q}^{1/2} = \mathbf{I} \quad (4)$$

where \mathbf{I} is the identity matrix. Define transformed (normalized by their standard deviations) parameters as:-

$$\mathbf{q} = \mathbf{Q}^{1/2} \mathbf{p} \quad (5)$$

Then:-

$$\mathbf{C}(\mathbf{q}) = \mathbf{Q}^{1/2} \mathbf{C}(\mathbf{p}) \mathbf{Q}^{1/2} = \mathbf{I} \quad (6)$$

From 1 and 5:-

$$s = \mathbf{y}^t \mathbf{p} = \mathbf{y}^t \mathbf{Q}^{-1/2} \mathbf{q} \quad (7)$$

Thus:-

$$s = \mathbf{z}^t \mathbf{q} \quad (8)$$

where:-

$$\mathbf{z} = \mathbf{Q}^{-1/2} \mathbf{y} \quad (9)$$

From (8) the variance of s is given by:-

$$\sigma_s^2 = \mathbf{z}^t \mathbf{C}(\mathbf{q}) \mathbf{z} = \mathbf{z}^t \mathbf{z} \quad (10)$$

Define t to be our prediction normalised by its standard deviation. If $\mathbf{C}(\mathbf{p})$ is multiGaussian, t is thus a normal deviate from which confidence intervals are thus easily determined from its value.

Thus:-

$$t = \frac{s}{\sqrt{\mathbf{z}^t \mathbf{z}}} = \frac{\mathbf{z}^t \mathbf{q}}{\sqrt{\mathbf{z}^t \mathbf{z}}} \quad (11)$$

The situation is shown diagrammatically for a parameter space of two dimensions in Figure 1.

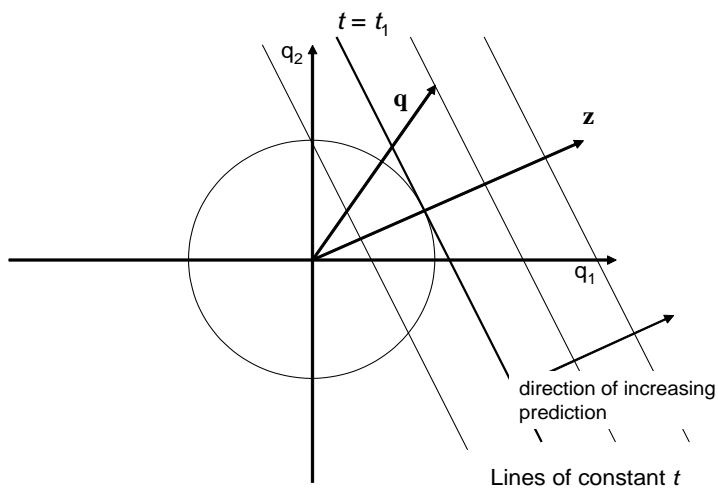


Figure F1. Contour lines in parameter space of a prediction made by a linear model.

The circle is an equi-probability contour for transformed parameters \mathbf{q} .

From equation 11 it is apparent that the prediction t is the projection of the vector \mathbf{q} onto the vector $\frac{\mathbf{z}^t}{\sqrt{\mathbf{z}^t \mathbf{z}}}$. Many different \mathbf{q} 's (and hence many different parameter sets) can result in the same projection (and hence the same prediction) – as is illustrated by the lines of constant t in the above figure (which are straight due to the fact that the model is linear). However it is obvious from the above that the smallest norm (and hence maximum likelihood) \mathbf{q} which gives rise to a particular prediction occurs when \mathbf{q} is parallel to \mathbf{z} . Looked at another way, as we maximise the prediction by travelling outwards along $\frac{\mathbf{z}^t}{\sqrt{\mathbf{z}^t \mathbf{z}}}$, the parameter vector \mathbf{q} of maximum likelihood which gives rise to this prediction must also point along this line, and hence be parallel to \mathbf{z} . Furthermore, because t is a normal variate, one standard deviation is encountered when t is 1.0, two standard deviations are encountered when t is 2.0 etc. From equation (11) this will occur (for maximum likelihood \mathbf{q}) when the magnitude of \mathbf{q} is 1.0, 2.0 etc. That is when:-

$$\mathbf{q}^t \mathbf{q} = 1 \quad (\text{one standard deviation of } t) \quad (12a)$$

$$\mathbf{q}^t \mathbf{q} = 2 \quad (\text{two standard deviations of } t) \quad (12b)$$

etc

From equation (5):-

$$\mathbf{q}^t \mathbf{q} = \mathbf{p}^t \mathbf{Q} \mathbf{p} \quad (13)$$

Where $\mathbf{C}(\mathbf{p})$ is diagonal, this is equivalent to summing squared weighted elements of \mathbf{p} , with the weight for each individual parameter (i.e. element) being the inverse of the standard deviation of the respective parameter.

It can be seen from Figure 1, that equation (13) represents the minimum value of $\mathbf{q}^t \mathbf{q}$ for which a prediction greater than t_1 can be made to occur at a confidence interval corresponding to the value of the t_1 normal deviate. Thus, for example, if a two sided 95% confidence interval is considered (this corresponding to 2 standard deviations from the mean), then $\mathbf{p}^t \mathbf{Q} \mathbf{p}$ must be greater than 4.0 for the prediction to be greater than t_1 . Thus if we use PEST's predictive analyzer to maximize/minimize the prediction subject to the constraint that an objective function calculated as $\mathbf{p}^t \mathbf{Q} \mathbf{p}$ rises no higher than a certain value, the mechanism for relating an objective function value to a confidence interval is thereby provided.

Nonlinear Analysis

In undertaking nonlinear analysis, a similar methodology is followed. That is, a prediction is maximized or minimized by varying parameters on which the prediction depends. For a particular value of that prediction, we seek the maximum likelihood parameter set (which is minimum norm for the transformed \mathbf{q} parameter set and hence minimum value for the objective function $\mathbf{p}^t \mathbf{Q} \mathbf{p}$) that can give rise to that prediction. Any prediction whose value is greater than this must then correspond to a lower confidence level as it cannot be achieved using a parameter set corresponding to an objective function that is equal to or lower than this. The situation is shown diagrammatically in Figure 2.

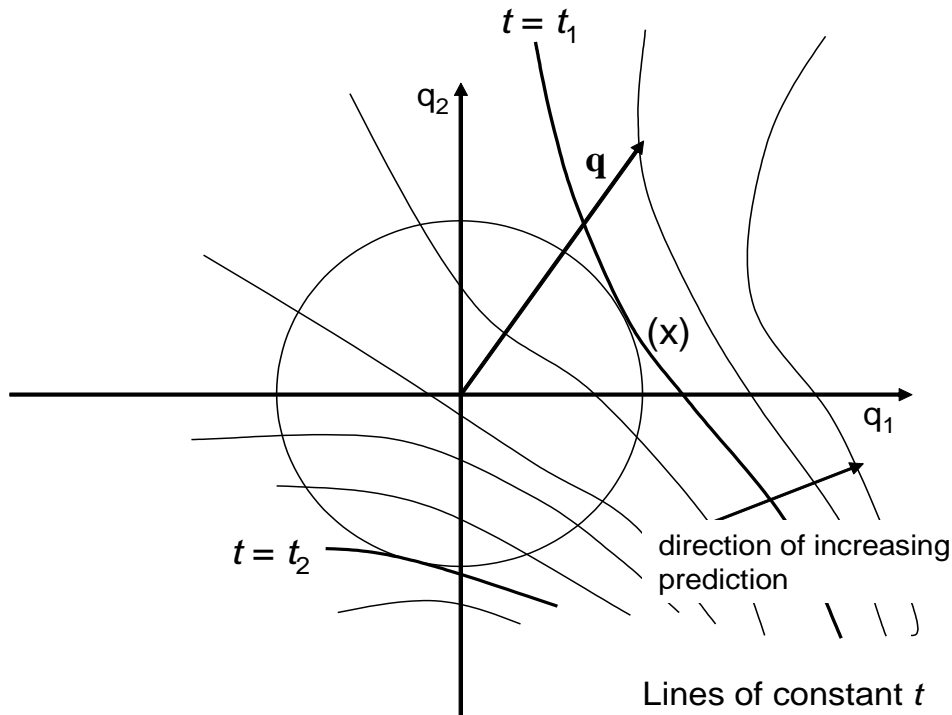


Figure F2. Contour lines in parameter space of a prediction made by a nonlinear model. The circle is an equi-probability contour for transformed parameters \mathbf{q} .

For the nonlinear case the dependence of a prediction on model parameters is not expressible as a vector \mathbf{z} . Nevertheless, as a prediction is maximized, a point is sought where a line of constant t is tangential to a contour of constant parameter probability (these are circles for transformed parameters \mathbf{q} , but are ellipses for native parameters \mathbf{p}). This point - point (x) in the above figure - defines the parameter set of highest likelihood that can give rise to a prediction of that value; thus no parameters of any greater likelihood (which are therefore any closer to the origin in Figure 2) can give rise to the same prediction.

Suppose that the circle in the above figure corresponds to a distance of $\sqrt{5.99}$ from the origin; that is, along this circle $\mathbf{q}^t\mathbf{q}$ (distance from the origin) is 5.99 and thus $\mathbf{p}^t\mathbf{Q}\mathbf{p}$ is also 5.99. For a Chi Square distribution with two degrees of freedom, this corresponds to a confidence interval of 95%. It is obvious that if $\mathbf{p}^t\mathbf{Q}\mathbf{p}$ is less than 5.99 the prediction will lie between values of t_1 and t_2 ; this allows us to define a confidence interval corresponding to the prediction interval. That is, we can notionally vary parameter values in order to raise (or lower) the prediction until $\mathbf{p}^t\mathbf{Q}\mathbf{p}$ is equal to 5.99 and then say that because there is only a 5% chance that $\mathbf{p}^t\mathbf{Q}\mathbf{p}$ will be greater than this, there is a 5% chance at most that the prediction will be greater than this. (“At most” is an important phrase here, because it is possible for $\mathbf{p}^t\mathbf{Q}\mathbf{p}$ to rise, without the prediction actually rising; all that is necessary for $\mathbf{p}^t\mathbf{Q}\mathbf{p}$ to rise is for \mathbf{q} to move out of the circle). This defines the so-called Scheffe (or “simultaneous”) confidence interval for the prediction interval. Unfortunately, as has already been mentioned, this approach to definition of predictive confidence intervals yields intervals that are too conservative; that is, the probability that the prediction is greater than t_1 or less than t_2 is actually smaller than the 5%. To illustrate this point further, let us return to the linear case.

Individual and Scheffe Confidence Intervals for a Linear Model

In Figure 3a, contours corresponding to predictions of t_1 and t_2 are shown bold. Also shown is a circle corresponding to the $\mathbf{p}^t \mathbf{Q} \mathbf{p}$ value of $(1.96)^2$; this circle thus has a radius of 1.96 in \mathbf{q} -space (corresponding to a 95% two-sided confidence interval for a normal deviate). If one were to notionally generate random realizations of \mathbf{q} in seeking to empirically determine the confidence with which a prediction lies between values of t_1 and t_2 (which are assumed to be symmetrically disposed with respect to mean parameter values corresponding to the origin in Figure 3a), this confidence interval would be evaluated by counting the fraction of parameter realisations that generate prediction values that lie between t_1 and t_2 (i.e. that lie within the shaded area of Figure 3a). By superimposing a normal distribution over the line defining the direction of the \mathbf{z} vector in Figure 3a (see Figure 3b), it is apparent that, as discussed above, definition of a two-sided confidence interval coincides with definition of points which are a distance of 1.96 from the origin along this line. This methodology is used to define the so-called “individual confidence interval” for the prediction in question.

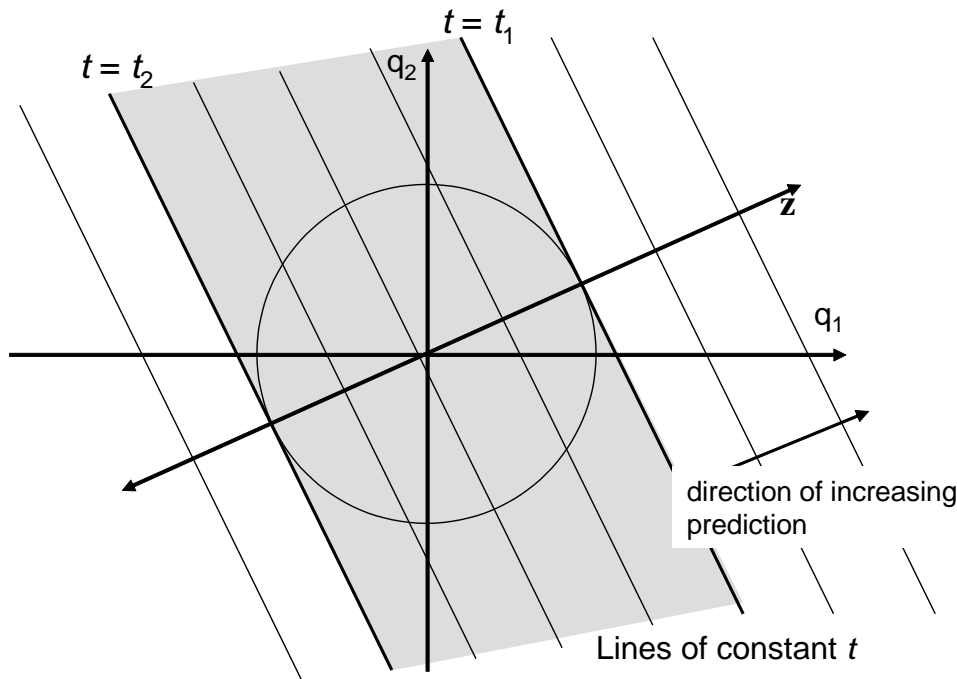


Figure F3a. Contour lines in parameter space of a prediction made by a linear model.

The circle is an equi-probability contour for transformed parameters \mathbf{q} .

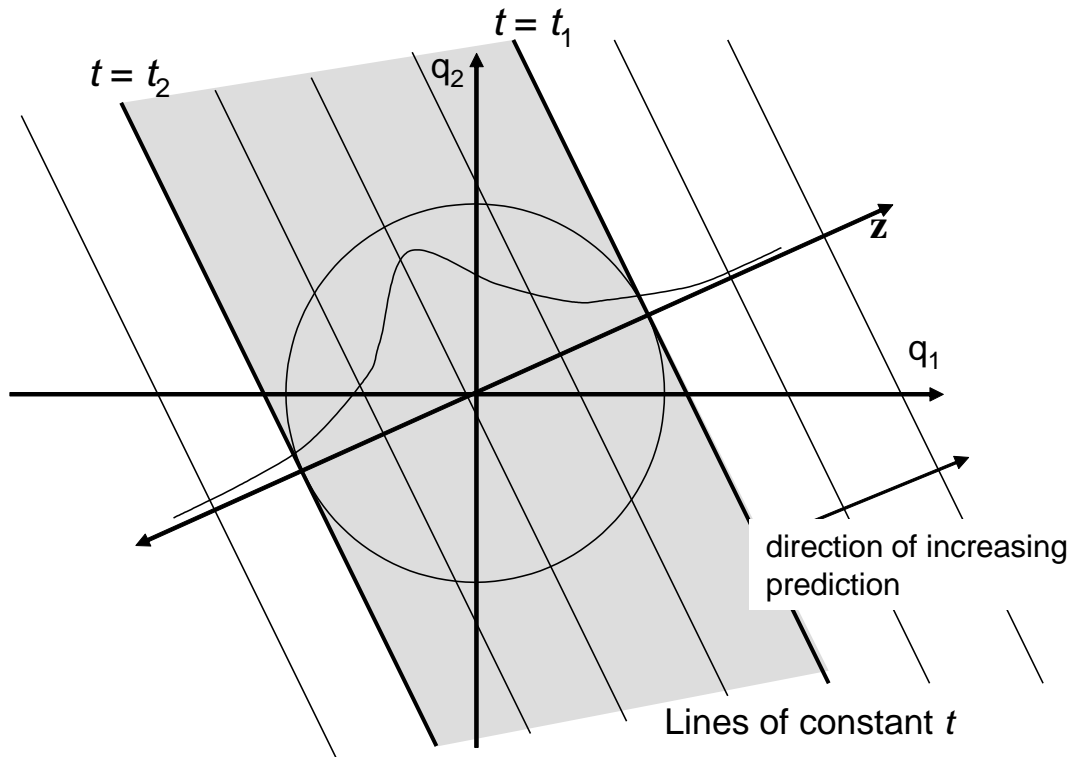


Figure F3b. Ninety-five percent of points generated for q would lie within the shaded region. Thus the confidence that a prediction is between t_1 and t_2 is 95%.

The 95% linear Scheffe confidence interval for the above prediction could be defined using a circle not with a radius of 1.96, but with a radius of $\sqrt{5.99}$ as discussed above (because 5.99 corresponds to a Chi Square confidence level of 95%). The fact that the Scheffe confidence limit circle is larger than the individual confidence limit circle is easily seen by notionally counting points, with each point representing a parameter realisation as discussed above. To guarantee that 95% of generated points lie within a circle of a given radius, the radius must be enlarged over that shown in Figure 3, because the circle in Figure 3 holds fewer than 95% of generated parameter points, as many points necessarily lie outside the circle but still in the shaded area of parameter space (all points within the shaded collectively summing to 95%). Hence Scheffe confidence intervals will always be larger than individual confidence intervals. In higher dimensional parameter spaces the discrepancy between the two is even larger. For example in a parameter space of 10 dimensions 95% individual confidence intervals are still defined by a $\mathbf{p}'\mathbf{Q}\mathbf{p}$ value of 1.96^2 . However the Scheffe confidence interval is defined by a $\mathbf{p}'\mathbf{Q}\mathbf{p}$ value of 18.31.

A problem arises when applying these concepts to a nonlinear model, however, if we are to escape the use of the statistically inefficient Scheffe confidence interval. The $t_1 - t_2$ confidence region for a linear model is shaded in Figure 4. Unfortunately, exact definition of this confidence region cannot be linked to the radius of a circle in parameter space in this case, due to the fact that lines of constant prediction are no longer equispaced or (what is even more problematical) even parallel, because of model nonlinearity. In contrast, the more statistically inefficient Scheffe

confidence intervals can, however, be exactly defined. However the fact that these are unnecessarily wide is also evident from Figure 4.

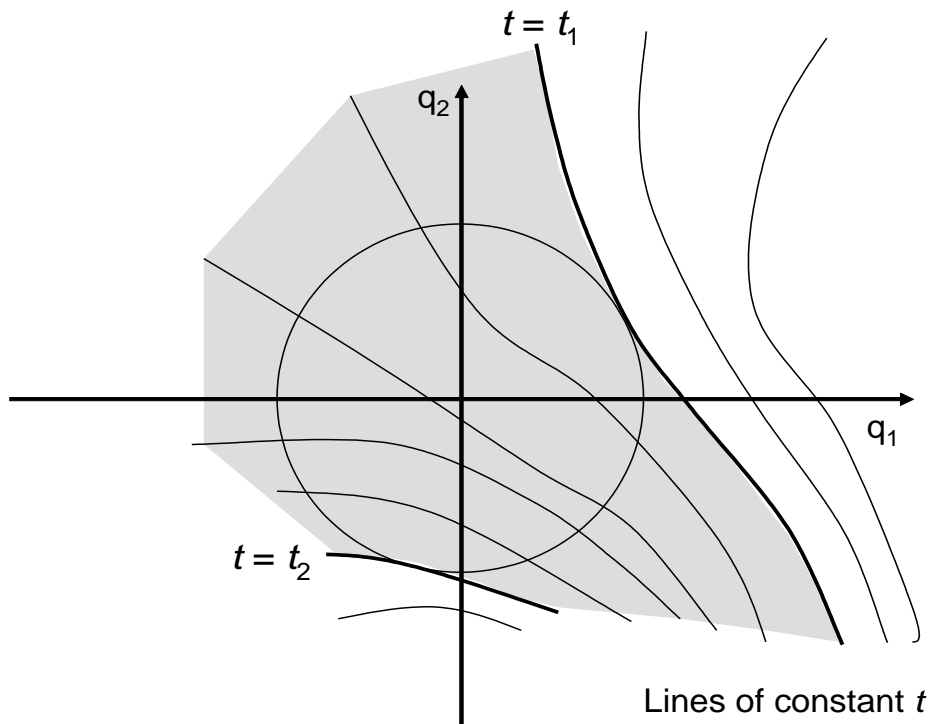


Figure F4. If ninety-five percent of points generated for q lie within the shaded region, the confidence that a prediction is between t_1 and t_2 is 95%.

Resolution of the Issue

Strictly, the best way to determine statistically efficient predictive confidence limits for a nonlinear model would be to abandon use of the maximization/minimization methodology for analysis of predictive confidence limits and employ Monte-Carlo analysis instead. The number of model runs required for such an analysis would probably not exceed by too much the number required for use of PEST's predictive analyser, especially if more than a few predictions were analysed. (Recall that in generating parameter values, no constraints on those values are imposed by historical measurements of system state).

Alternatively, if it is desired that use be made of previous work already undertaken using the predictive analyser, then I suggest that the use of individual confidence intervals constitutes an approximation which is not too bad, with the level of approximation decreasing with increasing model linearity. Thus confidence intervals are calculated by relating $\mathbf{p}'\mathbf{Q}\mathbf{p}$ to the square of a normal deviate, and using the confidence interval pertaining to that deviate as the confidence interval for a certain predictive interval. I wish to point out however, that at the time of writing this recommendation is based more on intuition than experience with this type of analysis.

It should be noted that the level of approximation involved in the use of individual confidence intervals in a calibration setting (for which PEST's predictive analyser is designed) is far smaller than in a setting such as that described herein where no calibration constraints are exerted, due to the generally smaller confidence regions which are involved in the latter type of analysis, especially where calibration data is abundant. Hence individual confidence intervals can be more confidently employed in that setting.

John Doherty
November 2007